

INFORMATION TO USERS

This manuscript has been reproduced from the microfilm master. UMI films the text directly from the original or copy submitted. Thus, some thesis and dissertation copies are in typewriter face, while others may be from any type of computer printer.

The quality of this reproduction is dependent upon the quality of the copy submitted. Broken or indistinct print, colored or poor quality illustrations and photographs, print bleedthrough, substandard margins, and improper alignment can adversely affect reproduction.

In the unlikely event that the author did not send UMI a complete manuscript and there are missing pages, these will be noted. Also, if unauthorized copyright material had to be removed, a note will indicate the deletion.

Oversize materials (e.g., maps, drawings, charts) are reproduced by sectioning the original, beginning at the upper left-hand corner and continuing from left to right in equal sections with small overlaps.

Photographs included in the original manuscript have been reproduced xerographically in this copy. Higher quality 6" x 9" black and white photographic prints are available for any photographs or illustrations appearing in this copy for an additional charge. Contact UMI directly to order.

ProQuest Information and Learning
300 North Zeeb Road, Ann Arbor, MI 48106-1346 USA
800-521-0600

UMI[®]

University of Alberta

**The Experimental Testing of the Impact of Interfacial Coupling on
Two Phase Flow in Porous Media**

by

Muhammad Ayub



**A thesis submitted to the Faculty of Graduate Studies and
Research in partial fulfillment of the
requirements for the degree of**

Doctor of Philosophy

in

Petroleum Engineering

Department of Civil and Environmental Engineering

Edmonton, Alberta, Canada

Spring 2000



National Library
of Canada

Acquisitions and
Bibliographic Services

395 Wellington Street
Ottawa ON K1A 0N4
Canada

Bibliothèque nationale
du Canada

Acquisitions et
services bibliographiques

395, rue Wellington
Ottawa ON K1A 0N4
Canada

Your file Votre référence

Our file Notre référence

The author has granted a non-exclusive licence allowing the National Library of Canada to reproduce, loan, distribute or sell copies of this thesis in microform, paper or electronic formats.

The author retains ownership of the copyright in this thesis. Neither the thesis nor substantial extracts from it may be printed or otherwise reproduced without the author's permission.

L'auteur a accordé une licence non exclusive permettant à la Bibliothèque nationale du Canada de reproduire, prêter, distribuer ou vendre des copies de cette thèse sous la forme de microfiche/film, de reproduction sur papier ou sur format électronique.

L'auteur conserve la propriété du droit d'auteur qui protège cette thèse. Ni la thèse ni des extraits substantiels de celle-ci ne doivent être imprimés ou autrement reproduits sans son autorisation.

0-612-59927-2

Canada

University of Alberta

Library Release Form

Name of Author: Muhammad Ayub

Title of Thesis: The Experimental Testing of the Impact of Interfacial Coupling on Two-Phase Flow in Porous Media

Degree: Doctor of Philosophy

Year this Degree Granted: 2000

Permission is hereby granted to the University of Alberta Library to reproduce single copies of this thesis and to lend or sell such copies for private, scholarly or scientific research purposes only.

The author reserves all other publication and other rights in association with the copyright in the thesis, and except as herein before provided, neither the thesis nor any substantial portion thereof may be printed or otherwise reproduced in any material form whatever without the author's prior written permission.



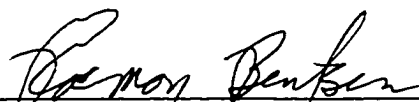
501-C, Shad Bagh
Lahore, Pakistan

Dated April 06, 2000

University of Alberta

Faculty of Graduate Studies and Research

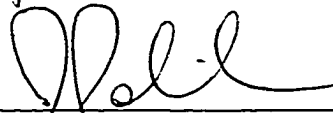
The undersigned certify that they have read, and recommended to the Faculty of Graduate Studies and Research for acceptance, a thesis entitled The Experimental Testing of the Impact of Interfacial Coupling on Two-Phase Flow in Porous Media submitted by Muhammad Ayub in partial fulfillment of the requirements for the degree of Doctor of Philosophy in Petroleum Engineering.



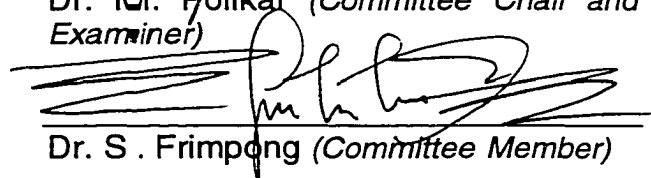
Dr. R. G. Bentsen (Supervisor)



Dr. B. Lepski (Co-supervisor)



Dr. M. Polikar (Committee Chair and Examiner)



Dr. S. Frimpong (Committee Member)



Dr. S. Liu (Committee Member)

MP

for Dr. D. W. Ruth (External Examiner)
University of Manitoba

Dated April 4, 2000

TO MY BELOVED MOTHER

Who passed away towards the end of this study, while desperately waiting for my return home. Whose everlasting passionate love and affection, blessings, patience, and encouragement were immensely important to the completion of this work.

I whole heartily pray to God for her soul to rest in peace in Heaven.

ABSTRACT

Traditional Darcian transport equations to describe two-phase flow through porous media ignore the influence of interfacial coupling between the two flowing phases. Because of this neglect, a significant amount of error may be introduced into two-phase flow properties such as relative permeability and capillary pressure, as indicated in some recent studies.

Several researchers have attempted to gain a better understanding of the probable impacts of interfacial coupling during two-phase flow through porous media. However, none of them has been able to provide a satisfactory explanation of its physical origin. Moreover, none of these attempts has provided a convenient method to estimate quantitatively the effects of interfacial coupling on two-phase flow through porous media.

In this study, a partition concept has been introduced into Kaladjian's transport equations to construct modified transport equations that enable a better understanding of the role of interfacial coupling in two-phase flow through natural porous media. Using these equations, it is demonstrated that, in natural porous media, the physical origin of interfacial coupling is the capillarity of the porous medium (capillary coupling), and not interfacial momentum transfer (viscous coupling), as is usually assumed. Moreover, it is suggested

that the magnitude of capillary coupling in a porous medium-fluids system is directly related to the porosity of the porous medium.

Furthermore, to test the new theory experimentally, a relatively new experimental apparatus to conduct steady state and unsteady-state two-phase flow experiments was constructed. Using this experimental set-up, several two-phase flow experiments were conducted successfully, where two different porous media and two different viscosity fluids were used.

Experimental testing of the new theory has shown that the pressure profiles predicted using the new transport equations are consistent with those determined experimentally. Moreover, it appears that the capillarity of the porous medium is the physical origin of interfacial coupling. Finally, the amount of interfacial coupling that takes place, which depends on porosity, appears to be consistent with the new theory.

ACKNOWLEDGEMENT

All the praise and gratitude be to God, the Creator, and the Sustainer of the Universe. The completion of this study was not possible without His grace and mercy. Nevertheless, this was not a solitary effort; many people and organizations were instrumental in the successful completion of this work. I extend my sincere appreciation to all of you, and I thank you all. However, I must single out a few organizations and individuals who played an extremely vital role throughout the course of this study.

The financial support to complete this study, provided by the Natural Sciences and Engineering Research Council of Canada, Imperial Oil Limited of Canada, and the Alberta Research Council of Canada, is gratefully acknowledged.

I am deeply indebted to Mr. Vasily Prudky for his great contribution to building the saturation measurement sensor and to Mr. Roy Gitzel for his extraordinary help in completing the data acquisition and instrument control system. Acknowledgment is also extended to Dr. S. M. Farouq Ali, who provided vital help when the financial situation looked rather bleak. Also, thanks to Dr. B. Lepski and all other members of the supervisory committee.

Very special thanks and sincere gratitude to Dr. Ramon G. Bentsen, who was always available to provide instant guidance, and who performed a pivotal role throughout the course of this work. His unmatched commitment, dedication, and devotion in pursuit of true knowledge are highly commendable. Certainly, these unique qualities of Dr. Bentsen kept me on the right track during the entire work, and, definitely, working under his supervision will remain a life time honour for me. Once again, thank you Dr. Bentsen for all your kindness and assistance, particularly for your thought provoking questions, unlimited discussions, and in particular for generously ignoring my shortcomings.

Finally, I must extend my special thanks and appreciation to my wife, Najam, son Ahsan and daughter Sahar, whose everlasting smile and a sense of great understanding, especially in moments of frustration, agony and stress, were immensely important for the successful culmination of this study. Last but not least, thanks to my entire family, brothers and sisters, friends, and specifically my sister Neelum, whose constant encouragement and good wishes have positively contributed throughout the course of this work.

Muhammad Ayub

TABLE OF CONTENTS

CHAPTER	PAGE
1. INTRODUCTION	1
2. LITERATURE REVIEW	4
2.1. Darcy's Law	4
2.2. Relative Permeability	5
2.2.1. Measurement of Relative Permeability	6
2.2.1.1. Laboratory Methods	7
2.2.1.1.1. Steady-State Methods	7
2.2.1.1.2. Unsteady-State Methods	8
2.2.1.2. Empirical Methods	8
2.2.1.3. Calculation From Field Data	9
2.2.2. Factors Affecting Relative Permeability	9
2.2.2.1. Effect of Saturation and Saturation History	10
2.2.2.2. Effect of Rock Properties	11
2.2.2.3. Effect of Wettability	11
2.2.2.4. Effect of Viscosity and Viscosity Ratio	12
2.2.2.5. Effect of Instability	12
2.2.2.6. Effect of Flow Regime	13
2.2.2.7. Effect of Hydrodynamics	14
2.3. Capillary Pressure	15
2.4. Interfacial Coupling	16
2.4.1. Viscous Coupling	16
2.4.1.1. Theoretical Developments	18
2.4.1.1.1. Volume Averaging Methods	19
2.4.1.1.2. Principles of Irreversible Thermodynamics	20
2.4.1.1.2.1. Applicability of Onsager's Relations	21
2.4.1.1.3. Analogous Models	23

2.4.1.1.3.1. Tubular Flow	24
2.4.1.1.3.2. Hele-Shaw Flow	26
2.4.1.2. A Common Message	26
2.4.1.3. Verification of Viscous Coupling	27
2.4.1.3.1. Laboratory Experiments	28
2.4.1.3.2. Conventional Numerical Methods	29
2.4.1.3.3. Lattice Gas Automata	30
2.4.1.4. Quantitative Impact of Ignorance	32
2.4.2. Capillary Coupling	34
2.5. Fluid Distribution and Measurement	35
3. STATEMENT OF THE PROBLEM	38
3.1. Objectives	39
4. THEORY	40
4.1. Introduction	40
4.2. Basic Equations	42
4.3. Determination of Partition Coefficients	43
4.4. One-Dimensional Transport Equations	48
4.4.1. Generalized Mobilities	49
4.5. Capillary Coupling Parameter	49
4.6. Viscous Coupling Versus Capillary Coupling	56
4.7. Unsteady-State Cocurrent Flow	58
4.7.1. Unstabilized Displacement	58
4.7.2. Fractional Flow	58
4.8. Measurement of Dynamic Saturation	61
4.8.1. Theoretical Background of the Capacitance Method	62
5. EXPERIMENTAL SET-UP AND PROCEDURE	65
5.1. Introduction	65
5.2. Experimental Set-Up	66
5.2.1. Core Holder and Injection Caps	68
5.2.2. Fluid Injection System	68
5.2.3. Effluent Collection System	71

5.2.4. Saturation Measurement System	71
5.2.4.1. Calibration of the Sensor	72
5.2.5. Dynamic Pressure Measurement System	75
5.2.6. Data Acquisition and Instrument Control	78
5.2.6.1. Hardware Configuration	79
5.2.6.1.1. UPC-L Interface Card	79
5.2.6.1.2. RS-232 Interface Card	79
5.2.6.1.3. GPIB Interface Card	81
5.2.6.1.4. DAS-8 Interface Card	81
5.2.6.2. Software Configuration	81
5.2.6.2.1. Running the Software System	85
5.3. Materials	89
5.4. Two-Phase Flow Experiments	89
5.4.1. Experimental Procedure	93
6. RESULTS AND DISCUSSION	98
6.1. Introduction	98
6.2. Two-Phase Flow Experiments	99
6.2.1. USCO Flow Experiments (all Sets)	99
6.2.1.1. USCO Saturation Profiles	101
6.2.1.1.1. Shock Formation	107
6.2.1.2. Fractional Flow	107
6.2.1.3. Capillary Pressure Gradient	115
6.2.1.4. R_{12} Calculation	124
6.2.2. SSCO Flow Experiments (all Sets)	126
6.2.2.1. SSCO Saturation Profiles	126
6.2.2.2. SSCO Effective Mobilities	137
6.3. Two Approaches to Test the Theory	138
6.3.1. First Approach	142
6.3.2. Second Approach	145
6.4. Sensitivity Analysis	146
7. SUMMARY AND CONCLUSIONS	160

7.1. Understanding Interfacial Coupling	160
7.2. The Experimental Set-up	162
7.3. Simplified Technique	163
7.4. Effect of Mobility Ratio	164
7.5. Effect of Grain Size Distribution	164
8. SUGGESTIONS FOR FUTURE RESEARCH	165
8.1. Theoretical	165
8.2. Experimental	166
8.2.1. Types of Two-Phase Flow Experiments	166
8.2.2. Saturation Measurement	166
8.2.3. Pressure Measurement	167
8.2.4. Injection System	167
8.2.5. Data Acquisition and Analysis	168
8.2.6. Materials	168
8.2.7. Travel Track	169
8.3. Numerical Simulation	169
REFERENCES	171
APPENDIX A: PHASE VELOCITY	193
APPENDIX B: PHASE PRESSURE (USCO)	196
APPENDIX C: CAPILLARY PRESSURE	199
APPENDIX D: PHASE PRESSURE (SSCO)	200
APPENDIX E: WETTING PHASE SATURATION	203
APPENDIX F: ADJUSTED MOBILITY	204
CURRICULUM VITAE	206

LIST OF TABLES

TABLE		PAGE
5.1	Properties of sandpacks.	90
5.2	Fluid properties at room temperature.	90
6.1	USCO flow experimental parameters (all Sets).	100
6.2	Macroscopic capillary numbers (all Sets).	100
6.3	SSCO flow experimental parameters (Set 1).	127
6.4	SSCO flow experimental parameters (Set 2).	128
6.5	SSCO flow experimental parameters (Set 3).	129
A1	Calculated phase velocities, USCO (Set 1).	193
A2	Calculated phase velocities, USCO (Set 2).	194
A3	Calculated phase velocities, USCO (Set 3).	195
B1	Measured phase pressure data, USCO (all Sets).	196
B2	Fitted phase pressure data, USCO (all Sets).	197
B3	Calculated phase pressure data, Beta = 0.5, USCO (all Sets).	198
C1	Fitted capillary pressure data, SSCO (all Sets).	199
D1	Measured phase pressure data, SSCO (Set 1).	200
D2	Measured phase pressure data, SSCO (Set 2).	201
D3	Measured phase pressure data, SSCO (Set 3).	202
E1	Saturation profiles and gradients, USCO (all Sets).	203
F1	Wetting phase adjusted mobility data, SSCO (all Sets).	204
F2	Nonwetting phase adjusted mobility data, SSCO (all Sets).	205

LIST OF FIGURES

FIGURE		PAGE
4.1	An idealized schematic of a representative macroscopic surface (RMS), one located in a phase-1 channel, and one located in a phase-2 channel.	51
4.2	Cross-sectional view of the resonator's jaw used to measure equivalent capacitance of the system.	63
5.1	Experimental set-up for SSCO & USCO two-phase flow.	67
5.2	General configuration of the core holder (not to scale).	69
5.3	End cap for the core holder (not to scale).	70
5.4	Circuit diagram of the water saturation measurement sensor.	73
5.5	Resonator for the saturation measurement system with cross-sectional view of the core holder.	74
5.6	Typical calibration curve to convert the frequency response into water saturation.	76
5.7	Hardware configuration for instrumental control and data acquisition.	80
5.8	Schematic for the stepping motor interface.	82
5.9	Software configuration for instrument control and data acquisition.	83
5.10	Front panel for the data acquisition and the instrument control.	86
5.11	Format of output file names for various types of collected data.	88
5.12	Viscosity variation of kerosene-mineral oil blend.	91
6.1	Typical unsteady-state raw frequency data at various times along the core holder, USCO (Set 3).	102
6.2	Saturation profiles obtained during USCO (Set 1).	103

6.3	Saturation profiles obtained during USCO (Set 2).	104
6.4	Saturation profiles obtained during USCO (Set 3).	105
6.5	Volume of injected water versus time for various saturation levels, USCO (Set 1).	109
6.6	Volume of injected water versus time for various saturation levels, USCO (Set 2).	110
6.7	Volume of injected water versus time for various saturation levels, USCO (Set 3).	111
6.8	Wetting and non-wetting phase velocities at 2182 seconds, USCO (Set 1).	112
6.9	Wetting and non-wetting phase velocities at 2213 seconds, USCO (Set 2).	113
6.10	Wetting and non-wetting phase velocities at 3235 seconds, USCO (Set 3).	114
6.11	Measured phase pressures, USCO (Set 1).	116
6.12	Measured phase pressures, USCO (Set 2).	117
6.13	Measured phase pressures, USCO (Set 3).	118
6.14	Capillary pressure versus wetting phase saturation, SSCO (Set 1).	119
6.15	Capillary pressure versus wetting phase saturation, SSCO (Set 2).	120
6.16	Capillary pressure versus wetting phase saturation, SSCO (Set 3).	121
6.17	Wetting phase saturation profiles at breakthrough times, USCO (all Sets).	122
6.18	Wetting phase saturation gradients at breakthrough times, USCO (all Sets).	123
6.19	Ratio of wetting phase pressure gradients to non-wetting phase pressure gradients versus normalized non-wetting	

	phase saturation, SSCO (all Sets)	125
6.20	Typical steady-state raw frequency data along the core holder, SSCO (Set 3).	130
6.21	Steady-state saturation profile for each run, SSCO (Set 1).	133
6.22	Steady-state saturation profile for each run, SSCO (Set 2).	134
6.23	Steady-state saturation profile for each run, SSCO (Set 3).	135
6.24	Typical comparison between measured saturations by the sensor and by using the material balance method, SSCO (Set 1).	136
6.25	Adjusted, measured and fitted effective mobility curves, SSCO (Set 1).	139
6.26	Adjusted, measured and fitted effective mobility curves, SSCO (Set 2).	140
6.27	Adjusted, measured and fitted effective mobility curves, SSCO (Set 3).	141
6.28	Typical curves for Beta 1 and Beta 2, versus wetting-phase saturation, first approach (Set 1).	144
6.29	Comparison of calculated and measured phase pressure profiles, Beta = 0.5, USCO (Set 1).	147
6.30	Comparison of calculated and measured phase pressure profiles, Beta = 0.5, USCO (Set 2).	148
6.31	Comparison of calculated and measured phase pressure profiles, Beta = 0.5, USCO (Set 3).	149
6.32	Comparison of calculated and measured phase pressure profiles for various values of Beta, USCO (Set 1).	153
6.33	Comparison of calculated and measured phase pressure profiles for various values of Beta, USCO (Set 2).	154
6.34	Comparison of calculated and measured phase pressure profiles for various values of Beta, USCO (Set 3).	155
6.35	Error sum of squares versus Beta (Set 1).	156

6.36	Error sum of squares versus Beta (Set 2).	157
6.37	Error sum of squares versus Beta (Set 3).	158

NOMENCLATURE*

ROMAN LETTERS

1	subscript for wetting phase
2	subscript for nonwetting phase
a_{ij}	fraction of fluid-fluid interface that is phase i - phase j interface; i, j = 1,2
A	cross-sectional area of porous medium
A	statistical parameter, Equation (5.1)
A_b	bulk area of the RMS
A_c	area under capillary pressure curve
b	width of the resonator's jaw, Figure 4.2
B	statistical parameter, Equation (5.1)
\bar{c}	velocity of light
C	capacitance of the resonator, Equation (4.67)
C_o	capacitance of the shielded strip line, Equation (4.69)
C_p	capacitance between sides of central and outer conductors, Figure 4.2
C'	capacitance between corners of central and outer conductors, Figure 4.2
d	distance between sides of outer and central conductors, Figure 4.2
f_i	fractional flow of phase i; i = 1,2
f_o	frequency response
F_{ij}	force acting on the phase i – phase j portion of the fluid-fluid portion of the RMS, i,j = 1,2

* The equations and the calculated results in this document are presented in a consistent set of units; thus, the units of variables and parameters are not specified here.

F_{is}	force acting on the phase i-solid part of the RMS, $i = 1,2$
g_i	statistical parameter, $i = 1,2,3,4$, Equation (6.1)
h	width of the central conductor, Figure 4.2
IFT	interfacial tension
k	intrinsic permeability of the medium
k_{or}	relative permeability to oil at initial water saturation
k_{wr}	relative permeability to water at irreducible oil saturation
$k_{r,i}$	coefficient of relative permeability matrix; $i, j = 1,2$
K_{ij}	generalized phase permeability for phase i ; $i, j = 1,2$, Equations (2.1) and (2.2)
l	length of the central conductor of the resonator
L_x	length of porous medium
$LAGO$	light atmospheric gas oil
LHS	left hand side of an equation
M_r	mobility ratio ($M_r = k_{wr}\mu_o / \mu_w k_{or} = \lambda_{1r}^o / \lambda_{2r}^o$)
n	number of pressure values along the core-holder
N_c	macroscopic capillary number ($N_c = A_c k_{wr} / \nu L \mu_w = A_c \lambda_{1r}^o / \nu L$)
p_i	pressure of phase i ; $i = 1,2$
\bar{p}_i	average pressure of phase i acting at the midpoint of an RMS, $i = 1,2$
P_c	capillary pressure
\bar{q}_i, v_i	darcy velocity of phase i ; $i = 1,2$
q	total flow rate
q_i	flow rate of phase i ; $i = 1,2$
Q_I	total quantity of injected wetting phase
R_{12}	function relating the pressure gradient in phase 1 to that in phase 2
RES	representative elementary surface

<i>RHS</i>	right had side of an equation
<i>RMS</i>	representative macroscopic surface
<i>S</i>	normalized saturation, Equation (6.4)
<i>S_i</i>	saturation of phase <i>i</i> ; <i>i</i> = 1,2
<i>S_{1i}</i>	initial saturation of the wetting phase
<i>S_{2r}, S_{or}</i>	residual saturation of the nonwetting phase
<i>S₁[*]</i>	specific saturation of the wetting phase
<i>SS_E</i>	error sum of squares
<i>SSCO</i>	steady-state cocurrent
<i>SSCT</i>	steady-state countercurrent
<i>t</i>	time
<i>t</i>	thickness of the central conductor, Figure 4.2
<i>USCO</i>	unsteady-state cocurrent
<i>v</i>	total velocity
<i>VI</i>	virtual instrument
<i>y_j</i>	measured (fitted) pressure values along the core-holder, <i>j</i> =1,n
<i>ŷ_j</i>	calculated pressure values along the core-holder, <i>j</i> =1,n
<i>Z_o</i>	characteristic impedance, Equation (4.68)

GREEK LETTERS

$\alpha = \alpha_i$	capillary coupling parameter, <i>i</i> = 1,2
α_{ij}	generalized partition coefficient for phase <i>i</i> ; <i>i,j</i> = 1,2
$\beta = \beta_i$	fraction of the fluid-fluid interface that is phase 1 – phase 2 (or phase 2 – phase 1) interface; <i>i</i> = 1,2, Equation (6.7)
μ_i	viscosity of phase <i>i</i> ; <i>i</i> = 1,2
λ_i	mobility of phase <i>i</i> ; <i>i</i> = 1,2

$\lambda_{ij}, \Lambda_{ij}$	generalized mobility of phase i ; $i, j = 1, 2$
λ_i°	mobility determined using cocurrent flow for phase i ; $i = 1, 2$
λ_i^*	mobility determined using countercurrent flow for phase i ; $i = 1, 2$
λ_{1r}°	mobility to wetting phase at residual saturation of nonwetting phase
λ_{2r}°	mobility to nonwetting phase at initial saturation of wetting phase
ϕ	porosity of a porous medium
ε	dielectric constant of air

CHAPTER 1

INTRODUCTION

Many developed and developing countries, despite current economic difficulties and improved conservation, still import significant quantities of petroleum. Because primary and enhanced recovery methods recover, on average, only about one third of the original oil in place, one way to alleviate this problem is to improve the recovery efficiency of known fields. In this regard, it should be noted that each one percent increase in recovery efficiency adds, on a worldwide basis, about four billion barrels of recoverable reserves. This suggests that a greatly expanded research effort in the area of enhanced recovery could pay large dividends.

Most enhanced recovery schemes involve the displacement of one fluid by another. In order to predict the way in which one fluid displaces another in porous media, it is usual to combine the transport and continuity equations for each phase to obtain a set of coupled partial differential equations. These equations are finite-differenced so that they can be used to construct a "reservoir simulator" that can be used to predict the manner in which, for example, water displaces oil towards the production wells in a given field.

The importance of fluid flow properties such as effective mobility and capillary pressure to predict waterflood performance in reservoir engineering studies (in particular, reservoir simulation) is well recognized in the petroleum industry. Data associated with these properties are essential for almost all two-phase flow studies related to petroleum reservoirs. This information is

used in making estimations and predictions of the productivity, injectivity and ultimate recovery from reservoirs for evaluation and future development plans. Moreover, the data can be used also to diagnose the formation damage expected under various operational conditions. Therefore, unquestionably, these data are one of the most important data sets required in reservoir engineering studies.

Conventionally, in immiscible two-phase (oil & water) flow through porous media problems, it is common practice to ignore the effect(s) of interfacial coupling between the two flowing phases. However, to account properly for interfacial coupling, a recently developed two-phase flow formulation suggests a need for some modifications to the existing transport equations. The source and magnitude of such coupling is not well understood. Some of the studies argue that the physical origin of interfacial coupling is the momentum transfer between the two flowing phases, while, more recently, other studies argue that the capillarity of a porous medium/fluid system should be held responsible for such coupling.

For a long time, it has been realized that interfacial coupling should be incorporated into immiscible, two-phase flow formulations. The importance of giving attention to this phenomenon is made all the more urgent because the degree of interfacial coupling to be expected in particular cases has not been established yet. This problem arises because the theoretical indicators by themselves cannot be relied on unless and until supporting experimentally derived confirmation has been obtained.

Whether interfacial coupling is important is a contentious issue (Ayub and Bentsen, 1999a). Some researchers ignore the possibility of such coupling (e.g. Collins, 1961), some researchers argue that it has no effect (e.g. Philip,

1972), some researchers say its effect is negligibly small in natural porous media (e.g. Zarcone and Lenormand, 1994), while still others contend that it has a significant role to play (e.g. Kalaydjian, 1987,1990). Moreover, as mentioned above, there is also the issue of the physical origin of interfacial coupling.

This study, by making use of the newly constructed transport equations for one-dimensional two-phase flow, is an attempt to address these issues. To develop these equations, a partition concept developed in an earlier study (Bentsen, 1998b) has been introduced into Kalaydjian's transport equations (Kalaydjian, 1987) to construct modified transport equations that enable a better understanding of the role of interfacial coupling in two-phase flow through porous media. If these modified transport equations are to be useful, and if they are to be accepted, it is necessary that these equations be tested experimentally.

Thus, the overall goal of this study is to come to a better understanding of the role of interfacial coupling in immiscible two-phase flow through porous media. To achieve this goal, not only a theoretical formulation was developed (as mentioned above), but also a vigorous effort to test the new theory experimentally was made. In order to accomplish the experimental part of this study, two types of porous media and two different viscosity fluids were used to conduct steady-state and unsteady-state two-phase flow runs. Moreover, the overall quantitative impact of interfacial coupling during two-phase flow through porous media was examined.

CHAPTER 2*

LITERATURE REVIEW

2.1. Darcy's Law

Researchers have studied problems in fluid flow through porous media for many years. These include Muskat (1949), Bear (1972), Collins (1961) and Scheidegger (1960). Darcy's (1856) well known empirical law is fundamental to a macroscopic description of single-phase fluid flow through porous media. This law has been used extensively by petroleum engineers for single-phase flow problems. However, the practical problems confronting petroleum engineers very frequently involve mixtures of immiscible fluids, such as water and oil or gas and oil. This type of multiphase flow through porous media is not well understood, and it is extremely difficult to describe analytically because of several factors such as the interaction between fluids and rock and the complexity of the pore structure (Islam and Bentsen, 1987).

Conventionally, it has been assumed that the Darcy law, which was developed to describe single-phase fluid flow through porous media, is equally good for two-phase flow through porous media. Because of the extremely complex nature of the fluid/fluid and the fluid/rock interactions, this assumption is highly questionable. To test the applicability of Darcy's law to two-phase flow problems, several experimental studies were performed using two immiscible phases (Cloud, 1930; Plumer *et al.* 1937; and Fletcher, 1949). These experimental studies found that the presence of a second phase can cause a reduction in the permeability to the first phase. However, the investigators

* A version of this chapter has been published. Ayub, M. and Bentsen, R.G. 1999a. *Journal of Petroleum Science and Engineering*. 23(13-26).

were unable to provide a satisfactory explanation. Several other investigators have attempted to overcome the difficulties involved in extending Darcy's law to two-phase fluid flow. Leverett (1941), for example, introduced the capillary pressure term in a formulation which was suggested initially by Muskat and Meres (1936) and Muskat *et al.* (1937) as an extension of Darcy's law to two-phase flow. In this formulation, it was assumed that Darcy's law is independently applicable, without any cross effect(s), to both of the fluids during two-phase flow through porous media. Fatt (1953) highlighted the importance of rock compressibility during multiphase flow and emphasized its inclusion into the equations of multiphase flow through porous media. Moreover, Moore (1938), Childs (1945), Muskat (1949), Hubbert (1950) and Rose (1954) discussed several useful aspects related to the principles of multiphase flow through porous media.

Another questionable assumption inherited by the conventional formulation for two-phase flow through porous media is the sole dependence of relative permeability on saturation, and that it is independent of the pressure and velocity of the fluids. To prove this assumption valid, many investigators such as Wyckoff and Botset (1936), Hassler *et al.* (1936) and Richardson *et al.* (1952) conducted experimental studies; however, this assumption is only an approximation, (Scheidegger, 1960). The mobility of a fluid relative to the other is the most important parameter of interest in all multiphase flow problems. In the following sections, some of the concepts and factors affecting relative permeability are presented briefly.

2.2. Relative Permeability

Underlying the extension of single-phase flow theory for the simultaneous flow of two or more fluids are the concepts of effective and relative permeability. The effective permeability is a relative measure of the conductance of a porous medium for one fluid phase when the medium is saturated with more

than one fluid (Amyx *et al.*, 1960). Relative permeability is defined as the ratio of the effective permeability of a phase to a base permeability. Three different base permeabilities are used: (1) the absolute air permeability, (2) the absolute water permeability and (3) the effective permeability to oil at residual wetting-phase saturation (Craig, 1971). Commonly, the three base permeabilities do not have the same value; therefore, it is important to know which base permeability was used to obtain a particular relative permeability curve. Relative permeability data are essential for almost all two-phase flow studies related to reservoirs. The data are used in making estimations and predictions of the productivity, injectivity and ultimate recovery from reservoirs for evaluation and future development plans. The relative permeability data can also be used to diagnose the formation damage expected under various operational conditions. Therefore, unquestionably, these data are one of the most important data sets required in reservoir engineering studies.

2.2.1. Measurement of Relative Permeability

The first experimental data based on the concept of an extended Darcy's law for two-phase flow were recorded by Wyckoff and Botset (1936). They used an unconsolidated porous medium to construct relative permeability curves for gas and water. Later, the typical trends of the relative permeability curves obtained by Wyckoff and Botset have been substantiated by many investigators (Amyx *et al.*, 1960). Some of the problems related to the measurement of relative permeability have been discussed by Rose (1951), and Fatt and Dykstra (1951). Manai (1991), Honarpour and Mahmood (1988) and Honarpour *et al.* (1986) have provided brief overviews of various techniques for relative permeability measurements. They have classified different methods into three broad categories: (1) laboratory methods, (2) empirical methods and (3) calculation from field data. Detailed specific information on the methods in each category are not given here; however, a general overview of each category follows.

2.2.1.1. Laboratory Methods

These methods are the most reliable sources for obtaining relative permeability data. Laboratory methods of relative permeability measurement are further classified into steady-state and unsteady-state methods. Aleman *et al.* (1989) have concluded that the difference in the relative permeabilities obtained by the two approaches is negligible, provided that the magnitude of the local (not macroscopic) capillary number is larger than a limiting value.

2.2.1.1.1. Steady-State Methods

Steady-state methods are widely used because they are more reliable than unsteady-state methods. In these methods capillary equilibrium prevails, saturation is measured directly and the calculation scheme is based on Darcy's law. Steady-state methods are time-consuming because equilibrium attainment may take several hours or days at different saturation levels. Also, independent measurements of fluid saturations in the core are required (Honarpour and Mahmood, 1988). Some of the more commonly used steady-state laboratory methods for measuring relative permeability are listed below (Craig, 1971 and Honarpour *et al.*, 1986).

1. Hassler method
2. Penn-State method
3. Single-sample dynamic method,
4. Stationary fluid methods
5. Hafford method
6. Dispersed feed method

These methods were originally developed and subsequently modified by Osoba *et al.* (1951), Morse *et al.* (1947), Caudle *et al.* (1951), Geffen *et al.* (1951), Leas *et al.* (1950), Rapoport and Leas (1953), Richardson *et al.* (1952), and further details are available in these references.

2.2.1.1.2. Unsteady-State Methods

Unsteady-state methods are also known as external-drive methods or displacement methods. In these techniques, saturation equilibrium is not attained; therefore, a few hours are usually needed to obtain an entire set of data. Although these are much faster methods as compared to steady-state methods, many operational difficulties are involved in these techniques, such as capillary end effects, viscous fingering and channeling. Kyte and Rapoport (1958) have discussed the behavior of a linear waterflood under the influence of end effects. Many uncertainties are also involved in the interpretation techniques because of gross simplifying assumptions. Bentsen and Sarma (1989) have discussed the inlet end effects and other problems associated with the unsteady-state techniques.

The Buckley and Leverett (1942) equation for linear displacement of incompressible and immiscible fluids is the basis of the analysis for almost all unsteady-state methods. Some of the commonly used unsteady-state methods were originally developed by Welge (1952), Johnson *et al.* (1959) and Jones and Roszelle (1978). Subsequently, several investigators have proposed many modifications to further enhance the reliability and accuracy of the unsteady-state methods proposed by the above mentioned researchers. Some of these investigators are Naar *et al.* (1962), Sigmund and McCaffery (1979), Batycky *et al.* (1981), O'Mera and Leas (1983), Tao and Watson (1984), Islam and Bentsen (1986), Kerig and Watson (1986, 1987), Sarma and Bentsen (1989a, 1989c, 1990) and King (1996).

2.2.1.2. Empirical Methods

Empirical models to estimate relative permeability data are mainly used to extrapolate limited laboratory data. These are not a good alternative to laboratory measurements, but they are used sometimes to by-pass the difficulties involved in laboratory methods. Usually, in these models, the

porous medium is assumed to be an idealized bundle of capillaries. Some of the available models based on this concept include Corey's model for drainage, Naar-Wygal's and Naar-Henderson's model for imbibition and Land's model for both drainage and imbibition processes (Honarpour and Mahmood, 1988; and Honarpour *et al.*, 1986). Watson *et al.* (1988) have provided a regression-based method for estimating relative permeabilities from displacement experiments.

2.2.1.3. Calculation From Field Data

Reservoir production history and fluid properties may also be used to estimate the relative permeability data. This technique provides average values of relative permeability which are greatly influenced by several factors such as pressure and saturation gradients, stages of depletion and saturation variations. Moreover, sometimes complete production-history data are not available, which may affect the validity of the relative permeability data obtained. Generally, a poor agreement is observed between the data obtained by this method and those obtained from laboratory methods. Pressure-transient analysis is another widely used method for in-situ determination of average relative permeability data (Honarpour and Mahmood, 1988; and Manai, 1991).

2.2.2. Factors Affecting Relative Permeability

Islam and Bentsen (1987) have reviewed the effect of different factors on relative permeability, such as the effect of viscous and capillary forces, wettability, saturation history and temperature. They pointed-out that it is natural and realistic to assume the dependence of relative permeability of a given fluid only on saturation of that fluid, but there is no theoretical basis for such an assumption. This view point is also discussed in detail by Bear (1972).

Numerous studies have been conducted to investigate the effect of other important parameters on relative permeability. In addition to saturation, the most important parameters affecting relative permeability are wettability, IFT, density, capillarity, viscosity and viscosity ratio, rock properties, flow rates, flow regimes, saturation history, overburden pressure and temperature. Geffen *et al.* (1951) and Lefebvre du Prey (1973) have presented experimental studies to investigate the factors affecting relative permeability measurements, such as IFT, pressure gradient, wettability, viscosity, velocity of fluids and saturation history. Perhaps, the most comprehensive review of the factors affecting relative permeability is provided by Honarpour *et al.* (1986). Some other important factors influencing relative permeability, such as the effect of flow regime, the effect of instability and the effect of hydrodynamic forces have also been studied by several investigators. A brief description of some of these parameters is given below.

2.2.2.1. Effect of Saturation and Saturation History

Leverett and Lewis (1941), Sarem (1966), Saraf and Fatt (1967) and Owens and Archer (1971) have shown that for strongly water-wet unconsolidated sands the permeability to a wetting phase is dependent solely upon its own saturation. However, Caudle *et al.* (1951), and Snell (1959) have indicated that the nonwetting phase relative permeability depends on the wetting phase as well as the nonwetting phase saturation for strongly water-wet systems. In preferentially oil-wet systems, the oil phase relative permeability is found to be strictly a function of oil saturation, while in water-wet rocks, the oil relative permeability is dependent on both water and oil saturation (Emmett *et al.*, 1971).

The effects of saturation history or the saturation hysteresis phenomenon have been described by several investigators, such as Geffen *et al.* (1951), Osoba *et al.* (1951), Levine (1954), Josendal *et al.* (1952) and Terwilliger *et al.*

(1951). They have observed that both water-oil and gas-oil relative permeability ratio curves, as well as individual wetting and nonwetting phase relative permeabilities of both sandstone and carbonate rocks, may exhibit saturation hysteresis.

2.2.2.2. Effect of Rock Properties

Arps and Roberts (1955) have presented a good study of gas-oil relative permeability ratios for 16 consolidated sandstones and 25 dolomites, cherts and limestones, all with 15% connate water saturation. A wide variation among relative permeabilities obtained from various rock samples was observed. Nind (1964) stated that an increase in the degree of consolidation increases the nonwetting phase relative permeability in a gas-oil system. Corey and Rathjens (1956) studied the effect of rock heterogeneity on drainage gas-oil relative permeability, and concluded that the relative permeability at a given saturation for flow parallel to the bedding plane was greater than the analogous value for flow perpendicular to the bedding plane.

2.2.2.3. Effect of Wettability

It has been recognized for a long time that the wettability of reservoir rock has an important effect on the relative permeability. The dissymmetry of relative permeability curves is attributed to the preferential wettability of the formation (Lorenz *et al.*, 1974; and Jennings, 1957). Geffen *et al.* (1951), Fatt *et al.* (1959), Mungan (1964, 1971), Schneider and Owens (1970), Owens and Archer (1971) and McCaffery (1973) have confirmed the importance of preferential wettability on two-phase flow in porous media. McCaffery and Bennion (1974) reported that wettability alterations over a relatively wide range produce a negligible effect on the relative permeability curve; however, conversely, Treiber *et al.* (1972) and several other investigators have found that relatively small variations in wettability produce considerable effects on the relative permeability curve.

2.2.2.4. Effect of Viscosity and Viscosity Ratio

Diverse opinions about the effects of fluid viscosity and viscosity ratio on relative permeability have been expressed by several investigators. Many investigators found either no effect or little effect of these parameters on relative permeability data; among these investigators are Wyckoff and Botset (1936), Muskat *et al.* (1937), Leverett *et al.* (1941), Leverett (1939), Craig (1952), Geffen *et al.* (1952), Levine (1954), Wilson (1956), Richardson (1957), Sandberg *et al.* (1958), Johnson *et al.* (1959) and Saraf and Fatt (1967). On the other hand, Yuster (1951) concluded that relative permeability increases with an increase of the viscosity ratio. This conclusion was later verified by the work of Morse *et al.* (1947), Odeh (1959) and Danis and Jacquin (1983). Moore and Slobod (1956) examined the combined effect of viscous and capillary forces on the displacement efficiency of one fluid by another, and found a significant effect of these forces. In view of the diverse opinions which have been expressed by various investigators related to the effect of viscosity and viscosity ratio, Honarpour *et al.* (1986) proposed conducting laboratory experiments with fluids which do not differ greatly in viscosity from the reservoir fluids.

2.2.2.5. Effect of Instability

High displacement rates and high oil/water viscosity ratios tend to make the displacement of oil by water unstable. An unstable displacement is characterized by the lack of a sharp front of the displacing phase. Instead, the displacing phase advances through the porous medium in the form of channels known as viscous fingers. In-depth instability phenomenon and its overall implications to two-phase flow through porous media have been studied by several investigators, such as Sarma and Bentsen (1989b, 1987), Sarma (1988), Bentsen (1985), Spanos and De la Cruz (1984), Peters and Flock (1981), Peters (1979), Rachford (1964), Outmans (1962a, 1962b),

Perrine (1961), Scheidegger (1960), Chouke *et al.* (1959), and Lin (1955). However, specifically, its immediate effect on relative permeability data have been studied by only a few investigators.

Peters and Khataniar (1987) have studied the effect of instability on relative permeability curves obtained by the dynamic-displacement method. They compared oil/water relative permeability curves from steady-state and dynamic-displacement methods at various levels of instability. They found a significant deviation between the two types of relative permeability data as the degree of instability increased. Sarma and Bentsen (1989a, 1989b) have not only presented the impact of instability on relative permeability and capillary pressure data, but also they have proposed a new method to obtain relative permeability data from experiments involving unstabilized fluid flow. Relative permeability curves obtained by using the newly proposed method were then compared to those obtained using the explicit external-drive method.

2.2.2.6. Effect of Flow Regime

Based on the combined effect of viscous, capillary and gravity forces on two-phase flow through porous media Bentsen (1978, 1985) introduced the concept of various flow regimes. Depending on the values of the instability and capillary numbers the flow behavior during external-drive methods of displacement can be characterized as, unstabilized, stabilized and stable, and unstable. Islam (1985) extended Bentsen's approach and developed a technique to estimate the effective permeabilities in all three flow regimes. He concluded that the effective permeability is a unique function of saturation only if the displacement is steady-state or if the displacement is stable and stabilized. However, if the displacement is unstabilized or unstable, different effective permeability curves are obtained. Moreover, local heterogeneities were found to have a strong effect on effective permeability for unstable displacements.

Recently, in their experimental work, Avraam and Payatakes (1995b) introduced four flow regimes rather than three as suggested by Bentsen (1978, 1985). They used optical observation and macroscopic measurements to determine the flow regimes, and to calculate the corresponding relative permeability data. The observed flow regimes were classified as large-ganglion dynamics (LGD), small-ganglion dynamics (SGD), drop-traffic flow (DTF) and connected pathway flow (CPF). However, only steady-state two-phase flow experiments were conducted, using an idealized pore network, etched in glass. Besides, from this type of work only qualitative mechanistic explanations can be extracted. On the other hand Bentsen's approach is more realistic, because it takes into account the most important parameters which are responsible for various types of flow regimes, i.e., viscous, capillary and gravity forces. Moreover, quantitative information about the limits of various flow regimes can be obtained. Despite these shortcomings, Avraam and Payatakes (1995b) were able to demonstrate the qualitative effect of different flow regimes on relative permeability data.

2.2.2.7. Effect of Hydrodynamics

Recently, Bentsen (1994a) used the idea that the total flux of a given phase may be partitioned into several individual fluxes, together with a new pressure difference equation (Bentsen, 1994b) to explore the possible impact that hydrodynamic forces might have on capillary pressure and, consequently, relative permeability. He concluded that capillarity has no impact on the relative permeability curves for homogeneous, water-wet porous media, provided that the pressure difference equation is implemented properly. Also, he demonstrated that, if the hydrodynamic effects are neglected, very little error is introduced into the analysis.

2.3. Capillary Pressure

Capillary pressure in porous media is simply defined as the pressure difference existing across the interface separating two immiscible fluids, one of which wets the surfaces of the rock in the presence of the other. The historical development of the capillary pressure phenomenon, and measurement methods and their shortcoming, are described briefly by Craig (1971). In another study, Melrose and Brandner (1974) have discussed the role of capillary forces in determining microscopic displacement efficiency for oil recovery by waterflooding. Many experimental measurement methods have been discussed and well documented by various investigators such as Leverett (1941), Hassler and Brunner (1945), Bruce and Welge (1947), Purcell (1949, 1950), Slobod *et al.* (1951), Brown (1951), Killins *et al.* (1953), Calhoun (1960) and Amyx *et al.* (1960). Therefore, they will not be covered here. For details of the methods discussed by these authors, the reader is referred to the above mentioned references.

Rose and Bruce (1949) proposed "Leverett's capillary pressure function" to correlate capillary pressure data. This function is also well known as the "*J*-function", which correlates the capillary pressure, wettability, pore-size distribution, contact angle, and IFT of the fluid pair involved. Brown (1951) successfully used the *J*-function to correlate capillary pressure data by using a number of core samples. However, Brown (1951) concluded that the usefulness of the *J*-function is limited to a specific lithology within the same formation.

Craig (1971) has mentioned that water-oil capillary pressure data are difficult to measure and thus too rarely are obtained. Commonly, capillary pressure data are measured by using an air-brine system. More frequently than not, the use of air-brine capillary pressure curves to estimate saturations in a water-oil system is misleading, particularly if the reservoir rock is oil-wet rather than

water-wet. The same argument holds for the methods which use the mercury injection technique to determine the capillary pressure curve.

2.4. Interfacial Coupling

Suspected cross effects (earlier mentioned in Section 2.1) between flowing fluids, and other non-Darcian behaviors discussed by Scheidegger (1960) and Bear (1972) during two-phase flow through porous media, were also investigated by Yuster (1951), Scott and Rose (1953), Klute (1967), and Bolt and Groenevelt (1969). These investigators indicated that the cause of non-Darcian behavior during multiphase flow could be due to the presence of a relatively new phenomenon, which in the recent literature is commonly known as 'viscous coupling'. Very few papers have been published in the recent literature (after 1990) on interfacial coupling. Moreover, no strong consensus has appeared with respect to the physical origin of such effects. Bentsen (1999), however, has argued strongly that the actual origin of such cross effects could be the capillarity of a porous medium-fluid system. In the following sections, these two concepts of interfacial coupling in two-phase flow through porous media are further discussed.

2.4.1. Viscous Coupling

Conventionally, in immiscible two-phase (oil and water) flow problems, it is common practice to assume that only one driving force, i.e., the potential gradient acting across each phase, is responsible for fluid flow in porous media. Such an approach neglects the possibility that momentum transfer between the two flowing phases may act also as a driving force. This additional driving force, which may occur at the fluid interfaces, is known as viscous coupling. In other words, as described by Rose (1991a), *"the term 'viscous coupling' connotes the idea that adjacent immiscible fluids flowing side-by-side in a porous medium will exert a reciprocal viscous drag on each other that will significantly affect the ensuing motions of the contiguous fluid"*

particles. This is the predicted consequence of the no-slip boundary condition, which allows the force of momentum to be transferred across the fluid-fluid interfaces”.

Coupled processes such as thermo-electric, electro-osmosis and chemical kinetics are well recognized. Similarly, many researchers (Rose, 1988b, 1989; Bourbiaux and Kalaydjian, 1990; Kalaydjian, 1990; Mannseth, 1991; and Bentsen and Manai, 1993) have suggested a considerable effect from viscous coupling during two-phase flow through porous media. The role of viscous coupling in multiphase flow, however, is controversial, as some of the studies (Zarcone and Lenormand, 1994) suggested either a negligible effect or no effect at all (Philip, 1972). Moreover, many of the text book writers on petroleum engineering such as Collins (1961), Scheidegger (1960), Muskat (1982) and Greenkorn (1983) have ignored the idea of viscous coupling.

For a complete understanding of the viscous coupling phenomenon, and its possible or probable effects on the behavior of multiphase flow through porous media, an extensive review of research conducted by various researchers is helpful. Therefore, in the following sections, it is intended to describe the previous work done related to viscous coupling. Specifically, three theoretical approaches are reviewed; these are:

1. volume averaging methods,
2. principles of irreversible thermodynamics, and
3. use of analogous models to understand the novel formulations for two-phase flow through porous media.

In addition, various modes for further theoretical and experimental development are discussed briefly. In order to understand the basic phenomenon, only the stable, co-linear flow of two immiscible, incompressible fluids through a water-wet isotropic and homogeneous porous medium is considered.

2.4.1.1. Theoretical Developments

Several papers referenced in Bear (1972) indicate that the effect of viscous coupling has been known from the early 1950's. Yuster (1951) was the first person to mention this phenomenon (Yuster's effect). Scott and Rose (1953) tried to explain the Yuster effect by introducing the concept of viscous coupling. Bear (1972) discussed the non-Darcian behavior of fluid-flow at very low hydraulic gradients, which serve as the driving force. Klute (1967) attributes this non-Darcian behavior to electro-osmosis effects, particle movement and quasicrystalline water structure, and so forth. Bolt and Groenevelt (1969), however, held coupling phenomena responsible for the non-Darcian behavior of fluid flow through porous media.

To understand the mechanism of multiphase flow through porous media, several theoretical approaches have been adopted by various investigators. Some of those approaches were:

1. the theory of mixtures (Wang, 1997; Wang and Cheng, 1996; Cheng and Wang, 1996; Wang and Beckermann, 1993; Murdoch and Kowalski, 1992; Bedford and Drumheller, 1983; Bowen, 1982, 1980; Drumheller, 1978),
2. the volume averaging methods (Whitaker, 1986, 1973, 1967; Bachmat and Bear, 1986; Bear and Bachmat, 1986; de la Cruz and Spanos, 1983; Hassanizadeh and Gray, 1980, 1979a, 1979b; Narasimhan, 1980; Gray and Lee, 1977; Gray, 1975; Bear, 1972; Slattery, 1970, 1969),
3. the principles of irreversible thermodynamics (Del Rio and de Harro, 1992; Kalaydjian, 1990, 1987; Kalaydjian and Marle, 1987; Longeron, 1987; Bear, 1972; Katchalsky and Curran, 1967; de Groot, 1951; Onsager, 1931a, 1931b), and
4. the use of analogous models (Rose, 1993 1990a; Bacri *et al.* 1990; Yuster, 1951) is also a common practice among researchers.

It should be noted that Trapp (1976) has presented a one-to-one correspondence between the various parameters of the continuum theory of mixtures and the volume averaging methods.

2.4.1.1.1. Volume Averaging Methods

In an effort to extend Darcy's law for single-phase flow to multiphase flow through porous media, de la Cruz and Spanos (1983) constructed a theoretical version of Darcy's empirical law by using volume averaging theorems (Bachmat and Bear, 1986; Bear and Bachmat, 1986; Hassanizadeh and Gray, 1980, 1979a, 1979b). For a horizontal, one-dimensional, homogeneous, porous medium, the flow equations developed by these investigators are:

$$\mu_1 \left(\frac{1}{K_{11}} \bar{q}_1 - \frac{1}{K_{12}} \bar{q}_2 \right) = -\frac{\Delta p_1}{L} \quad (2.1)$$

and

$$\mu_2 \left(\frac{1}{K_{22}} \bar{q}_2 - \frac{1}{K_{21}} \bar{q}_1 \right) = -\frac{\Delta p_2}{L}, \quad (2.2)$$

where K_{11} and K_{22} are the generalized phase permeabilities for phase 1 and 2, respectively, and where K_{12} and K_{21} are the viscous drag coefficients which represent the viscous drag that exists between phases 1 and 2. Note that the conventional Darcy law approach involves only a single permeability coefficient for each phase due to its neglect of interfacial viscous drag.

Another effort (Whitaker, 1986) involving the use of the volume averaging method to develop the governing equations for two immiscible fluids has resulted in a similar generalized theoretical version of Darcy's law which involves a system of two equations with four unknown parameters. The final outcomes of these two formulations are similar to each other; however, some of the parameters such as q_i and K_{ij} are defined differently in the two approaches. Nevertheless, the main point worth noting is that both of the

theoretical formulations indicate the presence of fluid-fluid drag or viscous coupling phenomena.

2.4.1.1.2. Principles of Irreversible Thermodynamics

Several attempts, using the ideas of irreversible thermodynamics, have been made to achieve a satisfactory explanation of the cross-effect of one fluid on the other in a multiphase flow system. Bear (1972) has provided a summary of Onsager's theory which is the basis of the thermodynamics of irreversible processes. In irreversible processes, by using the methods of continuum mechanics, it is assumed that the relationship between the fluxes and forces is linear. The assumption of linearity between fluxes and forces is common in other types of irreversible processes such as Fourier's law which relates heat flow to thermal gradient; Fick's law for a multicomponent system which relates the flow of each component to its concentration gradient; Ohm's law which relates the flow of electrons to the potential gradient; and Newton's law (for Newtonian fluids) which relates the shearing force to the velocity gradient. In all of these cases, however, the simple relationship of linearity between forces and fluxes does not always exist. The main cause of the overall non-linearity in a multicomponent system is thought to be the non-linear (or linear) coupling between one type of force to another type of flux (Bear, 1972). For further details of Onsager's theory and other concepts of irreversible thermodynamics, such as entropy and entropy production, the reader is referred to Onsager (1931a, 1931b), de Groot (1951) and Katchalsky and Curran (1967).

Unfortunately, a sufficient understanding of non-linear processes in non-equilibrium thermodynamics is not available. Hassanizadeh and Gray (1987), however, were able to develop a non-linear relationship between the pressure gradient and the flow velocity at the macroscopic level by employing the general continuum approach to the description of thermodynamic processes in

porous media. Berge and Bolt (1988) investigated the phenomena of heat flow and liquid flow through porous media, and established a connection between the two classical approaches. More recently, Del Riop and de Harro (1992) used a thermodynamics approach and developed approximate time evolution equations for fluxes in a porous system.

More importantly, an excellent theoretical development was reported by Kalaydjian (1987, 1990), who used the concepts of irreversible thermodynamics to develop a macroscopic understanding of two-phase flow through porous media. The flow equations developed by Kalaydjian (1990) are:

$$q_1 = \frac{k \cdot k_{r1}}{\mu_1} \left(-\frac{\partial P_1}{\partial x} \right) + \frac{k \cdot k_{r2}}{\mu_2} \left(-\frac{\partial P_2}{\partial x} \right) \quad (2.3)$$

and

$$q_2 = \frac{k \cdot k_{r2}}{\mu_1} \left(-\frac{\partial P_1}{\partial x} \right) + \frac{k \cdot k_{r2}}{\mu_2} \left(-\frac{\partial P_2}{\partial x} \right) \quad (2.4)$$

The diagonal terms k_{r1} and k_{r2} are the permeabilities of individual phases and the nondiagonal terms k_{r2} and k_{r1} represent the interfacial viscous coupling between the fluid phases. An experimental method to evaluate these nondiagonal terms has also been reported by the author, Kalaydjian (1990). As far as the cross-effect(s) between various species of two-phase flow through porous media is concerned, these equations are analogous to those developed by de la Cruz and Spanos (1983), and also to those developed by Whitaker (1986).

2.4.1.1.2.1. Applicability of Onsager's Relations

According to Onsager's fundamental theorem (Onsager, 1931a, 1931b), the cross coefficients, which in this case are λ_{12} and λ_{21} , are symmetric, provided that a proper choice of fluxes and forces is made. This principle of equality

between the cross coefficients is the central point of the Onsager's theory of irreversible processes at the microscopic level.

Kalaydjian (1990) tentatively assumed that Onsager's reciprocity relations of irreversible thermodynamics for microscopic systems may also be valid for macroscopic systems. In other words, non-diagonal terms in the equations above are equal to each other. This assumption, though tentatively adopted by Kalaydjian (1990), is questionable to many investigators who argue that the complex nature of the porous medium does not allow for such an assumption. Bentsen (1994c), for example, on the basis of the results presented in Mannseth (1991), showed that the non-diagonal transport coefficients responsible for viscous coupling, λ_{12} and λ_{21} , are not equal because of the non-linear relationship between the fluxes and the forces. More recently, Bentsen (1998b), by using the fractional flow theory, in conjunction with Kalaydjian's transport equations and Liang and Lohrenz's method for generalized mobilities, has constructed new equations for calculating effective mobilities. The author's investigations led to the conclusion of inequality between the cross coefficients, λ_{12} and λ_{21} , which control momentum transfer between fluid phases flowing in porous media; this implies non-applicability of Onsager's theory at the macroscopic level.

There are clearly two schools of thought regarding the applicability of Onsager's relationships to the generalized formulation involving four generalized permeability coefficients developed and advocated by Whitaker (1967, 1986), Slattery (1969, 1970), de la Cruz and Spanos (1983), Rose (1951, 1988a,b, 1990a,b, 1995, 1997), Kalaydjian (1987, 1990) and others. Among those who recently developed their theoretical formulations and consistently argued in favor of the applicability of Onsager's theory to coupled flows in porous media are Rose (1995, 1991a,b, 1990a,b, 1969), Auriault and

Lewandowska (1994), Auriault and Labaigue (1989) and Kalaydjian (1987, 1990). Those who do not favor full and/or partial implementation of Onsager's relations to coupled flow phenomena include Avraam and Payatakes (1995a,b), Bentsen (1994c), Bentsen and Manai (1993) and Goode and Ramakrishnan (1993). Some other studies such as Rakotomalala *et al.* (1995) conditionally recommended the applicability of the above mentioned theory of irreversible thermodynamics to coupling processes. They found that Onsager's relations hold only for unit mobility ratio and that a very small amount of viscous coupling was observed for other mobility ratios. Bentsen and Manai (1993), however, clearly observed unequal nondiagonal permeability coefficients, even for the case of unit mobility ratio, which implies non-applicability of Onsager's relations.

Keeping in view the diversity in opinions regarding the applicability of Onsager's relations to the viscous coupling phenomena, the situation seems to be very complicated. Therefore, it is desirable and logical to validate viscous coupling theory by further experimental research.

2.4.1.1.3. Analogous Models

A number of investigators (Ehrlich, 1993; Rose, 1993, 1990a; Bacri *et al.* 1990; Yuster, 1951) have used simple analogous models to gain insight into how two immiscible phases flow through a porous medium. In the porous media literature, two types of analogous models (tubular flow and Hele-Shaw flow) are frequently used. In these simple models, where possible interaction between the wetting fluid and the rock surface is commonly ignored, it is usual to assume that the boundary separating the wetting phase from the nonwetting phase is, in its entirety, a fluid-fluid interface (Bear, 1972; Chatenever and Calhoun, 1952; Rapoport and Leas, 1951). Neglect, in the simple analogous models, of the rock fluid surfaces in the interfacial boundary gives rise to two problems. First, the simple analogous models overestimate the amount of

momentum transferred across the interfacial boundary separating the two phases. Second, the relative permeabilities take on unrealistic physical values, in certain cases, at limiting values of the viscosity ratio. To overcome these difficulties, Scott and Rose (1953) adopted a more realistic approach by assuming that the wetting phase is separated from the nonwetting phase in part by a solid-phase boundary (of infinitesimal thickness) and in part by a fluid-fluid boundary. The flow equations developed by employing two types of analogous models (tubular flow and Hele-Shaw flow) are given next.

2.4.1.1.3.1. Tubular Flow

The analogous model described here is that used by Yuster (1951) and by Bacri *et al.* (1990). The system analyzed is a simple tube of small diameter with phase 2 (nonwetting) flowing in the central portion of the tube, and phase 1 (wetting) flowing concentrically in the annular space between phase 2 and the wall of the tube. It is supposed that the radius of the interface, R_i , is a function of x , the coordinate of the direction of flow, and that $dR_i(x)/dx \ll 1$. Under these conditions, the velocities in the direction of flow are dependent upon the radial coordinate only, and are defined by:

$$u_i = \frac{1}{4\mu_i} \frac{\partial p_i}{\partial x} r^2 + a_i \ln r + b_i; \quad i = 1, 2 \quad (2.5)$$

The four constants of integration, a_i, b_i , can be determined by applying the four boundary conditions: no slip condition at the wall of the tube [$u_1(R) = 0$]; finite shear stress at the center of the tube, $r = 0$; continuity of velocity at the fluid-fluid interface [$u_1(R_i) = u_2(R_i)$] and continuity of shear stress at the fluid-fluid interface [$\tau_{rx,1}(R_i) = \tau_{rx,2}(R_i)$]. The boundary separating the two fluids is supposed to be in part a fluid-solid surface and in part a fluid-fluid interface. The latter two boundary conditions are assumed to apply only on the fluid-fluid part of the boundary. That is, continuity of velocity and shear stress is not

invoked on the fluid-solid part of the boundary. Rather, boundary conditions appropriate for a fluid-solid surface are utilized. Moreover, the lubrication approximation for film flow is employed so that:

$$\frac{\partial p_1}{\partial r} = \frac{\partial p_2}{\partial r} = 0 \quad (2.6)$$

Finally, the fluxes are assumed to be defined by

$$v_1 = \frac{2}{R^2} \int_{R_i}^R r u_1 dr \quad (2.7)$$

and

$$v_2 = \frac{2}{R^2} \int_0^{R_i} r u_2 dr \quad (2.8)$$

where R is the radius of the tube. By applying the four boundary conditions to Equation (2.5), and by making use of Equations (2.7) and (2.8), it may be shown that

$$v_1 = -\lambda_{11} \frac{\partial p_1}{\partial x} - \lambda_{12} \frac{\partial p_2}{\partial x} \quad (2.9)$$

and

$$v_2 = -\lambda_{21} \frac{\partial p_1}{\partial x} - \lambda_{22} \frac{\partial p_2}{\partial x} \quad (2.10)$$

where, the phenomenological coefficients, λ_{ij} , are generalized conductances or mobilities.

It is to be noted that, Equations (2.9) and (2.10) are the tubular analogues to the transport equations proposed by Kalaydjian (1990, 1987), that is, Equations (2.3) and (2.4). Moreover, it is possible to derive tubular analogues to the transport equations proposed by de la Cruz and Spanos (1983) and Whitaker (1986). In the interest of brevity, however, these results are not reported here.

2.4.1.1.3.2. Hele-Shaw Flow

The analogous model is that employed by Rose (1990a). That is, the system which is analyzed is a Hele-Shaw cell wherein two fluids are flowing, with the less dense fluid located between the interface and the top of the cell, and the more dense fluid located between the interface and the bottom of the cell. Utilizing the same approach as before, it may be shown that:

$$v_1 = -\Lambda_{11} \frac{\partial p_1}{\partial x} - \Lambda_{12} \frac{\partial p_2}{\partial x} \quad (2.11)$$

and

$$v_2 = -\Lambda_{21} \frac{\partial p_1}{\partial x} - \Lambda_{22} \frac{\partial p_2}{\partial x}. \quad (2.12)$$

Equations (2.11) and (2.12) are the Hele-Shaw analogues to the flow equations obtained by utilizing the other theoretical approaches, as described in the preceding sections.

2.4.1.2. A Common Message

Although, for the sake of brevity, the final formulations obtained by utilizing only three theoretical approaches are described in the preceding sections, the other theoretical approach mentioned in Section 2.4.1.1, that is, the continuum theory of mixtures (Wang, 1997; Murdoch and Kowalski, 1992) has arrived also at a more or less similar final formulation. Because of the various definitions of different parameters involved in the theoretical development, however, the appearance of the final formulations obtained by means of the various theories may differ slightly from each other. For example, Wang (1997), using the theory of mixtures, has developed a formulation for immiscible fluids flowing through a porous medium, where he has introduced the concept of 'mixture pressure', just like the concept of 'global pressure' which earlier was introduced by Chavent (1976) and Yortsos (1987) for immiscible displacement in porous media. The other porous media theories,

such as the one adopted by Kalaydjian (1990, 1987), use separate pressure gradients, rather than a mixture pressure or global pressure, for each fluid during multiphase flow through porous media. Note that, Wang (1997), although taking a different approach to investigate the viscous coupling phenomenon, has indicated a considerable effect of viscous coupling on the relative mobility and the cross-interaction mobility terms used in his formulation.

A common message is conveyed by all of the research reviewed above; that is, the interfacial viscous coupling phenomenon in multiphase flow through porous media is an important phenomenon, which must be addressed by more vigorous research efforts. In 1996, Walter Rose (a prominent researcher of the viscous coupling phenomenon), while addressing a seminar held by the Alberta Research Council of Canada, emphasized the need of such vigorous efforts and said, *“if the VC (viscous coupling) model is selected, a correct result will be obtained whether or not VC actually is occurring. On the other hand, if a K_r (relative permeability or conventional) model is selected, a correct result will be obtained only in the case that VC is not present”*. Obviously, a genuine question can be raised; why then, despite all this theoretical evidence, has the viscous coupling phenomenon been unable to achieve its due recognition within the scientific community? One answer to this question is: because it is extremely difficult to validate the theoretical indicators by experimental means! In the following section some of the efforts to validate the theoretical findings are reviewed.

2.4.1.3. Verification of Viscous Coupling

In an applied scientific discipline, such as multiphase flow through porous media, no theoretical claim(s) is acceptable unless and/or until supported by the *physical* evidence. Several investigators have adopted and/or adapted various *physical approaches* to validate the viscous coupling phenomenon.

Three main approaches to validate the newly postulated viscous coupling theory are described below.

2.4.1.3.1. Laboratory Experiments

Various theoretical approaches as described above have resulted in a set of large-scale flow equations for two immiscible phases in a porous medium with four generalized permeability coefficients. Spanos *et al.* (1986) further extended the formulations by re-interpreting the parameters of the Buckley-Leverett (1942) theory. They were able to incorporate the four generalized permeability coefficients into the Buckley-Leverett conventional formulation. In another similar study, Rose (1988b) has shown that the Buckley-Leverett equation can be modified and applied to linear displacement processes involving viscous coupling.

Having pointed-out that a generalized theory [Equations (2.3) and (2.4)] is available, and that Buckley-Leverett theory may be modified to include the effects of viscous coupling, attention is now focused on experimental procedures to measure the four newly developed generalized permeability coefficients. These are the coefficients which are needed to validate the new generalized theory of immiscible displacement.

To obtain the values of the generalized permeability coefficients, various experimental schemes have been reported in the literature. At least two types of experiments are needed to quantify the matrix of four generalized transport coefficients (Rose, 1988a). Rose (1988a) suggested conducting two types of experiments, namely, horizontal flow and vertical flow experiments to obtain the required parameters. However, in this scheme two major difficulties are involved which are associated with measuring the gravitational effect, and the difference in the vertical and horizontal velocities. In their experimental research, Manai (1991) and Bentsen and Manai (1993, 1991) presented a

scheme involving cocurrent flow and countercurrent flow to overcome the difficulties associated with Rose's approach which used horizontal and vertical flows (Rose, 1988a). Goode (1991) suggested indirect measurement methods involving two types of experiments. Liang and Lorenz (1994) and Liang (1993) proposed a combination of steady-state and unsteady-state experiments, once again, overcoming the above mentioned difficulties of Rose's method.

Recently, Dullien and Dong (1996) presented an experimental approach to determine the four generalized permeability coefficients by setting the pressure gradient in one of the two flowing fluids equal to zero. The values of the cross coefficients with respect to the effective permeability to water and oil were found to be significant. Their approach of using one flowing fluid, while keeping the other stationary, is a limiting case of two-phase flow phenomena; that is, it does not represent the overall mechanism of two-phase flow through a porous system. Moreover, they were unable to determine the net contribution of viscous coupling to the water or oil flow, when the respective pressure gradient across the water or oil phase was set equal to zero.

2.4.1.3.2. Conventional Numerical Methods

Commonly, the laboratory experimental approach is considered as the best option to validate any novel theoretical formulation. Perhaps, this is the reason that conventional numerical approaches (finite-difference methods and finite-element methods) are very scarce in the literature related to the validation of the viscous coupling theory. By using a finite-difference algorithm based on a Lagrangian modeling of two-phase porous media flow, Rose (1990c), presented some results such as the importance of including the effects of viscous coupling, capillarity and gravity into the conventional numerical algorithm.

For an idealized porous medium, Goode (1991) developed a percolation algorithm by using a finite-difference scheme to demonstrate the momentum transfer during two-phase porous media flow. In another study, Goode and Ramakrishnan (1993) used a network model to simulate the invasion of nonwetting phase using their percolation-like algorithm. In this study, however, by making use of triangular grids, a finite-element scheme rather than a finite-difference scheme was employed. They observed a significant effect of the off-diagonal terms on the behavior of fluid flow. Moreover, the cross coefficients were found to be a strong function of saturation and viscosity ratio.

Investigative studies to validate the viscous coupling theory by utilizing conventional numerical methods are extremely limited. Therefore, based on the few available articles, it is very difficult to conclude something definite.

2.4.1.3.3. Lattice Gas Automata

Lattice gas automata, a branch of cellular automata, is a relatively new method for computational fluid dynamics and is essentially a discrete model in time and space, where on a regular lattice, particles of identical mass move from one site to another with a unit speed. Upon collision at a site or vertex, the particles conserve their mass and momentum according to pre-specified simple mathematical rules. Remarkably, at an extended level, this simplicity is able to handle extremely complex systems, such as porous media flow, at a macroscopic scale. For further details and relevant studies the reader is referred to Wolfram (1986a, 1986b); Rothman (1988, 1990); Rothman and Keller (1988); Kadanoff *et al.* (1989); Monaco (1989); Zanetti (1989); Doolen *et al.* (1990); Gutman (1990); Gao and Sharma (1994a, 1994b); Ferreol and Rothman (1995); van Genabeek and Rothman (1996); and Olson and Rothman (1997).

Frisch *et al.* (1986) suggested a lattice gas automata technique for incompressible Navier-Stokes equations and its behavior at a macroscopic scale. Later, this work was extended by other investigators such as Kadanoff *et al.* (1989) and Zanetti (1989). Rothman and Keller (1988), and Rothman (1990) showed that this can be used to simulate two-phase flow through a porous medium at the macroscopic scale. Rothman (1990) conducted a numerical simulation study to validate the macroscopic laws [earlier developed by Kalaydjian (1987, 1990) and others] for immiscible two-phase flow in porous media. Under conditions of negligible capillarity, the macroscopic laws were validated, and a linear relationship between forces and fluxes, at a sufficiently high level of forcing, was observed. Moreover, Onsager's relations were found to be valid only in the above-mentioned linear regime. At high flow rates, however, where inertial effects become significant (i.e., Reynolds number $\gg 1$), the symmetry in Onsager's reciprocal relations was unobservable.

In a recent study, Olson and Rothman (1997) attempted to compute both coupling coefficients κ_{wn} and κ_{nw} (same as K_{12} and K_{21} , respectively) in a complex digitized rock geometry which was determined by X-ray microtomography (Auzerais *et al.* 1996; Kinney *et al.* 1993). The coupling coefficients were computed independently and found to be equal, thus maintaining the reciprocity of Onsager's relations; however, the authors found that, while Onsager's relationship appeared to hold for equilibrium flows, it did not hold for non-equilibrium flows because such flows are outside the domain of applicability of the Onsager theory. Moreover, the author's claim that every previous experimental determination of viscous coupling was conducted by utilizing an artificial porous medium is not, strictly speaking, true. For example, Bentsen (1992a, 1992b), Bentsen and Manai (1993, 1991), and Manai (1991) used unconsolidated cores (Ottawa sand), which are likely to be a better representation of a porous medium than most other types of porous

medium (with the possible exception of actual reservoir cores) used in other experimental, simulation or lattice gas automata technique(s).

Although lattice gas automata and conventional numerical simulation methods for validation of the theoretical hypothesis provide certain limited advantages over laboratory experiments (Rothman, 1990; Olson and Rothman, 1997), the requirements of advanced computational techniques and the use of fictitious particles to represent the fluids make these approaches more difficult to adopt on a routine basis.

2.4.1.4. Quantitative Impact of Ignorance

From the discussions in the preceding sections, a major observation is that most of the available literature on the subject at hand is either in full or partial support of the existence of viscous coupling phenomenon during two-phase flow through porous media. Some of the experts, however, argued rightly or wrongly, that the transfer of momentum is small; hence, it can be ignored. Some investigators, such as Philip (1972), have rejected the idea of viscous coupling completely. The main issue, however, seems to be the question: how much?

Kalaydjian (1990) described an experimental approach to quantify the effect of viscous coupling on both microscopic and macroscopic levels in a square cross-section capillary tube and in porous media, respectively. His investigation showed non-negligible viscous coupling terms in the matrix of generalized permeability coefficients, even at the macroscopic level.

In a similar effort, Rose (1991b) compared two models: one which included viscous coupling, the "C-model", and one which did not, the "D-model". Equality of the reciprocal coupling coefficients ($K_{12} \equiv K_{21}$) was assumed. He showed that, when conventional methods (viscous coupling not included) were

used to determine the effective mobilities, a significant amount of error was incurred. As discussed in the preceding sections, however, the assumption of equality of the reciprocal coupling coefficient is controversial. In a previous study, to demonstrate the effect of ignorance of viscous coupling, Rose (1990c) presented a Lagrangian algorithm for the simulation of coupled two-phase flow in porous sediments. He observed a considerable effect of viscous coupling by predicting various positions of the flood-front against different saturations for two cases where coupling was and was not involved.

Moreover, Bentsen (1998b) explored the impact of neglecting viscous coupling between fluid phases on the effective mobility curves. He demonstrated that the effective mobility curves that include the effect of viscous coupling between fluid phases differ significantly from those that exclude such coupling. Moreover, he showed that the conventional effective mobilities that pertain to steady-state, cocurrent flow, steady-state, countercurrent flow and pure countercurrent imbibition differ significantly. Thus, it appears that traditional effective mobilities are not true parameters; rather, they are infinitely nonunique.

Recently, Bentsen (1997) attempted to quantify the effect(s) of neglecting viscous coupling by estimating the relative error incurred when this effect(s) is neglected. By investigating several one-dimensional problems, he concluded, that relative errors of about 40 percent are introduced into the analysis when viscous coupling across fluid-fluid interfaces is neglected. This is important in pure countercurrent imbibition problems, vertical flow problems and when using quasi-analytical methods for estimating relative permeability.

In another recent investigation, as mentioned in the Section 2.2.1, Bentsen (1998a), in addition to suggesting the non-applicability of Onsager's relation to two-phase flow problems for the sand-fluid system used in the study, also

shows that the neglect of viscous coupling between the two flowing phases can result in the introduction of relative error as large as 30 percent into the calculated values of the effective mobilities.

Obviously, the work done to quantify the effect of viscous coupling and the ultimate consequences of its ignorance is relatively limited. In certain cases, however, as shown by Bentsen (1997, 1998a,b), an error of about 30 to 40 percent is significant and cannot be overlooked for one reason or another. At least these findings should be enough to alert the scientific community involved in the study of multiphase flow through porous media. Particularly, the oil industry, where reservoir simulation is commonly used to represent the behavior of multiphase flow, must take extra precautions by introducing the newly suggested modifications in the conventional Darcian approach.

2.4.2. Capillary Coupling

Recently, contradicting his previous observations about the source of interfacial coupling during two-phase flow through porous media, Bentsen (1999) has introduced a partitioning concept into Kalaydjian's transport equations to construct modified transport equations that enable a better understanding of the role of interfacial coupling in two-phase flow through natural porous media. Using the new modified transport equations, the author demonstrated that, in natural porous media, the physical origin of interfacial coupling is the capillarity of the porous medium, and not interfacial momentum transfer, as is usually assumed. However, on the basis of recent results presented in the literature (Zarcone and Lenormond, 1994; Rakotomalala *et al.* 1995), the author has not precluded the possibility that some negligibly small viscous coupling may also take place. Further details of this new theoretical development are given in Chapter 4.

2.5. Fluid Distribution and Measurement

Fluid distribution refers to the relative location of two or more phases in the pore space of a reservoir. The fluid distribution of immiscible phases in reservoir rock is an important parameter that has a direct effect on the flow rates of each phase and the oil recovery efficiency (Willhite, 1986). Amyx *et al.* (1960) have indicated that the distribution of the liquid in a porous system is dependent upon the wetting characteristics of the rock. Moreover, Craig (1971) has mentioned that liquid distribution does not depend upon the wetting or nonwetting phase saturation; rather, it depends upon the direction of the saturation change.

Usually, direct quantitative measurement of the fluid distribution is not feasible; however, fluid saturation, the volume fraction of a pore occupied by a phase, can be measured directly. There are several indirect methods of inference drawn from the results of laboratory flow tests and other techniques.

Chatenever and Calhoun (1952) conducted microscopic studies of dynamic fluid behavior in synthetic porous matrices. The simultaneous flow of oil and water through a transparent model was observed and photographed, and the results appeared as a motion picture that received wide distribution and acclaim. Kimbler and Caudle (1957) also used a photographic technique to study fluid distribution in a transparent model similar to that used by Chatenever and Calhoun (1952). Swanson (1979) suggested a method in which the nearest approximation to a direct measurement of the fluid distribution combines SEM (scanning electron microscope) with replicas of the fluid phase at specified saturations. This technique provides valuable insight into the fluid distributions under strong wetting conditions. The author also has described a way of getting information about the fluid distribution in a porous medium by interpreting capillary pressure data. Yadav *et al.* (1987) have developed a novel technique to study the distribution of wetting and

nonwetting phases in reservoir rocks during immiscible displacement. The technique uses a method of fluid solidification (wetting, nonwetting, or both) in conjunction with photomicrography to obtain the fluid distribution in porous media. However, the estimation of relative permeability of a fluid, while the other fluid is solidified, is questionable because the nature of the interaction between the fluids is entirely different than the interaction between a fluid and a solid. Moreover, the technique is very time consuming.

Some early investigators, such as Bail and Marsden (1957), have suggested the use of electrical resistivity measurements across the core to measure the saturation distribution. Geffen and Gladfelter (1952) and Laird and Putman (1951, 1959) have used X-rays in their studies. Recently, Kantzas (1990) has summarized various potential methods to determine the non-destructive, in-situ fluid distribution such as radioactive tracer measurements, microwave attenuation techniques, nuclear magnetic resonance imager (NMRI) techniques, ultrasound mapping and computer assisted tomography (CAT) techniques. This author has presented a comprehensive review of industrial applications of CAT techniques with greater emphasis on CAT applications in the oil industry. This technique, though becoming popular now-a-days, can be considered as hazardous because it involves the measurement of X-rays that are transmitted through the core. Islam (1985) reported that the X-ray absorption method for generating saturation profiles is not single-valued and involves some hysteresis effects. Moreover, very high costs are involved, not only for purchasing the equipment, but also for its regular maintenance.

In an elegant piece of experimental research, Parsons (1975) used the selective absorption of electromagnetic radiation to measure fluid saturation. This technique is considered to be relatively better because it overcomes the difficulties that the other techniques suffer from. The microwave attenuation method of saturation measurement does not require the addition of a foreign

material, and the continuous fluid saturation profiles generated by this method are of better quality, Manai (1991).

CHAPTER 3

STATEMENT OF THE PROBLEM

Relative permeability data, as stated in the previous chapter, are of great importance to reservoir engineering studies. Such data are fundamental for all reservoir simulators dealing with two-phase fluid flow problems. However, there exist several factors that may affect the shape of relative permeability curves. Some of those factors have been reviewed in the previous chapter.

A general observation can be made from the discussion in the preceding chapter. That is, despite various vigorous efforts which have been made to understand the mechanisms of interfacial coupling, which take place during immiscible displacement processes, there is still much to learn about interfacial coupling phenomena. Therefore, a comprehensive understanding of direct and/or indirect influence(s) of interfacial coupling on immiscible displacement processes is the prime objective of this study.

Another major observation is that most of the available literature on the subject at hand is either in full or partial support of the existence of interfacial coupling phenomena during two-phase flow through porous media. Some of the experts, however, argued rightly or wrongly, that the interfacial coupling is small; hence, it can be ignored. Some investigators, such as Philip (1972), have rejected the idea of interfacial coupling completely. The main issue, however, as noted in the previous chapter, seems to be the question; how much?

Obviously, the work done to quantify the effect of interfacial coupling and the ultimate consequences of its ignorance is relatively limited. In certain cases, however, as shown by Bentsen (1997, 1998a,b), an error of about 30 to 40 percent is significant and cannot be overlooked for one reason or another. Because of these results during some specific cases of two-phase flow through porous media studies, it seems imperative to gain in-depth understanding of interfacial coupling phenomena. The knowledge gained during and after the course of this study may help the oil industry in improving reservoir simulation techniques by introducing the newly suggested modifications in the conventional Darcian approach for two-phase flow through porous media.

Moreover, it is strongly desirable to develop experimental techniques to collect accurate quantitative data to test the newly evolved theoretical formulation involving a partitioning coefficient that controls the amount of capillary coupling during two-phase flow through porous media. More specifically, the main objectives of this study are listed below.

3.1. Objectives

1. To gain further understanding of interfacial coupling phenomena.
2. To ensure the functional capabilities of the existing experimental set-up by introducing the necessary modifications in the system. Particularly, a new saturation measurement device and a data acquisition and instrument control system will be developed.
3. To develop simplified technique(s) to quantify the interfacial coupling effect.
4. To examine the effect(s) of various mobility ratios experimentally.
5. To examine the effect(s) of grain size distribution experimentally.

CHAPTER 4*

THEORY

4.1. Introduction

On the basis of experimental results presented in the literature (Lelièvre, 1966; Bourbiaux and Kalaydjian, 1990; Bentsen and Manai, 1991, 1993), it appears that mobilities determined in a countercurrent flow experiment are less than those determined, for the same sand-fluid system, in a cocurrent flow experiment. Such a result can not be explained, if one assumes that the conventional transport equations (Muskat, 1982) describe correctly two-phase flow through porous media. That is, one must resort to more sophisticated transport equations, such as those constructed by Kalaydjian (1987), or others (de la Cruz and Spanos, 1983; Whitaker, 1986) to explain such a result.

In Muskat's transport equations (Muskat, 1982), the flux is taken to be proportional to one driving force, the pressure gradient acting across the phase. On the other hand, in the more sophisticated transport equations, Muskat's equation for a given phase is modified to include a cross, or coupling, term that is proportional to the pressure gradient of the other phase. The need for such a modification is argued usually on the basis of symmetry, or results arising out of irreversible thermodynamics (Katchalsky and Curran, 1967). Moreover, it is postulated usually that the coupling effect arises from the interfacial contact between the wetting and non wetting fluids.

* A version of this chapter has been accepted for publication. Bentsen, R.G. 1999. *Transport in Porous Media*.

In constructing the more sophisticated transport equations, it is usual to start at the microscopic scale with the Navier Stokes equation, and then use volume averaging, or some equivalent technique, to construct equations that pertain at the macroscopic scale. When the volume averaging approach is used, the mobilities that appear in the transport equations are defined in terms of surface integrals. Because of the complicated nature of the pore space in natural porous media, it is necessary to determine these integrals experimentally. As a consequence, one must be aware that the information lost in passing from the microscopic to the macroscopic scale may not be recaptured easily in the experiment used to determine the mobilities.

Thus, when conducting experiments to determine mobility, it is important to keep in mind two realities. First, the definition for mobility is an operational definition. That is, mobility is defined by the equation in which it appears. If the form and/or underlying physics of the defining equation are inappropriate, model error will be introduced into the experimentally determined mobilities. Second, in the transport equations, the mobilities and pressure gradients appear as a product. This can make it difficult to discern whether a particular interfacial coupling effect should be associated with the mobility, or whether it should be associated with the pressure gradient. Hence, if care is not taken when determining mobilities experimentally, interfacial effects, that should be associated more properly with the appropriate pressure gradient, may be incorporated into the definition of mobility. Again, model error may be incorporated into the experimentally determined mobilities.

Whether a particular interfacial effect should be associated with the mobility, or the pressure gradient, depends upon the source of the interfacial coupling. If the effect is due to interfacial momentum transfer, it should be associated with the mobility. If, however, the effect is due to the capillarity of the porous medium, it should be associated with the appropriate pressure gradient.

In the following analysis a partitioning concept is introduced into Kalaydjian's (Kalaydjian, 1987) transport equations to construct modified transport equations that enable a better understanding of interfacial coupling in two-phase flow through natural porous media. It is shown that, in natural porous media, interfacial coupling arises not because of interfacial momentum transfer, as is usually assumed, but rather because of the capillarity of the porous medium. These analyses are confined to the stable, collinear, horizontal flow of two immiscible, incompressible fluids through a water-wet, isotopic and homogeneous porous medium where phase 1 is the wetting phase and phase 2 is the nonwetting phase. Note that, the theory presented in the following sections (Section 4.2 to 4.4) closely follows the one earlier developed by Bentsen (1999).

4.2. Basic Equations

Kalaydjian (1987) has shown that, consistent with the assumptions made above, the transport equations for the flow of two continuous phases may be written as:

$$v_1 = -\lambda_{11} \frac{\partial p_1}{\partial x} - \lambda_{12} \frac{\partial p_2}{\partial x} \quad (4.1)$$

and

$$v_2 = -\lambda_{21} \frac{\partial p_1}{\partial x} - \lambda_{22} \frac{\partial p_2}{\partial x} \quad (4.2)$$

where $\lambda_{ij} = k_{ij} / \mu_i$; $i, j = 1, 2$. Bentsen (1992a, 1994a, 1997, 1998a) has established, for all types of one-dimensional flow, that:

$$\frac{\partial P_c}{\partial x} = R_{12} \frac{\partial p_2}{\partial x} - \frac{\partial p_1}{\partial x} \quad (4.3)$$

where R_{12} is a weak function of normalized saturation that is introduced to account for the fact that, for horizontal, steady-state cocurrent (SSCO) flow, the pressure profile for the wetting phase is not parallel to that for the

nonwetting phase (Bentsen and Manai, 1991, 1993). Introducing Equation (4.3) into Equations (4.1) and (4.2) yields:

$$v_1 = - \left(\lambda_{11} + \frac{\lambda_{12}}{R_{12}} \right) \frac{\partial p_1}{\partial x} - \frac{\lambda_{12}}{R_{12}} \frac{\partial P_c}{\partial x} \quad (4.4)$$

and

$$v_2 = - (\lambda_{22} + R_{12} \lambda_{21}) \frac{\partial p_2}{\partial x} + \lambda_{21} \frac{\partial P_c}{\partial x} \quad (4.5)$$

Moreover, the conventional transport equations, again consistent with the assumptions made above, may be written as:

$$v_1 = - \lambda_1 \frac{\partial p_1}{\partial x} \quad (4.6)$$

and

$$v_2 = - \lambda_2 \frac{\partial p_2}{\partial x} \quad (4.7)$$

where $\lambda_i = k_i / \mu_i$; $i = 1, 2$.

4.3. Determination of Partition Coefficients

Based on the experimental results presented by Bentsen and Manai (1991, 1993), it can be inferred that (Bentsen, 1998b):

$$\lambda_{ij} = \alpha_{ij} \lambda_i^\circ ; i, j = 1, 2 \quad (4.8)$$

where α_{ij} are generalized partition coefficients for phase i ; $i, j = 1, 2$, and where λ_i° , $i=1, 2$, are mobilities determined in a SSCO experiment. Upon introducing Equation (4.8) into Equations (4.4) and (4.5), one obtains:

$$v_1 = - \lambda_1^\circ \left[\left(\alpha_{11} + \frac{\alpha_{12}}{R_{12}} \right) \frac{\partial p_1}{\partial x} + \frac{\alpha_{12}}{R_{12}} \frac{\partial P_c}{\partial x} \right] \quad (4.9)$$

and

$$v_2 = - \lambda_2^\circ \left[(\alpha_{22} + R_{12} \alpha_{21}) \frac{\partial p_2}{\partial x} - \alpha_{21} \frac{\partial P_c}{\partial x} \right] \quad (4.10)$$

Thus, given the validity of Equation (4.9), it appears that the total pressure force per unit volume available to act on a volume element of phase 1, $\partial p_1/\partial x$, may be partitioned into two components: a phase component, $\alpha_{11} \partial p_1/\partial x$, and a coupling (or capillary) component, $\alpha_{12}/R_{12} \cdot \partial p_1/\partial x$, which arises because of the introduction of the capillary pressure equation [Equation (4.3)] into Equation (4.1). Because the pressure forces per unit volume, $\partial p_1/\partial x$ and $\partial p_2/\partial x$, act in the same direction, the phase and coupling components of the total pressure force per unit volume also act in the same direction. Similar comments can be made with respect to Equation (4.10), the equation that determines the flux of phase 2. Moreover, the partition coefficients, α_{ij} , may be viewed as being the fraction of the pressure force per unit volume of phase j that is available to act on a volume element of phase i ; $i, j=1,2$.

Under conditions of steady-state flow, the capillary pressure gradient, $\partial P_c/\partial x$, is identically equal to zero. Moreover, the flux of a given phase may be defined by either Kalaydjian's (1987) transport equations or by the conventional transport equations. Thus for SSCO, Equations (4.6) and (4.7) may be combined with Equations (4.9) and (4.10) to obtain:

$$\alpha_{11} + \frac{\alpha_{12}}{R_{12}} = 1 \quad (4.11)$$

and

$$\alpha_{22} + R_{12}\alpha_{21} = 1 \quad (4.12)$$

In countercurrent flow, the pressure gradients for the two flowing phases act in opposite directions. Consequently, for countercurrent flow, the function R_{12} must be the negative of that which pertains for cocurrent flow (Bentsen, 1992a). Thus, for countercurrent flow, Equations (4.9) and (4.10) become:

$$v_1 = -\lambda_1^* \left[\left(\alpha_{11} - \frac{\alpha_{12}}{R_{12}} \right) \frac{\partial p_1}{\partial x} - \frac{\alpha_{12}}{R_{12}} \frac{\partial P_c}{\partial x} \right] \quad (4.13)$$

and

$$v_2 = -\lambda_2^* \left[(\alpha_{22} - R_{12}\alpha_{21}) \frac{\partial p_2}{\partial x} - \alpha_{21} \frac{\partial P_c}{\partial x} \right] \quad (4.14)$$

Note that, because the pressure forces per unit volume, $\partial p_1/\partial x$ and $\partial p_2/\partial x$, act in opposite directions, the phase and coupling (or capillary) components of the total pressure force per unit volume, $\partial p_1/\partial x$, must also act in opposite directions. Moreover, as shown below, the phase and coupling components can sum algebraically to only a fraction of the total pressure force per unit volume, $\partial p_1/\partial x$. Similar comments can be made with respect to Equation (4.14), the defining equation for the phase 2 flux.

Based on the experimental results presented by Bentsen and Manai (1991, 1993), it can be inferred that (Bentsen, 1998b):

$$\lambda_i^* = \alpha_i \lambda_i^* \quad ; i = 1, 2 \quad (4.15)$$

where the $\lambda_i^*, i = 1, 2$, are the mobilities measured in a steady-state, countercurrent (SSCT) flow experiment, and where the $\alpha_i, i = 1, 2$, are parameters that control the amount of capillary coupling that can take place. By combining Equations (4.6) and (4.7) with Equations (4.13) and (4.14), and by introducing Equation (4.15) into the resulting equations, it may be shown that, for SSCT flow:

$$\alpha_{11} - \frac{\alpha_{12}}{R_{12}} = \alpha_1 \quad (4.16)$$

and

$$\alpha_{22} - R_{12}\alpha_{21} = \alpha_2 \quad (4.17)$$

To ensure that the capillary pressure gradient for SSCT flow is consistent with that for SSCO flow, one more condition must be imposed. Because, for SSCT flow, the pressure gradients for the two flowing phases are opposite in sign, Equation (4.3) becomes, for SSCT flow:

$$-\frac{\partial P_c}{\partial x} = R_{12} \frac{\partial p_2}{\partial x} + \frac{\partial p_1}{\partial x} \quad (4.18)$$

Introducing Equation (4.8) into Equations (4.1) and (4.2), and setting the resulting equations equal to Equations (4.6) and (4.7), respectively, yields:

$$\alpha_{11} \frac{\partial p_1}{\partial x} + \alpha_{12} \frac{\partial p_2}{\partial x} = \frac{\partial p_1}{\partial x} \quad (4.19)$$

and

$$\alpha_{21} \frac{\partial p_1}{\partial x} + \alpha_{22} \frac{\partial p_2}{\partial x} = \frac{\partial p_2}{\partial x} \quad (4.20)$$

Multiplying Equation (4.20) through by R_{12} , adding the resulting equation to Equation (4.19), and collecting like terms, one obtains, for the negative of the countercurrent capillary gradient:

$$R_{12} \frac{\partial p_2}{\partial x} + \frac{\partial p_1}{\partial x} = (\alpha_{12} + R_{12}\alpha_{22}) \frac{\partial p_2}{\partial x} + (\alpha_{11} + R_{12}\alpha_{21}) \frac{\partial p_1}{\partial x} \quad (4.21)$$

Equating the coefficients of like terms:

$$\alpha_{11} + R_{12}\alpha_{21} = 1 \quad (4.22)$$

and

$$\alpha_{12} + R_{12}\alpha_{22} = R_{12} \quad (4.23)$$

Note that only one of the Equations (4.22) and (4.23) is needed; that is, use of either of these two equations leads to the same result.

Equations (4.11), (4.12), (4.16), (4.17) and either Equation (4.22) or (4.23) comprise a set of five equations involving six unknowns: α_{11} , α_{12} , α_{21} , α_{22} , α_1 and α_2 . This system of equations may be solved for five of the unknowns in terms of the sixth unknown to obtain:

$$\alpha_{11} = \alpha_{22} = \frac{1+\alpha}{2} \quad (4.24)$$

$$\alpha_{12} = \frac{R_{12}(1-\alpha)}{2} \quad (4.25)$$

and

$$\alpha_{21} = \frac{1-\alpha}{2R_{12}} \quad (4.26)$$

where

$$\alpha_1 = \alpha_2 = \alpha \quad (4.27)$$

The parameter α controls the amount of capillary coupling that can take place. Mathematically, α can range between 0 and 1. For physical reasons [see Equation (4.15)], it seems unlikely that α would ever take on a value of zero. However, by setting $\alpha=0$, an upper limit can be placed on the amount of capillary coupling that can take place. Thus, if $\alpha=0$, $\alpha_{12} = 0.5R_{12}$ while $\alpha_{21} = 0.5/R_{12}$. That is, when $\alpha=0$, the phase and coupling components of the force per unit volume of a given phase have the same magnitude. Consequently, for SSCT flow, the pressure gradient for a given phase [see Equation (4.13) or (4.14)] is eliminated, leaving only the capillary pressure gradient as a driving force, an unlikely scenario. If $\alpha=1$, $\alpha_{12} = \alpha_{21} = 0$; that is, no capillary coupling can take place. Note that, because $\alpha_1 = \alpha_2 = \alpha$, only three sets of experiments are needed to determine the α_{ij} : two sets of SSCO flow experiments, one for each phase, to determine R_{12} ; and one set of SSCT flow experiment to determine α . Finally, it should be noted that, even though it is suggested herein that the physical origin of the coupling is different, Equations (4.24) to (4.27) are consistent with recently presented results for viscous coupling (Bentsen, 1998b; Babchin *et al.*, 1998).

4.4. One-Dimensional Transport Equations

The introduction of Equations (4.24), (4.25) and (4.26) into Equations (4.9) and (4.10) leads, for one-dimensional, cocurrent flow, to:

$$v_1 = -\lambda_1^o \left(\frac{\partial p_1}{\partial x} + \frac{1-\alpha}{2} \frac{\partial P_c}{\partial x} \right) \quad (4.28)$$

and

$$v_2 = -\lambda_2^o \left(\frac{\partial p_2}{\partial x} - \frac{1-\alpha}{2R_{12}} \frac{\partial P_c}{\partial x} \right) \quad (4.29)$$

Note that, if $\alpha=1$, and/or if $\partial P_c/\partial x = 0$, the conventional transport equations for one dimensional, cocurrent, two-phase flow are obtained, as should be the case. Note also that $\partial P_c/\partial x$ and $\partial p_i/\partial x$, $i=1,2$, are opposite in sign. Consequently, the unsteady-state, cocurrent (USCO) fluxes, v_1 and v_2 , are less than or greater than, respectively, the SSCO fluxes, v_1^o and v_2^o . Moreover, in view of Equation (4.28) and (4.29), it appears that the $\partial P_c/\partial x$ term is the mechanism by which the wetting-phase saturation front steepens in an unstabilized displacement.

The introduction of Equations (4.24), (4.25) and (4.26) into Equations (4.13) and (4.14) yields, for one-dimensional, countercurrent flow:

$$v_1 = -\lambda_1^o \left(\alpha \frac{\partial p_1}{\partial x} - \frac{1-\alpha}{2} \frac{\partial P_c}{\partial x} \right) \quad (4.30)$$

and

$$v_2 = -\lambda_2^o \left(\alpha \frac{\partial p_2}{\partial x} - \frac{1-\alpha}{2R_{12}} \frac{\partial P_c}{\partial x} \right) \quad (4.31)$$

Again note that if $\alpha=1$ and/or $\partial P_c/\partial x = 0$, conventional equations for one-dimensional, two-phase flow are obtained. Note also that because, in countercurrent flow, the phase 1 and phase two gradients act in opposite directions, only a fraction (α) of the total pressure force per unit volume of a

given phase is available to act on a volume element of that phase. Moreover, in view of Equations (4.30) and (4.31), it appears that the same mobility may be used for both cocurrent and countercurrent flow. Note that Equations (4.30) and (4.31) have not been used in this study; rather, these are given here only for the sake of completeness.

4.4.1. Generalized Mobilities

In several earlier papers (Bentsen, 1997, 1998a, 1998b), it has been suggested that, in order to describe completely the flow characteristics of a porous medium, four generalized mobilities are required. In view of Equations (4.28) and (4.29), it appears that such is not the case. That is, only the two conventional mobilities, λ_1° and λ_2° , are required, provided a proper partitioning of the driving forces has been undertaken. Moreover, in the light of Equations (4.30) and (4.31), it seems that the mobility of a given phase for countercurrent flow is the same as that for cocurrent flow, if the driving forces have been partitioned properly. Thus, there is no need to suppose that the countercurrent mobility for a given phase is less than that for cocurrent flow, as has been done in the past (Bentsen, 1997, 1998a, 1998b). In the earlier experimental studies (Bentsen and Manai, 1991, 1993), different mobilities for cocurrent and countercurrent flow were determined because of the operational nature of the definition for mobility. That is, without a proper partitioning of the driving forces, the parameter α is incorporated as a part of the definition for mobility, whereas, in view of Equations (4.30) and (4.31), it is more properly associated with the driving force (pressure gradient) for a given phase.

4.5. Capillary Coupling Parameter

If one is to understand the role of interfacial coupling in two-phase flow it is essential to come to a better understanding of the physics underlying the capillary coupling parameter, α . The source of such coupling is usually taken to be the interfacial contact between the wetting and nonwetting fluids flowing

through the porous medium. Some insight into the nature of such interfacial coupling can be gained provided the channel-flow theory (Rapoport and Leas, 1953; Chatenever and Calhoun, 1952) is accepted. In channel-flow theory, it is postulated that each fluid flows through a different set of channels, and that the channels are bounded in part by fluid-solid surfaces and in part by fluid-fluid interfaces.

Let us consider first the steady-state flow of wetting fluid (phase 1) in a specific channel. In order to estimate an average pressure for the wetting phase within this channel, it is convenient to introduce the concept of a representative macroscopic surface (RMS). An RMS is supposed to be larger than a representative elementary surface (RES), but smaller than the dimensions of a channel wall, so that macroscopic pressures may be used in the analysis that follows. It is supposed that such an RMS is located in the channel in such a way that the RMS is parallel to the direction of flow, and that the RMS is comprised in part by fluid-solid surface and in part by fluid-fluid interface. Moreover, it is supposed that the fluid-fluid portion of the RMS is comprised in part by phase 1-phase 1 interface and in part by phase 1-phase 2 interface. A highly idealized schematic of such an RMS, located in a channel flowing wetting fluid, is depicted in Figure 4.1. Note that, for reasons of clarity, Figure 4.1 is not drawn to scale.

To estimate the average pressure for phase 1, it is supposed that

$$F_{1s} = A_b(1-\phi)p_1 \quad (4.32)$$

$$F_{11} = A_b\phi a_{11}p_1 \quad (4.33)$$

and

$$F_{12} = A_b\phi a_{12}p_1 \quad (4.34)$$

where F_{1s} is the force acting on the fluid 1-solid part of the RMS, and where F_{11} and F_{12} are the forces acting on the phase 1-phase 1 and phase 1-phase

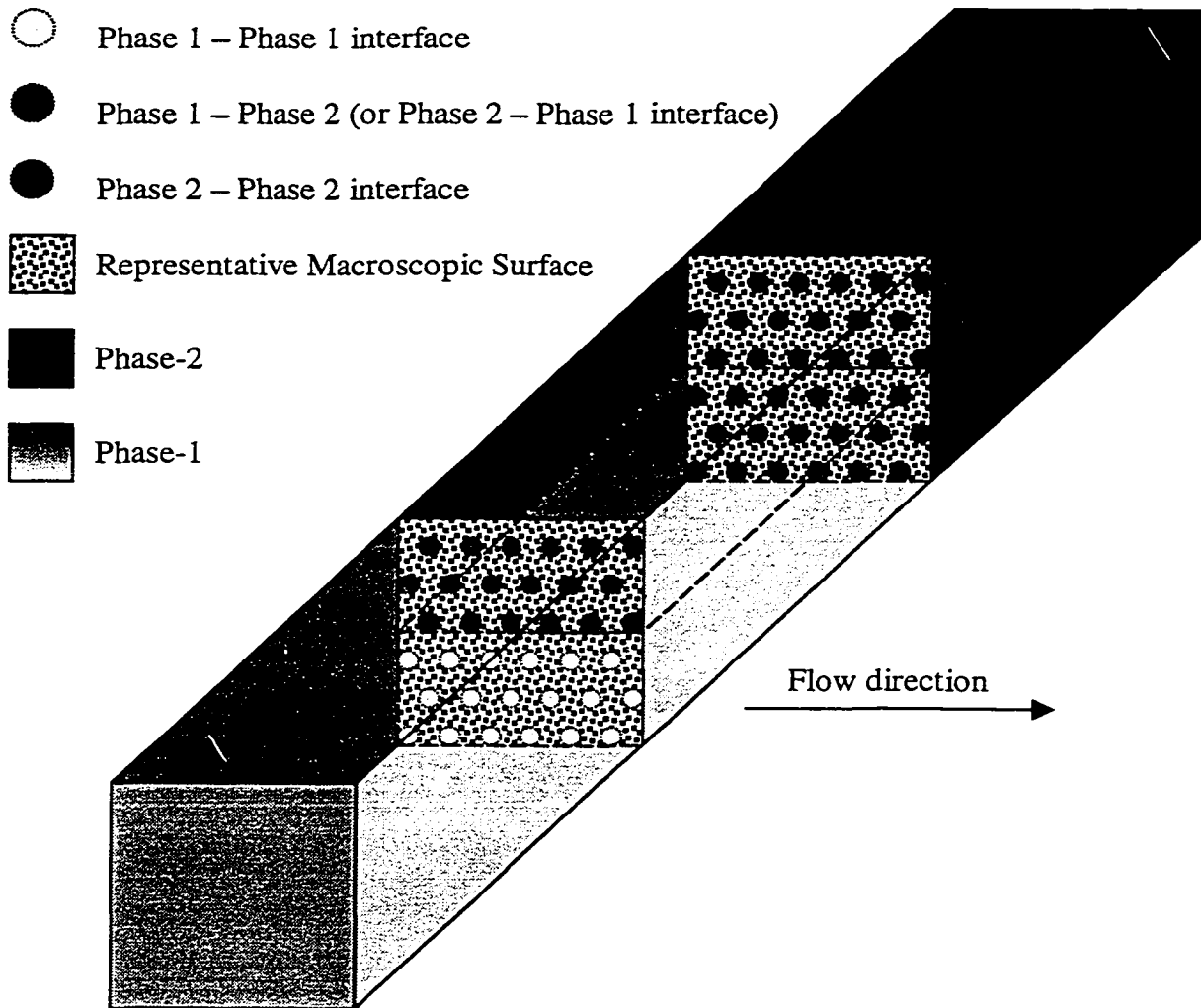


Figure 4.1: An idealized schematic of the representative macroscopic surfaces (RMS) one located in a phase-1 channel, and one located in a phase-2 channel.

2 portions of the fluid-fluid portion of the RMS, respectively. The bulk area of the RMS is defined by A_b , the porosity by ϕ and a_{11} and a_{12} are the fractions, on the phase 1 side, of the fluid-fluid interface that are phase 1-phase 1 and phase 1-phase 2 interface, respectively. The phase pressures, p_1 and p_2 , are assumed to be measured at the midpoint of the RMS.

The capillary pressure, P_c , defines the pressure drop across the phase 1-phase 2 portion of the fluid-fluid interface, where

$$p_2 - p_1 = P_c \quad (4.35)$$

Solving Equation (4.35) for p_1 and introducing the result into Equation (4.34), there results

$$F_{12} = A_b \phi a_{12} (p_2 - P_c) \quad (4.36)$$

By summing the forces defined by Equations (4.32), (4.33) and (4.36) and by dividing by A_b , the average pressure of the wetting phase, acting at the midpoint of the first RMS, may be shown to be

$$\bar{p}_1 = [1 - (1 - a_{11})\phi] p_1 + a_{12}\phi(p_2 - P_c) \quad (4.37)$$

In view of the fact that

$$A_b \phi a_{11} + A_b \phi a_{12} = A_b \phi$$

it follows that

$$a_{11} + a_{12} = 1 \quad (4.38)$$

The introduction of Equation (4.38) into Equation (4.37) yields

$$\bar{p}_1 = (1 - a_{12}\phi) p_1 + a_{12}\phi(p_2 - P_c) \quad (4.39)$$

Consider next a channel flowing, under steady-state conditions, phase 2, the nonwetting phase. It is supposed that another RMS, parallel to the one located in the channel flowing wetting fluid (see Figure 1), is located in this channel. An analysis similar to that presented above for phase 1 may be used

to demonstrate that the average pressure of the nonwetting phase, acting at the midpoint of the second RMS, is defined by

$$\bar{p}_2 = (1 - a_{21}\phi) p_2 + a_{21}\phi(p_1 + P_c) \quad (4.40)$$

where

$$a_{21} + a_{22} = 1 \quad (4.41)$$

and where a_{21} and a_{22} define the fractions, on the phase 2 side, of the fluid-fluid interface that are phase 2-phase 1 interface and phase 2-phase 2 interface, respectively.

Two more equations are needed to define completely the $a_{ij}, i, j = 1, 2$, parameters. To obtain these equations, two compatibility conditions are imposed. To be consistent the area of the phase 1-phase 2 interface on the wetting side of the first RMS should equal the area of the phase 2-phase 1 interface on the nonwetting side of the second RMS. This can be achieved by setting

$$a_{12} = a_{21} \quad (4.42)$$

At steady-state, there should be no local saturation gradients in the transverse direction to flow. For this to be the case, it is necessary that

$$a_{11} = a_{22} \quad (4.43)$$

Equations (4.38), (4.41), (4.42) and (4.43) comprise a system of four equations in four unknowns, the $a_{ij}, i, j = 1, 2$, which may be solved to show that

$$a_{11} = a_{12} = a_{21} = a_{22} = 0.5 \quad (4.44)$$

Note that the $a_{ij}, i, j = 1, 2$, should not be considered as saturations inasmuch as saturation is dictated by the relative number of channels, and their cross-sectional area (orthogonal to the direction of flow), that are transporting phase 1 and phase 2, respectively.

If Equation (4.44) is introduced into Equations (4.39) and (4.40), it follows that

$$\bar{p}_1 = (1 - \frac{\phi}{2})p_1 + \frac{\phi}{2}(p_2 - P_c) \quad (4.45)$$

and

$$\bar{p}_2 = \frac{\phi}{2}(p_1 + P_c) + (1 - \frac{\phi}{2})p_2 \quad (4.46)$$

Taking the partial derivatives of Equations (4.45) and (4.46) with respect to x , keeping in mind the assumption of steady-state flow, yields

$$\frac{\partial \bar{p}_1}{\partial x} = (1 - \frac{\phi}{2})\frac{\partial p_1}{\partial x} + \frac{\phi}{2}\frac{\partial p_2}{\partial x} \quad (4.47)$$

and

$$\frac{\partial \bar{p}_2}{\partial x} = \frac{\phi}{2}\frac{\partial p_1}{\partial x} + (1 - \frac{\phi}{2})\frac{\partial p_2}{\partial x} \quad (4.48)$$

For steady-state cocurrent flow, $\partial p_1/\partial x = \partial p_2/\partial x$. Introducing this result into Equations (4.47) and (4.48) yields

$$\frac{\partial \bar{p}_1}{\partial x} = \frac{\partial p_1}{\partial x} \quad (4.49)$$

and

$$\frac{\partial \bar{p}_2}{\partial x} = \frac{\partial p_2}{\partial x} \quad (4.50)$$

As expected, it can be inferred from Equations (4.49) and (4.50) that for cocurrent, steady-state flow, the average (or effective) driving force for a given phase is the appropriate phase pressure gradient. This is consistent with results presented in an earlier paper (Bentsen, 1999). For steady-state, countercurrent flow, $\partial p_1/\partial x = -\partial p_2/\partial x$. If this result is introduced into Equations (4.47) and (4.48), it follows that

$$\frac{\partial \bar{p}_1}{\partial x} = (1 - \phi)\frac{\partial p_1}{\partial x} \quad (4.51)$$

and

$$\frac{\partial \bar{p}_2}{\partial x} = (1-\phi) \frac{\partial p_2}{\partial x} \quad (4.52)$$

Hence, on the basis of Equations (4.51) and (4.52), it appears that, for steady-state, countercurrent flow, the average (or effective) driving force for a given phase is smaller, by the factor $(1-\phi)$, than the appropriate phase pressure gradient. The reason for this is that the wetting and nonwetting phase pressure gradients are acting in opposite directions. Again, this result is consistent with results presented in an earlier paper (Bentsen, 1999). Moreover, Equations (4.51) and (4.52) can be used to demonstrate that the interfacial coupling parameter, α , is defined by

$$\alpha = 1 - \phi \quad (4.53)$$

In constructing Equation (4.53), the defining equation for α , the porosity, ϕ , was assumed to be that in a plane parallel to the direction of flow. For isotropic, homogeneous, natural porous media being considered here, the porosity of a plane is independent of the direction of the plane. Hence, in view of Equation (4.53), $0 < \alpha < 1$. That is, in isotropic, homogeneous, natural porous media, α cannot take on the limiting values of 0 and 1, because, for such values, the porous medium ceases to exist.

The introduction of Equation (4.53) into Equations (4.28) and (4.29) yields

$$-\frac{v_1}{\lambda_1^o} = \left(\frac{\partial p_1}{\partial x} + \frac{\phi}{2} \frac{\partial P_c}{\partial x} \right) \quad (4.54)$$

and

$$-\frac{v_2}{\lambda_2^o} = \left(\frac{\partial p_2}{\partial x} - \frac{\phi}{2R_{12}} \frac{\partial P_c}{\partial x} \right) \quad (4.55)$$

Equations (4.54) and (4.55) are the final form of flow equations where the phenomenon of capillary coupling has been incorporated into the existing two-

phase flow formulations. Moreover, in Chapter 6, various scenarios to test the validity of these equations experimentally are presented.

4.6. Viscous Coupling Versus Capillary Coupling

It has been determined experimentally (Bentsen and Manai, 1991,1993) that the effective mobilities determined in a steady-state, countercurrent flow experiment are less than those determined in a steady-state, cocurrent flow experiment. Such a result cannot be explained, if the conventional transport equations [Equations (4.6) and (4.7)] are assumed to describe correctly two-phase flow through porous media. That is, in order to explain such results, one must resort to more sophisticated transport equations, such as those constructed by Kalaydjian (1987) and others (de la Cruz and Spanos, 1983; Whitaker, 1986). It has been usual, in such equations, to postulate that the coupling that takes place between the two flowing phases arises because of interfacial momentum transfer. However, in view of Equations (4.30) and (4.31), it seems preferable to refer to such interfacial coupling as capillary rather than viscous coupling. This position is taken for two reasons. First, as can be seen in Equations (4.30) and (4.31), the parameter α is associated with the pressure gradients, and not with the mobilities. Second, the coupling component of the driving force for a given phase [see Equations (4.9) and (4.10)] arises because of the capillarity of the porous medium, and not because of interfacial momentum transfer.

Over the years, simple analogous models of porous media (see, for example, Bacri, et al., 1990; Rose, 1990a,1993; Ayub and Bentsen, 1999a) have been used to gain insight into the role interfacial momentum transfer plays in flow through porous media. In these models, it is possible to specify the conditions that must apply on the boundary separating the two flowing fluids. Moreover, it is practicable to derive not only transport equations that are analogous to those of Kalaydjian (1987), but also to specify the functional forms of the

mobilities. However, two problems arise when one tries to extend these results to flow through natural porous media. First, in order to meet the requirement that the velocity must be zero at the wall(s) of the analogous porous medium, it is necessary that the cross mobilities become zero at both limiting values ($S = 0$ and $S = 1$) of saturation. In natural porous media, on the other hand, the cross mobilities were found to be zero at only one of the limiting values of saturation, not both (Bentsen and Manai, 1991, 1993). Second, in the analogous models of porous media, it is usually found that the cross mobilities are equal, a result that is consistent with ideas arising out of nonequilibrium thermodynamics (Katchalsky and Curran, 1967). Again, however, available experimental results do not support the extension of this result to natural porous media (Dullien and Dong, 1996; Avraam and Payatakes, 1995a; Bentsen and Manai, 1993).

In analogous models of porous media, the interfacial coupling that takes place is truly due to interfacial momentum transfer. On the other hand, it appears that, in natural porous media, such coupling is due to the capillarity of the porous medium. Thus, because viscous coupling occurs in analogous models of porous media, while capillary coupling occurs in natural porous media, results obtained for the former are not extendable to the latter. Moreover, it should be pointed out that, while the results presented herein provide a plausible explanation as to why, in natural porous media, steady-state, countercurrent mobilities appear to be less than steady-state, cocurrent mobilities, they do not preclude the possibility that some viscous coupling is also taking place. On the basis of recent results presented in the literature (Zarcone and Lenormond, 1994; Rakotomalala et al., 1995), however, it can be inferred that, in natural porous media, the viscous coupling effect is likely to be negligibly small.

4.7. Unsteady-State Cocurrent Flow

The above theory has been developed by making use of SSCO and SSCT two-phase flow experiments; however, it is equally applicable to one-dimensional USCO flow experiments. In this study, to quantify the amount of interfacial coupling, SSCO and USCO flow experiments were conducted. On a routine basis, SSCT experiments are rather difficult to perform as compared to SSCO and USCO experiments. So, keeping in mind one of the main objectives of this study, that is, to develop relatively easier technique(s) to quantify interfacial coupling, it was decided to conduct a set of experiments involving SSCO and USCO type two-phase flow through porous media. The SSCO flow experiments were conducted to obtain the phase mobilities, $\lambda_i^o; i = 1, 2$, whereas, the USCO flow experiments were used to determine the capillary coupling parameter, α .

4.7.1. Unstabilized Displacement

Sarma (1988) and Sarma and Bentsen (1989a) have introduced a unique method for estimating relative permeabilities from unstabilized displacement data. Using this method one can estimate the effective permeabilities over the entire saturation range of interest, whereas, conventional external-drive methods cannot be used because of the difficulty of measuring both saturation and pressure accurately in the immediate vicinity of a displacement front. Therefore, in this study, to calculate the unsteady-state fluxes, the method developed by Sarma and Bentsen (1989a) will be used. For the reader's convenience, the following section has been taken from the reference, Sarma and Bentsen (1989a).

4.7.2. Fractional Flow

If a displacement is unstabilized, use can no longer be made of the standard (Eluerian) methods for estimating the fraction of water (or oil) flowing at a

particular location in the core. Rather, a Lagrangian approach must be taken. Buckley and Leverett (1942) have shown that:

$$\frac{\partial x(S_1, t)}{\partial t} = \frac{q}{A\phi} \frac{\partial f_1(S_1, t)}{\partial S_1} \quad (4.56)$$

For a specific saturation, say S_1^* , Equation (4.56) may be integrated to yield:

$$x(S_1^*, t) = \frac{q}{A\phi} \int_0^t \frac{\partial f_1(S_1^*, t)}{\partial S_1} dt \quad (4.57)$$

where it has been assumed that $x(S_1^*, 0) = 0$. Because Equation (4.57) must hold for all possible values of S_1^* ($S_{1i} \leq S_1^* \leq 1 - S_{or}$), it may be written:

$$x(S_1, t) = \frac{q}{A\phi} \int_0^t \frac{\partial f_1(S_1, t)}{\partial S_1} dt \quad (4.58)$$

If $x(S_1, t)$ is a single-valued function of S_1 , both sides of Equation (4.58) may be integrated with respect to S_1 to obtain:

$$\int_{S_{1i}}^{S_{1i}^*} x(S_1, t) dS_1 = \int_{S_{1i}}^{S_{1i}^*} \frac{q}{A\phi} \int_0^t \frac{\partial f_1(S_1, t)}{\partial S_1} dt dS_1 \quad (4.59)$$

Moreover, if $f_1(S_1, t)$ is a well-behaved function, the order of integration may be changed and

$$\int_{S_{1i}}^{S_{1i}^*} x(S_1, t) dS_1 = \frac{q}{A\phi} \int_0^t \int_{S_{1i}}^{S_{1i}^*} \frac{\partial f_1(S_1, t)}{\partial S_1} dS_1 dt \quad (4.60)$$

or, upon carrying out the integration with respect to S_1 ,

$$\int_{S_{1i}}^{S_{1i}^*} x(S_1, t) dS_1 = \frac{q}{A\phi} \int_0^t f_1(S_1^*, t) dt \quad (4.61)$$

where it has been assumed that $f_1(S_{1i}, t) = 0$.

At time t , a certain quantity of water will have been injected into the core. Let the portion of this water which is stored in the core between the initial water saturation S_{1i} , and S_1^* be defined by:

$$Q_1(S_1^*, t) = q \int_0^t f_1(S_1^*, t) dt = A\phi \int_{S_{1i}}^{S_1^*} x(S_1, t) dS_1 \quad (4.62)$$

Then, upon differentiating Q_1 with respect to t , it follows that

$$f_1(S_1^*, t) = \frac{1}{q} \frac{dQ_1(S_1^*, t)}{dt} = \frac{A\phi}{q} \frac{d}{dt} \int_{S_{1i}}^{S_1^*} x(S_1, t) dS_1 \quad (4.63)$$

To evaluate the integral in Equation (4.63), the values of x as a function of saturation are required. This can be done by obtaining a least squares fit of x as a function of S_1 . However, in actual experimental work, values of saturation as a function of x were measured. Therefore, to incorporate the measured saturation profiles more appropriately, the following modification of the above formulation was utilized.

Considering the integral from Equation (4.63),

$$\int_{S_{1i}}^{S_1^*} x(S_1, t) dS_1, \quad (4.64)$$

and, using the well-known formula for integration by parts, one can write the modified form of Equation (4.64) as

$$\int_{S_{1i}}^{S_1^*} x(S_1, t) dS_1 = x(S_1, t) \cdot S_1(x, t) \Big|_{S_{1i}}^{S_1^*} - \int_{S_{1i}}^{S_1^*} S_1(x, t) \frac{dx}{dS_1} dS_1 \quad (4.65)$$

Simplifying the above equation and substituting the resulting equation into Equation (4.63) yields the final form of the equation that was used in this study to determine fractional flow data for the wetting phase.

$$f_1(S_1^*, t) = \frac{A\phi}{q} \frac{d}{dt} \left[x(S_1^*, t) \cdot S_1^* - x(S_{1i}, t) \cdot S_{1i} + \int_{x(S_1^*)}^{x(S_{1i})} S_1 dx \right] \quad (4.66)$$

To estimate $f_1(S_1, t)$ for some specific saturation, say S_1^* , $Q_1(S_1^*, t)$ must be estimated at a number of different times. This can be done, with the aid of Equation (4.62), provided saturation profiles measured at a number of different times are available. Then, by using least squares techniques to fit a

parametric equation to these data, it becomes possible to differentiate analytically the parametric equation to obtain an estimate for $f_1(S_1^*, t)$ at the time of interest. Moreover, by undertaking this procedure for a number of different values of S_1^* , the f_1 saturation curve which pertains to a specific point in time can be constructed.

4.8. Measurement of Dynamic Saturation

Initially, it was intended to use a microwave attenuation system for the current study, which had previously been used successfully by several researchers such as, Islam (1985), Manai (1991), Sarma (1988) and Saeedi (1979), at the University of Alberta, Canada. However, the original microwave generator failed, and the replacement microwave generator was unable to generate sufficient power to measure saturation accurately in cores having the desired thickness. Consequently, a new way to measure saturation had to be developed. After reviewing various saturation measurement techniques, and keeping in mind the limited availability of technical expertise and funding, it was decided to develop a method based on capacitance to measure saturation.

The capacitive characteristics of water and oil are vastly different, and can be described by a relative dielectric constant. When expressed in units relative to the dielectric constant of vacuum at room temperature, which is 1, the dielectric constant of water is close to 80, while that for oil is about 2. This wide contrast in dielectric properties of water and oil can be used to estimate the fractional distribution of water and oil in laboratory waterflood experiments. As the water saturation in a porous medium increases, the dielectric constant of the matrix also increases. In other words, the capacitance of a water saturated porous medium is directly proportional to the amount of water present in the core. This proportionality relationship, however, is not linear,

mainly because of the complex nature of the interaction among the electromagnetic waves, the oil, and the porous medium. Generally, the dielectric behavior of heterogeneous mixtures such as water/oil/porous medium has a complicated dependence on frequency and the matrix (Arulanandan and Smith, 1973). Therefore, in order to determine the saturation profiles in a porous medium, this complex behaviour must be determined empirically to establish a proper measurement method (Davis, 1980).

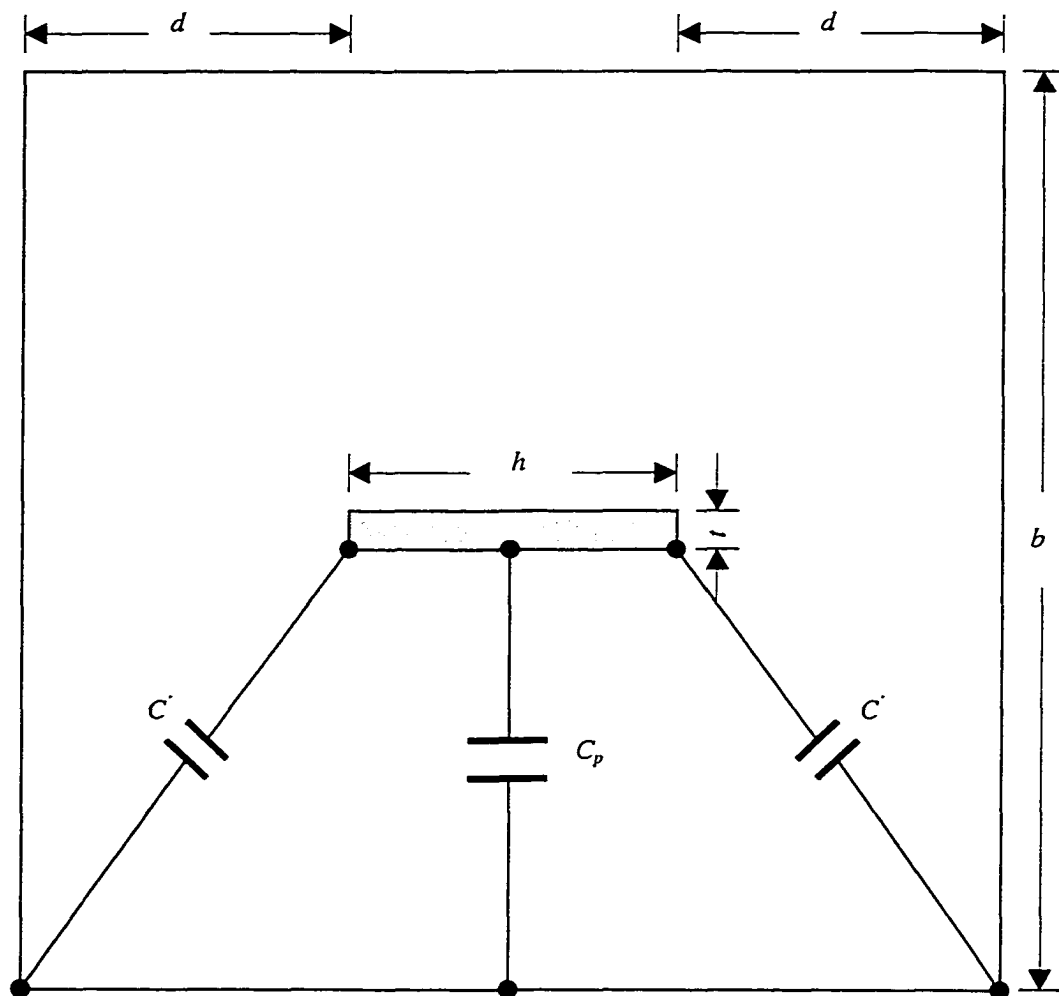
A variety of frequency ranges starting from RF to virtually any frequency level in the microwave range can be used to detect water saturation level(s) in porous media. For the current application, however, the VHF range of the electromagnetic spectrum was found to be the most appropriate level because, at the operating frequencies from 100 MHz to 200 MHz, the anomalous response of the fluids/porous media system was found to be minimum (Davis, 1980; Kraszewski 1996).

4.8.1. Theoretical Background of the Capacitance Method

The cross-sectional view of the resonator's jaw used to determine the capacitance for the current study is shown in Figure 4.2. The equation used (Orlov, 1970) to correlate the frequency response to that of the capacitance of the sample placed between the two jaws of the resonator is:

$$\frac{1}{2\pi f_o C} = Z_o \tan\left(\frac{2\pi f_o l}{\bar{c}}\right) \quad (4.67)$$

where f_o is the frequency response in MHz, C is the capacitance of the resonator in pF, l is the length of the central conductor of the resonator in cm, \bar{c} is the velocity of light in m/sec, and Z_o is the characteristic impedance of the shielded strip line in ohms. The characteristic impedance, Z_o , can be determined with the help of the following equation (Orlov, 1970):



$d = 40$ mm (distance between sides of outer and central conductors)

$h = 20$ mm (width of the central conductor)

$t = 1$ mm (thickness of the central conductor)

$b = 100$ mm (cross-sectional width of the resonator's jaw)

C_p = capacitance between sides of central and outer conductors, pF

C' = capacitance between corners of central and outer conductors, pF

Figure 4.2: Cross-sectional view of the resonator's jaw used to measure equivalent capacitance of the system.

$$Z_o = \frac{377}{\sqrt{\epsilon} C_o} \quad (4.68)$$

where ϵ , in this case, is the dielectric constant of air, and C_o is the capacitance of the shielded strip line, measured when there is no sample material placed in the jaws of the resonator. Mathematically, C_o can be determined, if the various dimensions of the resonator are known, using:

$$C_o = 2C_p + 4C' \quad (4.69)$$

where C' is defined in Figure 4.2. Moreover, C_p in the above equation may be determined with the help of the following equation (Orlov, 1970):

$$C_p = 2 \frac{\frac{h}{b}}{1 - \frac{t}{b}} \quad (4.70)$$

where h is the width, t is the thickness of the central conductor of the resonator and b is the overall width of the jaw (see Figure 4.2).

CHAPTER 5*

EXPERIMENTAL SET-UP AND PROCEDURE

5.1. Introduction

One of the main objectives of this study was to ensure the functional capabilities of the existing experimental set-up. Several modifications to accomplish this task were made to the equipment, the procedure, and the data acquisition system. This chapter describes the modifications made during the course of this study.

The experimental set-up, equipment, and measurement techniques used in this study were vastly different than those used by the previous researchers (Saeedi, 1979; Islam, 1985; Sarma, 1988; Manai, 1991; Chang, 1996) at the University of Alberta. A microwave attenuation method, originally developed by Parsons (1975) to determine the dynamic saturation profiles, was used by Saeedi (1979), Islam (1985), Sarma (1988), and Manai (1991).

Chang (1996), however, introduced some major modifications to the experimental set-up. Some of the modifications proposed by Chang (1996) include: upgraded microwave instrumentation, a data acquisition system developed in Visual Basic programming codes, and an improved pressure transducer calibration system. However, the microwave generator installed by Chang (1996), after replacing the original generator, was unable to generate sufficient power to measure saturation accurately in cores having the desired thickness. Moreover, several operational problems were noticed with the data

* A version of this chapter (Section 5.2.4) has been accepted for publication. Ayub, M. and Bentsen, R.G. 1999b. *Journal of Canadian Petroleum Technology*.

acquisition system. Consequently, a new way to measure the saturation profiles and to acquire data with improved efficiency had to be developed.

After reviewing various saturation measurement techniques, and keeping in mind the limited availability of technical expertise and funding, it was decided to develop a method based on capacitance to measure dynamic saturation profiles. Some more discussion about the capacitance based method used in this study is available in Chapter 4. In the following sections, each of the major components of the recently developed and successfully tested experimental set-up and procedure are described briefly.

5.2. Experimental Set-up

The schematic diagram of the experimental set-up used to conduct the SSCO and USCO flooding experiments is shown in Figure 5.1. This experimental set-up was rebuilt, when it was discovered that the equipment proposed by Chang (1996) to conduct the current experimental study was not adequate. Some of the major modifications made in the previous system include the saturation measurement system, the fluid injection system, and the data acquisition and control system. A general classification of the equipment used in this study is given as:

- core holder and injection caps;
- fluid injection system;
- effluent collection system;
- dynamic saturation measurement system;
- dynamic pressure measurement system;
- data acquisition and instrument control system.

In the following sections each of the above components of the entire experimental set-up is described briefly.

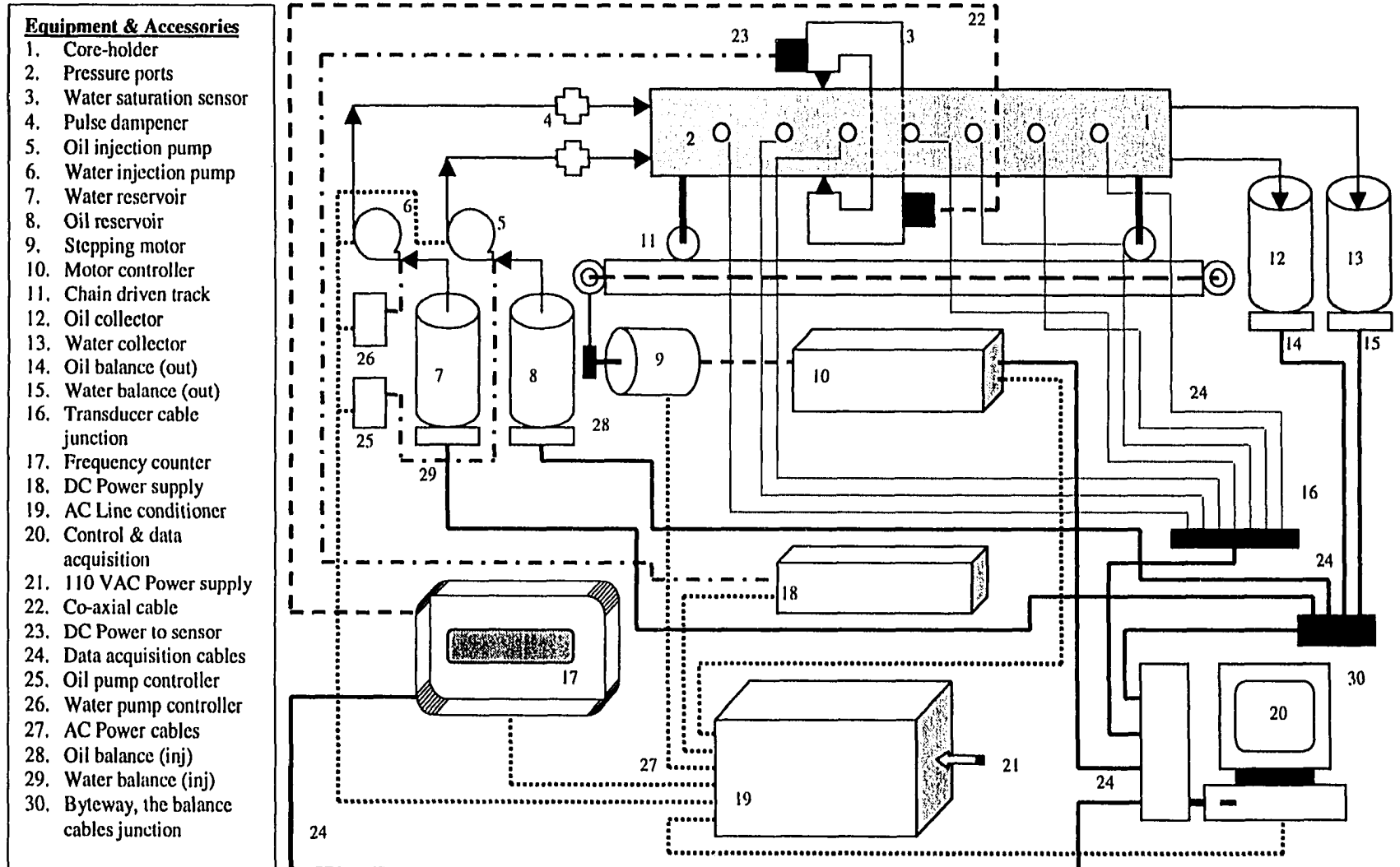


Figure 5.1: Experimental set-up for SSCO & USCO two-phase flow.

5.2.1. Core Holder and Injection Caps

A rectangular core holder made of acrylic sheet was used in this study. The main reason for choosing acrylic was its low dielectric constant which is close to that of the oil used in this research. This avoids an additional possible complexity of capacitance measurement which may arise by using some other material with a different dielectric constant. Moreover, acrylic is easy to machine, readily available and it is a relatively more transparent material for visual observations. The core holder was designed to be at least 60 cm in length to allow for the accurate measurement of dynamic water saturation profiles. The overall length of the core holder, however, was 85 cm; that is, an additional 10 cm on the injection end and 15 cm on the production end was left to eliminate the inlet and outlet end-effects. The core holder was tested at 30 psi pressure; however, it was decided to keep a working pressure of 25 psi as an upper limit, thus giving a safety margin of about 5 psi.

The core holder can hold a 1 cm thick and 5 cm wide unconsolidated porous medium. Moreover, the core holder allows all the transducers to be mounted at the same reference datum with equal spacing. A copper sheet of 1 mm thickness was also attached on both sides of the core holder to facilitate electrical conductivity across the two jaws of the saturation measurement device. The configuration of the core holder and the injection end cap are given in Figures 5.2 and 5.3, respectively.

5.2.2. Fluid Injection System

Two FMI (Fluid Metering Inc.) "Q" model pumps were used to inject oil and water. This type of pump features a unique valveless, rotating and reciprocating pumping action with variable stroke length and stroke rate. An extremely minor level of pulses was observed at various injection rates; however, to achieve essentially pulse free fluid flow, FMI pulse dampeners were installed before the inlet of the core holder, as shown in Figure 5.1. The

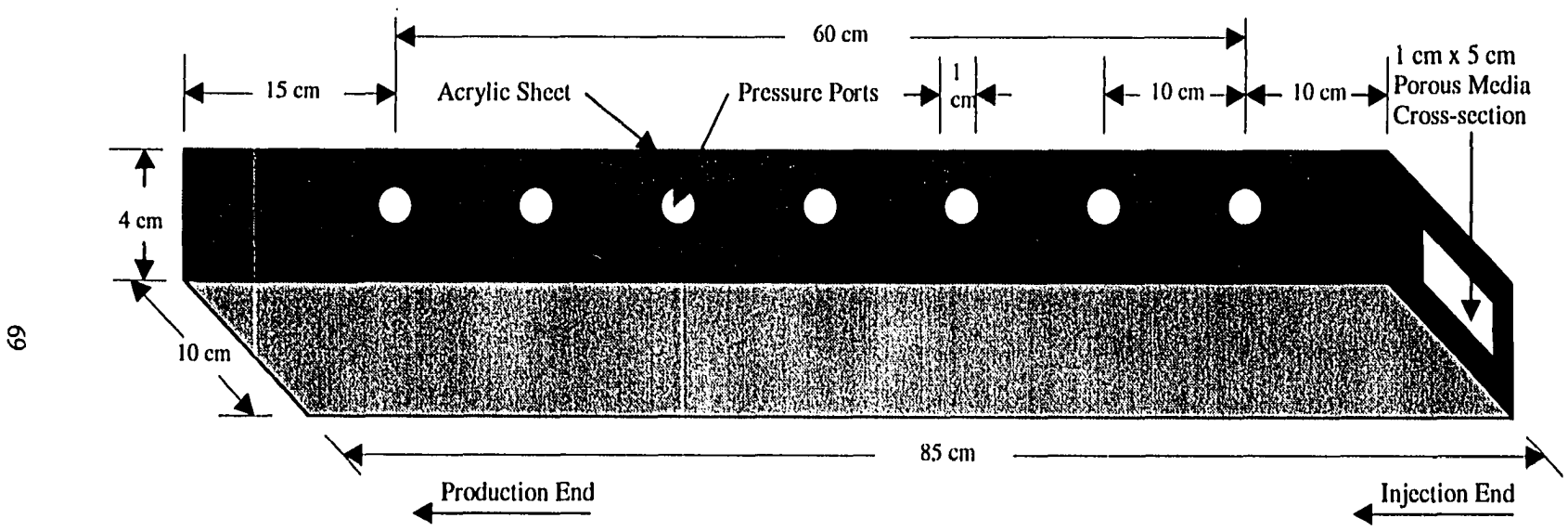


Figure 5.2: General configuration of the core holder (not to scale).

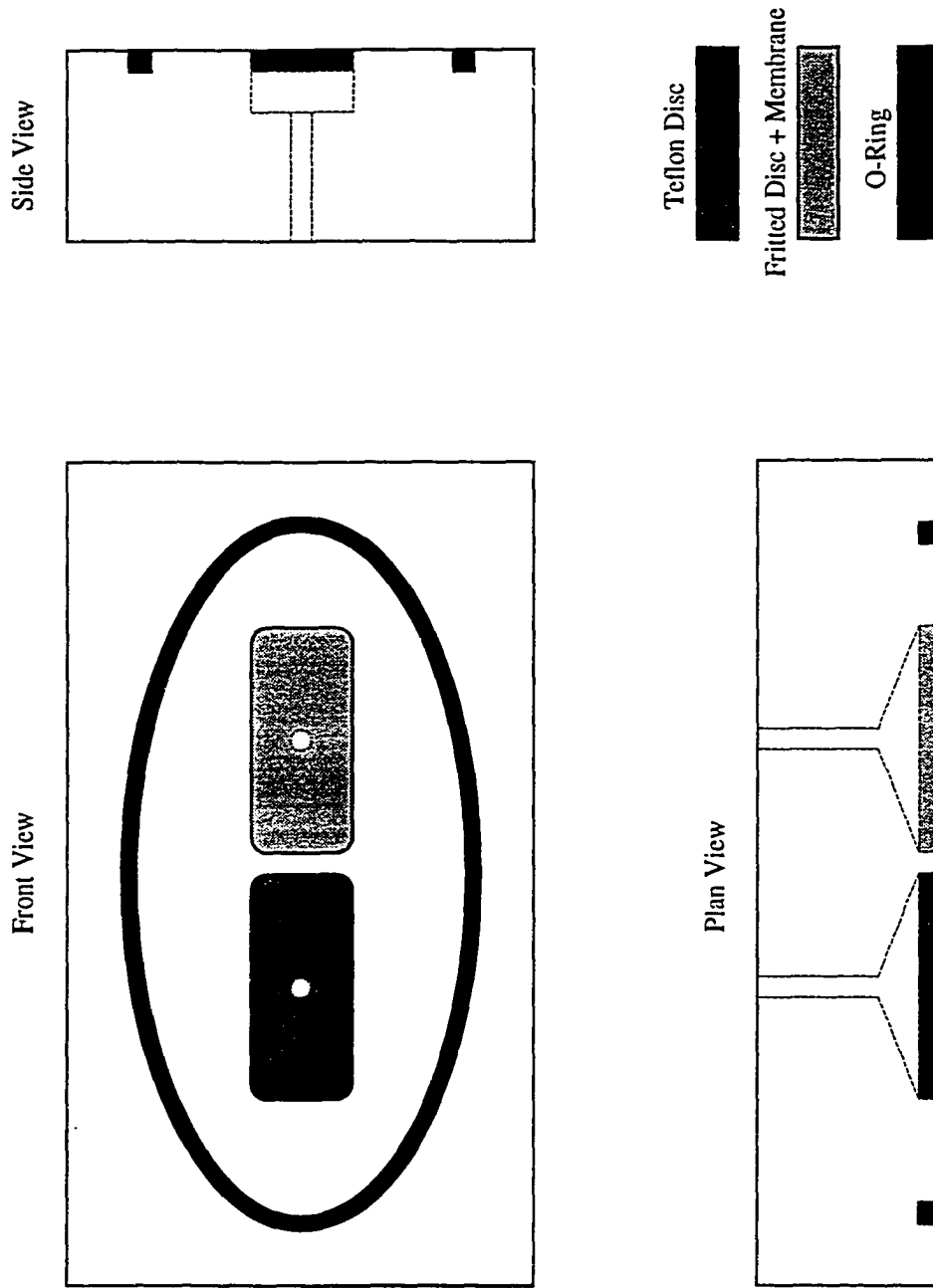


Figure 5.3: End cap for the core holder (not to scale).

other main reason to opt for this pumping system was its ability to provide a variety of flow rates controlled by the adjustable stroke length and stroke rate. Moreover, unlike the previously used Ruska pumps, an unlimited volume of fluids could be injected to achieve steady-state flow conditions.

To facilitate the accurate measurement of injection rates and cumulative fluid injected with respect to time, two electronic balances (manufactured by Setra Systems, Inc.), one for water and the other for oil, were installed. The injection data were directly stored in the computer for further analysis.

5.2.3. Effluent Collection System

Because of the error introduced due to improper visual readings of the fluid(s) meniscus, the commonly used method of measuring volumes of the effluents was not used. Instead, a system similar to that used for injection rate measurement, an incremental weight measurement method, was used to measure the effluent production rates. The incremental weights of the produced fluids were measured at pre-set time intervals with the help of two electronic balances (manufactured by Mettler Toledo Company) placed at the exit end of the core holder. Weight data were directly stored in the computer for further analysis.

5.2.4. Saturation Measurement System

The principle underlying the water saturation measurement, i.e., the capacitance based method, has already been presented in the previous chapter. In the current application of capacitance-based methods, the equivalent dielectric constant of the porous medium, the oil and the core holder (acrylic) is assumed to be negligible as compared to the dielectric constant of water. Most of the shift in frequency response is considered to be a direct indication of water presence during two-phase flow through the packed core holder.

The circuit diagram of the water saturation measurement sensor is shown in Figure 5.4. This diagram provides general insight into the measurement methodology adopted for the current application. To employ the autogeneration method of dielectric constant measurement, a push-pull scheme was used. In this type of scheme two oscillators, instead of the commonly used single oscillator, have to be installed in the circuit. The push-pull scheme used in this circuit allows us to eliminate all of the even frequency harmonics; this leads to a highly stable frequency response, better resolution and a higher Q-quality resonator (Figure 5.5).

5.2.4.1. Calibration of the Sensor

The major drawback of the equations given in Section 4.8.1 of the previous chapter is that they are applicable to a single component system. Mathematically, it is rather difficult to determine an equivalent measure of capacitance of a multi-component system. In this study, the multi-component system is comprised of water, the sand, the oil, and the acrylic sheet, which make it extremely difficult to rely upon the concept of equivalent capacitance obtained mathematically. Moreover, local heterogeneity and permeability variation in the sand pack, outer roughness of the core holder body, electromagnetic interference with the surrounding electrical equipment, and temperature and humidity variation in the laboratory are additional factors which may affect the frequency response of the resonator for the measurement of capacitance.

In order to minimize the adverse effect(s) of these factors, it was decided to recalibrate the sensor before each set of flooding experiments. This process involves the statistical readjustment of the calibration formula (presented next) against some of the known values of water saturation levels obtained by the standard volumetric material balance method.

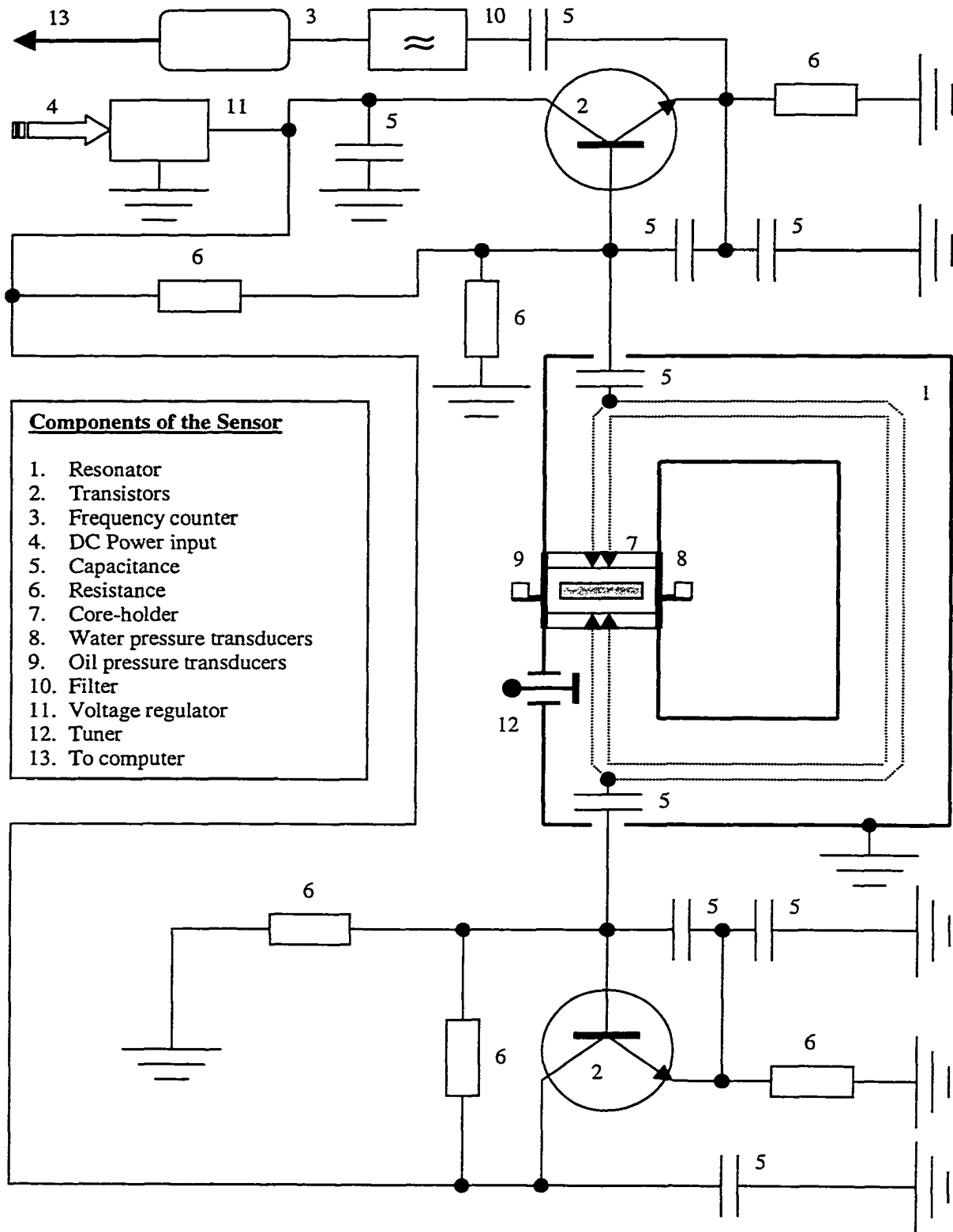


Figure 5.4: Circuit diagram of the water saturation measurement sensor.

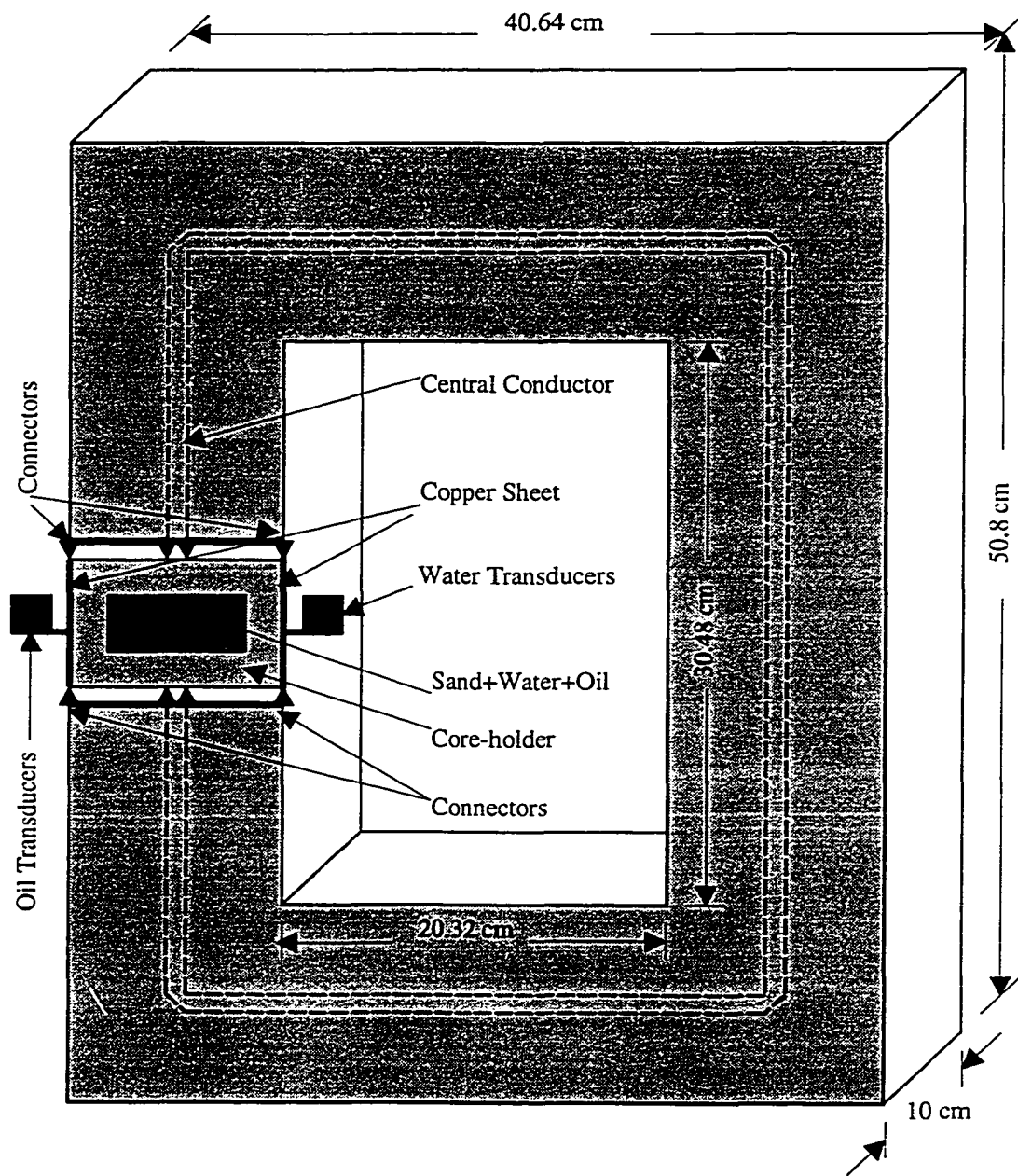


Figure 5.5: Resonator for the saturation measurement system with cross-sectional view of the core holder.

To overcome difficulties arising because of the influence of several factors mentioned above, it was decided to use the lumped frequency response of the saturation measurement sensor against various levels of water saturation, while other components (sand, oil, acrylic) are also present under the sensor. In order to apply this approach Equation (4.67) was simplified as follows:

$$\frac{1}{Af_o S_1} = \tan(Bf_o) \quad (5.1)$$

or

$$S_1 = \frac{1}{Af_o \tan(Bf_o)} \quad (5.2)$$

where $A = 2\pi Z_o$, $B = 2\pi l/\bar{c}$, and S_1 is directly equivalent to C for a specific set of conditions of room temperature and humidity, which are usually assumed as constant. The parameters A and B were determined using nonlinear regression analysis, once the frequency response f_o against various water saturation levels was determined experimentally. Typical calibration data and their comparison with the measured data are shown in Figure 5.6. The range of water saturation levels used to obtain this type of standard calibration trend extends from the irreducible water saturation (S_{1i}) to irreducible oil saturation. Frequency responses at $S_1 = 0\%$ and $S_1 = 100\%$ were not included in the calibration process, because they do not represent meaningful data points for a flooding process; however, they do provide some estimate of the porous medium and the core holder heterogeneity. Some more discussion and the performance of the water measurement system used in this study are presented in the next chapter.

5.2.5. Dynamic Pressure Measurement System

To quantify the capillary coupling parameter, α , and to perform other analysis, it is necessary to obtain the dynamic phase pressure profiles along the length of the core during SSCO and USCO flooding experiments. To facilitate the

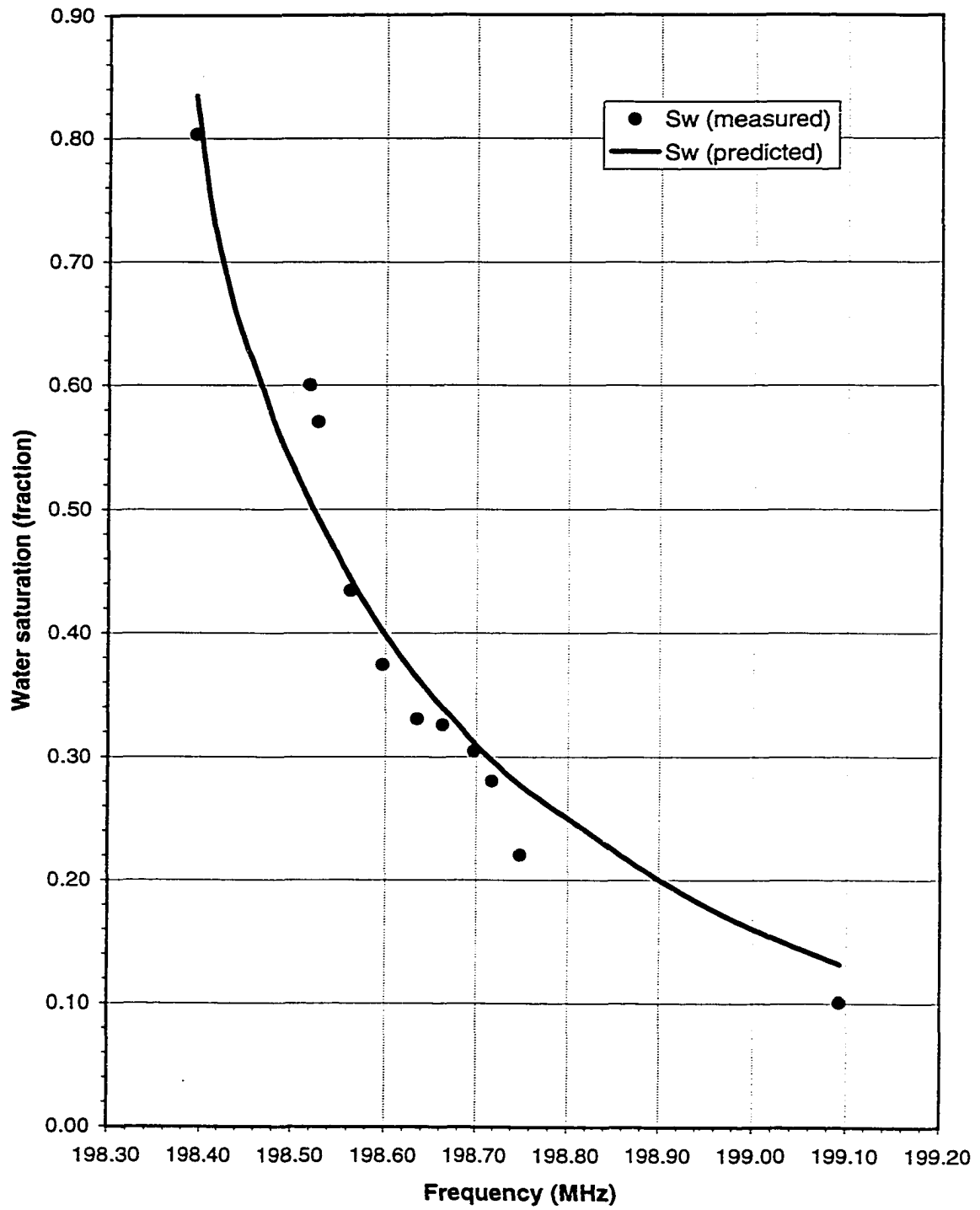


Figure 5.6: Typical calibration curve to convert the frequency response into water saturation.

phase pressure measurement, 14 pressure transducers (manufactured by Validyne Engineering Corp.) were installed.

Out of these 14 pressure transducers, 7 pressure transducers were installed to measure the pressure in the oleic phase on the one side of the core holder, and the other 7 were installed to measure the pressure in the aqueous phase on the opposite side of the same core holder. This arrangement of pressure transducers was found to be extremely satisfactory. However, to further authenticate the accuracy of this scheme, a different installation arrangement of pressure transducers at the core holder, whereby, oil and water transducers on both sides of the core holder were installed alternatively, was tested in a preliminary two-phase flow run. No difference in the dynamic phase pressure readings was observed during the two-phase flow runs for both of the transducer installation arrangements.

To sense the pressure in the oleic phase, strongly hydrophobic Teflon discs (manufactured by KONTES Scientific Glassware/Instrument) were mounted on the fluid intake ports of the pressure transducers. The fritted discs (locally manufactured) used in the previous studies (Manai, 1991; Chang 1996), to sense the pressure in the aqueous phase, were found to be inefficient. A change in the wettability of the fritted discs was suspected after a few hours of flooding, particularly during SSCO experiments. This appeared to impede communication of water pressures to the pressure transducer diaphragms. No such change in wettability of the Teflon discs was observed. To overcome this difficulty, several types of hydrophilic filter membranes (such as used by Hammervold *et al.*, 1998; Hammervold and Skjaeveland, 1992; and Longeron *et al.*, 1994) manufactured by various companies were tested. Eventually, it was discovered that the membranes supplied by the Millipore Corporation with minimum protein binding and high bubble-point pressure were best suited for this study. Therefore, in addition to the fritted discs manufactured by

CORNING Corp., which merely provided a support, the above mentioned filter membranes were also attached to the intake ports of the water pressure transducers.

Prior to each flow experiment, all the pressure transducers were calibrated with the help of an elegant in-house built calibration apparatus used in a previous study (Chang, 1996). The best feature of this system is that all the transducers may be calibrated simultaneously at the same reference level. Further details of the calibration set-up are available in Chang (1996). Data from all the transducers were recorded automatically, via an interface card (UPC-L) supplied by the Validyne Engineering Corp.

5.2.6. Data Acquisition and Instrument Control

The original data acquisition system used by Chang (1996) was developed using Visual Basic. Editing and debugging of Visual Basic is relatively difficult for the non-expert. Moreover, previously the movement of the core holder was not continuous; instead, the core holder had to be stopped momentarily under the microwave sensor to get the water saturation readings at 100 stations along the core holder. With the new water saturation measurement sensor, however, the data acquisition becomes a continuous and instantaneous process and there is no need to stop momentarily along the core holder to obtain a saturation data point. Consequently, to incorporate these modifications and to overcome the various operational difficulties, a new data acquisition system has been developed and tested. The code used in the new data acquisition system is written using LabVIEW. As a result, in addition to better equipment control, debugging and editing was much easier and faster.

LabVIEW is a highly productive graphical programming environment that combines easy-to-use graphical development with the flexibility of a powerful programming language. It offers an intuitive environment, tightly integrated

with measurement hardware, for engineers and scientists for data acquisition, data analysis, and data presentation. However, in this study, LabVIEW was used mainly for data acquisition and instrument control. For data analysis and presentation, Microsoft Office and SPSS were employed.

5.2.6.1. Hardware Configuration

A block diagram, representing the hardware configuration, for data collection and instrument control is given in Figure 5.7. The computer used for data acquisition was an IBM compatible Pentium 200 with Microsoft Windows 95 as an operating system. Four interface cards, that is, UPC-L, RS-232, GPIB and DAS-8, manufactured by various companies were installed on the computer.

5.2.6.1.1. UPC-L Interface Card

The UPC-L interface card is manufactured by the Validyne Engineering Corp. The Validyne UPC-L provides the ability to interface a computer directly to LVDT and variable reluctance sensors. No external signal conditioning is required. Any combination of LVDT, variable reluctance, and DC voltages may be measured by this card by simply wiring the sensor into any input terminal, and programming the function of the input channel. In this study, to measure the phase pressure, Validyne's model DP-15 pressure transducers were used. Pressure data communication and calibration were facilitated through UPC-L, which takes commands from various VIs (Virtual Instruments), developed with the help of LabVIEW. Note that the original software (The Easy Sense Software) supplied by the Validyne Engineering Corp. was not used in this study.

5.2.6.1.2. RS-232 Interface Card

This is a standard serial port data communication card that normally comes with most computers. Incremental and cumulative weight of injection and production fluids were measured with the help of four electronic balances.

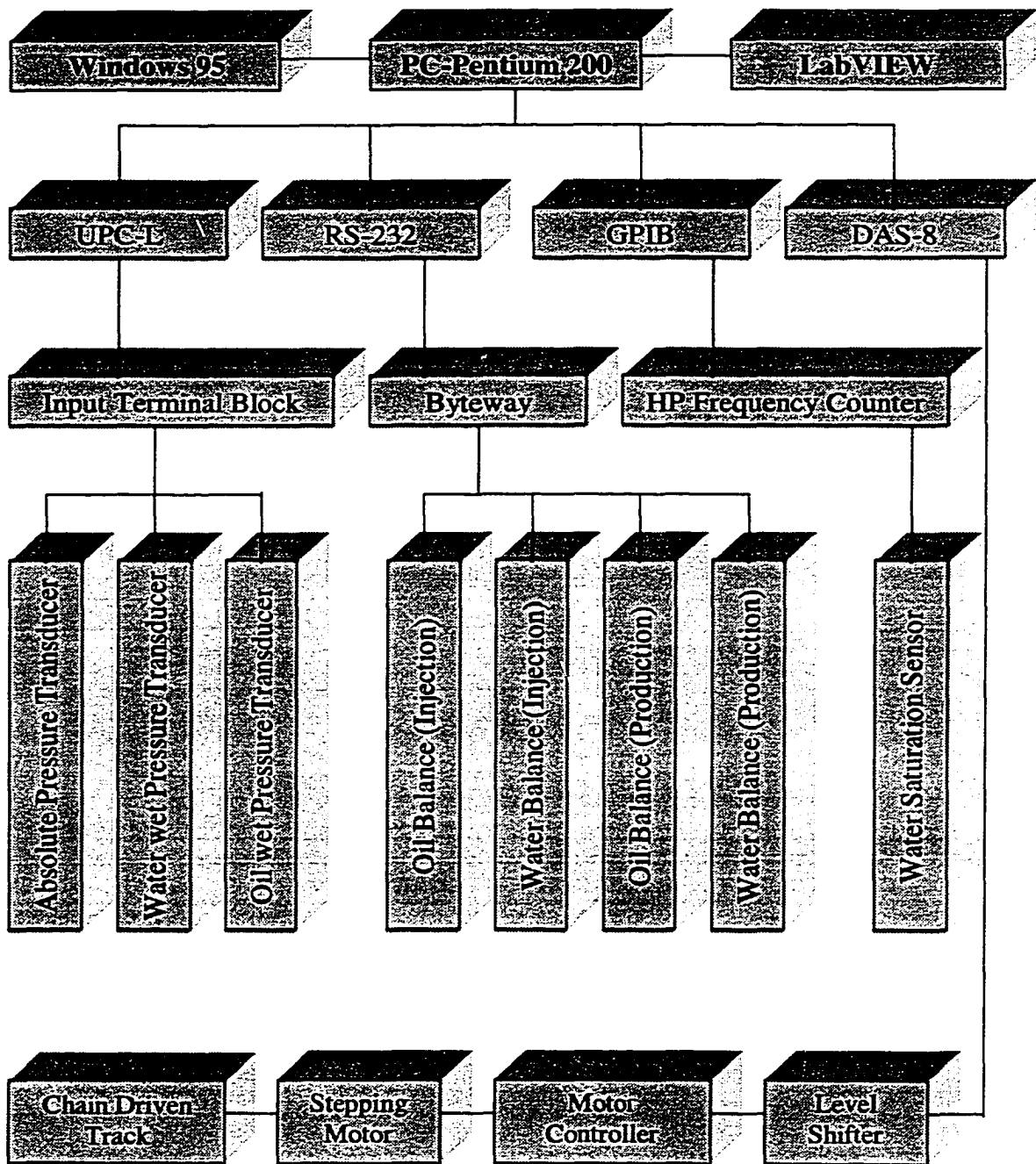


Figure 5.7: Hardware configuration for instrument control and data acquisition.

These balances were equipped with serial ports that can communicate with the computer through the Byteway. The Byteway (manufactured by Protec Microsystems, Inc.), a microprocessor based peripheral sharer, can multiplex up to 8 serial ports; it connects all the balances to the computer.

5.2.6.1.3. GPIB Interface Card

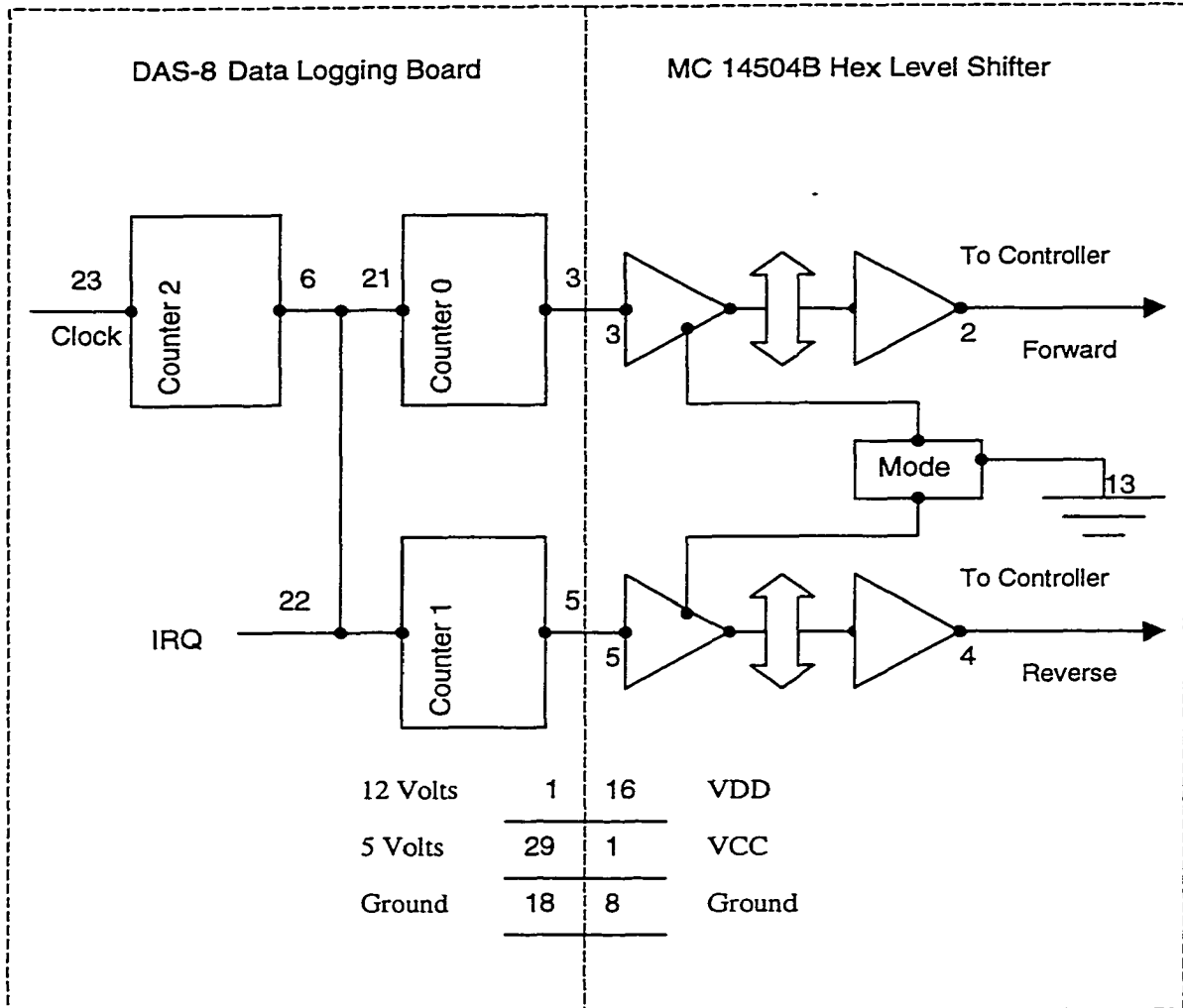
In 1965, Hewlett-Packard designed the HP-IB to connect their line of programmable instruments to their computers. Because of its high transfer rate, this interface bus quickly gained popularity. It was later accepted as IEEE Standard 488-1975. Today, the general purpose interface bus (GPIB) is more widely used than HP-IB. A series of GPIB cards has been developed by National Instruments. This type of card can be used as talker, listener, and/or controller to various programmable instruments. In this study, the frequency signals from the water measurement sensor were captured with the help of a frequency counter (HP Universal Counter 225 MHz, Model 53131-A). These frequency data were recorded and stored in the computer using one of the GPIB interface cards.

5.2.6.1.4. DAS-8 Interface Card

A DAS-8 card is capable of handling data under computer interrupt control. This feature was used to control the start/stop functions, and the speed (forward/backward) of the stepping motor. An existing LabVIEW driver provided by the manufacturer (Computer Board, Inc.) of the DAS-8 card was used to interface the card with the main LabVIEW program. Figure 5.8 provides the schematic for the stepping motor interface.

5.2.6.2. Software Configuration

The configuration and the execution hierarchy for data acquisition and instrument control are shown on Figure 5.9. The code used in the new data acquisition system was written using LabVIEW. As a result, in addition to



Note: Numbers shown on this schematic represent the pin numbers.

Figure 5.8: Schematic for the stepping motor interface.

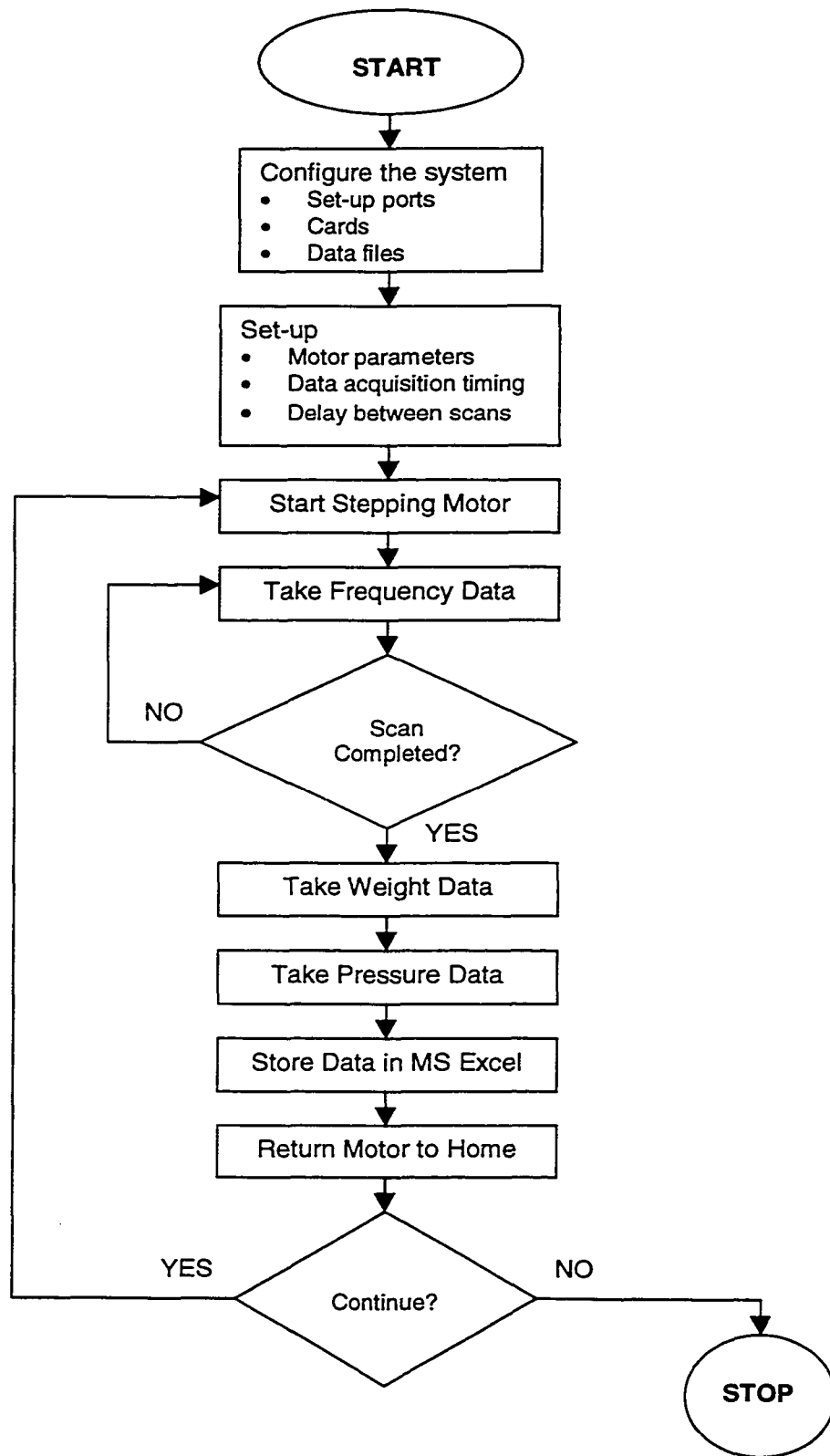


Figure 5.9: Software configuration for instrument control and data acquisition.

better equipment control, debugging and editing was much easier and faster. The following information about LabVIEW was obtained from the *LabVIEW User Manual*.

LabVIEW is a program development environment, much like modern C or BASIC development environments; however, LabVIEW is different from those applications in one important aspect. Other programming systems use text-based languages to create lines of code, while LabVIEW uses a graphical programming language, G, to create programs in block diagram form.

LabVIEW is a general-purpose programming system, but it also includes libraries of functions and development tools designed specifically for data acquisition and instrument control. LabVIEW programs are called virtual instruments (VIs) because their appearance and operation can imitate actual instruments. However, VIs are similar to the functions of conventional languages programs.

A VI consists of an interactive user interface, a data-flow diagram that serves as the source code, and icon connections that allow the VI to be called from higher level VIs. More specifically, VIs are structured as follows:

- The interactive user interface of a VI is called the *front panel*, because it simulates the panel of a physical instrument. The front panel can contains knobs, push buttons, graphs, and other controls and indicators. One can enter data using a mouse and keypad, and then view the results on the computer screen.
- The VI receives instructions from a *block diagram*, constructed in G. The block diagram is a pictorial solution to a programming problem. The block diagram is also the source code for the VI.
- VIs are hierarchical and modular. One can use them as top-level programs and subprograms within other programs. A VI within another VI is called a

sub VI. The icon and connector of a VI work like a graphical parameter list so that other VIs can pass data to a sub VI.

The front panel for the VI written using LabVIEW for the current experimental study is shown in Figure 5.10.

5.2.6.2.1. Running the Software System

To start the data acquisition and instrument control system, one has to follow the following steps:

1. Turn on all equipment (the frequency counter, the motor controller, the DC power meter, all balances, the Byteway, pump controllers, and the computer).
2. Leave the entire system for initial warm-up for at least one hour. This is very important to get stable frequency data from the saturation measurement sensor.
3. Set the core holder at its initial starting position.
4. For a steady-state run, set an appropriate stroke length and stroke rate for both pumps. However, for an unsteady-state run, one has to set only the water pump.
5. Make sure all balances indicate a zero reading on their displays in the beginning.
6. Double click on the icon named "Main Experimental Control", and follow the instructions. Note that the entire data acquisition source code was saved in a folder "PhD".
7. Click the start icon (an arrow indicating toward right direction) on the main tool bar, and follow the prompted instructions. However, do not forget to switch on the pump(s) just before the last prompted instruction; that is, "Start Motor".
8. The delay time between scans can be adjusted at any time during the execution of the acquisition system.

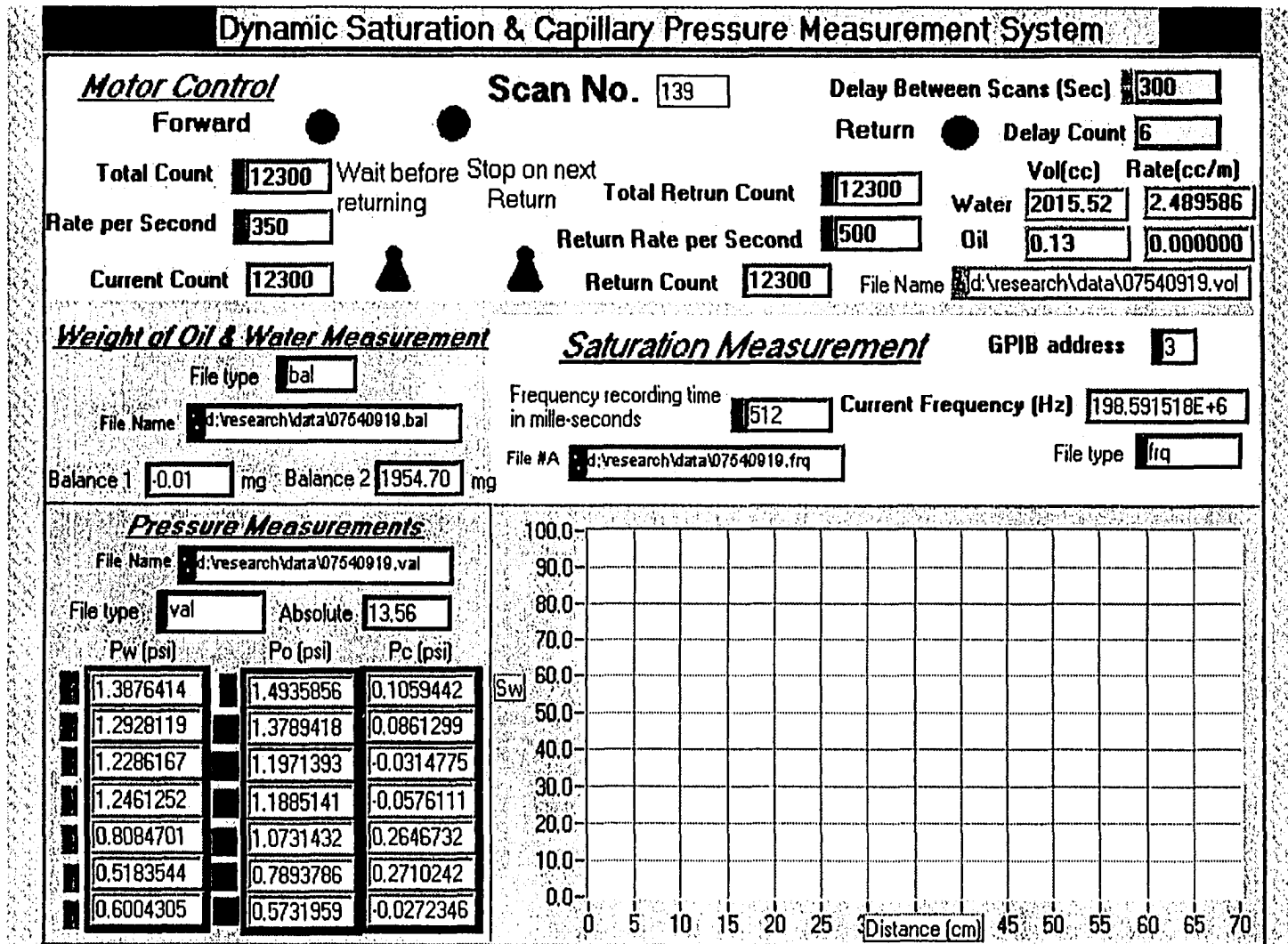


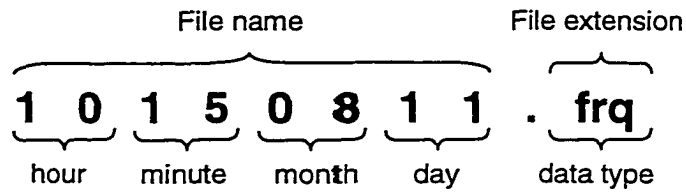
Figure 5.10: Front panel for the data acquisition and the instrument control.

9. To stop a run, click on the stop icon, and turn off the pump(s). Other instruments, however, may be switched off at a later time.
10. Some important precautions during the run time of an experiment must be observed strictly; these include: avoid any vibration in the lab, try to keep room temperature as constant as possible, do not use any high frequency equipment such as radio or cell-phone in the lab.
11. The single most important precaution is that the saturation measurement sensor and its associated equipment must never be stopped during an experimental set of runs (SSCO and USCO flow runs). If this precaution is not followed, one may observe a considerable shift in the frequency response from the saturation measurement sensor.

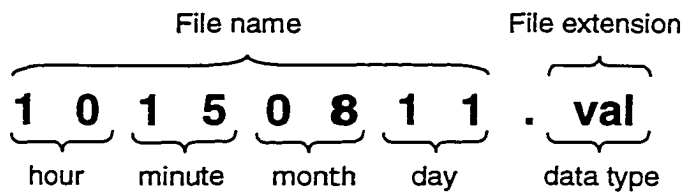
A large amount of data has to be collected and later interpreted for each set of SSCO and USCO flow runs. This may become an unnecessary source of confusion and chaos if the collected data are not labeled and organized properly. Therefore, to manage the huge process of data handling efficiently, a unique system of naming and tagging input and output data files was introduced into the current data acquisition system.

Upon starting the system (Step 7), file names for various types of data (such as pressure data, injection data, production data, and frequency data), are allocated automatically to all of the data output files. The structure for naming a file can best be understood from Figure 5.11. The numbers shown on a file name represent the time and date, while various file extensions indicate the type of data stored in a particular file. Other detailed information about an experiment may be stored before clicking the "Continue" button on the input information form, which will then appear at the beginning of each output file. Note that all output files were automatically stored in MS Excell spreadsheets for further analysis.

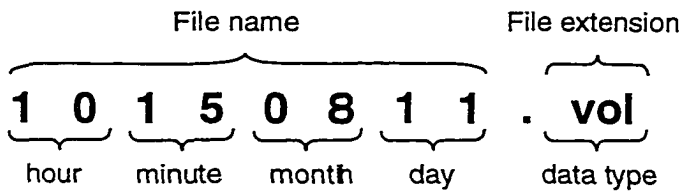
Frequency Data



Pressure Data



Injection Data



Production Data

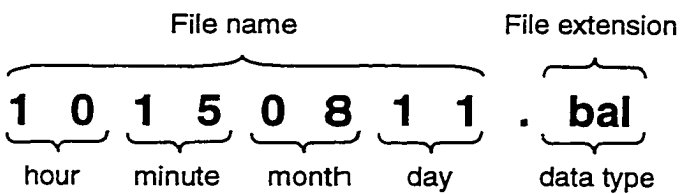


Figure 5.11: Format of output file names for various types of collected data.

5.3. Materials

To investigate the effect of grain size distribution on the parameter α , it was decided to use two different grain sizes of unconsolidated porous media. For this purpose, Ottawa silica sand of 80-120 mesh, and 100-170 mesh, were selected to obtain uniform sandpacks. The procedure adopted for the core preparation and to determine the other core properties such as, porosity and absolute permeability is described in the next sections. Table 5.1 provides average porosities and absolute permeability values of the sandpacks obtained for the various experiments.

Distilled water was used not only to create an irreducible water saturation, but also as a displacing fluid. To investigate the effect of oil viscosity on the parameter α , two oils of different viscosities were used. LAGO was the oil used in several preliminary experiments; however, it was not used for actual runs, once it was suspected that it may affect the wettability of the sandpacks and the fritted discs. For actual flow experiments kerosene (supplied by Fisher Scientific), and a blend of kerosene and light mineral oil (supplied by Fisher Scientific) were used. Table 5.2 provides the relevant properties of the fluids used in this study. Figure 5.12 depicts the variation of the blend (mineral oil + kerosene) viscosity versus volumetric variation of the kerosene in the blend. This figure was used as a guideline to obtain the desired viscosity of the blend. Later, the blend viscosity was independently confirmed by using a Brookfield viscometer.

5.4. Two-Phase Flow Experiments

Keeping in view the theoretical development in Chapter 4, if one is to determine the magnitude of α , the capillary coupling coefficient, it seems clear that two separate types of flow experiments must be undertaken.

Table 5.1: Properties of sandpacks.

Exp. No.	Grain Size [mesh (μm)]	Porosity (fraction)	Abs. Perm. (darcy)	S_{li} (fraction)	S_{2r} (fraction)
1-10*	80-120(180-125)	0.370**	17.00**	0.1000**	0.1100**
11(Set 1)	80-120(180-125)	0.370	17.88	0.1069	0.0916
12(Set 2)	80-120(180-125)	0.373	19.30	0.1177	0.0999
13(Set 3)	100-170(150-90)	0.325	1.700	0.1615	0.1165

* Preliminary runs

** Average values

Table 5.2: Fluid properties at the room temperature.

Fluid	Density (gm/cc)	Viscosity (mPa.s)	IFT (dyne/cm)
Distilled Water	0.99	1.00	--
LAGO	0.81	7.50	22
Kerosene	0.77	1.685	32
Light Mineral Oil	0.88	47.62	48
Kerosene + Light Mineral Oil	0.83	15.00	45

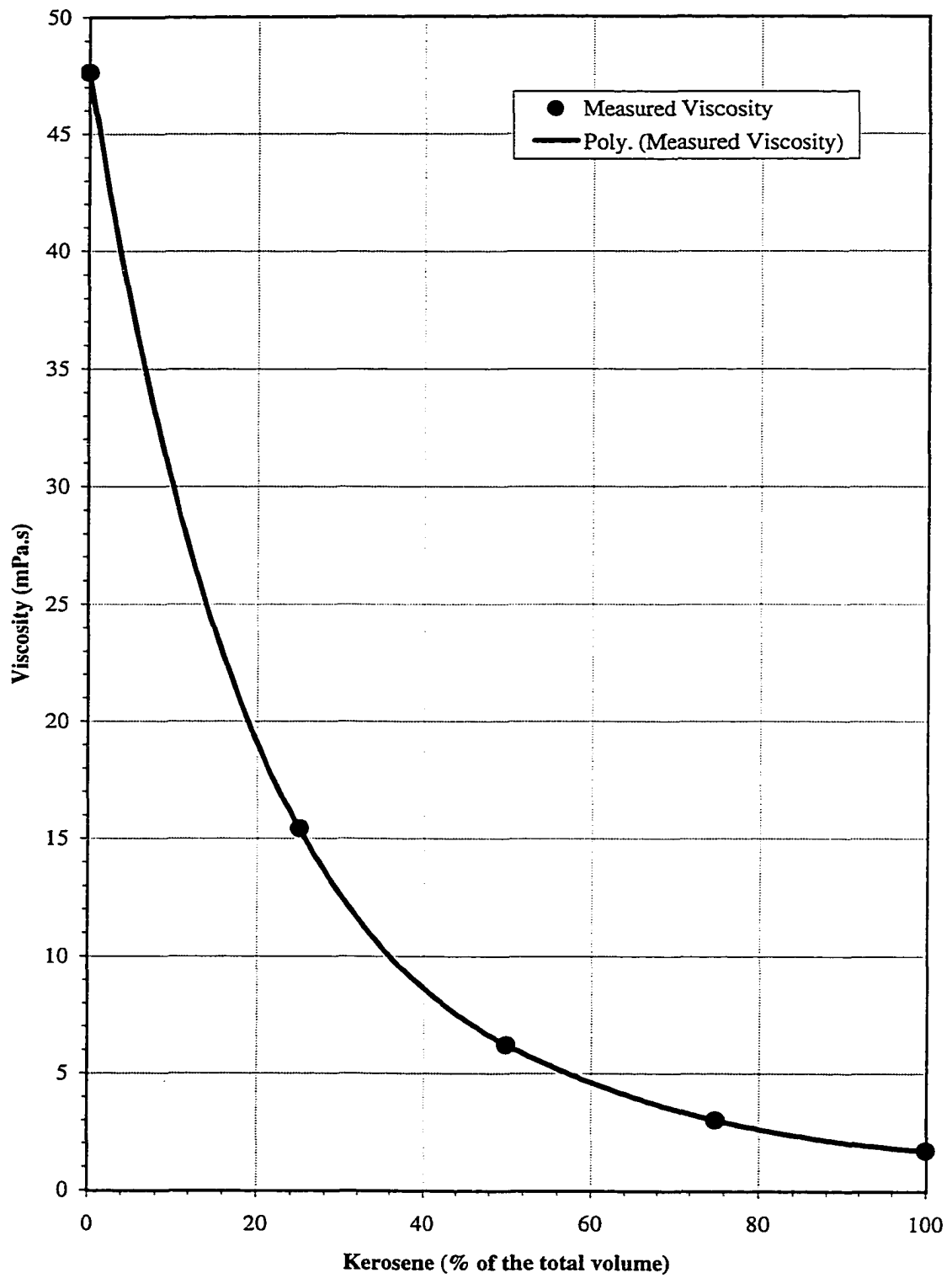


Figure 5.12: Viscosity variation of kerosene-mineral oil blend.

Initially, it was intended to conduct three different types of flow experiments: SSCO, SSCT, and USCO. The reason for undertaking an extra type of experiment was to validate the observations made during the other two types of experiments; hence, leaving less room for doubt in the experimental results. No operational problems were experienced while conducting the SSCO and the USCO flow experiments. Several attempts were made to conduct the SSCT flow experiments, but unfortunately, none of them proved to be successful. The main reasons for these unsuccessful attempts seem to be various operational difficulties such as improperly fabricated end-caps and non-availability of fritted and Teflon discs of relatively higher displacement pressure.

Consequently, it was decided to conduct only two types of experiments: SSCO and USCO experiments. Another reason for not performing SSCT experiments was to simplify the laboratory work needed to quantify the amount of interfacial coupling, one of the main objectives of this study. Moreover, SSCT flow experiments are rather tedious to undertake on a routine basis.

In addition to several preliminary flow experiments, three sets of SSCO and USCO flow experiments were performed. The first set of SSCO and USCO experiments was conducted using kerosene, distilled water, and 80-120 mesh sand. The second set of SSCO and USCO runs used a blend of kerosene and light mineral oil, distilled water, and 80-120 mesh sand. The third set of flow experiments was similar to the first set, except that silica sand of 100-170 mesh, instead of silica sand of 80-120 mesh, was used. The step by step experimental procedure used to perform the proposed SSCO and USCO flow experiments is listed below.

5.4.1. Experimental Procedure

In order to complete a set of two-phase flow experiments, the following steps were followed to conduct each USCO and SSCO run.

1. **Core Preparation and Properties:** To obtain as uniform a sandpack as possible, the core holder was suspended in the vertical position with the bottom end-cap and the dummy plugs inserted into the pressure ports.
2. The core holder was filled with a constant height of distilled water.
3. The sand was poured from the top end of the core holder.
4. The core holder was hammered gently with a rubber hammer while pouring the sand into the core holder. A better and quicker sandpack was obtained by hammering as compared to that commonly obtained by using a regular mechanical vibrator (Chang, 1996).
5. To avoid the formation of different distinct layers of the porous medium in the core, sand pouring, water filling, and hammering were done continuously without any time break, until the core holder was completely packed.
6. The top end-cap was then attached to the core holder to start air drying the packed core by circulating compressed air from top of the core holder for about 48 hours.
7. Weigh the dry core holder with the end-caps, the fittings and the dummy plugs.
8. Suspend the core holder in vertical position, and pull a vacuum for about 12 hours.
9. Saturate the core by imbibing distilled water from the bottom-end of the core holder at a very slow rate.
10. Weigh the core holder again with the same accessories as mentioned in Step 7.
11. Calculate the porosity of the core by estimating the pore volume with the help of the weight values obtained in Step 7 and Step 10.

12. Replace the dummy plugs from one side of the core holder with the water wet pressure transducers. To avoid any air entrapment during the installation of the water-wet transducers, extreme care was taken by keeping water circulation in progress at a very slow rate.
13. Obtain the average absolute permeability of the core with distilled water at various injection rates, using Darcy's law.
14. Allow the core to rest for about 24 hours with 100% water saturation to render it completely water wet.
15. Replace the water-wet transducers with dummy plugs. This step was necessary to avoid oil contact with the water-wet membrane for an elongated time period. It was observed that the pores of the hydrophilic membrane got clogged after about 12 hours of continuous contact with oil only; this considerably reduced the ability of water transfer through the hydrophilic membrane. Consequently, accurate sensing of true water pressures during two-phase flow becomes extremely difficult. To overcome this limitation of the membrane, it was imperative to keep the membrane in contact with water during the whole two-phase flow experiment. Moreover, it was also observed that the presence of the irreducible water saturation in the porous medium is probably not enough to overcome the above-mentioned limitation of the membrane. Because of this experimental difficulty, it was decided to obtain the irreducible water saturation prior to installing the water wet pressure transducers.
16. Keeping in mind the pressure limitations (25 psi maximum) of the core holder, start oil injection at an appropriate injection rate.
17. Record weights of the fluid injected and the fluid produced to calculate the irreducible water saturation level using the material balance method.
18. Install the oil wet pressure transducers by adding additional oil into the oil ports of the core holder to avoid any air entrapment. Moreover, bleed the pressure transducers to make sure that no air is trapped in the transducers.

19. Obtain the average effective permeability to the oil at the irreducible water saturation by using Darcy's law. Repeat the process at various injection rates to get an average value of the effective permeability.
20. Replace the preparatory end-cap on the injection side with a regular injection end-cap that allows injection of both oil and water simultaneously. Make sure no air is trapped during this procedure.
21. In order to reinstall the water wet pressure transducers, inject both water and oil, with the oil at a very high injection rate, and the water at a very low injection rate (total pressure in the core holder should not exceed the maximum limit of the pressure). Keep on injecting both fluids until steady-state is achieved. This step was undertaken to overcome the experimental difficulty mentioned in Step 15. It was observed that a slightly higher level of water saturation than the irreducible water saturation level helps keep the membrane from clogging.
22. Calculate the value of steady-state water saturation by the material balance method.
23. Avoiding trapping of air, reinstall the water-wet transducers.
24. Now, load the core holder, with all the 14 transducers fixed in-place, on the travelling trolley of the chain driven track. Extreme care must be taken to avoid any violent contact between the core holder and the saturation measurement sensor and its components such as the side connectors and the central conductor.
25. Turn on the main data acquisition and instrument control system, and leave the entire system on for an initial warm-up for at least one hour.
26. Scan the core prior to the flooding experiment. Record the frequency response. This response will represent the steady-state water saturation along the length of the core obtained in Step 22.
27. **USCO Flow Experiments:** Because of the problem discussed in Steps 15 and 21, and because of the fact that the USCO experiments are much faster than the SSCO experiments, it was decided to conduct the USCO

flow experiments prior to the SSCO flow experiments. It is unusual to conduct an unsteady-state displacement at a slightly higher water saturation level, rather than at the irreducible water saturation level; however, no major problem in the subsequent analysis was anticipated.

28. Replace the two-phase injection end-cap with the water injection end-cap to initiate the USCO displacement experiment.
29. Start injecting the distilled water at a pre-determined injection rate (by trial and error method) to achieve an unstabilized displacement.
30. Keep on scanning the core at regular time intervals to determine the saturations, the phase pressures, and the weight data for further analysis.
31. Every USCO run was stopped after obtaining a couple of scans, once water breakthrough at the outlet end of the core holder was noticed.
32. **SSCO Flow Experiments:** To begin the SSCO flow experiment, remove the water injection end-cap, and reinstall the two-phase injection end-cap, avoiding air entrapment.
33. Readjust the injection rates of oil and water to values the same as those used in Step 21.
34. Inject both oil and water for at least 24 hours (or equivalent to 10 to 15 pore-volumes) to reestablish the initial conditions of saturations. Scan the core.
35. Compare the frequency response obtained in Step 34 to that obtained in Step 26 to confirm that the current saturation level is same as the one calculated in Step 22.
36. Repeat the injection of both oil and water several times by readjusting the pumping rate of both fluids in such a way that a complete imbibition set of SSCO relative permeability curves can be obtained.
37. Collect and store the frequency data, the phase pressure data, and the inlet and outlet weight data after every run, once steady-state has been

achieved. Steady-state has been achieved usually after continuous injection of 8 to 10 pore volumes.

This completes a set of USCO and SSCO flow experiments for a particular fluid and porous medium. Note that it is important to undertake both SSCO and USCO flow experiments using the same core so that the analysis leading to the estimation of the capillary coupling parameter has the same basis.

CHAPTER 6

RESULTS AND DISCUSSION

6.1. Introduction

As mentioned in Chapter 5, several preliminary two-phase flow experiments using LAGO as a nonwetting phase and distilled water as a wetting phase were conducted to test the theoretical findings presented in Chapter 4. However, LAGO was not used in actual experiments, once it was suspected that it might affect the wettability of the sandpacks and the fritted disks. Pertinent sandpack properties are given in Table 5.1. Table 5.2 provides the important properties of the fluids used as wetting and nonwetting phases during SSCO and USCO experimental runs.

In addition to several preliminary flow experiments, three sets of SSCO and USCO flow experiments were performed. In the following sections, data analyses, procedures, and results and their interpretation for each of the experimental sets are presented. Note that an experimental set comprises two types of two-phase flow experiments: SSCO and USCO experiments using the same core and the same fluids for both of the runs. Most of the data analyses were performed using Microsoft Spreadsheet; however, wherever nonlinear regression was needed SPSS-9 was employed.

During the data analysis for each set of experiments, attention has been focused on testing the theory pertaining to the physical origin of interfacial coupling developed in Chapter 4. Specifically, attempts have been made to test Equations (4.54) and (4.55) with the help of measured and calculated experimental data. Capillary pressure gradients and mobility values for both

phases were taken from SSCO runs, while phase velocities to substitute into Equations (4.54) and (4.55) were determined with the help of USCO flow runs. Further details are available in the following sections. Finally, the sensitivity of the most important parameter, the coupling parameter, and the impact of the variation of other parameters on it have been examined.

6.2. Two-Phase Flow Experiments

The first set of SSCO and USCO flow experiments was conducted using a sandpack of 80-120 mesh Ottawa sand; kerosene was used as the nonwetting phase. A blend of light mineral oil and kerosene was used as the nonwetting phase to conduct the second set of experiments, using the same 80-120 mesh Ottawa sand. In the third set of experiments, however, a 100-170 mesh silica sand was used with kerosene as the nonwetting phase. Distilled water was used as the wetting phase in each case. In other words, two different porous media and two different viscosity fluids were used to conduct the two-phase flow experiments.

6.2.1. USCO Flow Experiment (all Sets)

Because of the problem described in Steps 15 and 21 of Section 5.4.1, and because of the fact that the USCO experiments are less time consuming than the SSCO experiments, it was decided to conduct the USCO flow experiments prior to the SSCO flow experiments. However, saturation profiles for the USCO flow experiments were processed only after the calibration curve, with the help of SSCO saturation profiles, was obtained. Table 6.1 provides the experimental parameters for all of the USCO flow runs. To make sure that USCO runs were indeed unstabilized flow runs, the macroscopic capillary number (N_c) as defined by Bentsen (1978) and Islam and Bentsen (1987) was calculated for each USCO run. Table 6.2 shows values of N_c and some other parameters necessary to calculate N_c values for each experimental set. Note

Table 6.1: USCO flow experimental parameters (all Sets).

Set No.	S_{li} (fraction)	S_l^* (fraction)	S_{2r} (fraction)	BT time (sec)	q_l (m ³ /sec)
Set 1	0.1069	0.3140	0.1200	2182	1.85x10 ⁻⁸
Set 2	0.1177	0.2630	0.1000	2213	1.78x10 ⁻⁸
Set 3	0.1615	0.3850	0.1200	3235	1.32x10 ⁻⁸

* Breakthrough time

Table 6.2: Macroscopic capillary numbers (all Sets).

Set No.	A_c (Pa)	λ_{1r}^* (m/Pa.s)	λ_{2r}^* (m/Pa.s)	M_r	N_c
Set 1	971.1013	8.583E-09	5.980E-09	1.4354	0.3473
Set 2	764.4894	6.365E-09	1.202E-09	5.2945	0.2134
Set 3	293.3152	1.169E-09	6.300E-10	1.8561	0.0204

that an unsteady-state displacement process is considered to be unstabilized if the value of N_c is more than 0.01 (Islam and Bentsen, 1986; Sarma, 1988).

6.2.1.1. USCO Saturation Profiles

To obtain USCO saturation profiles, the core holder was scanned periodically once the unsteady-state displacement process started. Such scans were continued until shortly after breakthrough occurred in each of the USCO flow runs. Figure 6.1 shows the raw frequency profiles obtained during the USCO runs of Set 3. Similar raw frequency profiles were obtained during the USCO runs of Sets 1 and 2. Raw frequency data were then processed with the help of the calibration equation obtained from the associated SSCO flow experiment data set (see Section 6.2.2.1). Note that in the USCO frequency profiles, one can observe two distinct zones of saturation, the first in the invaded zone and the second in the non-invaded zone. However, Equation (5.2), which was used to convert the USCO frequency response to saturation, does not recognize this type of distinction in the frequency data. Consequently, the data from the SSCO runs were used to obtain the coefficients for this equation because, in these runs, each profile represents only a single value of saturation.

Figures 6.2 to 6.4 depict the processed saturation profiles for the USCO runs. Two points need to be made with respect to these profiles. First, theory predicts (Bentsen, 1978) that, for homogeneous, isotropic porous media, the saturation profiles should be nearly linear, as they approach the initial saturation to wetting phase, S_1^* . It can be seen from Figures 6.2 to 6.4 that such was not the case in this study. That is, most of the saturation profiles exhibit a “foot” in the immediate vicinity of S_1^* . The porous media used in this study were not perfectly homogeneous. As a consequence, local heterogeneities give rise to perturbations on the saturation profiles. Moreover,

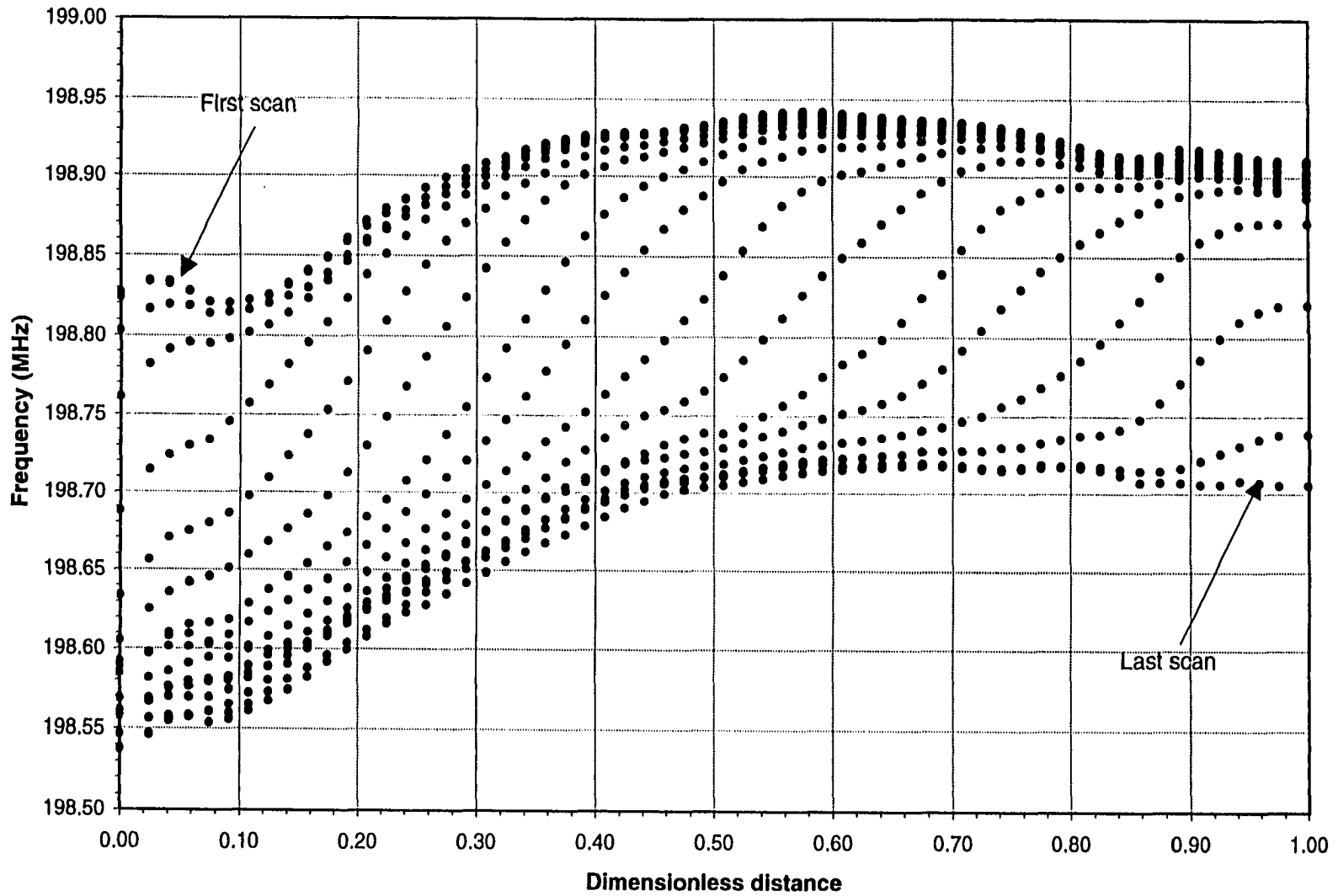


Figure 6.1: Typical unsteady-state raw frequency data at various times along the core holder, USCO (Set 3).

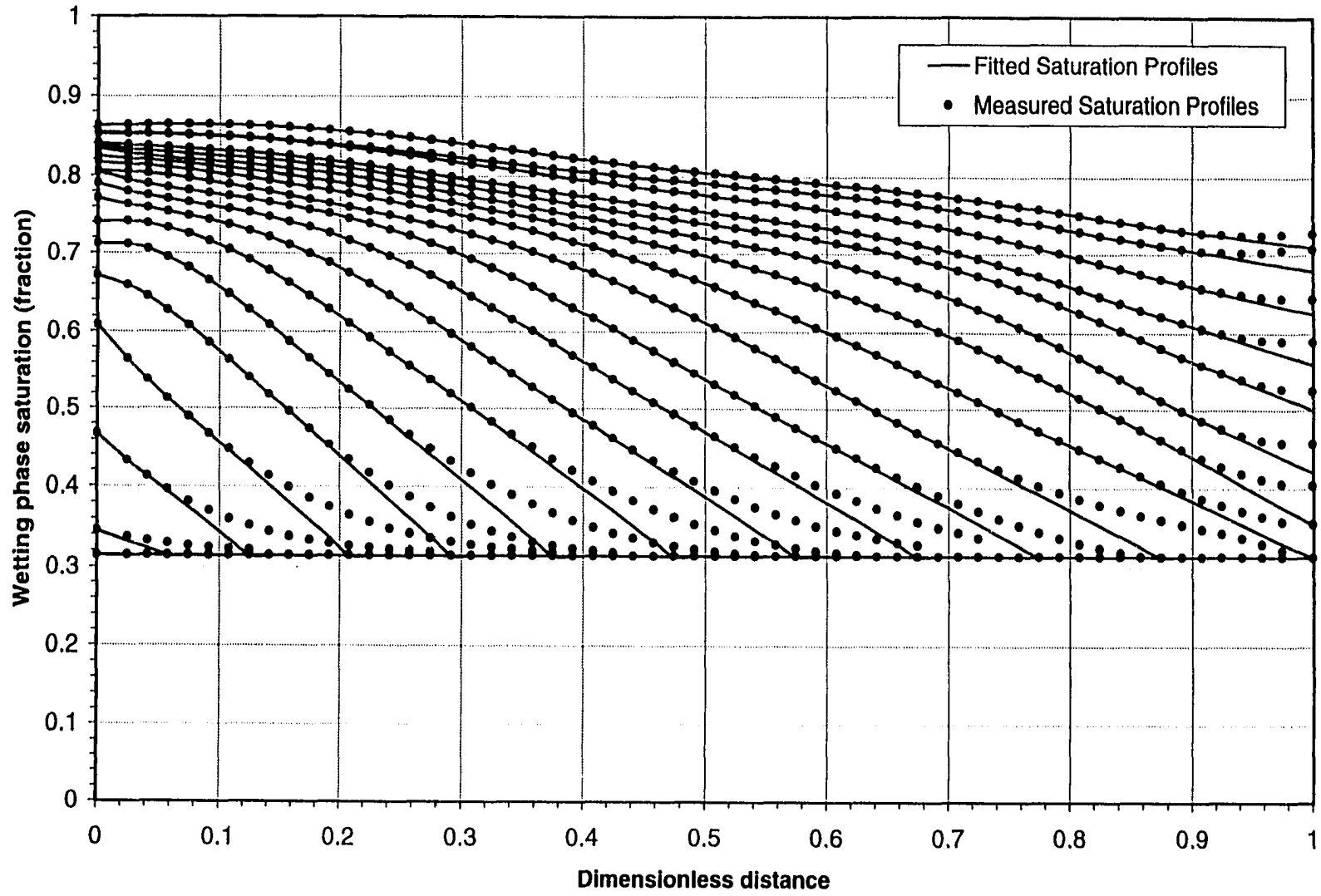


Figure 6.2: Saturation profiles obtained during USCO (Set 1).

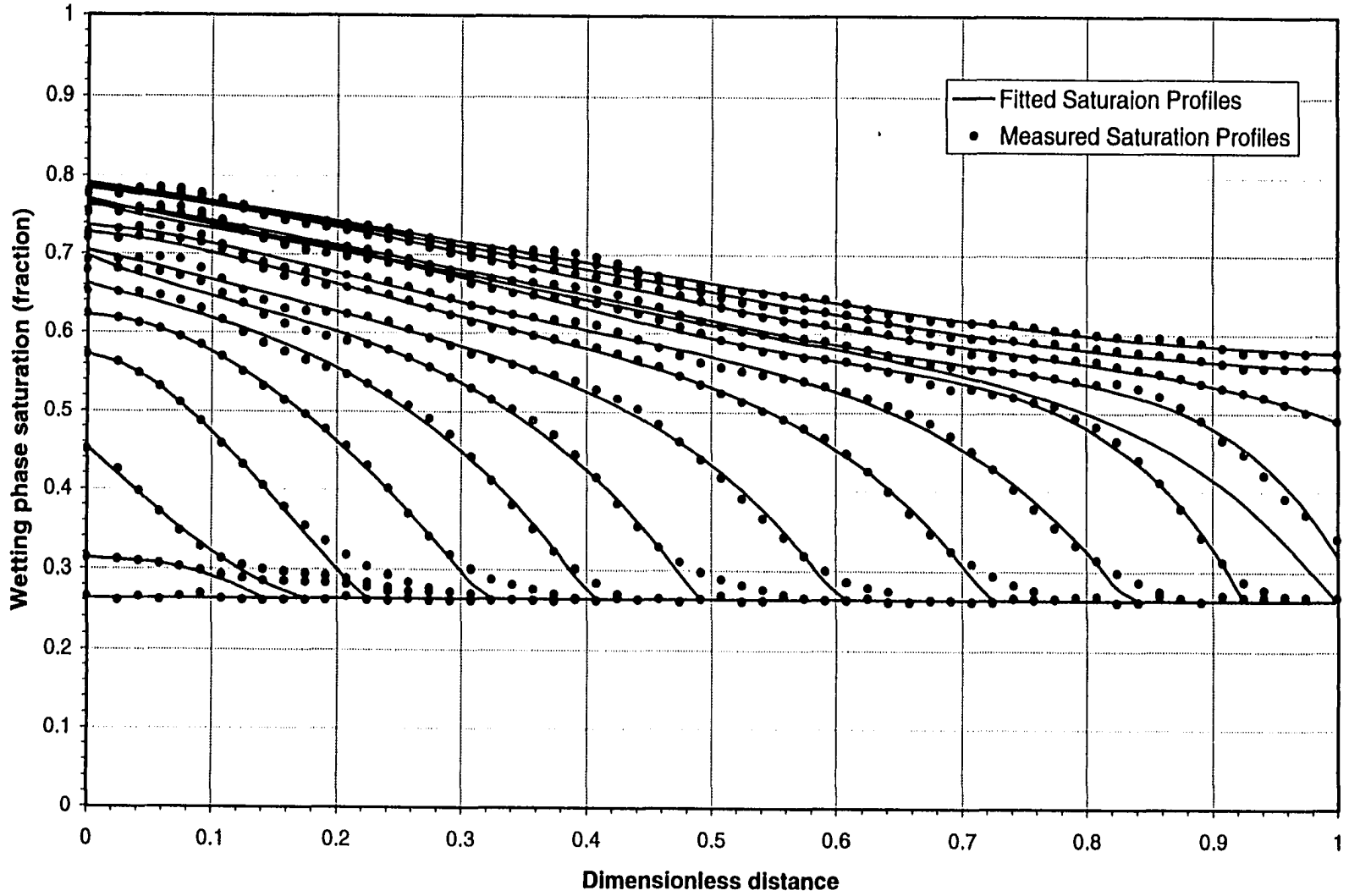


Figure 6.3: Saturation profiles obtained during USCO (Set 2).

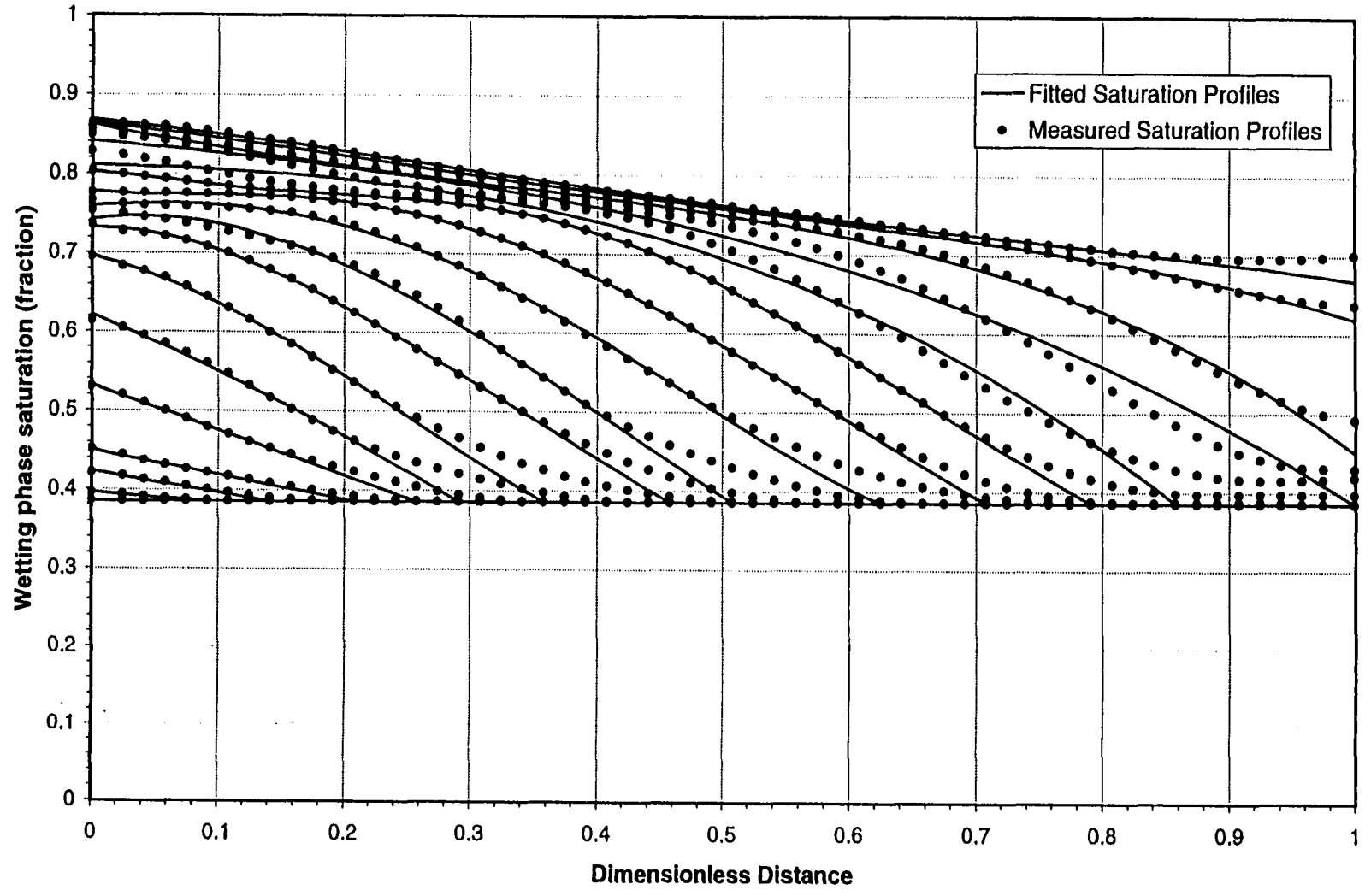


Figure 6.4: Saturation profiles obtained during USCO (Set 3).

when the displacement is stable, capillary forces act to suppress such perturbations. This can be seen in Figure 6.3 where the “foot” on Profile 5 appears to be smaller than that on Profile 4. The magnitude of the capillary force acting to suppress such perturbations depends on saturation, increasing as saturation decreases. This can be seen by comparing Figure 6.3 with Figure 6.4. That is, in Figure 6.3, where $S_1^* = 0.263$, the “feet” associated with the profiles are smaller than those in Figure 6.4, where $S_1^* = 0.385$. Further discussion of these ideas can be found in Section 6.2.1.1.1.

Second, when the original saturation profiles (including the “foot”) were used to determine f_1 , the fraction of the wetting phase flowing at a given saturation, material balance problems occurred. This was a particular problem in the immediate vicinity of the maximum wetting phase saturation ($1 - S_{2r}$) where values of f_1 greater than 1 were obtained, when the original profiles were used to determine f_1 . Material balance dictates that $f_1 = 1 @ S_1 = 1 - S_{2r}$. To deal with this problem, it was decided to remove the “feet” from the saturation profiles. It is to be noted that, when the “feet” were removed, f_1 became very close to 1 at $S_1 = 1 - S_{2r}$, as should be the case.

The USCO saturation profiles were corrected in the following way. The straight-line portion of the saturation profile, in the immediate vicinity of the flood front, was extrapolated towards the down stream end so as to intersect the horizontal saturation profile representing the initial saturation level. This resulted in USCO saturation profiles similar to those obtained in earlier studies (Saeedi, 1979; Sarma, 1988) in which similar unstabilized displacement experiments were conducted.

6.2.1.1.1. Shock Formation

In one-dimensional displacements in which the conditions upon which Buckley-Leverett (Buckley and Leverett, 1942) theory is based are not violated, a sharp front (or shock) eventually establishes itself. However, in unstabilized displacements, such as those conducted in this study (and by Sarma, 1988), steepening of the flood front as the front progresses along the core was observed. The mechanism by which stabilization (steepening) of the saturation profile occurs can be understood by referring to Equations (4.28) and (4.29). With regard to these two equations, it is important to note that, while the phase pressure gradients are both negative, the capillary pressure gradient is positive. Thus, the effect of the capillary pressure gradient is to decrease the magnitude of the wetting phase flux, and increase that of the nonwetting phase flux. Because the magnitude of the capillary pressure gradient increases as the wetting phase saturation decreases, the magnitude of this decrease (increase) in flux increases as the wetting phase saturation decreases. This is so because the magnitude of the slope of the capillary pressure curve increases markedly as the wetting phase saturation decreases. This is particularly the case in the immediate vicinity of the irreducible saturation of the wetting phase. The overall result of a decreasing wetting phase flux and an increasing nonwetting phase flux is a significant steepening of the saturation front, particularly in the immediate vicinity of the irreducible saturation to the wetting phase.

6.2.1.2. Fractional Flow

Figures 6.2 to 6.4 show comparisons of measured and fitted saturation profiles along the length of the core holder scanned at a fixed time interval for each set of experiments. The least squares method with various degree polynomials was used to determine the best fit saturation profiles. Using the method described in Section 4.7.2, the best-fit saturation profiles versus dimensionless distances for each set were used to construct Q_1 versus time curves (Figures

6.5 to 6.7) for various saturation levels. Fractional flow data versus wetting phase saturation was then determined by differentiating the fitted polynomial equations obtained for the Q_i versus time curves (Figures 6.5 to 6.7) with respect to a specific time (see Equation 4.66). The time chosen for this purpose for each case was the breakthrough time (Table 6.1) that corresponds to the saturation profile obtained at the time when the unstabilized flood front reaches the outlet end of the core.

In actual calculations [see Equations (4.54) and (4.55)], velocities rather than fractional flows of wetting and nonwetting phases are required. They were determined by multiplying the fractional flow values by the total volumetric injection rate and dividing it by the cross-sectional area of the core (APPENDIX A). Moreover, for each experimental set, Figures 6.8 to 6.10 depict the velocity variation of the wetting and nonwetting phases with the wetting phase saturation. It is important to mention here that the parametric equation used to fit the fractional flow curve was the one that was used by Sarma (1988). For the reader's convenience, this equation is given below.

$$f_1 = \frac{S_1 - S_{1i}}{S_{1m} - S_{1i} - g_1(S_{1m} - S_1) - g_2(S_{1m}^2 - S_1^2) - g_3(S_{1m}^3 - S_1^3) - g_4(S_{1m}^4 - S_1^4)} \quad (6.1)$$

By observing the saturation profiles shown in Figures 6.2 to 6.4 and comparing them with those shown in Figures 6.21 to 6.23 (Section 6.2.2.1), it becomes obvious that neither of the USCO runs were started at the actual connate water saturation levels nor were they stopped at the actual residual oil saturation levels. This was done because of the operational difficulty described in Step 15 of Section 5.4.1. Consequently, fractional flow data have to be adjusted accordingly. That is to say, it was imperative to assume zero fractional flow at a higher initial water saturation level than the actual connate water saturation determined during the SSCO flow runs. This assumption appeared to be consistent with reality as no water production was observed

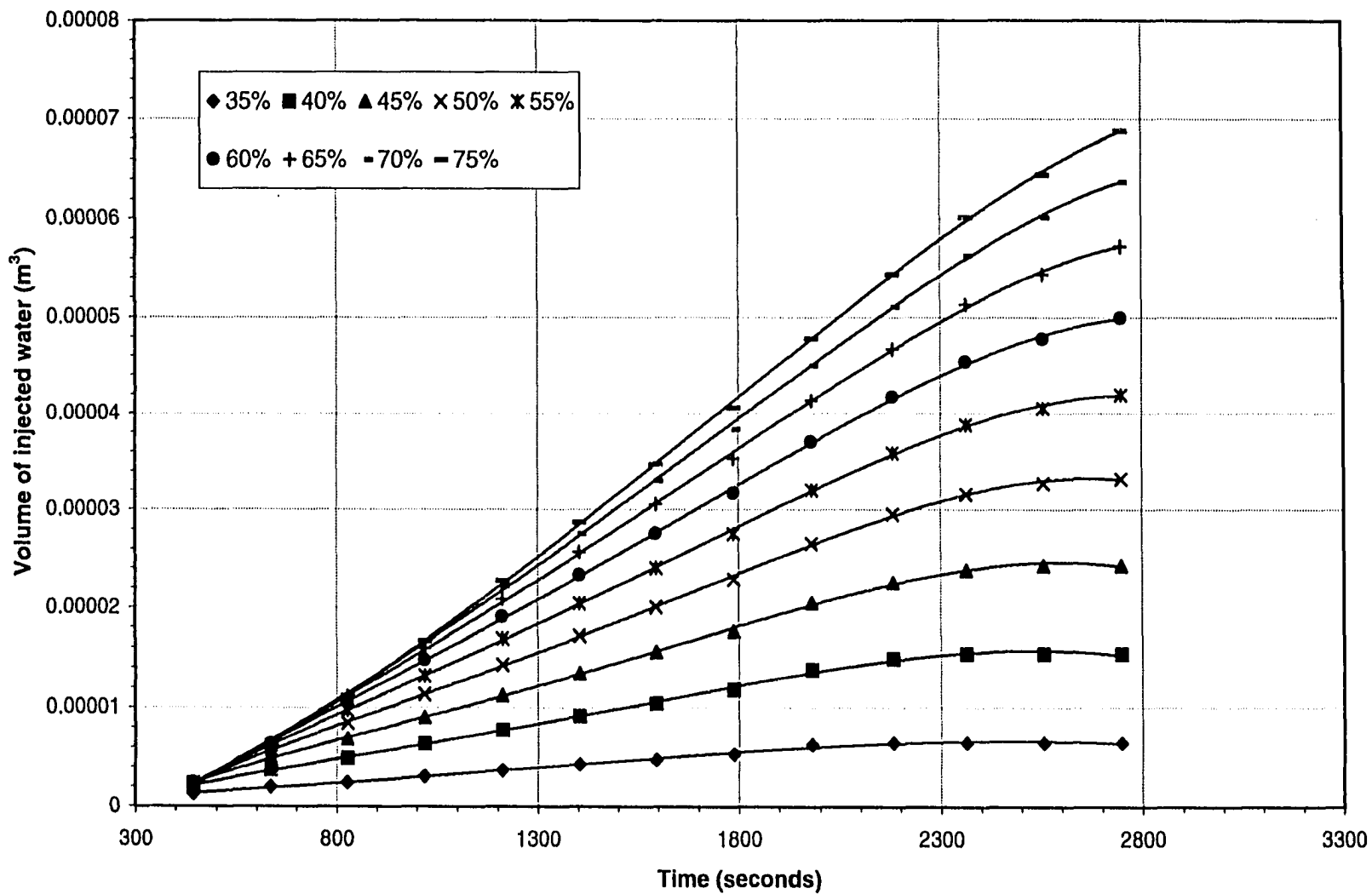


Figure 6.5: Volume of injected water versus time for various saturation levels, USCO (Set 1).

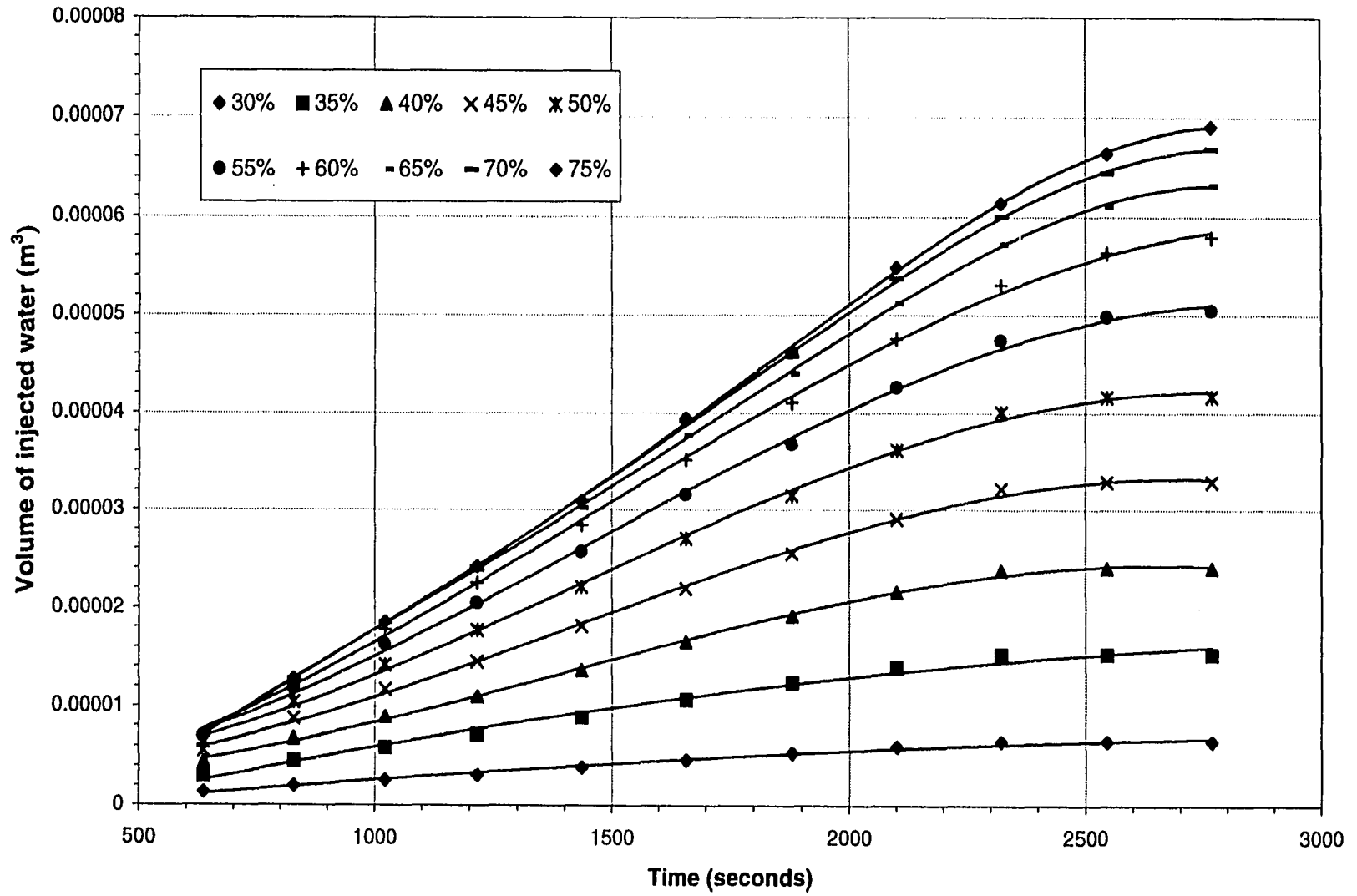


Figure 6.6: Volume of injected water versus time for various saturation levels, USCO (Set 2).

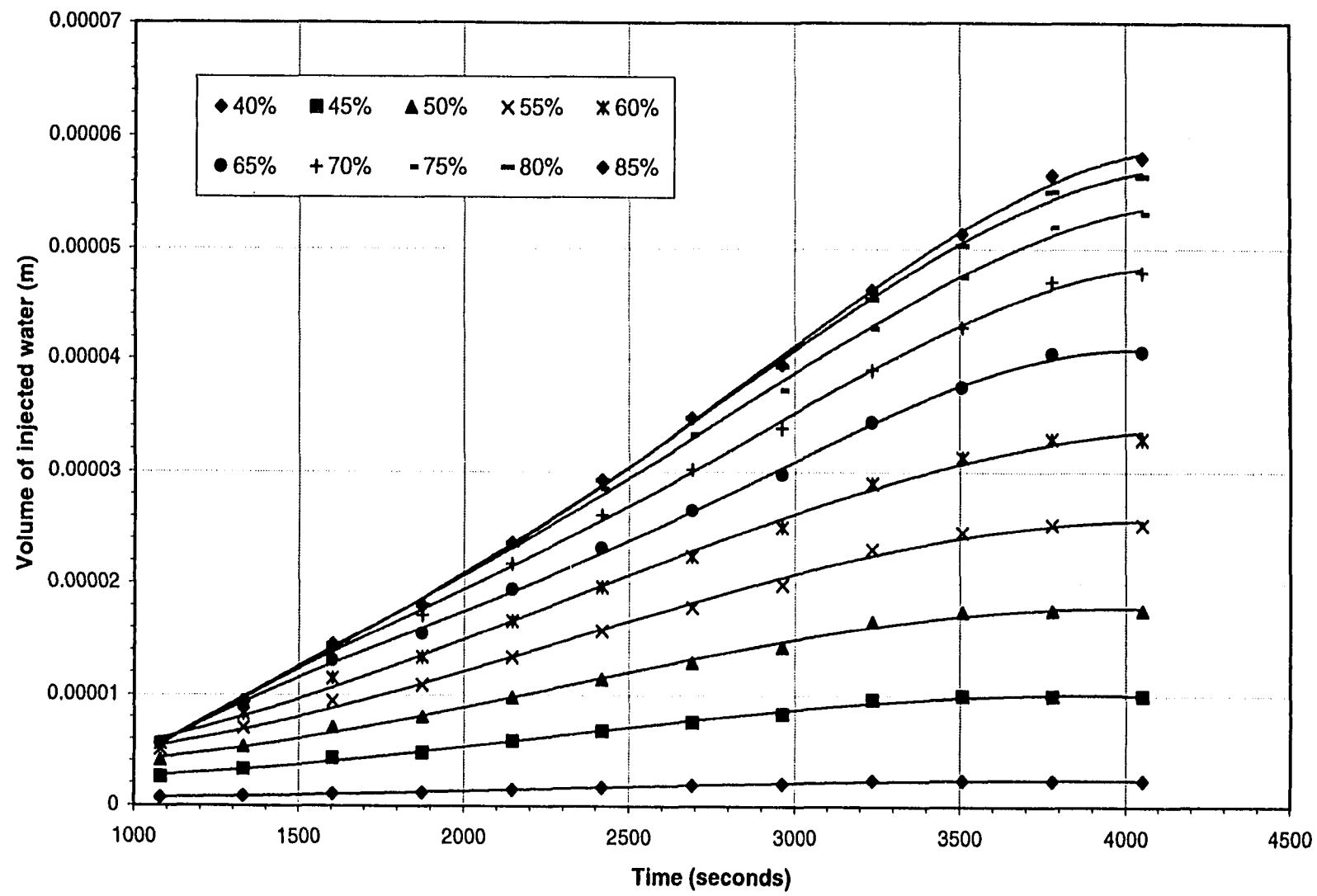


Figure 6.7: Volume of injected water versus time for various saturation levels, USCO (Set 3).

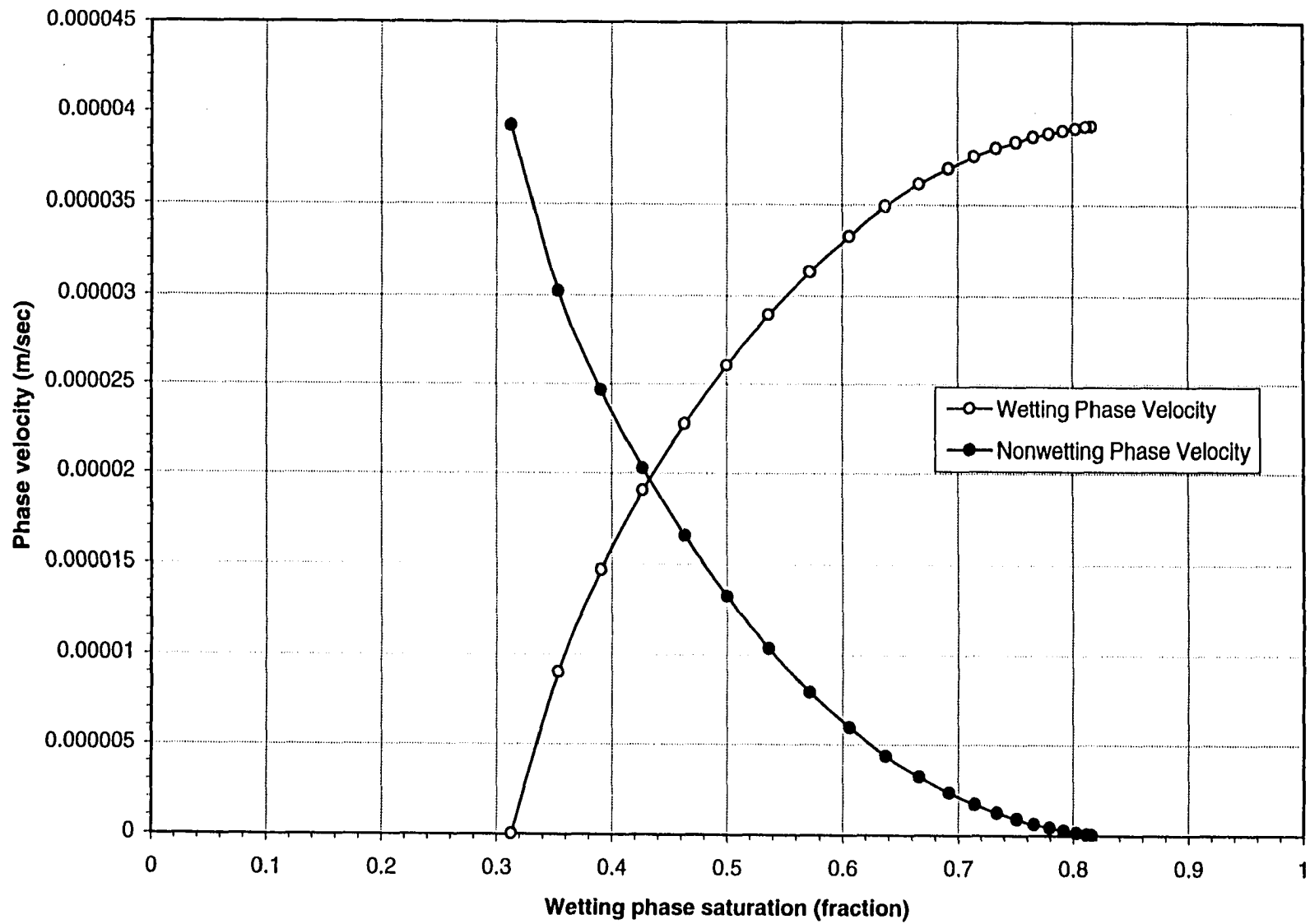


Figure 6.8: Wetting and nonwetting phase velocities at 2182 seconds, USCO (Set 1).

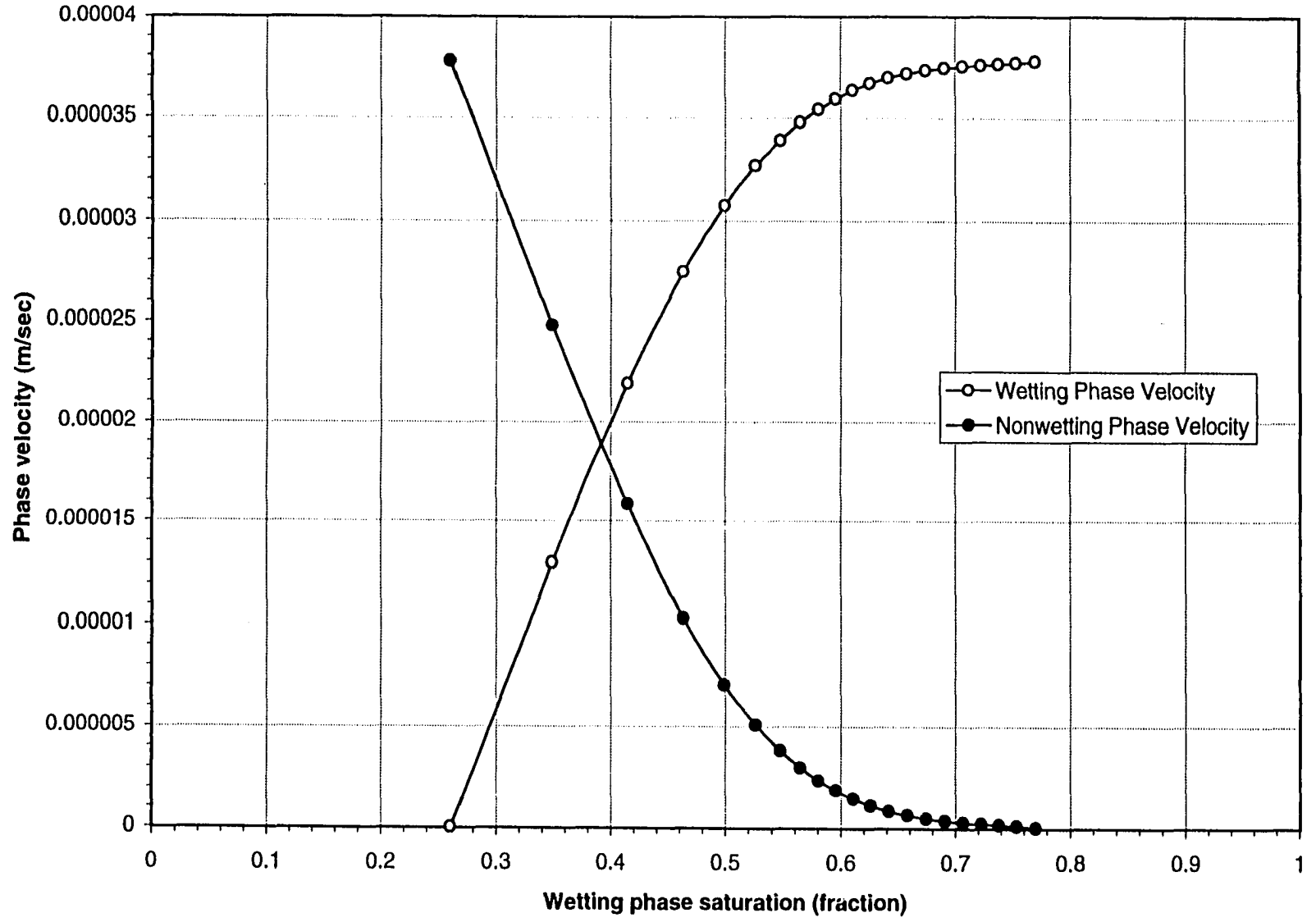


Figure 6.9: Wetting and nonwetting phase velocities at 2213 seconds, USCO (Set 2).

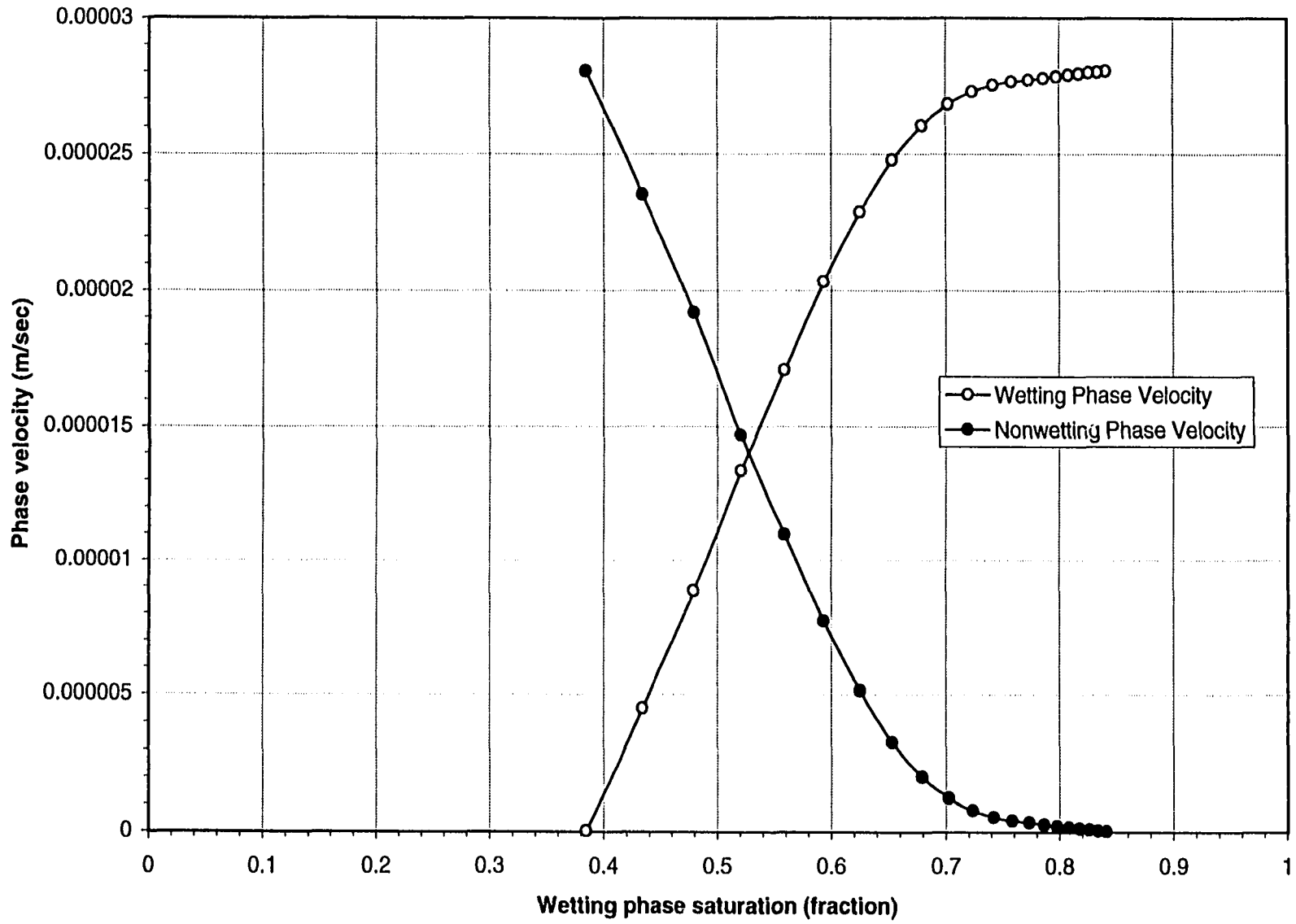


Figure 6.10: Wetting and nonwetting phase velocities at 3235 seconds, USCO (Set 3).

until breakthrough occurred during all of the USCO runs. Similarly, as no significant amount of oil production after the breakthrough was observed, fractional flow was assumed to have attained its maximal level, even when the actual (steady-state) residual oil saturation was not achieved during the displacement runs.

6.2.1.3. Capillary Pressure Gradient

By looking at Equations (4.54) and (4.55), it becomes clear that $\partial P_c / \partial x$ must be determined by using unsteady-state phase pressure gradients; that is,

$$\frac{\partial P_c}{\partial x} = R_{12} \cdot \frac{\partial p_2}{\partial x} - \frac{\partial p_1}{\partial x}. \quad (6.2)$$

Because of the operational difficulty described in Step 15 of Section 5.4.1, it appeared that during USCO runs insufficient time was available to attain good pressure data. Moreover, because of the scatter in the measured values of the phase pressures (Figures 6.11 to 6.13 and APPENDIX B), it becomes extremely difficult to get an appropriate best-fit curve with monotonic characteristics. To overcome this difficulty, it was decided to use the capillary pressure (Figures 6.14 to 6.16 and APPENDIX C) data obtained during the SSCO runs (APPENDIX D) along with the breakthrough saturation gradient (Figures 6.17, 6.18 and APPENDIX E) data obtained during the USCO runs to construct the capillary pressure gradient.

In addition to the observed scatter in phase pressure data, this approach was adopted because of the fact that, for a particular porous medium/fluid system, a capillary pressure curve remains unchanged regardless of the procedure (SSCO or USCO) used to measure the data (observed by Sarma 1988). Moreover, sufficient time was available to measure SSCO phase pressure data whereas there appeared to be insufficient time to obtain accurate USCO phase pressure data. Therefore, for capillary pressure calculations, SSCO phase pressure data were considered to be more reliable as compared to the

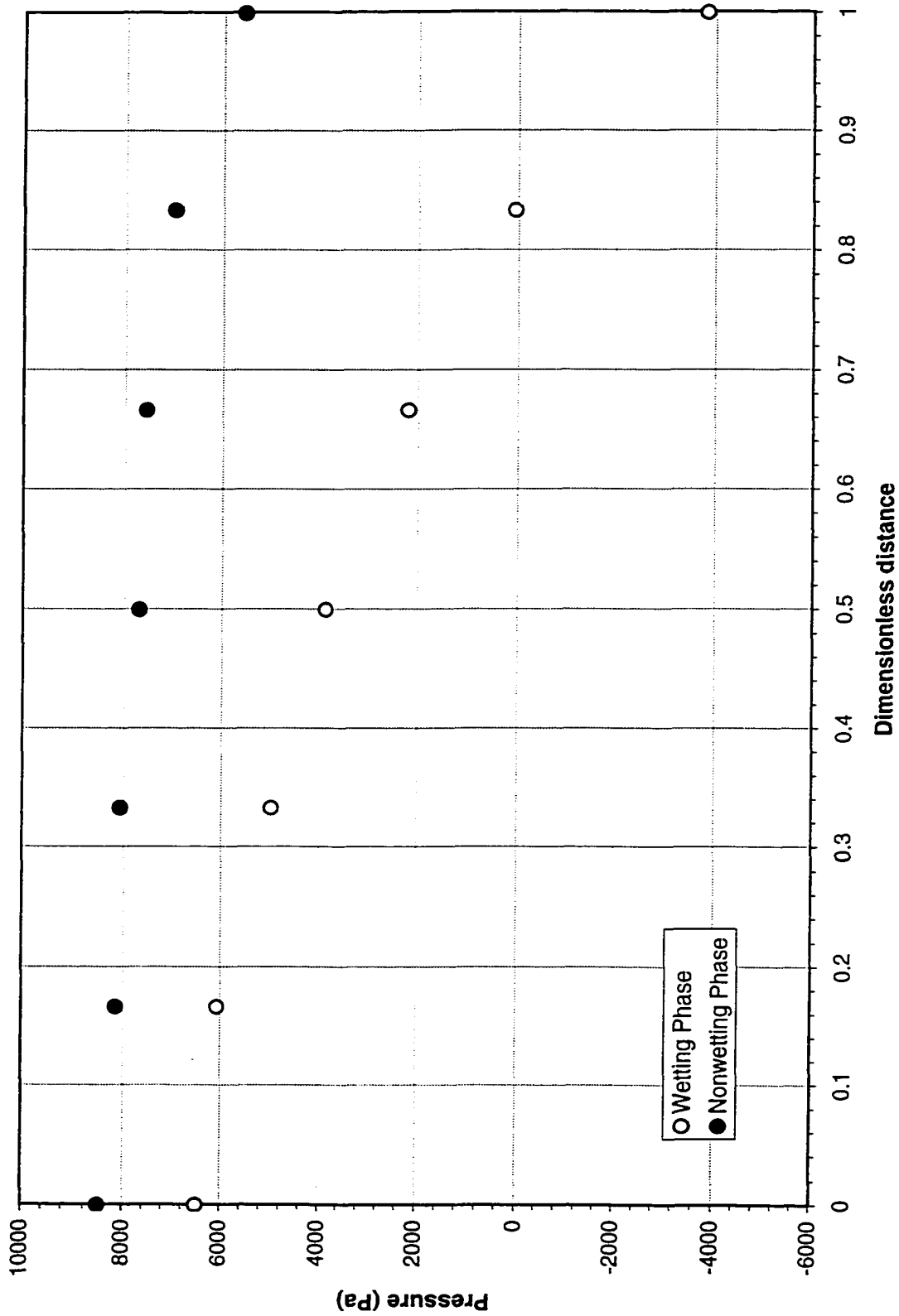


Figure 6.11: Measured phase pressures, USCO (Set 1).

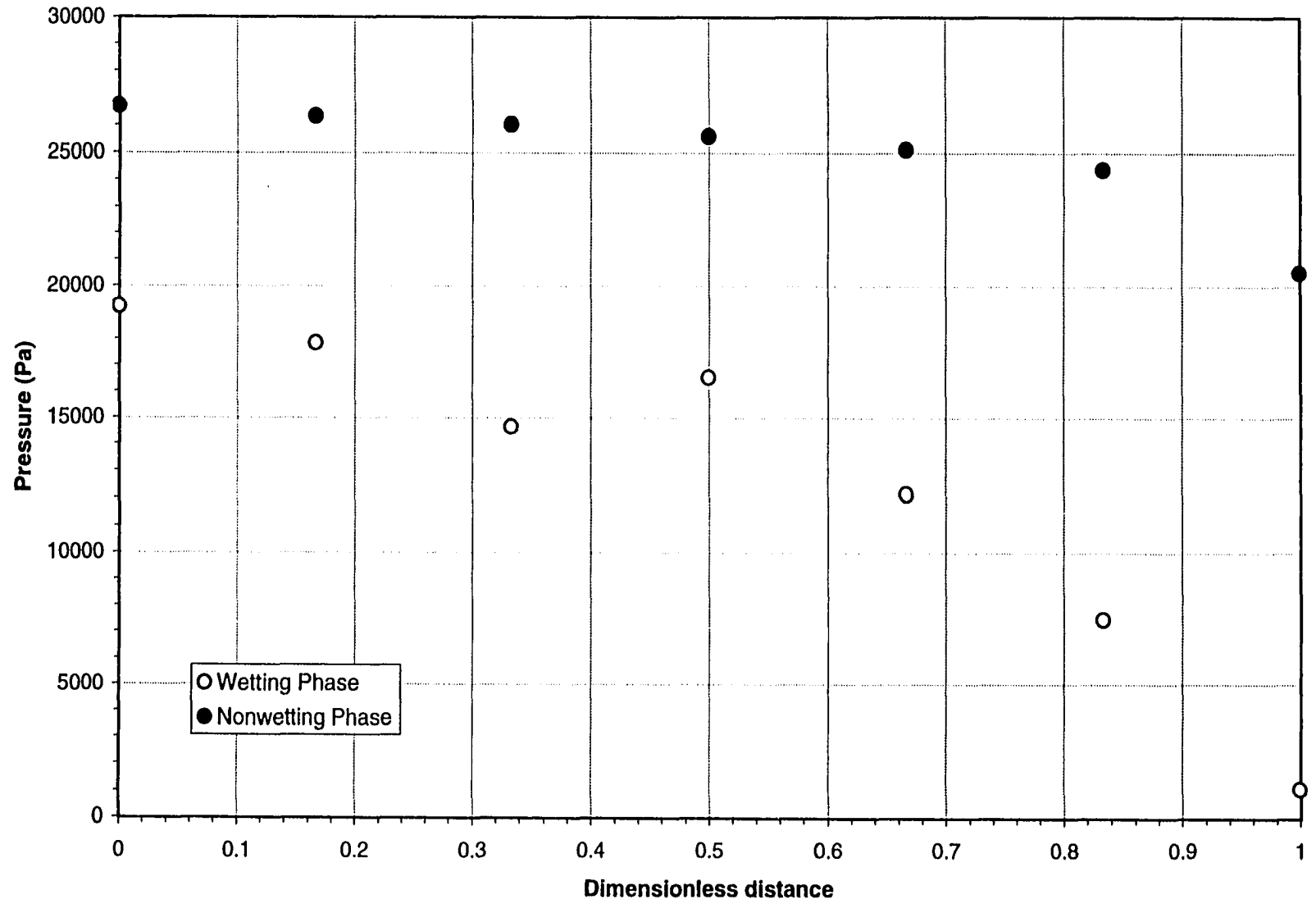


Figure 6.12: Measured phase pressures, USCO (Set 2).

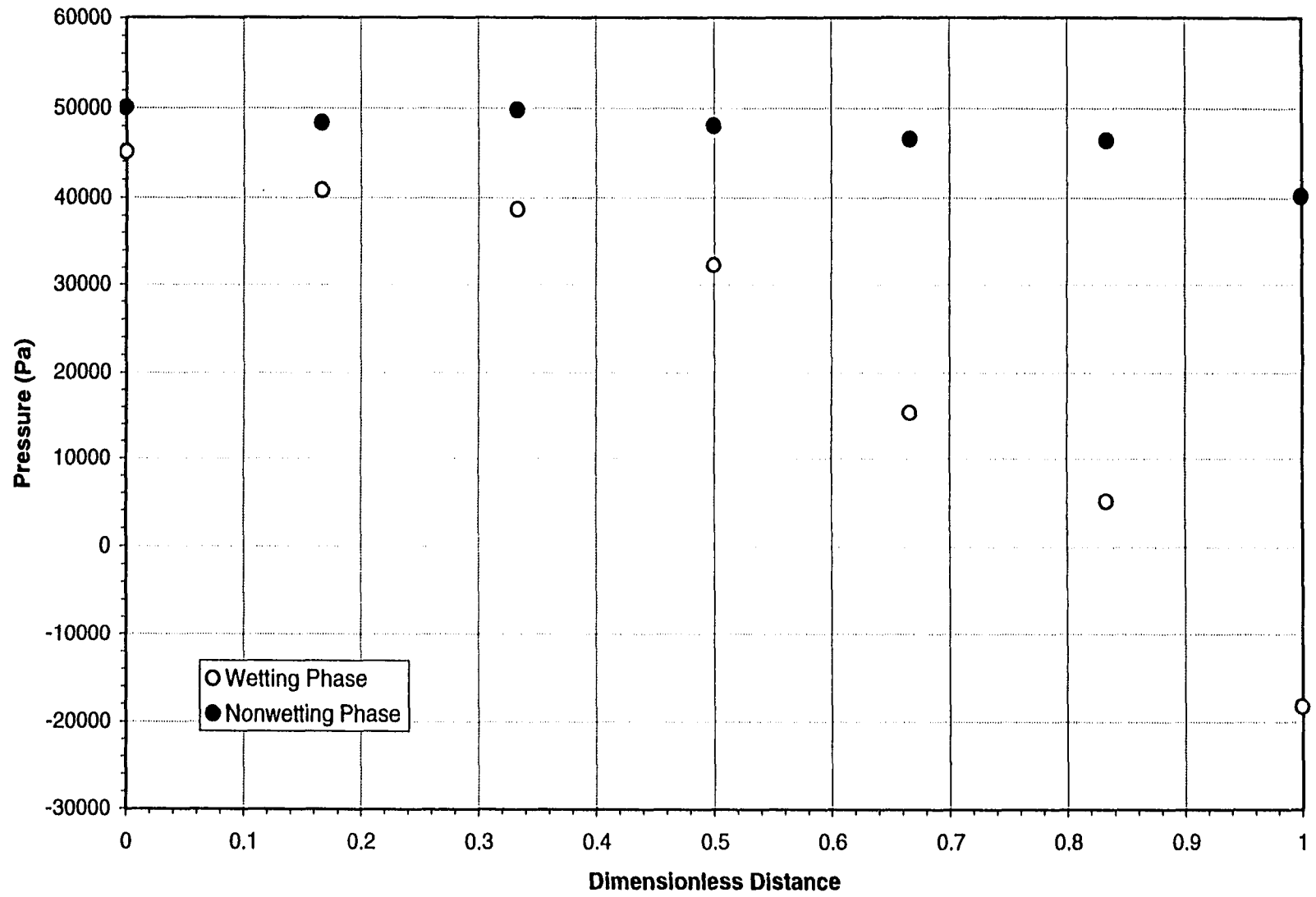


Figure 6.13: Measured phase pressures, USCO (Set 3).

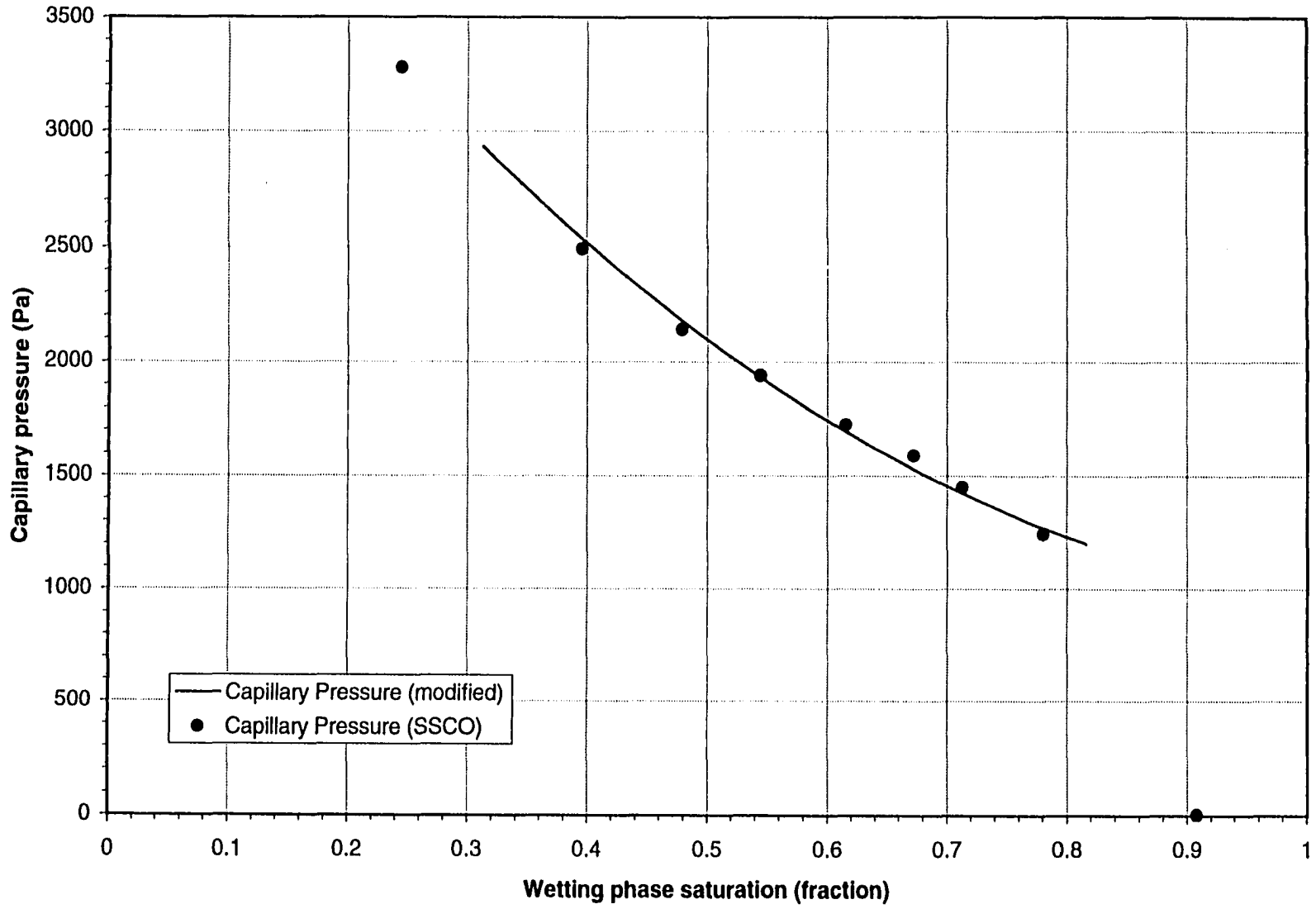


Figure 6.14: Capillary pressure versus wetting phase saturation, SSCO (Set 1).

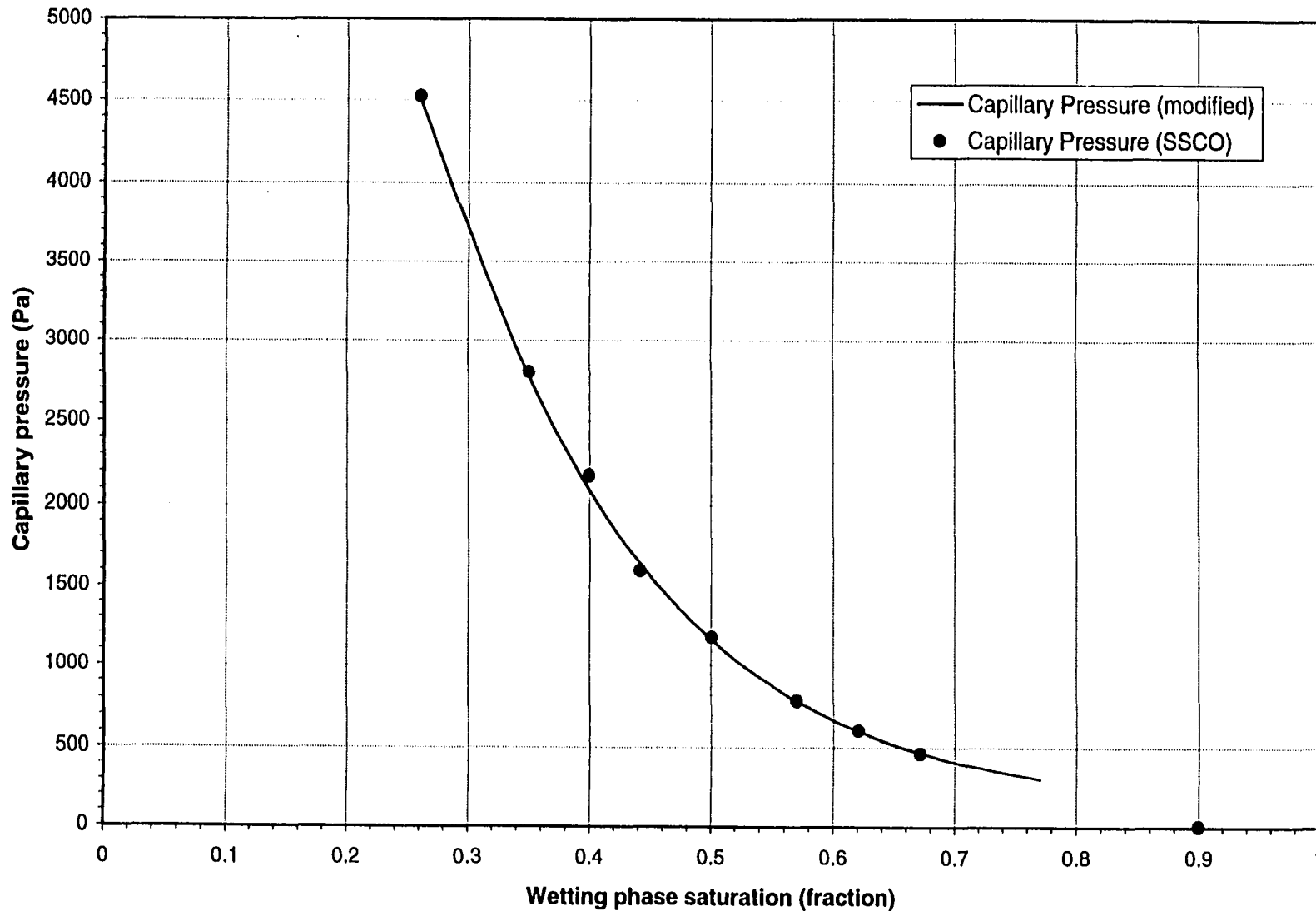


Figure 6.15: Capillary pressure versus wetting phase saturation, SSCO (Set 2).

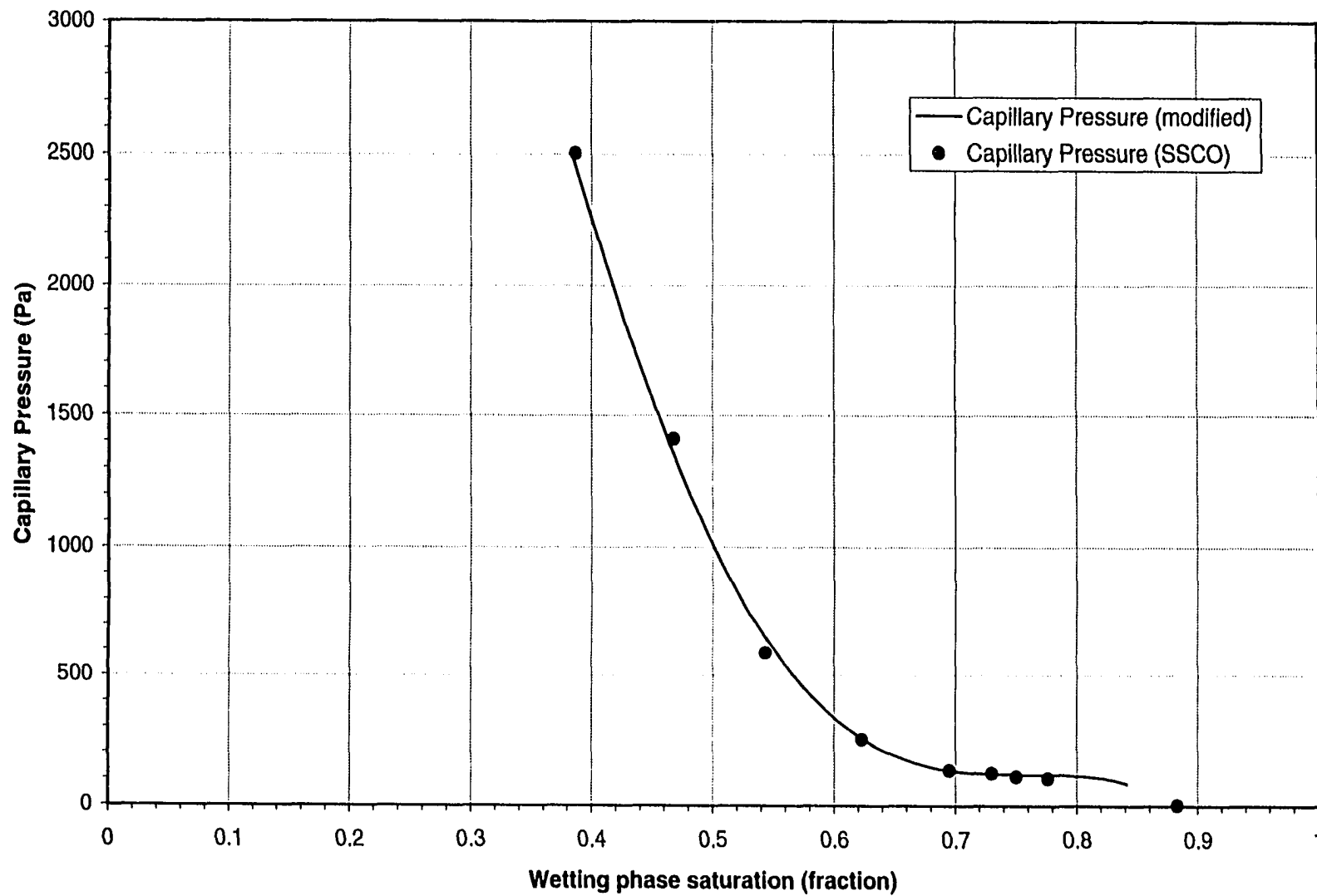


Figure 6.16: Capillary pressure versus wetting phase saturation, SSCO (Set 3).

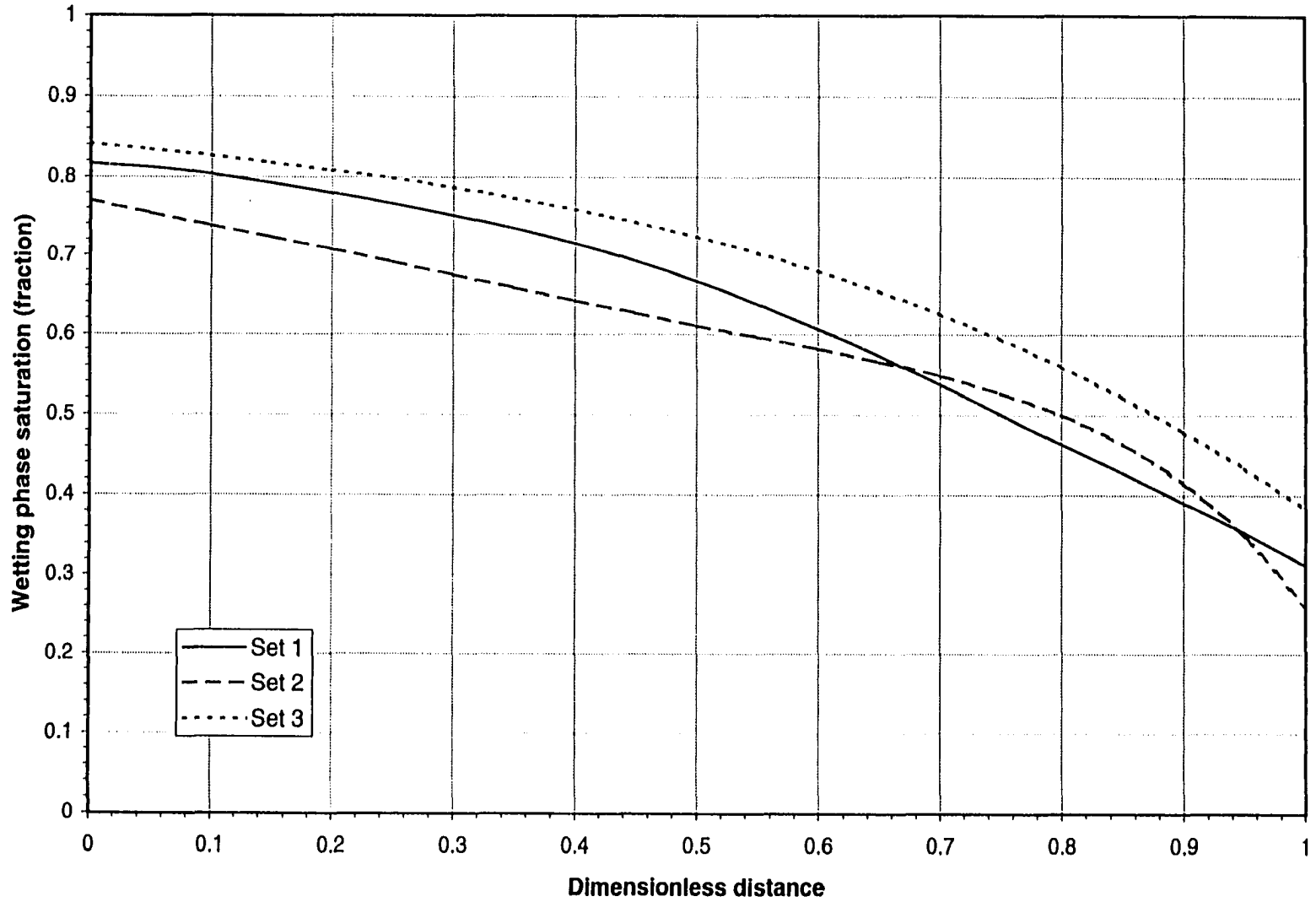


Figure 6.17: Wetting phase saturation profiles at breakthrough times, USCO (all Sets).

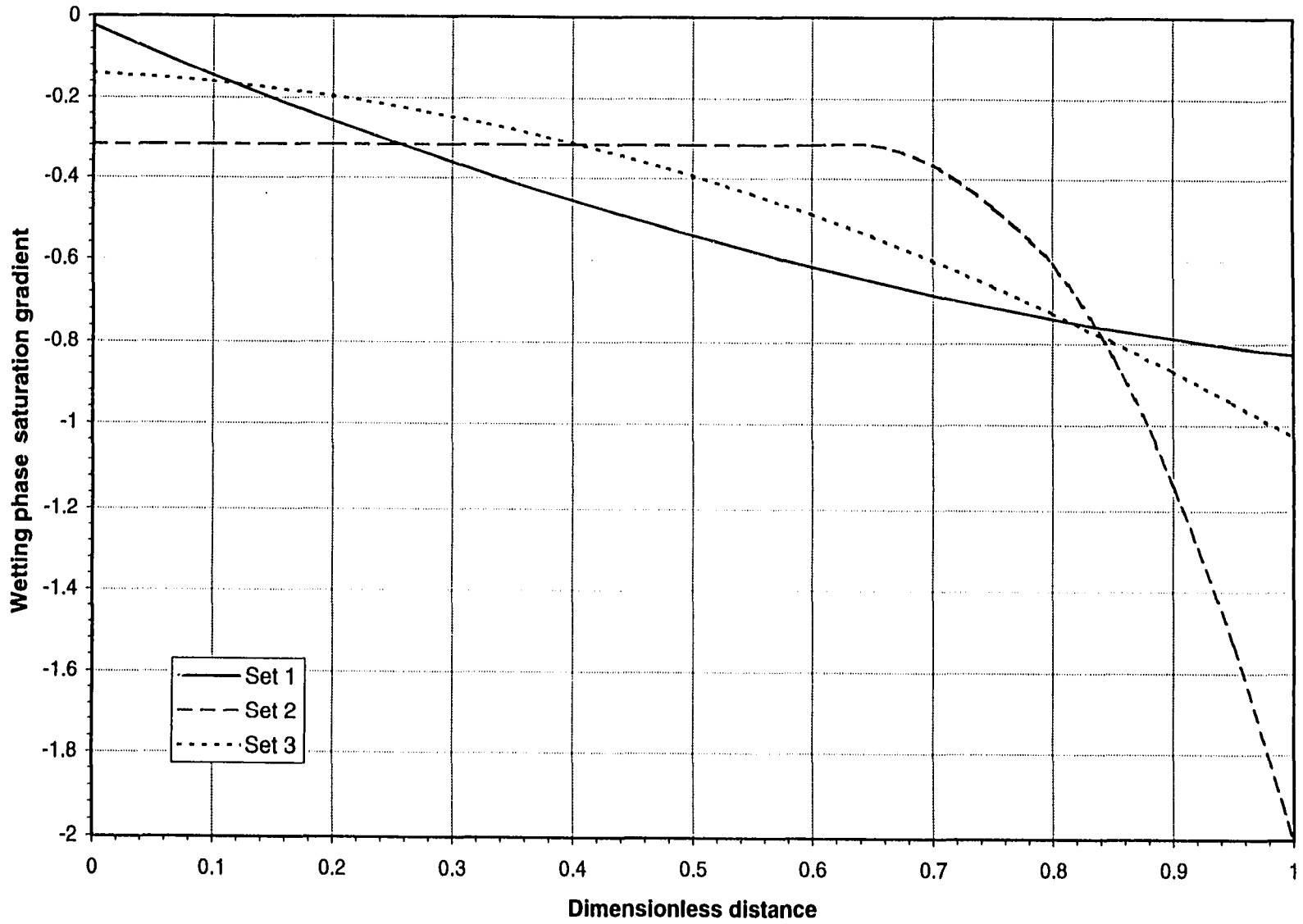


Figure 6.18: Wetting phase saturation gradients at breakthrough times, USCO (all Sets).

phase pressure data obtained during USCO runs. Equation (6.3) represents this approach.

$$\frac{\partial P_c}{\partial x} = \frac{\partial P_c}{\partial S_1} \cdot \frac{\partial S_1}{\partial x} \quad (6.3)$$

6.2.1.4. R_{12} Calculation

In a previous experimental study at the University of Alberta, using the same porous medium (Ottawa sand), Manai (1991) observed unequal pressure gradients for the wetting and the nonwetting phases. However, the nonwetting phase used in his study was not the same as those used in this study. Bentsen (1992a) used the limited experimental data obtained by Manai (1991) to construct a relation between the phase pressure gradients ratio (R_{12}) and the normalized nonwetting phase saturation ($1-S$). Based on an analysis of these data, he concluded that R_{12} was a weak function of normalized nonwetting phase saturation. The relation proposed by Bentsen (1992a) is given below.

$$R_{12} = 1 - a(1 - S) \quad (6.4)$$

Using the results of the SSCO flow runs conducted in this study, data analyses were performed to verify Equation (6.4). Unfortunately, based on the data plotted in Figure 6.19, no specific conclusions could be drawn with respect to the validity of Equation (6.4). Nevertheless, the R_{12} versus $1-S$ graph for Set 2 seems to be in agreement with Equation (6.4). However, as indicated on the plot (Figure 6.19), R^2 values for all of the curves are very poor. Because of the outlying data points, a best-fit straight line for Set 3 was not plotted, as such a plot might mislead the reader. Moreover, in Set 1 and Set 3, the dimensionless parameter (a) was found as a positive entity, rather than a negative, as should be the case according to Equation (6.4). Therefore, to overcome these inconsistencies, for the data analysis during the current study,

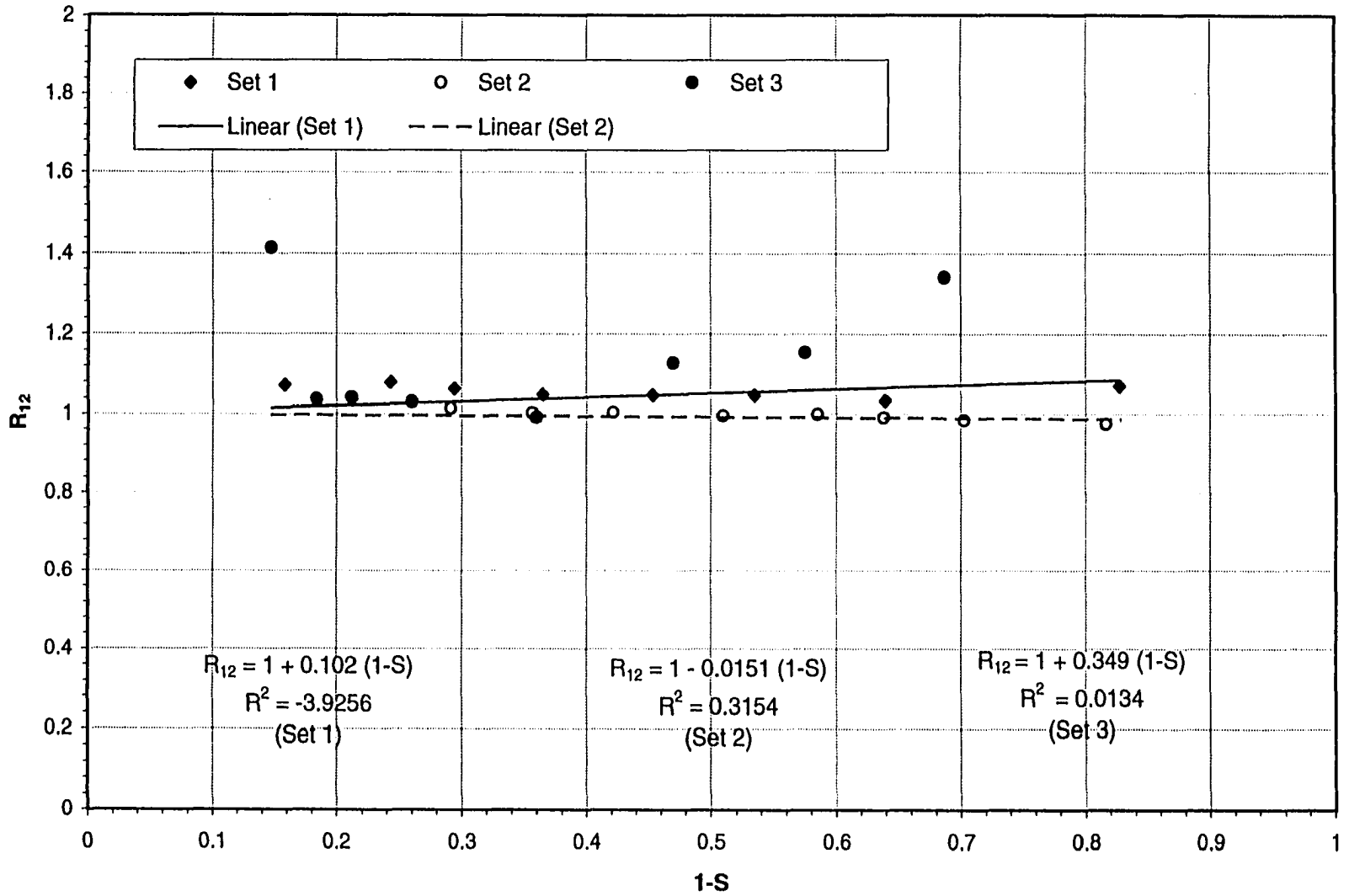


Figure 6.19: Ratio of wetting phase pressure gradients to nonwetting phase pressure gradients, versus normalized nonwetting phase saturation, SSCO (all Sets).

it was decided to use $R_{12} = 1$ for all cases. This should not introduce a significant amount of error into the analysis (Bentsen, 1998a, 1994a).

6.2.2. SSCO Flow Experiment (all Sets)

In order to determine steady-state effective mobilities to the wetting and nonwetting phases during an imbibition process, oil and water were injected at various constant flow rates while keeping the total pressure build-up in the core holder within its operational limit (25 psi). Various experimentally measured and calculated parameters related to Sets 1, 2 and 3 are given in Tables 6.3, 6.4 and 6.5, respectively. It should be noted that the mobilities reported in Tables 6.3, 6.4 and 6.5 are not true mobilities; rather, they are mobilities divided by the length (0.60 m) of the core. It was convenient to report the mobilities in this way because plotting the saturation and phase pressure versus dimensionless distance, rather than distance, facilitated the curve fitting process.

6.2.2.1. SSCO Saturation Profiles

In SSCO flow runs, the core holder was scanned at the beginning of injection and at the time when steady-state had been achieved. Steady-state was achieved usually after continuous injection of 8 to 10 pore volumes. Various ratios of wetting phase injection rates to nonwetting phase injection rates (Tables 6.3 to 6.5) were used to achieve different saturation levels during all SSCO flow runs.

Figure 6.20 shows the raw frequency profiles obtained during the SSCO runs of Set 3. Similar raw frequency profiles were obtained during the SSCO runs of Sets 1 and 2. A close observation of Figure 6.20 reveals that, while all of the profiles are essentially parallel to one another, they are certainly not horizontal. Moreover, there appear to be minor anomalies on each of the profiles. To understand why this should be the case, it is important to keep in

Table 6.3: SSCO flow experimental parameters (Set 1).

Run No.	q_1/q_2	S_1 (fraction)	dp_1/dx (Pa)	dp_2/dx (Pa)	λ_1 (m/Pa.s)	λ_2 (m/Pa.s)
1	0	0.1069	0	-15548.47	0	8.01E-09
2	0.0583	0.2449	-19484.58	-18202.16	3.68E-10	6.75E-09
3	0.2724	0.3957	-17952.69	-17364.91	1.37E-09	5.19E-09
4	0.5552	0.4796	-15960.16	-15239.63	2.37E-09	4.46E-09
5	0.7633	0.5448	-14975.41	-14313.51	2.52E-09	3.45E-09
6	1.3026	0.6158	-14230.78	-13568.88	3.58E-09	2.88E-09
7	2.1608	0.6723	-13362.03	-12576.04	4.69E-09	2.3E-09
8	3.5233	0.7133	-11914.14	-11045.40	5.5E-09	1.68E-09
9	6.2193	0.7811	-10590.34	-9887.08	7.29E-09	1.26E-09
10	infinity	0.9084	-5750.23	0	1.31E-08	0

Table 6.4: SSCO flow experimental parameters (Set 2).

Run No.	q_1/q_2	S_1 (fraction)	dp_1/dx (Pa)	dp_2/dx (Pa)	λ_1° (m/Pa.s)	λ_2° (m/Pa.s)
1	0	0.1177	0	-19898.27	0	1.368E-09
2	0.1030	0.2610	-68175.36	-69995.57	1.247E-10	1.179E-09
3	0.2696	0.3502	-59074.28	-60149.86	2.950E-10	1.075E-09
4	0.5674	0.4001	-53489.52	-54068.68	5.400E-10	9.415E-10
5	0.9354	0.4420	-50469.62	-50510.99	8.697E-10	9.290E-10
6	1.7352	0.5010	-40872.12	-41120.33	1.336E-09	7.651E-10
7	2.9051	0.5702	-32184.73	-32101.99	2.021E-09	6.976E-10
8	5.2599	0.6210	-23828.28	-23786.91	2.954E-09	5.626E-10
9	7.3675	0.6720	-25813.97	-25483.02	3.788E-09	5.209E-10
10	infinity	0.9001	-6412.12	0	1.347E-08	0

Table 6.5: SSCO flow experimental parameters (Set 3).

Run No.	q_1/q_2	S_I (fraction)	dp_1/dx (Pa)	dp_2/dx (Pa)	λ_1^* (m/Pa.s)	λ_2^* (m/Pa.s)
1	0	0.1615	0	-33021.01	0	9.170E-10
2	0.0810	0.3872	-104827.88	-78219.01	3.810E-11	6.306E-10
3	0.2043	0.4680	-93906.59	-81405.12	9.350E-11	5.280E-10
4	0.4295	0.5439	-82530.24	-73193.65	1.644E-10	4.317E-10
5	0.9200	0.6235	-72850.00	-73638.59	3.075E-10	3.307E-10
6	2.1295	0.6953	-64865.87	-62987.72	4.954E-10	2.396E-10
7	3.2434	0.7302	-69623.26	-67009.45	6.096E-10	1.953E-10
8	4.2580	0.7503	-74463.38	-71975.87	6.988E-10	1.698E-10
9	8.3589	0.7768	-79965.39	-56573.27	8.051E-10	1.362E-10
10	infinity	0.8835	-44471.18	0	1.456E-09	0

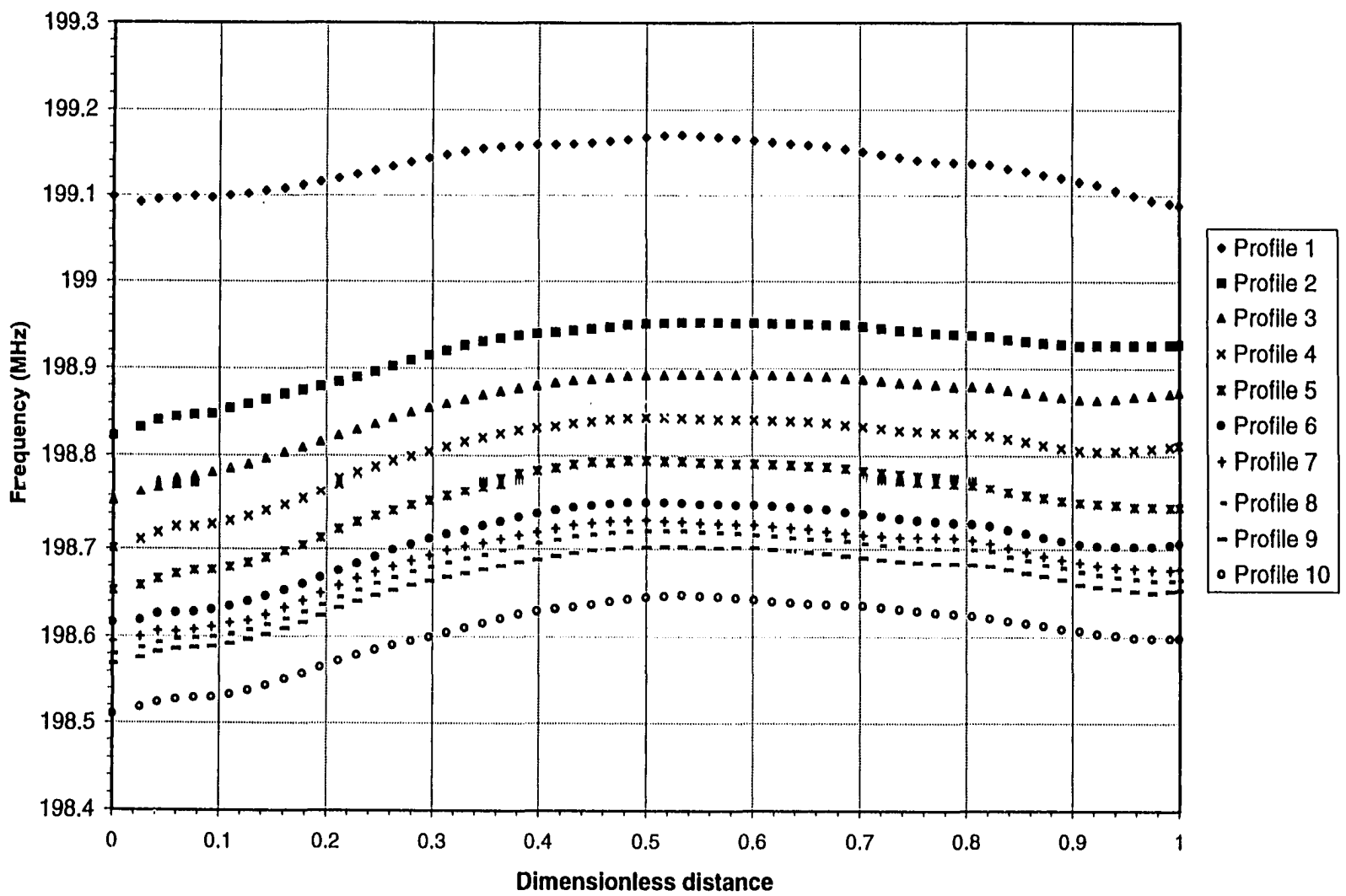


Figure 6.20: Typical steady-state raw frequency data along the core holder, SSCO (Set 3).

mind that capacitance based methods for measuring saturation are extremely sensitive to very minor variations in the thickness, width, surface roughness and attitude of the core holder as it passes through the water saturation sensor. Moreover, minor variations in packing and/or porosity along the length of the core are expected to have an effect on the frequency profiles. It is thought that minor variations in the core holder dimensions, surface roughness and porosity give rise to the minor perturbations observed on the frequency profiles. With respect to the observed curvature in the frequency profiles, it is thought that the attitude of the core holder is the most important factor. In particular, because of mechanical limitations in the travel-track system currently being used, it was not possible to keep the core holder perfectly horizontal as it was drawn through the water saturation sensor. Such variations in the attitude of the core holder as it passes through the water saturation sensor are thought to be the most likely explanation for the curvature observed in the frequency profiles.

In a steady-state displacement, saturation should be essentially constant along the length of the core holder (Manai, 1991). Consequently, the frequency response, for a given constant value of saturation, should also be essentially invariant with distance. However, because of problems associated primarily with the attitude of the core holder, the frequency profiles depicted in Figure 6.20 exhibit curvature. To eliminate such curvature, and to obtain true saturation profiles, the following procedure was used. First, it was assumed that, for each of the frequency profiles shown in Figure 6.20, the saturation, as determined by material balance, was constant along the length of the core. Second, for each of the 60 datum points along the length of the core holder, the nonlinear regression methods found in SPSS-9, a Windows based software program, together with the saturation and frequency data associated with a particular datum point, were used to determine the best values of the A and B parameters in Equation (5.2). Third, the raw frequency data, together

with Equation (5.2), was used to construct Figure 6.23. This process was repeated to obtain the saturation profiles shown in Figures 6.21 and 6.22.

It is to be noted that the sensitivity of the frequency response increases with wetting phase saturation level; therefore, most of the saturation profiles at low levels of the wetting phase saturation are much smoother than those for higher levels of the wetting phase saturation (Figures 6.21 to 6.23). This behavior was also observed by earlier researchers (Manai, 1991; Sarma, 1988); however, they used microwaves instead of VHF electromagnetic waves. It is also important to note that the frequency counter (HP 53131A) used to capture the frequency response provided a very stable frequency response in the MHz and KHz ranges. Most of the fluctuations in frequency response were observed in the Hz range only. Because the MHz range of the frequency counter was used in this study, stable and accurate frequency responses were obtained.

Generally, the overall quality of these profiles was excellent with the exception of a few undesirable fluctuations. Most probably, these fluctuations were due to external electromagnetic interference and/or due to the heterogeneity of the core holder and porous medium. To assign a specific value to a particular saturation profile, an arithmetic average of all saturation values along the core was used. This method of saturation measurement was then compared with the standard material balance method. A typical comparison between steady-state saturations obtained by the standard material balance method and the above-described method is shown in Figure 6.24.

Standard calibration curves (Figure 5.6) represented by Equation (5.2) were obtained separately for each experimental set using SSCO processed saturation profiles (Figures 6.21 to 6.23). Using raw frequency data collected

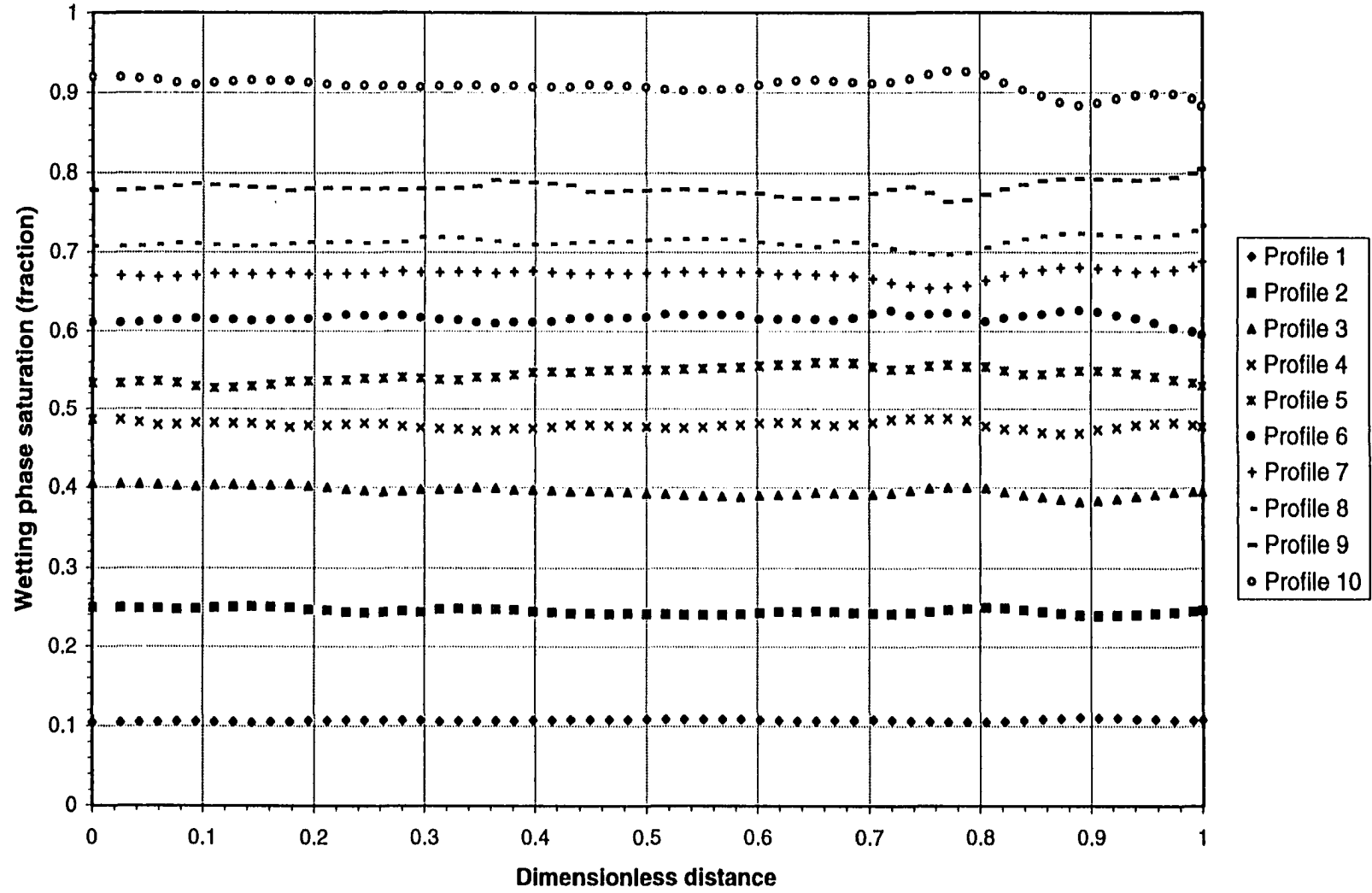


Figure 6.21: Steady-state saturation profile for each run, SSCO (Set 1).

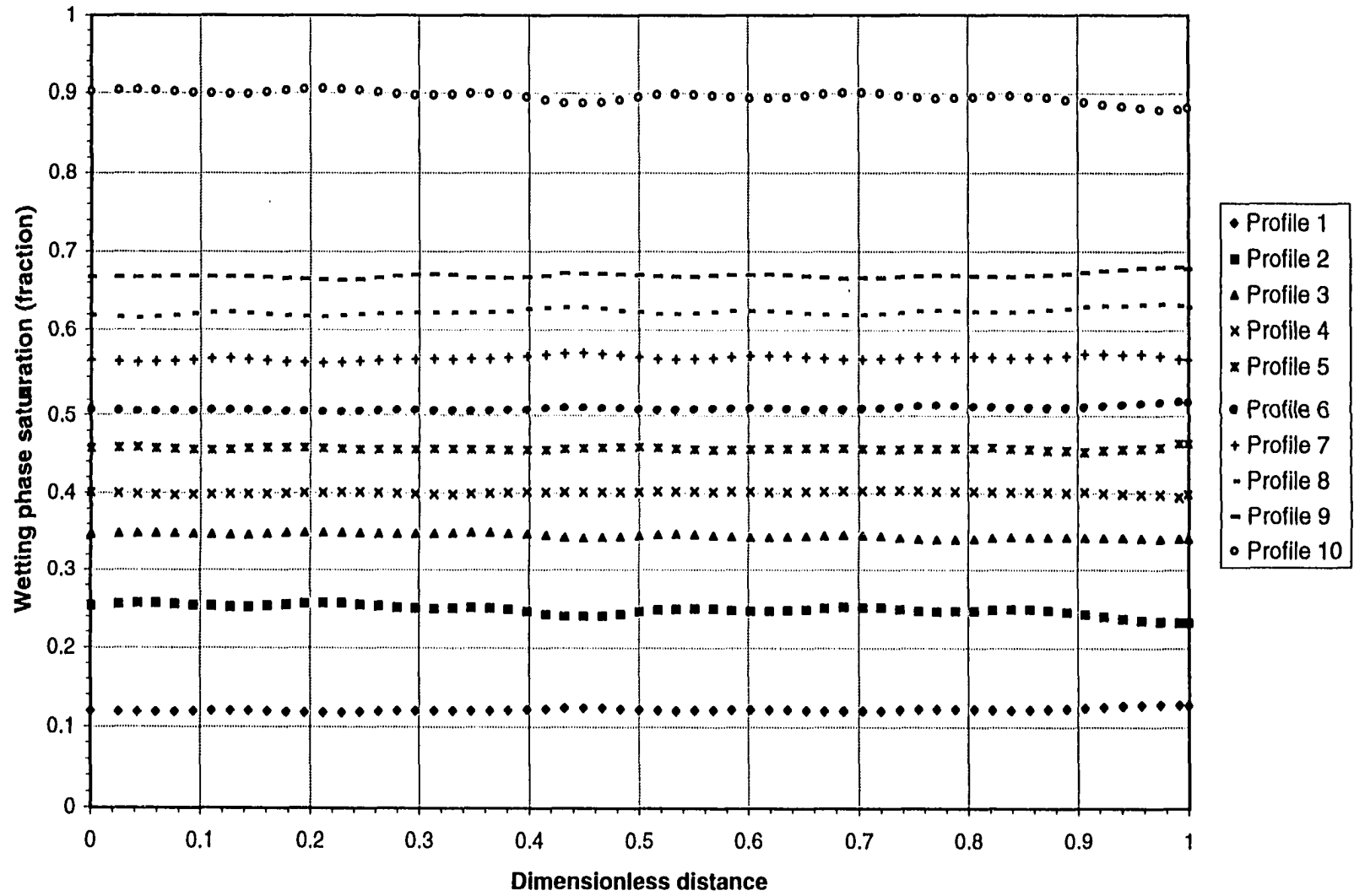


Figure 6.22: Steady-state saturation profile for each run, SSCO (Set 2).

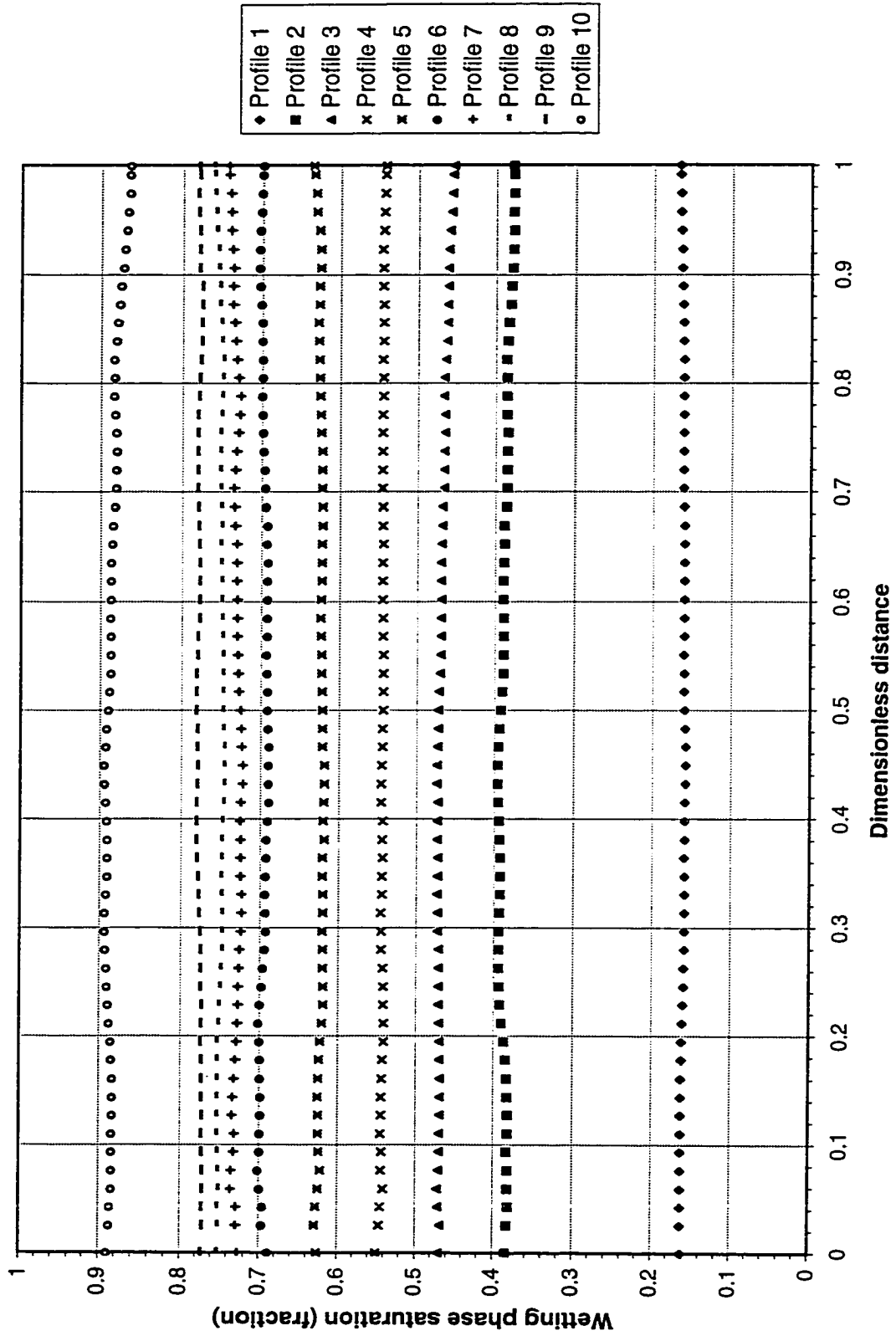


Figure 6.23: Steady-state saturation profile for each run, SSCO (Set 3).

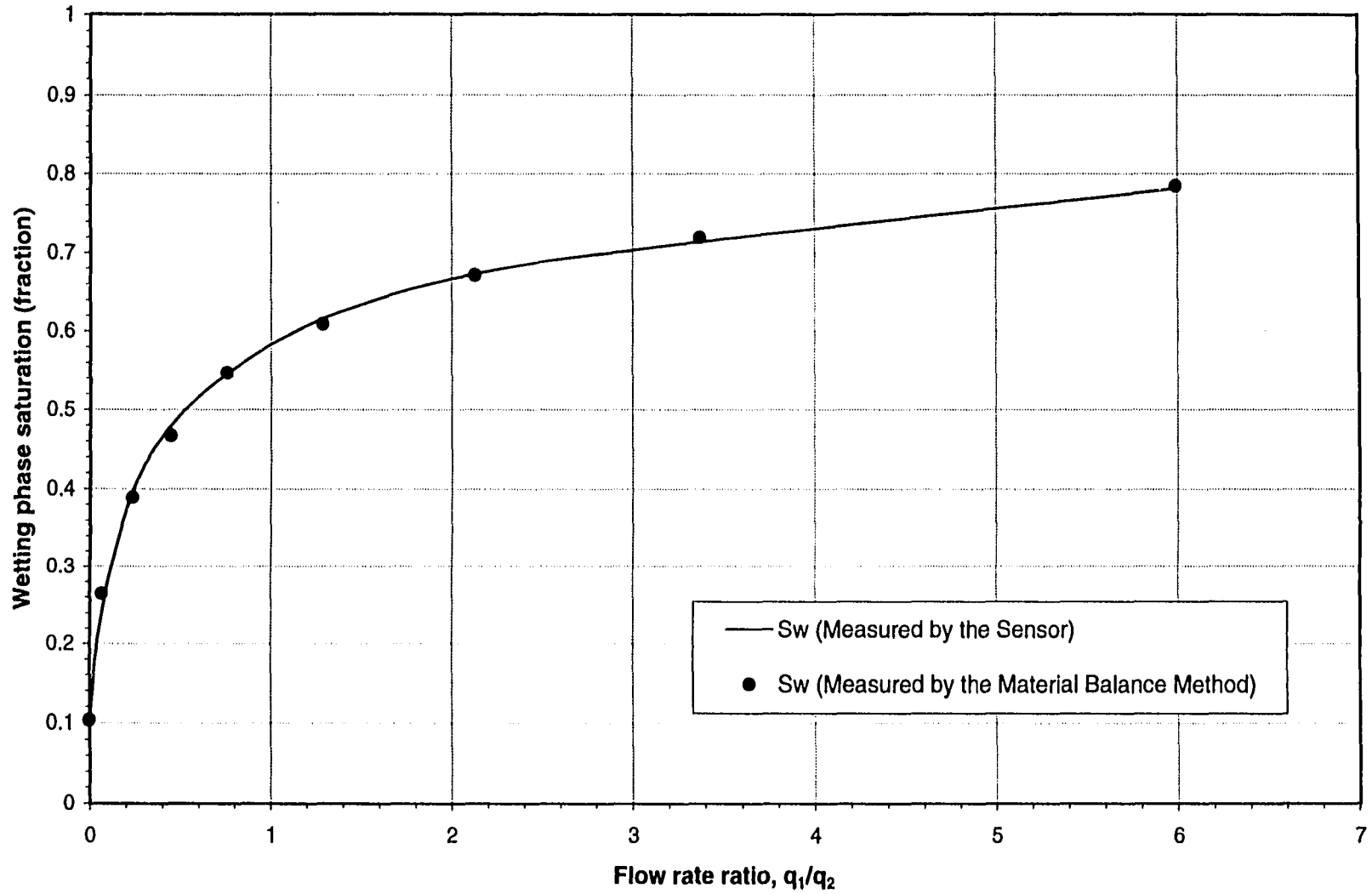


Figure 6.24: Typical comparison between saturations measured by the sensor and by using the material balance method, SSCO (Set 1).

during each of the USCO flow runs, these calibration curves were then used to obtain USCO saturation profiles (Figures 6.2 to 6.4) for each of the data sets.

6.2.2.2. SSCO Effective Mobilities

Calculated mobilities for the wetting and nonwetting phases are given in Tables 6.3, 6.4 and 6.5 for Sets 1, 2 and 3, respectively. These values were not used directly to test Equations (4.54) and (4.55); rather they were modified by adjusting the end-point saturation (observed during USCO runs) and effective mobility values (APPENDIX F). As a consequence, all other intermediate saturation and effective mobility values have to be adjusted accordingly. The need for this type of adjustment arose because of the problem mentioned in Step 15 of Section 5.4.1. Due to this operational problem, all of the USCO flow runs were initiated at a slightly higher initial wetting phase saturation level and they were stopped before the actual residual nonwetting phase saturations were attained.

Consequently, effective mobility curves, which were originally calculated by making use of SSCO flow runs, have to be adjusted accordingly to cope with the new dynamic saturation range for USCO flow runs. In other words, it was necessary to assume zero mobility to water at a slightly higher initial water saturation level (used to start a USCO run) than the actual connate water saturation determined during the SSCO flow runs. This adjustment appeared to be realistic because no water production was observed until breakthrough occurred for all of the USCO runs.

To adjust the effective mobilities for the wetting and nonwetting phases, original best-fitted values of both mobilities and wetting phase saturations were normalized. These normalized values were then used to recalculate the modified or adjusted effective mobility and saturation values by making use of the new end-point saturations (observed during USCO runs) and effective

mobility values. Adjusted, measured and fitted steady-state effective mobility curves for Sets 1, 2 and 3 are shown in Figures 6.25, 6.26 and 6.27, respectively.

6.3. Two Approaches to Test the Theory

At this stage, it is convenient to rewrite the final form of the theory developed in Chapter 4; that is,

$$-\frac{v_1}{\lambda_1^o} = \left(\frac{\partial p_1}{\partial x} + \frac{\phi}{2} \frac{\partial P_c}{\partial x} \right) \quad (4.54)$$

and

$$-\frac{v_2}{\lambda_2^o} = \left(\frac{\partial p_2}{\partial x} - \frac{\phi}{2R_{12}} \frac{\partial P_c}{\partial x} \right). \quad (4.55)$$

As described above (Section 6.2.1.3), because of some observed inconsistencies in the phase pressure gradients, it was not possible to make proper use of Equation (6.4). Consequently, R_{12} values have been assumed to be 1 in all cases of the SSCO flow experiments. In other words, pressure gradients along the length of the core for both wetting and nonwetting phases during all SSCO runs were supposed to be equal to each other. Moreover, keeping in mind the underlying assumptions with respect to the fluid/fluid contact area in an RMS [Equations (4.42) and (4.43)], Equations (4.54) and (4.55) may further be simplified as follows:

$$-\frac{v_1}{\lambda_1^o} = \left(\frac{\partial p_1}{\partial x} + \beta_1 \cdot \phi \cdot \frac{\partial P_c}{\partial x} \right) \quad (6.5)$$

and

$$-\frac{v_2}{\lambda_2^o} = \left(\frac{\partial p_2}{\partial x} - \beta_2 \cdot \phi \cdot \frac{\partial P_c}{\partial x} \right) \quad (6.6)$$

where, β_1 and β_2 are fractions of fluid/fluid contact area in an RMS for the wetting phase equation and the nonwetting phase equation, respectively. If

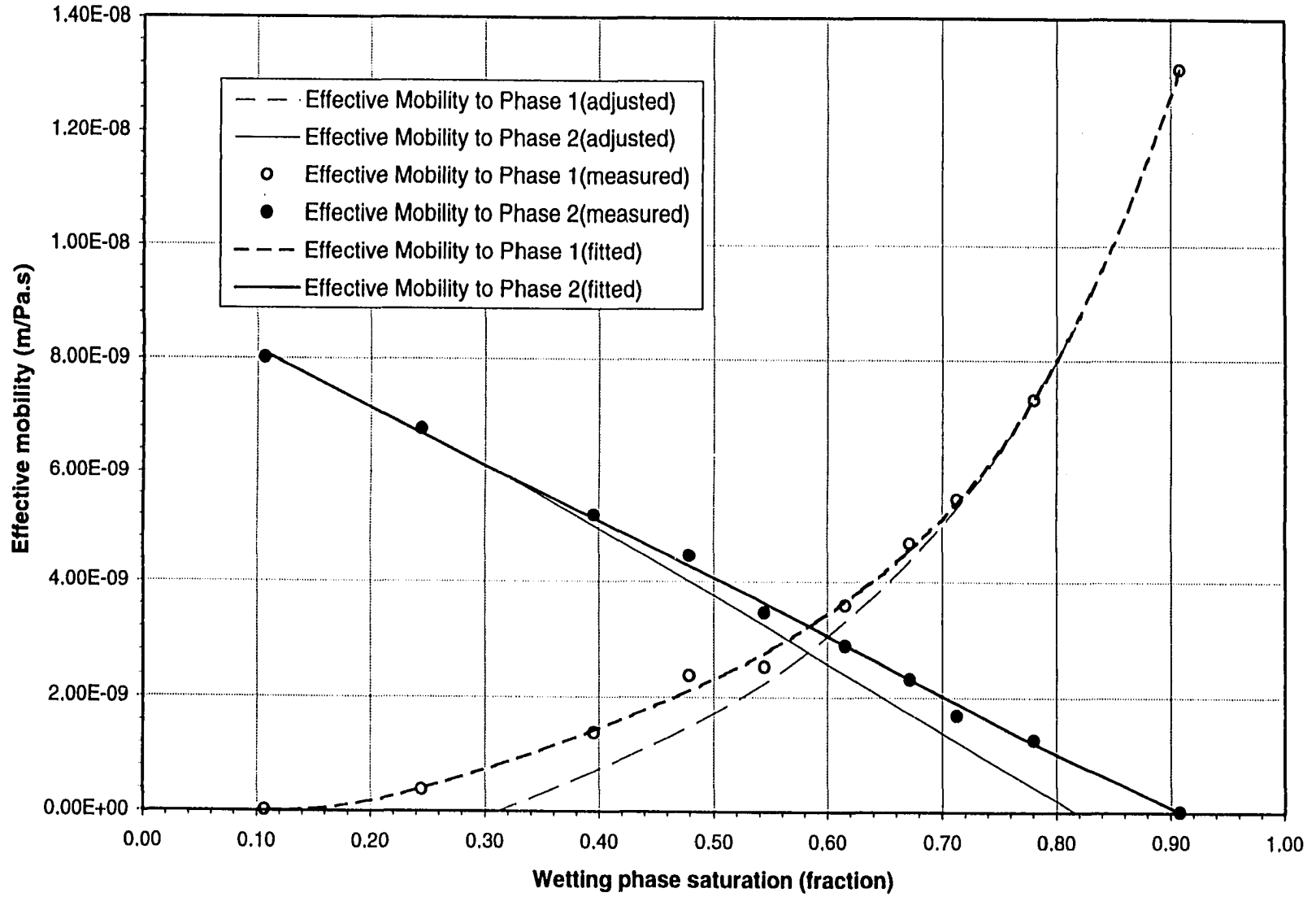


Figure 6.25: Adjusted, measured and fitted effective mobility curves, SSCO (Set 1).

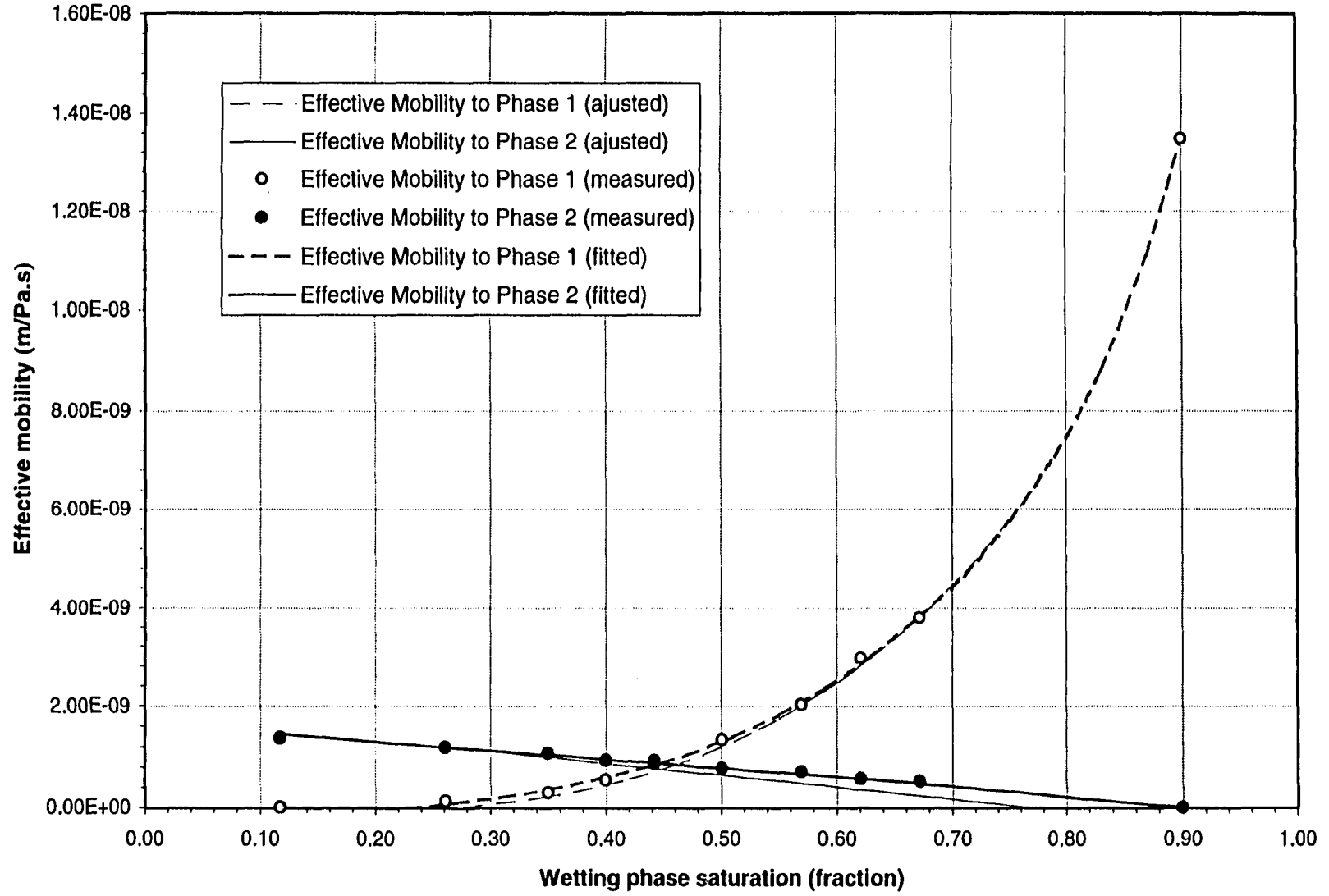


Figure 6.26: Adjusted, measured and fitted effective mobility curves, SSCO (Set 2).

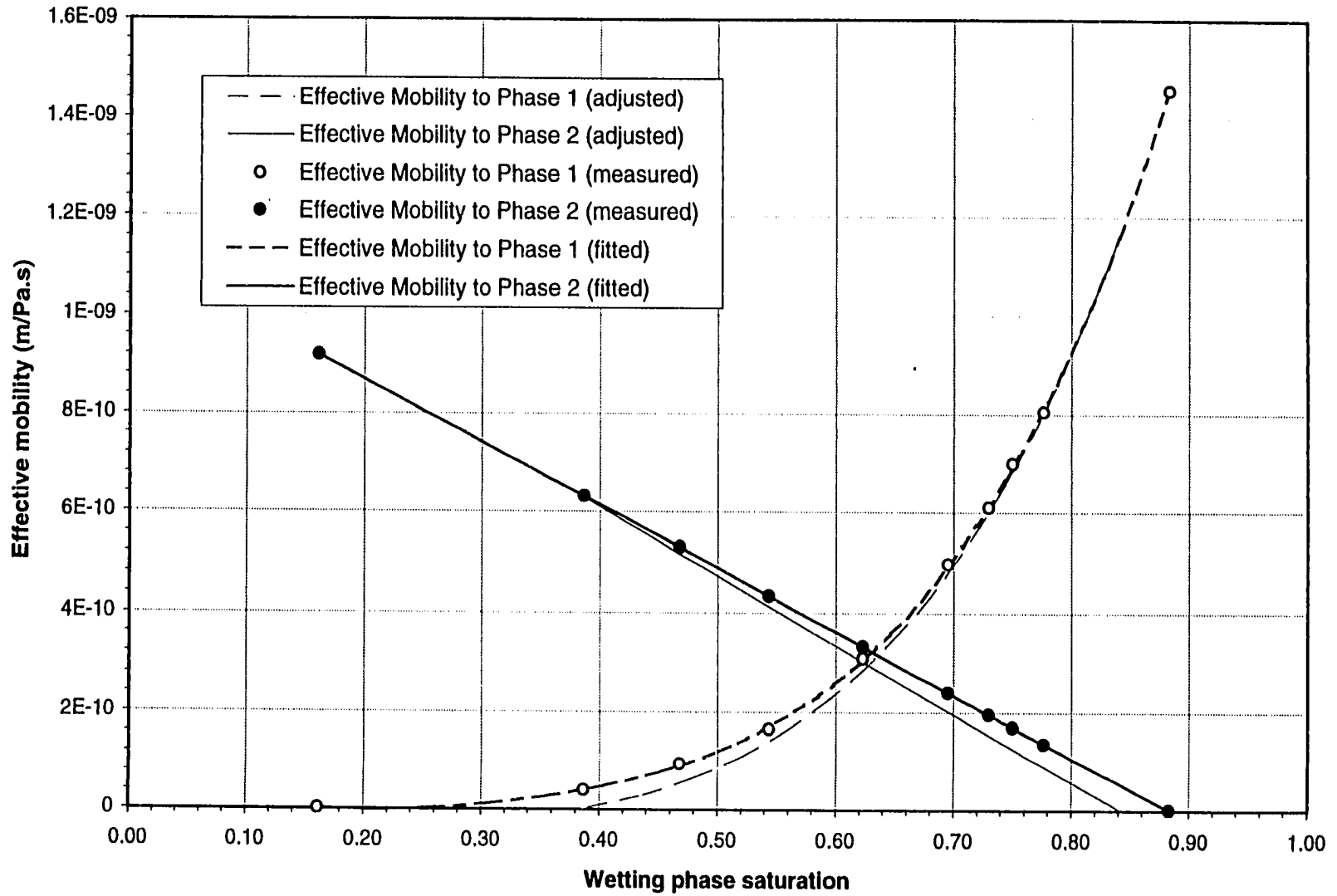


Figure 6.27: Adjusted, measured and fitted effective mobility curves, SSCO (Set 3).

the assumptions underlying Equations (4.42) and (4.43) are correct, then, one can write:

$$\beta_1 = \beta_2 = \beta = 0.5 \quad (6.7)$$

This equation is consistent with Equation (4.44). Moreover, as explained in Chapter 4, mathematically $0 \leq \beta \leq 1$. In the following sections two approaches to test the theory are presented. In the first approach, an attempt was made to determine β_1 and β_2 experimentally. In the second approach, various values of β were assumed to calculate the phase pressure profiles (see Section 6.3.2).

6.3.1. First Approach

To follow this approach for testing the theory, Equations (6.5) and (6.6) were rearranged as follows:

$$\beta_1 = -\frac{\frac{v_1}{\lambda_1^0} + \frac{\partial p_1}{\partial x}}{\phi \frac{\partial P_c}{\partial x}} \quad (6.8)$$

and

$$\beta_2 = \frac{\frac{v_2}{\lambda_2^0} + \frac{\partial p_2}{\partial x}}{\phi \frac{\partial P_c}{\partial x}} \quad (6.9)$$

The first approach for testing the theory used measured and calculated data from USCO and SSCO flow runs to calculate the right hand side (RHS) of Equations (6.8) and (6.9). That is, v_1 , v_2 , $\partial p_1/\partial x$, $\partial p_2/\partial x$, and $\partial P_c/\partial x$ were taken from USCO flow runs, while λ_1^0 and λ_2^0 were obtained using SSCO flow runs. In other words, in this approach, an attempt was made to determine experimentally the values of β_1 and β_2 . If the theory is valid, calculations performed to determine these values should lead us [in the light of Equation (6.7)] to values for β in the vicinity of 0.5.

Figure 6.28 depicts typical trends for β_1 and β_2 , determined by adopting this approach, versus wetting phase saturation for Set 1. Similar trends were found for experimental Sets 2 and 3. From Figure 6.28, one can observe three obvious contradictions with the theory postulated earlier in Chapter 4: first, β_1 and β_2 are not equal to each other; second, β_1 and β_2 are not equal to 0.5; and third, β_1 and β_2 seem to be a function of wetting phase saturation. However, β_2 values lie between 0 and 0.5 in the range of wetting phase saturations from 0.5 to 0.74; while most of the values of β_1 lie below zero with the exception of a few values in a very narrow range of wetting phase saturations (0.75 to 0.78), where they almost approach zero.

Based on these observations, one may wrongly conclude that the theory presented in Chapter 4 may not adequately incorporate interfacial coupling effects into the existing two-phase flow formulation. Most of the fluctuations and variations in β_1 and β_2 did not arise because of the underlying physics; rather, they probably came about because of the data manipulation methods used in this study. For example, the least squares curve-fitting method was found to be difficult to apply in certain cases.

In particular, the pressure gradient calculations ($\partial p_1/\partial x$, $\partial p_2/\partial x$, and $\partial P_c/\partial x$) were found to be extremely sensitive to the degree of the polynomial used to fit the measured phase pressure data along the length of the core holder. In most cases, more than one polynomial equation seemed to provide an excellent best-fit curve for the raw pressure data. However, pressure gradient data ($\partial p_1/\partial x$, $\partial p_2/\partial x$, and $\partial P_c/\partial x$) calculated by differentiating the best-fitted curves showed a significant difference with a change in the degree of the polynomial used to fit the raw pressure data.

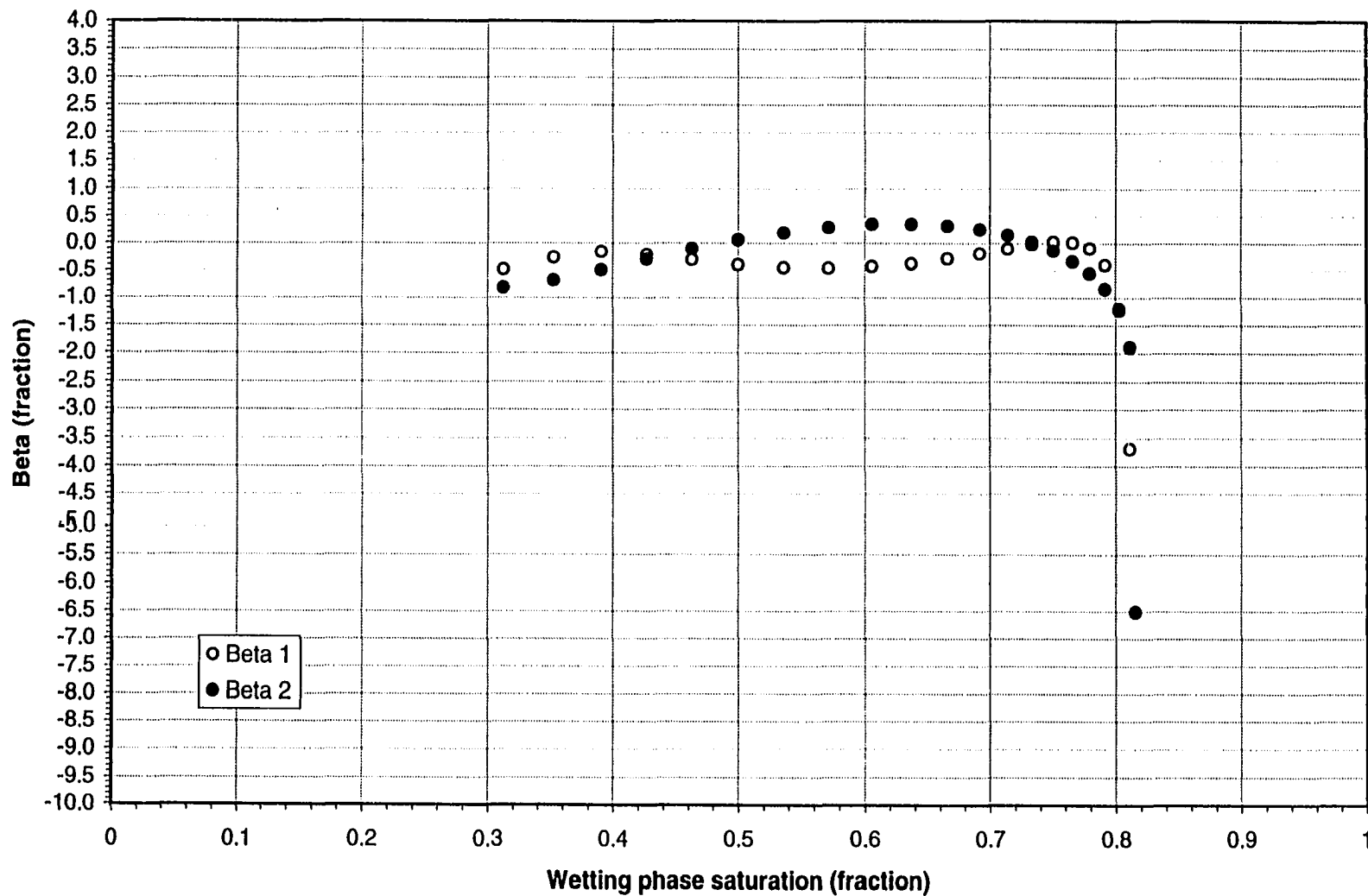


Figure 6.28: Typical curves for Beta 1 and Beta 2, versus wetting phase saturation, first approach (Set 1).

Obviously, the way in which Equations (6.8) and (6.9) were arranged for testing the theory indicates that this is an indirect or inverse problem, which may have an infinite number of non-unique solutions. To get a “good” solution, one needs extremely accurate experimental data, when this approach is followed. Unfortunately, because of operational difficulties, the quality of the data (particularly phase pressure data during USCO runs) was not adequate. This appears to be the main reason for getting non-unique values of β_1 and β_2 , (Figure 6.28). Consequently, to overcome the apparent anomalies and to avoid the misleading conclusions of this approach to test the theory, it was decided to attempt a second approach.

6.3.2. Second Approach

For this approach, it was assumed that $\beta_1 = \beta_2 = \beta$, so that Equations (6.5) and (6.6) become:

$$\frac{\partial p_1}{\partial x} = -\frac{v_1}{\lambda_1^{\circ}} - \beta \cdot \phi \cdot \frac{\partial P_c}{\partial x} \quad (6.10)$$

and

$$\frac{\partial p_2}{\partial x} = -\frac{v_2}{\lambda_2^{\circ}} + \beta \cdot \phi \cdot \frac{\partial P_c}{\partial x} \quad (6.11)$$

The second approach for testing the theory uses Equation (6.3) to calculate $\partial P_c / \partial x$, which is the product of the data obtained using SSCO and USCO flow runs; that is, $\partial P_c / \partial S_1$ and $\partial S_1 / \partial x$, respectively. Moreover, other parameters of the RHS of Equations (6.10) and (6.11) taken from SSCO runs include λ_1° and λ_2° , whereas v_1 and v_2 were taken from USCO flow runs. Using all required parameters of the RHS of Equations (6.10) and (6.11), values of $\partial p_1 / \partial x$ and $\partial p_2 / \partial x$, as functions of dimensionless distance, were calculated for $\beta = 0.5$. Calculated phase pressure gradients ($\partial p_1 / \partial x$ and $\partial p_2 / \partial x$) data were then

best-fitted using the least squares method to obtain empirical equations for all the data sets. Finally, these empirical best-fit equations were integrated (see Section 6.4) with respect to dimensionless distance to calculate the phase pressure profiles for all the data sets.

Comparisons between calculated phase pressure profiles using this approach and measured phase pressure profiles (Figures 6.11 to 6.13) during actual USCO flow runs for Sets 1, 2 and 3 are shown in Figures 6.29, 6.30 and 6.31, respectively. Obviously, the match between measured and calculated unsteady-state pressure profiles (Figures 6.29 to 6.31 and APPENDIX B) for $\beta = 0.5$ was found to be very good for all the data sets. However, some scatter in the measured phase pressure data, particularly in the wetting phase, is also obvious from the figures. Certainly, the reasons stipulated earlier in Section 5.4.1 (Steps 15 and 21) are most likely responsible for this type of scatter in the wetting phase pressure values.

Keeping experimental limits and operational errors in view, Figures 6.29 to 6.31 demonstrate a very strong indication that the current problem of the experimental testing for the theory must be tackled by using the second approach, rather than the first approach described in Section 6.3.1.

6.4. Sensitivity Analysis

From Section 6.3.1, it appears that the first approach for testing the theory is an inverse approach with infinitely non-unique characteristics, as depicted in Figure 6.28. However, although the first approach for testing the theory does not appear to work well, it does give some indication that the theory may be valid. That is, from Figure 6.28, one may see that some of the β values (though, in a very narrow range of the wetting phase saturation) seem to approach 0.5, or at least take on values larger than zero. This is an indication that one may adopt the first approach for testing the theory, provided that the

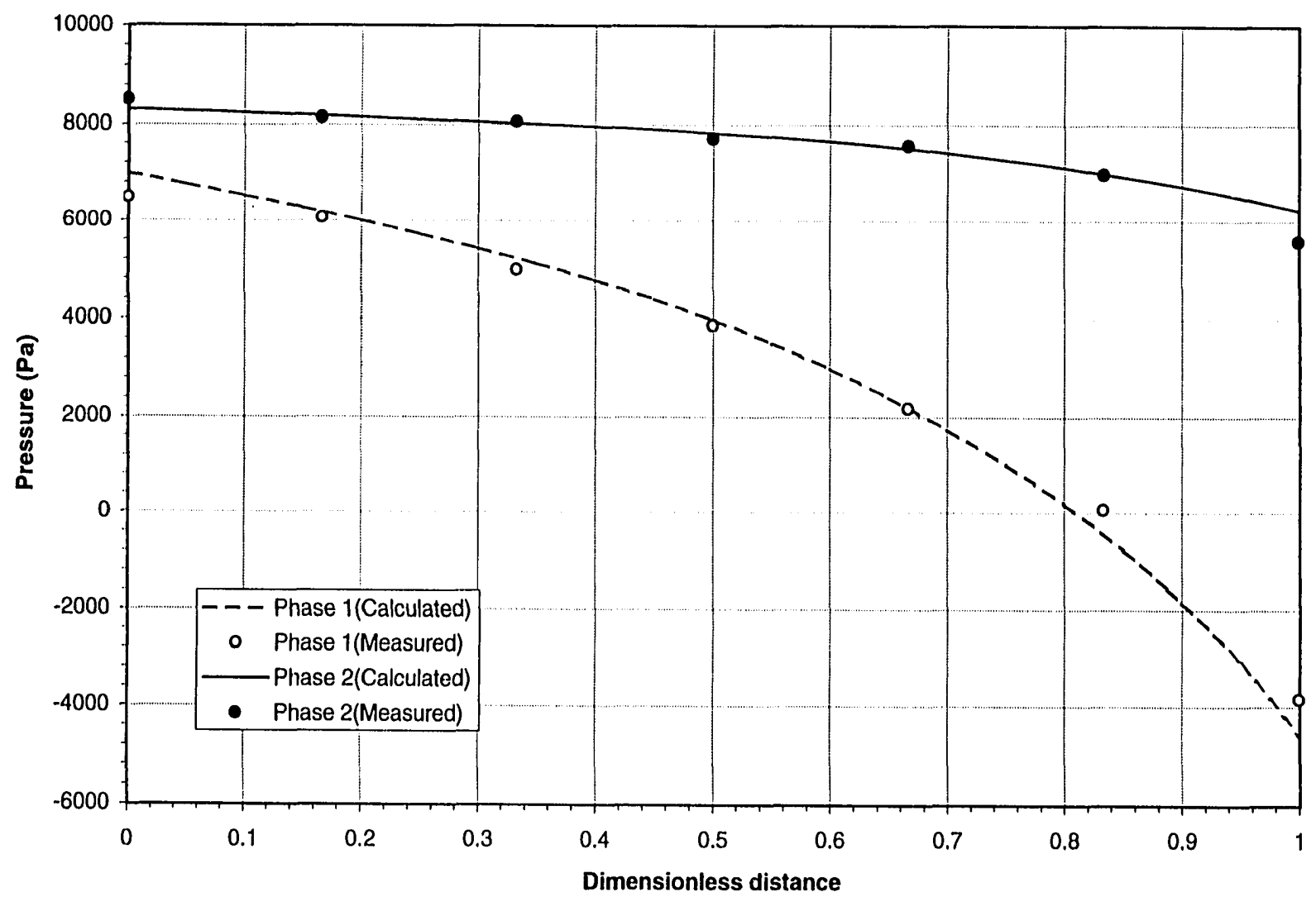


Figure 6.29: Comparison of calculated and measured phase pressure profiles, Beta = 0.5, USCO (Set 1).

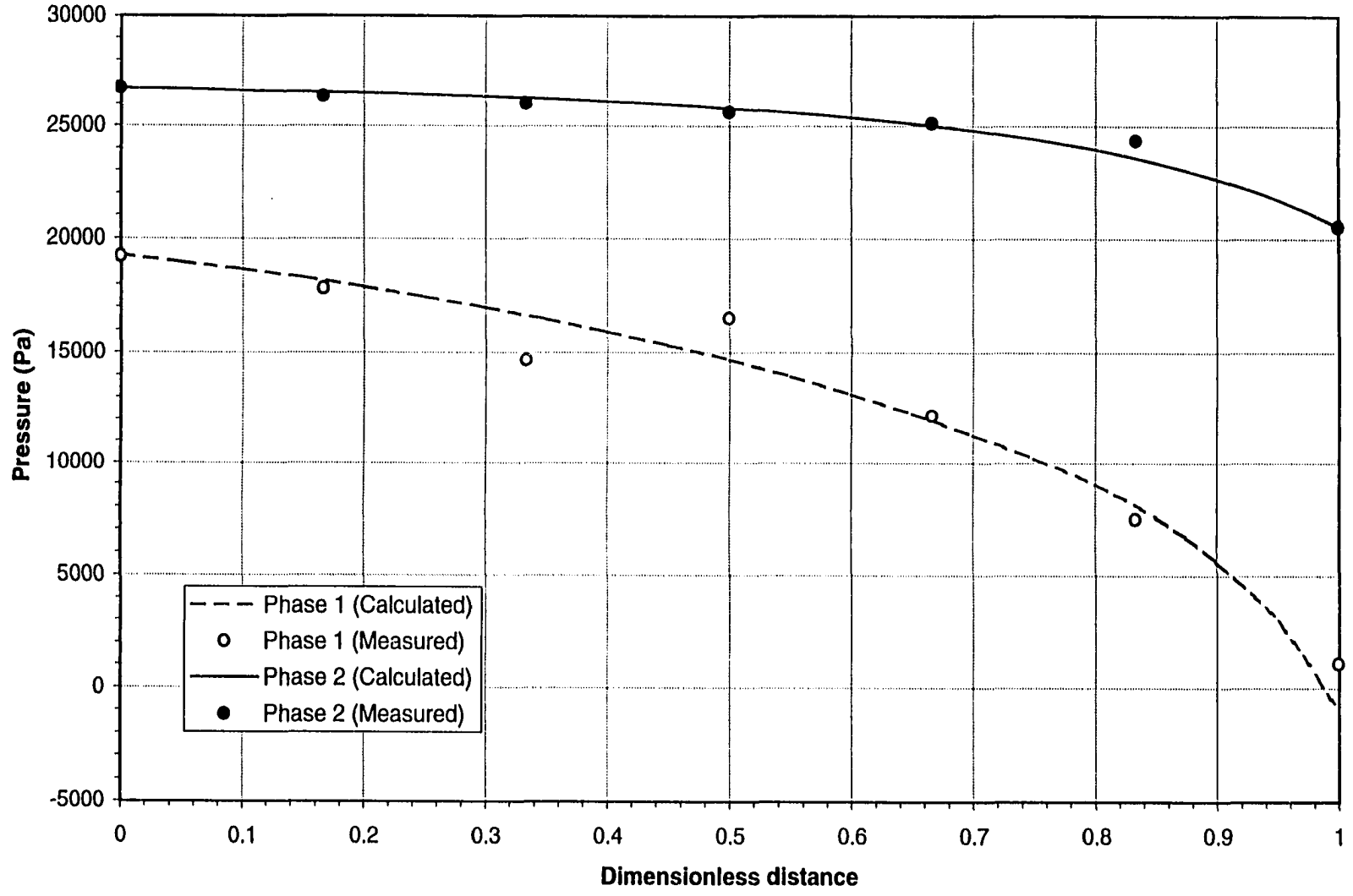


Figure 6.30: Comparison of calculated and measured phase pressure profiles, Beta = 0.5, USCO (Set 2).

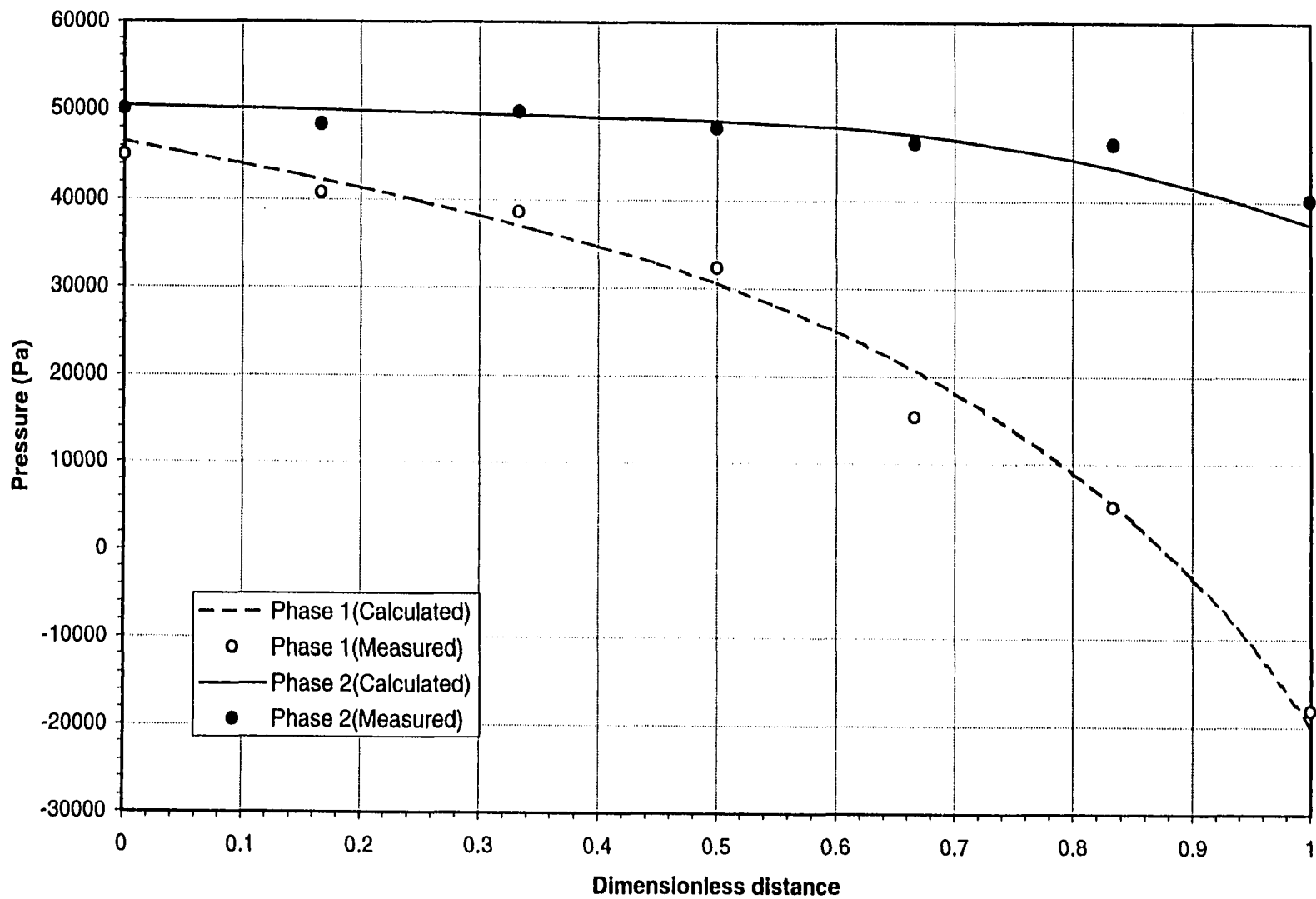


Figure 6.31: Comparison of calculated and measured phase pressure profiles, Beta = 0.5, USCO (Set 3).

statistical noise that arises during the data analysis is overcome. It should be noted that the operational problems described in Step 15 of Section 5.4.1 contributed also to the apparent inadequacy of the first approach.

Despite the operational difficulty (during USCO runs) related to the measurement of extremely accurate phase pressure profiles, the second approach for testing the theory appears to be more successful. Figures 6.29 to 6.31 show a very good match between the measured pressure profiles for each of the phases and the calculated phase pressure profiles for the case where β was assumed to be 0.5. However, this case ($\beta = 0.5$) is only a plausible scenario, where the assumptions underlying (4.42) and (4.43) were assumed to be valid. Mathematically, depending on rock/fluids properties and/or experimental conditions (such as the flow rate and/or the type of flow, that is, SSCO, USCO or SSCT), β may take any value between zero and one. Therefore, it seemed appropriate to perform a sensitivity analysis, so that the impact of β variation on the calculated phase pressure profiles with respect to the measured phase pressure profiles could be examined.

To perform the sensitivity analysis, β values of 0.0, 0.25, 0.5, 0.75, and 1.0 were chosen to calculate the phase pressure profiles for each experimental set by making use of Equations (6.10) and (6.11). Note that Equations (6.10) and (6.11) provide the pressure gradients for each of the flowing phases. To calculate the corresponding pressure profiles, the calculated phase pressure gradient data were best fitted by using a least-squares method. The resultant polynomial equation was then integrated with respect to dimensionless distance to calculate the phase pressure profile for each of the experimental data sets.

To accomplish the integration process, integration constants for each case were required. These constants were estimated by best fitting the measured phase pressure data for each phase during each USCO flow run.

Generally, during USCO runs, it was speculated that the time available to measure accurate phase pressures was insufficient. Therefore, estimated phase pressure data points in the vicinity of the inlet end of the core were assumed to be more reliable as compared to the data points estimated closer to the outlet end of the core. This assumption was justified because of the fact that, during an unsteady-state displacement process, the pressure sensors installed in the vicinity of the inlet end of the core holder get more time to measure accurate pressure values as compared to the sensors installed in the vicinity of the outlet end of the core holder.

Therefore, after best fitting the measured pressure data points along the core, the pressure values at a dimensionless distance of zero (inlet end) were taken as the integration constants to perform the integration process for each phase pressure profile of all the USCO runs. The only exception was the wetting phase pressure profile for the USCO run of Set 1, where this process (determination for the integration constant) was modified slightly.

For some unknown reason, the first pressure value (at the inlet end of the core) for the wetting phase during the USCO run for Set 1 appeared to be slightly lower than the expected pressure value. Therefore, to avoid any wrong estimation for the integration constant for this particular case, only six pressure values were used to obtain a best-fit curve. Then, by ignoring the first pressure value, the best-fitted curve was extrapolated to determine the pressure value (integration constant for this particular case) at the inlet end of the core.

Figures 6.32, 6.33 and 6.34 depict the comparison of calculated and measured phase pressure profiles, for various values of β for Sets 1, 2 and 3, respectively. As far as the determination of the correct values of β for all experimental sets is concerned, these figures provide very little information because all the calculated phase pressure profiles (for various values of β) seem to exhibit a reasonable match with their respective measured phase pressure data.

Thus, to estimate a representative value of β for each case, the error sum of squares (SS_E) for each calculated and measured (best-fitted) phase pressure profile for all runs was obtained with the help of the following equation:

$$SS_E = \sum_{j=1}^n (y_j - \hat{y}_j)^2 \quad (6.12)$$

Where, the y_j are the measured best-fitted phase pressure values, the \hat{y}_j are the calculated phase pressure values, and n is the total number of phase pressure values along the core. Figures 6.35, 6.36 and 6.37 show plots of SS_E versus β for the experimental Sets 1, 2 and 3, respectively. Again, apparently from a β determination point of view, it is not easy to analyze these plots.

For the wetting phase, for all of the experimental sets, the best β value seems to be one (because of minimum SS_E), while for the nonwetting phase (for all of the sets), the best β value appears to be zero (because of minimum SS_E). Both of these scenarios, that is, $\beta = 0$ (for nonwetting phase) and $\beta = 1$ (for wetting phase), are most unlikely (see Chapter 4).

Despite the above-mentioned mixed behavior of SS_E versus β for each of the phases, it seems plausible that the β value at the point of intersection of both

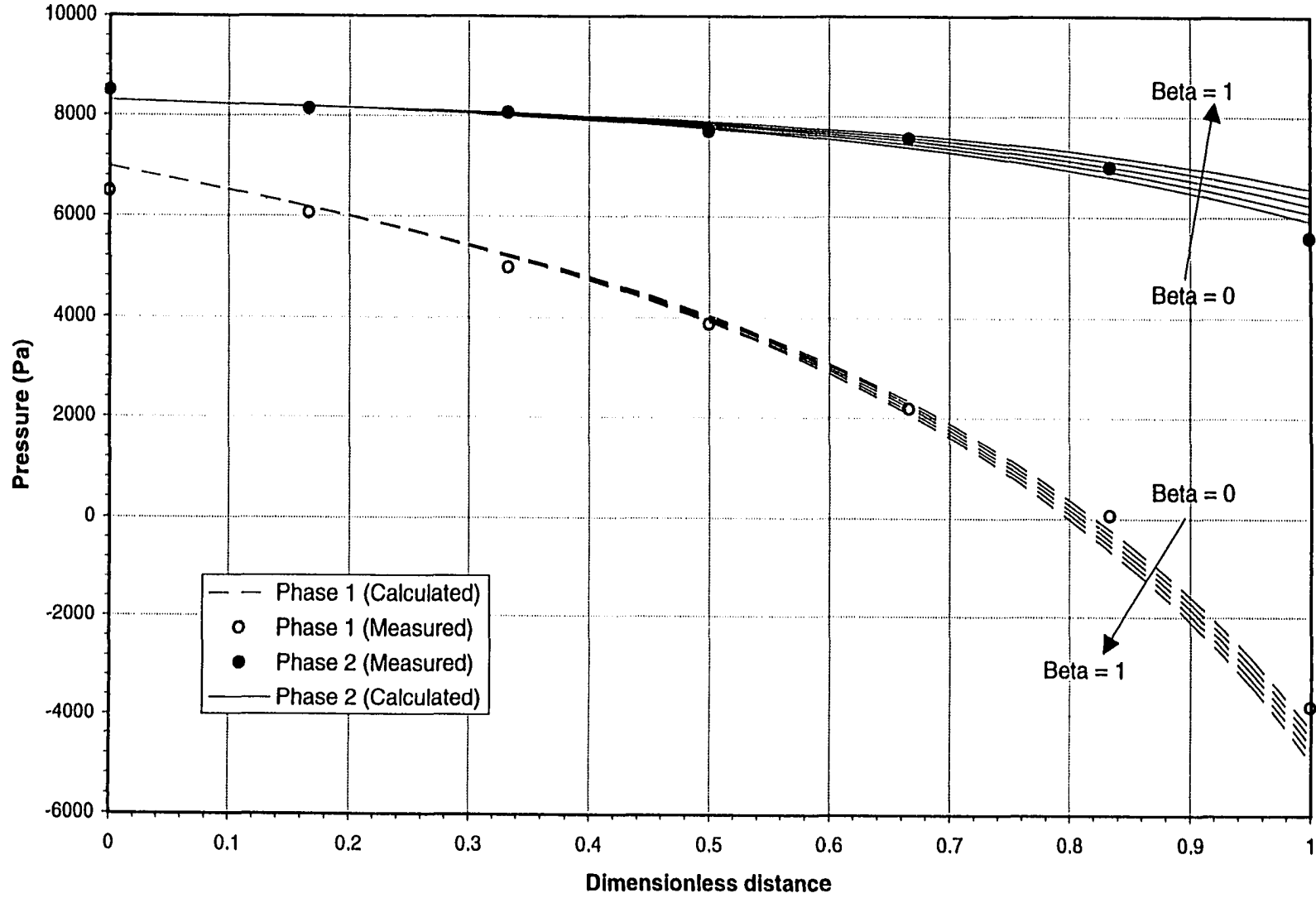


Figure 6.32: Comparison of calculated and measured phase pressure profiles for various values of Beta, USCO (Set 1).

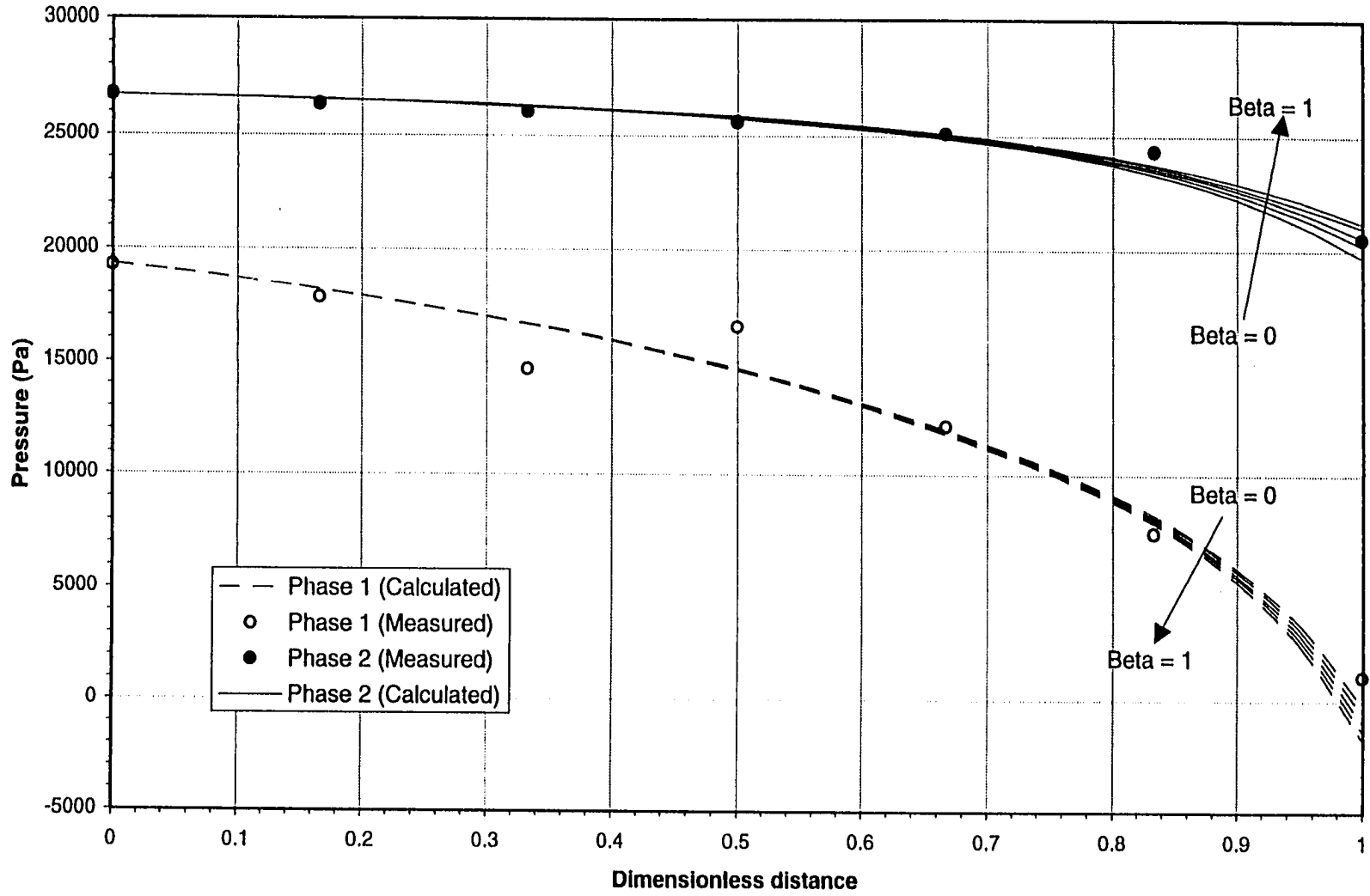


Figure 6.33: Comparison of calculated and measured phase pressure profiles for various values of Beta, USCO (Set 2).

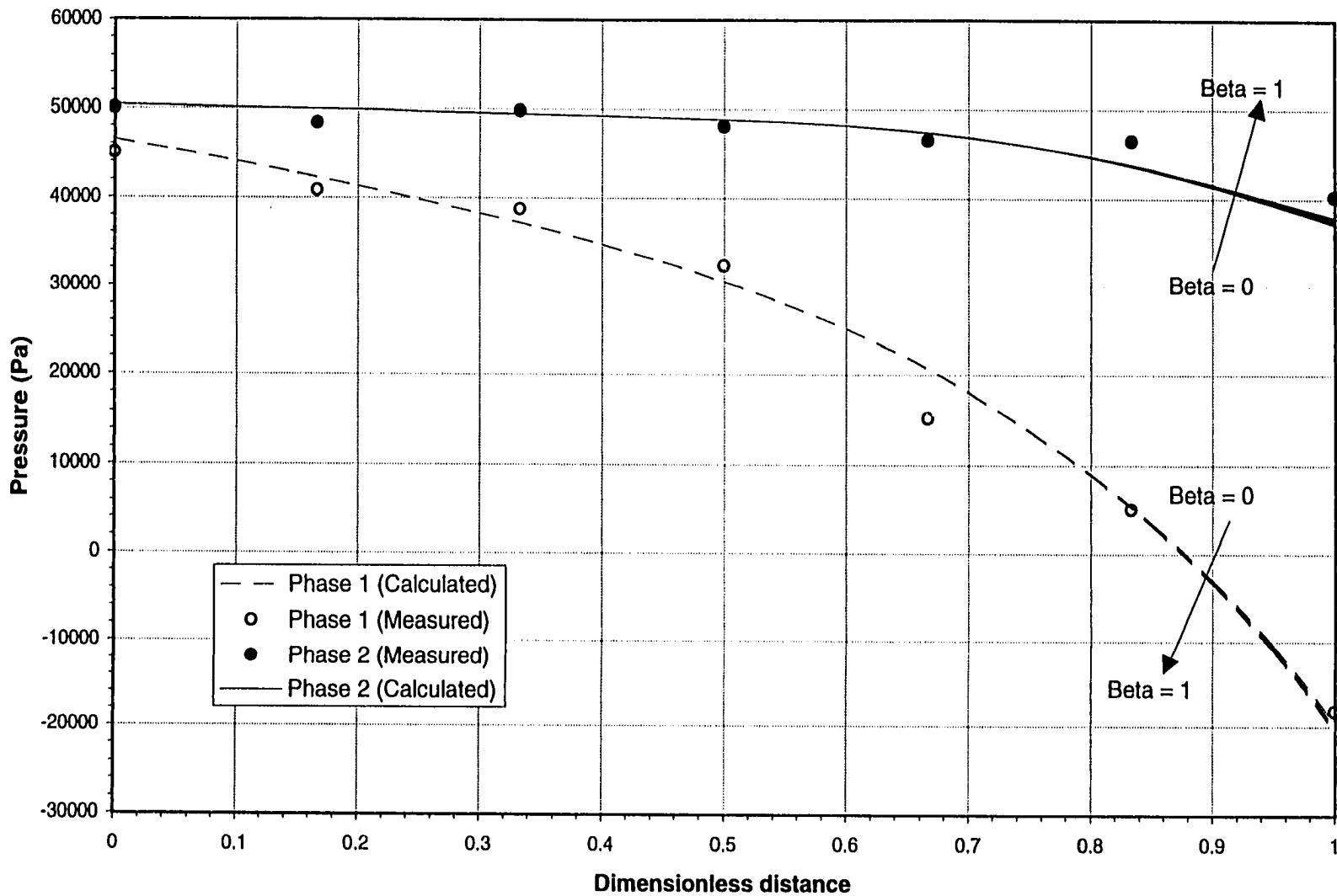


Figure 6.34: Comparison of calculated and measured phase pressure profiles for various values of Beta, USCO (Set 3).

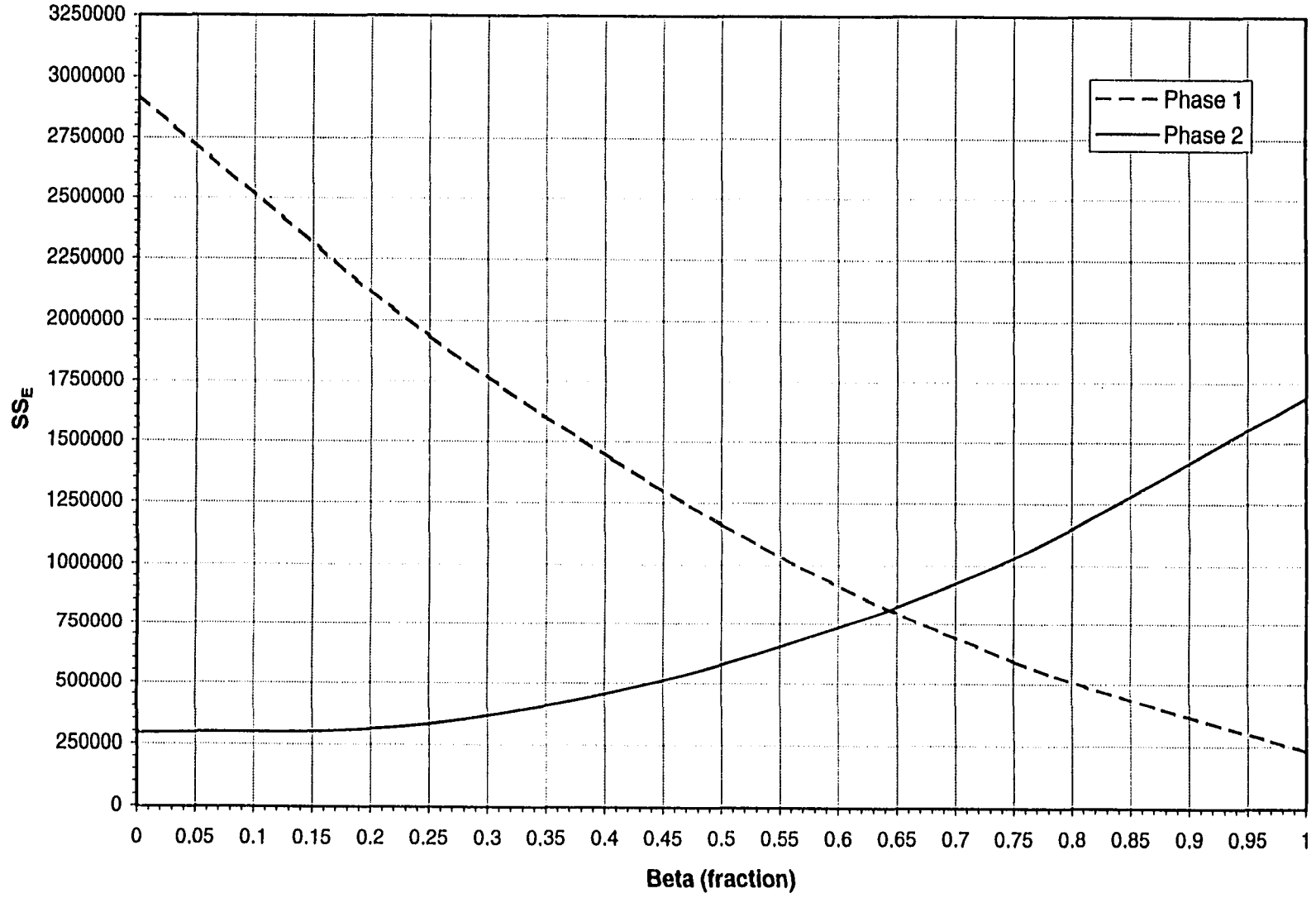


Figure 6.35: Error sum of squares versus Beta (Set 1).

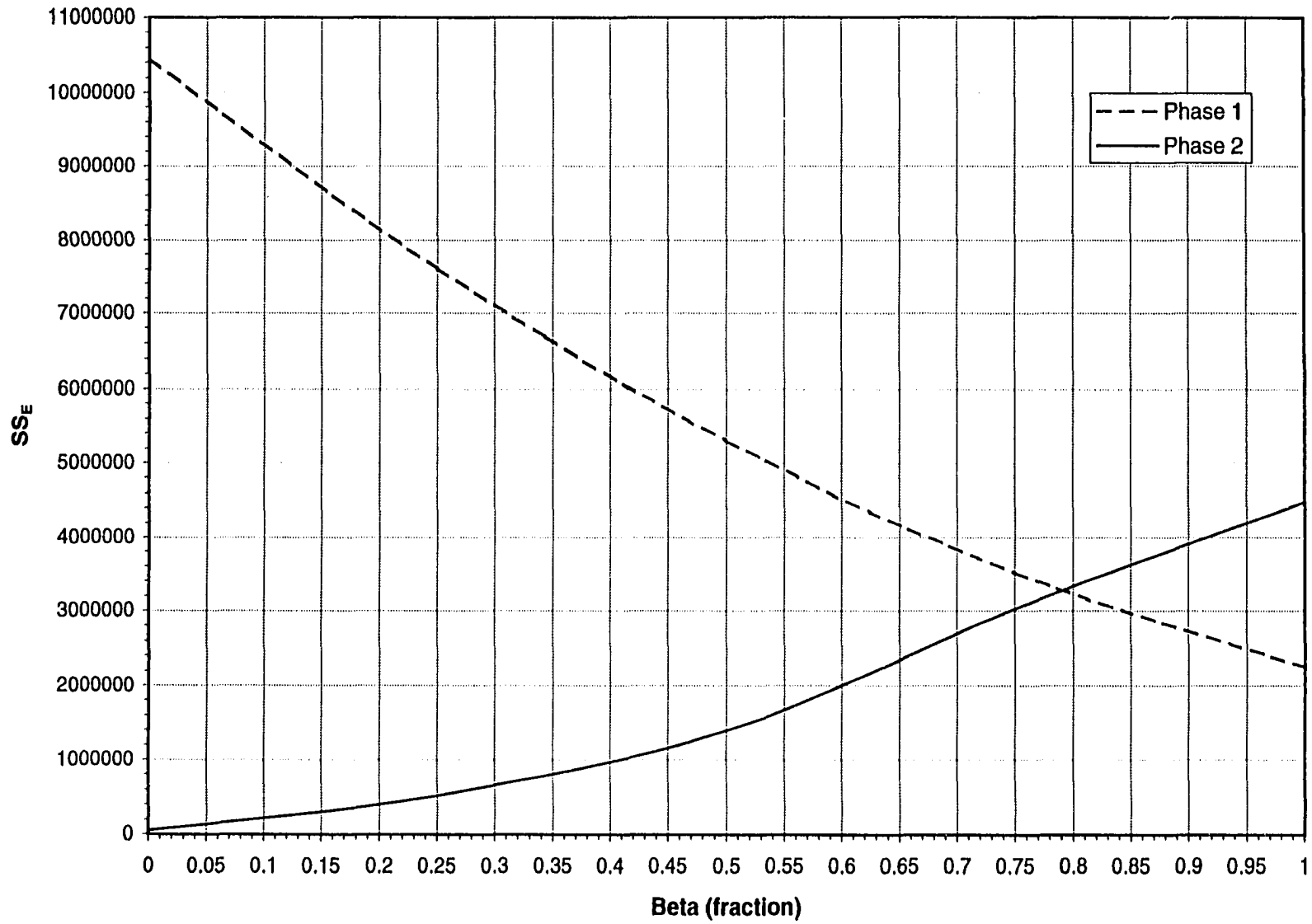


Figure 6.36: Error sum of squares versus Beta (Set 2).

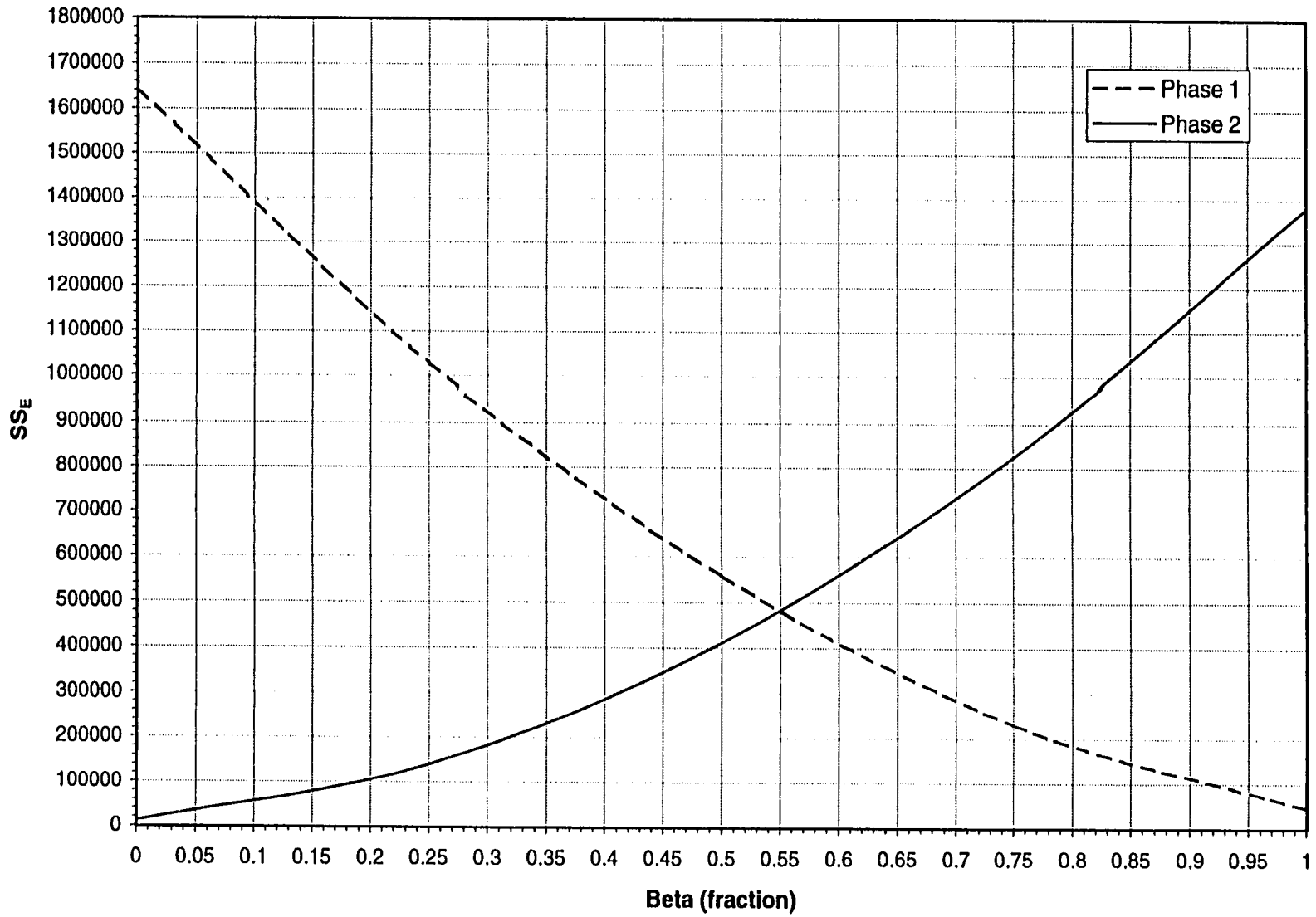


Figure 6.37: Error sum of squares versus Beta (Set 3).

curves (Phase-1 and Phase-2) may be chosen as the representative value of β for a specific set of experimental runs. This is because this is the β value where SS_E for both of the phases is found to be minimal.

From Figures 6.35 to 6.37, an estimate for the β value (at the point of intersection) for each of the experimental set can be made. The value of β for Set 1 was found to be around 0.64, for Set 2 β was 0.79, while for Set 3, β was estimated to be about 0.55.

Keeping in mind the underlying assumptions for the theory development in Chapter 4, these observations, if accepted, lead toward a conclusion that the representative value of β (as defined in Section 6.3) may vary between zero and one, as should be the case. Moreover, as mentioned above, it is unlikely that β would take on the extreme values of zero or one, (see Chapter 4). This is particularly true when both of the curves (Figures 6.35 to 6.37) are looked at together, rather than the individual trends, which are certainly misleading. Generally, overall observations made during the testing of the theory by adopting the second approach and subsequent sensitivity analyses indicate that the second approach for testing the theory is somewhat more successful.

CHAPTER 7

SUMMARY AND CONCLUSIONS

Five main objectives of this study were set out in Chapter 3. In the following sections, for the sake of clarity, each of them is summarized separately. Moreover, relevant conclusions drawn from this study are also listed with each of the objectives of this study.

7.1. Understanding Interfacial Coupling

The prime objective of this study was to gain a better understanding of interfacial coupling phenomena that may occur during two-phase flow through porous media. The suspected cross effect between two flowing fluids in porous media has been a matter of debate for the last couple of decades. Several views about its quantitative significance and about its physical origin are available in the literature, (Ayub and Bentsen, 1999a). Based on the literature review presented in Chapter 2, three main schools of thought were recognized. First, those who believe that the effects of interfacial coupling are significant; second, those who argue that these effects are small and must be ignored; while, the third school of thought completely disagrees with the existence of such phenomena.

Most researchers who belong to the first school of thought strongly believe that the physical origin of interfacial coupling was the mutual transfer of momentum (viscous coupling) between flowing fluids through porous media. Bentsen (1999), however, contradicting his previous observations about the source of interfacial coupling, has suggested that the actual source of

interfacial coupling was the capillarity of the porous medium, and not interfacial momentum transfer, as is usually assumed.

As noted in the literature review, mobilities determined in a countercurrent flow experiment are less than those determined, for the same sand-fluid system, in a cocurrent flow experiment. Such a result cannot be explained, if one assumes that the conventional transport equations describe correctly two-phase flow through porous media. This is because the conventional equations are incapable of accounting for interfacial coupling between the two flowing phases. Therefore, if interfacial coupling is to be accounted for properly, use must be made of the newly formulated transport equations. In this study, a partitioning concept was introduced into Kalaydjian's (Kalaydjian, 1987) transport equations to construct modified equations that could be used to study interfacial coupling in two-phase flow. Moreover, an attempt was made to test experimentally the new transport equations.

Ideally, the new transport equations should have been tested using steady-state, cocurrent and countercurrent flow experiments. This is because the magnitude of the interfacial coupling effect is larger in such experiments. However, because of difficulties associated with the proper design and fabrication of the end-caps needed to conduct countercurrent flow experiments, the attempts made to conduct SSCT flow experiments were unsuccessful. Consequently, SSCO and USCO experiments had to be conducted to test the theory. As it turned out, the choice of such experiments to test the theory was unfortunate. That is, as can be seen in Figures 6.32 to 6.34, the magnitude of the interfacial coupling effects when using SSCO and USCO flow experiments, was of the same order as the magnitude of the error in the experimental data. This makes it difficult to argue convincingly that the new transport equations are valid, or that a correction for interfacial coupling is

even needed. Keeping in mind these limitations, the following conclusions can be drawn:

1. The pressure profiles predicted using the new transport equations [Equations (4.28) and (4.29)], together with the appropriate data, were consistent with those determined experimentally.
2. The amount of interfacial coupling that takes place appeared to be consistent with that predicted using Equation (4.53).
3. The experimentally determined difference in the magnitude of the steady-state pressure gradients was not consistent with that predicted using Equation (6.4).
4. Of the two approaches used to test the theory, the second approach was found, because it was not an inverse method, to be more successful.

7.2. The Experimental Set-up

The second major objective of this study was to ensure the functional capabilities of the existing experimental set-up. To achieve this objective, several modifications to the equipment, the procedure, and the data acquisition system, were introduced. In fact, almost all of the components of the experimental set-up were rebuilt (see Chapter 5). Based on the demonstrated performance of the newly built experimental set-up, the following conclusions can be drawn:

1. A relatively new saturation measurement technique using a capacitance-based method to obtain the dynamic saturation profiles during the core flooding experiments has been developed and tested successfully (Ayub and Bentsen, 1999b).
2. It has been demonstrated that the VHF range of electromagnetic spectrum can be used to determine the instantaneous saturation levels without the requirement of a settling or attenuation time.

3. Dynamic saturation profiles, during SSCO and USCO two-phase flow experiments, along the length of a core can be measured with a reasonable level of accuracy.
4. The agreement between the measured dynamic saturation profiles using the new technique, and those calculated using the standard material balance method, can be rated as good.
5. In most of the SSCO flow runs, the dynamic phase (wetting and nonwetting) pressure profiles were fairly good.
6. The newly installed fluid injection and production system, which uses weight-data of injected and produced fluids to calculate various experimental parameters, such as injection and production rates, was found to be very accurate and easy to use. As a result, the accuracy for the material balance calculations was significantly improved.
7. The newly developed data acquisition and instrument control system using LabVIEW was found to be excellent.
8. Front panel VI for the data acquisition system was very user friendly. Moreover, output data files and their format were found to be easy to understand and manipulate in a spreadsheet environment.
9. A unique automatic system of naming various output data files was introduced and found to be extremely helpful in subsequent data analysis during and after two-phase flow experiments.

7.3. Simplified Technique

The third objective of this study was to simplify the laboratory work needed to quantify the amount of interfacial coupling. Based on the experimental testing carried out, and keeping in mind all of the underlying assumptions, Equations (4.54) and (4.55) seem to be consistent with experimental measurements. In other words, after the successful testing of the theory experimentally in this study, one may not need to pass through the entire testing process. Instead, an accurate estimate of the porosity of the porous medium may be enough to

determine accurate relative permeability data, provided, interfacial coupling phenomena have been properly accounted for. This has immensely simplified the whole process of taking care of interfacial coupling phenomena and its proper incorporation into the existing Darcian approach for describing two-phase flow through porous media.

7.4. Effect of Mobility Ratio

The fourth objective of this study was to investigate the probable effect of mobility ratio (viscosity ratio) on the newly discovered phenomena of interfacial coupling (capillary coupling). To achieve this objective, two different mobility ratios were used in the experimental part of this study. No qualitative and/or quantitative effects were observed during the analysis of the output data. In both cases, capillary coupling appeared to be only porosity dependent. However, more experimental work is needed for further confirmation of this observation.

7.5. Effect of Grain Size Distribution

The fifth objective of this study was to authenticate whether or not the above-mentioned conclusions were valid for a porous medium with a different grain size distribution. To achieve this objective, two porous media having different grain size distributions were used in the experimental part of this study. No effect of grain size distribution on analyzed data was observed. Once again, in both cases, capillary coupling appeared to be only porosity dependent. However, more work is needed to confirm this conclusion.

CHAPTER 8

SUGGESTIONS FOR FUTURE RESEARCH

Research work is seldom problem and trouble free. This research work is no exception. However, while most of the problematic issues may be rated as minor, it is imperative to address all possible means to improve the quality and authenticity of this type of sophisticated research work. Generally, within experimental limits, the overall quality of the research work proved to be fairly good. In the following section, however, some suggestions to further improve the theoretical and the experimental components of this study are offered.

8.1. Theoretical

1. There is a need to develop a more comprehensive theoretical model, which must be able to handle more complex cases such as those where chemical reactions and/or phase change may occur.
2. A similar theory based on three-phase flow through porous media should be developed.
3. The current theory is valid only for two-phase flow, where both phases are assumed to flow linearly. Attempts should be made to develop a similar theory based on radial flow through porous media.
4. The current theory is valid only for 1-D two-phase flow. A similar theory based on 2-D and/or 3-D flow through porous media should be developed.
5. To quantify the relative magnitudes of capillary coupling and viscous coupling during multiphase flow through porous media, more theoretical attempts should be made.

8.2. Experimental

In general, the current experimental set-up is fairly adequate to conduct further experimental research to investigate the phenomena of interfacial coupling; however, some room for further improvement still exists. Specific areas for further improvement are presented below:

8.2.1. Types of Two-Phase Flow Experiments

In this study, three types of two-phase flow experiments (SSCO, USCO, and SSCT) were conducted. However, because of operational difficulties, SSCT types of flow experiments were not successful. It is recommended, therefore, that further attempts should be made to conduct SSCT flow experiments. Moreover, though USCO flow experiments are less time consuming and easy to perform, analysis of USCO flow to obtain the required parameters is rather lengthy and tedious. However, the best scenario would be to conduct all three types of flow experiments successfully, so that all speculation about testing of the theory and/or its validation would be removed.

8.2.2. Saturation Measurement

1. More controlled laboratory environments (such as room temperature, vibration, external electromagnetic interference or electrical noise, and humidity) may help improve the quality of the dynamic saturation profiles.
2. To avoid artifacts and the observed curvature in the raw frequency data, it would be very helpful to explore a new method to convert raw frequency profiles into water saturation profiles. This can be done by improved statistical means and/or by replacing the current travel-track system with a better system.
3. To calibrate the wetting phase saturation data, Equation (5.2) was used in this study. The parameters A and B of this equation have to be determined by using a nonlinear regression method. Although, from an operational point of view, this calibration scheme provides very good

quality dynamic saturation profiles, some additional information about the core and its contents may be obtained, and/or the calibration process itself may be improved further by using the concept of “equivalent capacitance” (Orlov, 1970). With the help of equivalent capacitance, in addition to wetting phase saturation data, other core related information such as nonwetting phase saturation data, and the heterogeneity of the core and the core holder, may also be estimated directly.

8.2.3. Pressure Measurement

1. There is a need to search further for a better selective wetting capillary barrier for the pressure taps. Use of a different wetting medium for proper oil-water separation at the inlet and the outlet end of the core-holder should be considered.
2. To increase the hydrophilicity of the intake ports (water-wet membranes and/or fritted discs) of water-wet pressure transducers, they may be treated with a solution of NaOH.
3. An alternate pressure transmission system with a higher level of sensitivity and accuracy may be used. One such system, (Honeywell® Pressure Transmitter), was employed by Hammervold, *et al.* (1998). Alternatively, more sensitive pressure transducers from Validyne® and/or Omega® may also be tested.
4. The kind of accuracy for the phase pressure data required in this type of laboratory research work may possibly be achieved by making use of manometer(s), provided that an automatic system of data logging from the manometer(s) is available.

8.2.4. Injection System

1. At this stage, an ON/OFF option for both of the injection pumps has not been hooked-up with the rest of the data acquisition and instrument

control system. It would be convenient to attach both pumps through their respective controllers with the existing data acquisition system.

2. Although the current Q type FMI pumps, along with the pulse dampeners, provide essentially pulse free flow, it would be preferable to use a screw type (or some other equivalent type) pumping system. This would help in eliminating the extremely minor pressure pulses associated with pumping rates at higher stroke lengths.

8.2.5. Data Acquisition and Analysis

1. As far as the data acquisition by using LabVIEW is concerned, the current system provides an excellent format for output data files. One can easily use the output data files for further analysis in MS Excel environments.
2. However, since LabVIEW is a complete data acquisition and analysis software, further modifications to the data acquisition and instrument control system may be introduced.
3. It is possible to analyze the collected data within the environment of LabVIEW. This may enhance the efficiency and effectiveness of the current analysis system.
4. Moreover, efforts should be made to extend the current data acquisition system to the next higher level where the analyzed data, in addition to the raw data, may be observed visually on the computer screen in real time.

8.2.6. Materials

1. A core holder constructed with acrylic sheet is used in this study. Fabrication and machining of acrylic is relatively easy; however, a perfectly smooth surface is rather difficult to achieve. Therefore, an alternate core holder material with a minimum dielectric constant should be tested in future research work.

2. Porous media of two different grain sizes (porosity values) were used in this study. To gain further and rather better understanding of the role of porosity in interfacial coupling phenomena, a wider range of grain sizes should be used.
3. Similarly, to investigate the effect of mobility ratio on interfacial coupling, nonwetting phases of two different viscosity values were used in this study. It is recommended that a wide variety of fluids be used to understand the possible impact of fluid properties on interfacial coupling phenomena.
4. The current choice of fluids and porous media should be expanded so that application of the modified two-phase flow formulation developed in this study may be extended to and verified for heavy oil reservoirs and/or tar sand deposits.

8.2.7. Travel Track

1. At present, a chain driven travel track to obtain dynamic saturation and pressure scans along the length of core is used. A significant level of noise and vibration was noticed during the scanning process. This type of noise and vibration may exert adverse effects on the quality of dynamic saturation and pressure profiles. To overcome this problem, a better travel track such as the one manufactured by PIC[®] may be used to replace the existing travel track.
2. To conduct the flooding experiments in vertical and/or in any other angle, it is recommended that the complete layout of the whole mechanical set-up be modified.

8.3. Numerical Simulation

It is extremely important to develop a reservoir simulator using the newly found understanding of interfacial coupling phenomena during linear and 1-D two-

phase flow through porous media. For this purpose, finite difference, finite element, and/or cellular automata techniques may be employed.

Once the interfacial coupling theory is proved experimentally, then, logically, the next step should be to investigate its implications by comparing the results obtained with and without its incorporation in the existing two-phase flow formulation. This goal can be best achieved by developing a numerical simulator. Therefore, in addition to conducting more experimental research, the development of a reservoir simulator is strongly recommended for any future study.

REFERENCES

1. Aleman, M.A., Ramamohan, T.R. and Slattery, J.C., (1989), "The difference between steady-state and unsteady-state relative permeabilities", *Transport in Porous Media*, Vol. 4, pp. 448-493.
2. Amyx, J.W., Bass, D.M., Jr. and Whiting, R.L., (1960), "*Petroleum Reservoir Engineering*", McGraw Hill Book Co., New York.
3. Arps, J.J. and Roberts, T.G., (1955), "The effect of relative permeability ratio, the oil gravity, and the solution gas-oil ratio on the primary recovery from depletion type reservoir", *Trans. AIME*, Vol. 204, pp. 120-127.
4. Arulanandan, K. and Smith, S.S., (1973), "Electrical dispersion in relation to soil structure", *Journal of the Soil Mechanics and Foundations Division*, December, pp. 1113-1133.
5. Auriault, J.L. and Lewandowska, J., (1994), "On the cross-effects of coupled macroscopic transport equations in porous media", *Transport in Porous Media*, Vol. 16, pp. 31-52.
6. Auriault, J.L. and Lebaigue, O., (1989), "Dynamics of two immiscible fluids flowing through deformable porous media", *Transport in Porous Media*, Vol. 4, pp. 105-128.
7. Auzeais, F.M., Dunsmuir, J., Ferreol B.B., Martys, N., Olson, J., Ramakrishnan, T.S., Rothman, D.H. and Schwartz, L.M., (1996), "Transport in sandstone: A study based on three dimensional microtomography", *Geophysical Res. Lett.*, April 1, Vol. 23(7), pp. 705-708.
8. Avraam, D.G. and Payatakes, A.C., (1995a), "Generalized relative permeability coefficients during steady-state two-phase flow in porous media, and correlation with the flow mechanisms", *Transport in Porous Media*, Vol. 20, pp. 135-168.
9. Avraam, D.G. and Payatakes, A.C., (1995b), "Flow regimes and relative permeabilities during steady-state two-phase flow in porous media", *J. Fluid Mech.*, Vol. 293, pp. 207-236.

10. Ayub, M. and Bentsen, R.G., (1999a), "Interfacial viscous coupling: a myth or reality?", *Journal of Petroleum Science & Engineering*, Vol. 23, pp. 13-26.
11. Ayub, M. and Bentsen, R.G., (1999b), "Measurement of dynamic saturation profiles", paper accepted for publication, *Journal of Canadian Petroleum Technology*.
12. Babchin, A.J., Yuan, J.Y. and Nasr, T., (1998), "Generalized phase mobilities in gravity drainage processes", Paper No. 98-09, presented at the 49th Annual Technical Meeting of The Petroleum Society of CIM in Calgary, Canada, June 8-10.
13. Bachmat, Y. and Bear, J., (1986), "Macroscopic modelling of transport phenomena in porous media. 1: The continuum approach", *Transport in Porous Media*, Vol. 1, pp. 213-240.
14. Bacri, J., Chaouche, M. and Salin, D., (1990), "Modèle simple de perméabilités croisées", *C. R. Acad. Sci., Paris*, Vol. 311, Series II, pp. 591-596.
15. Bail, P.T. and Marsden, S.S., (1957), "Saturation distribution in a linear system during oil displacement", *Producers Monthly*, June, Vol. 21(8), pp. 22-32.
16. Batycky, J.P., McCaffery, F.G., Hodgins, P.K. and Fisher, D.B., (1981), "Interpreting relative permeability and wettability from unsteady-state displacement measurements", *SPEJ.*, Vol. 21(3), pp. 296-308.
17. Bear, J. and Bachmat, Y., (1986), "Macroscopic modeling of transport phenomena in porous media. 2: Application to mass, momentum and energy transport", *Transport in Porous Media*, Vol. 1, pp. 241-269.
18. Bear, J., (1972), *"Dynamics of Fluids in Porous Media"*, Elsevier Publishing Co. Inc., New York.
19. Bedford, A. and Drumheller, D.S., (1983), "Recent advances - theories of immiscible and structured mixtures", *Int. J. Engg. Sci.*, Vol. 21(8), pp. 863-960.

20. Bentsen, R.G., (1999), "The physical origin of interfacial coupling in two-phase flow through porous media", submitted for publication to *Transport in Porous Media*.
21. Bentsen, R.G., (1998a), "Influence of hydrodynamic forces and interfacial momentum transfer on the flow of two immiscible phases", *Journal of Petroleum Science & Engineering*, Vol. 19, pp. 177-190.
22. Bentsen, R.G., (1998b), "Effect of momentum transfer between fluid phases on effective mobility", *Journal of Petroleum Science & Engineering*, Vol. 21, pp. 27-42.
23. Bentsen, R.G., (1997), "Impact of model error on the measurement of flow properties needed to describe flow through porous media", *Revue de L'institut Francais du Petrole*, Vol. 52(3), pp. 299-315.
24. Bentsen, R.G., (1994a), "Effect of hydrodynamic forces on the pressure-difference equation", *Transport in Porous Media*, Vol. 17, pp. 133-144.
25. Bentsen, R.G., (1994b), "Effect of hydrodynamic forces on capillary pressure and relative permeability", *Transport in Porous Media*, Vol. 17, pp. 121-132.
26. Bentsen, R.G., (1994c), "An investigation into whether the nondiagonal mobility coefficients which arise in coupled, two-phase flow are equal", *Transport in Porous Media*, Vol. 14(1), pp. 23-32.
27. Bentsen, R.G., (1992a), "Construction and experimental testing of a new pressure difference equation", *AOSTRA J. Res.*, Vol. 8, pp. 159-168.
28. Bentsen, R.G., (1992b), "Effect of neglecting viscous coupling and dynamic capillary pressure on the one-dimensional flow of two immiscible phases through a porous medium", *SPE unsolicited paper No. SPE-26016*.
29. Bentsen, R.G., (1985), "A new approach to instability theory in porous media", *SPE J.*, Vol. 25, pp. 765-779.
30. Bentsen, R.G., (1978), "Conditions under which the capillary term may be neglected", *Journal of Canadian Petroleum Technology*, Vol. 17(4), pp. 25-30.

31. Bentsen, R.G. and Manai, A.A., (1993), "On the use of conventional cocurrent and countercurrent effective permeabilities to estimate the four generalized permeability coefficients which arise in coupled, two-phase flow", *Transport in Porous Media*, Vol. 11, pp. 243-262.
32. Bentsen, R.G. and Manai, A.A., (1991), "Measurement of cocurrent and countercurrent relative permeability curves using the steady-state method", *AOSTRA J. Res.*, Vol. 7, pp. 169-181.
33. Bentsen, R.G. and Sarma, H.K., (1989), "The external-drive method: Its use and abuse", *AOSTRA J. Res.*, Vol. 5, pp. 61-74.
34. Berge, H.F.M.T. and Bolt, G.H., (1988), "Coupling between liquid flow and heat flow in porous media: A connection between two classical approaches", *Transport in Porous Media*, Vol. 3, pp. 35-49.
35. Bolt, G.H. and Groenevelt, (1969), "Coupling phenomenon as a possible cause for non-Darcian behavior of water in soil", *Bull. I.A.S.H.* Vol. 14(2), pp. 17-26.
36. Bourbiaux, B.J. and Kalaydjian, F.J., (1990), "Experimental study of cocurrent and countercurrent flows in natural porous media", *SPEERE*, Aug., Vol. 5, pp. 361-368.
37. Bowen, R.M., (1982), "Compressible porous media models by use of the theory of mixtures", *Int. J. Eng. Sci.*, Vol. 20(6), pp. 697-735.
38. Bowen, R.M., (1980), "Incompressible porous media models by use of the theory of mixtures", *Int. J. Eng. Sci.*, Vol. 18, pp. 1129-1148.
39. Brown, H.W., (1951), "Capillary pressure investigations", *Trans. AIME.*, Vol. 192, pp. 67-74.
40. Bruce, W.A. and Welge, H.J., (1947), "The restored-state method for determination of oil in place and connate water", *Drill. and Prod. Prac.*, API, pp. 166-174.
41. Buckley, S.E. and Leverett, M.C., (1942), "Mechanism of fluid displacement in sands", *Trans. AIME*, Vol. 146, pp. 107-116.
42. Calhoun, J.C., Jr., (1960), "*Fundamentals of Reservoir Engineering*", The University of Oklahoma Press, Norman, USA.

43. Caudle, B.H., Slobod, R.L. and Brownscombe, E.R., (1951), "Further developments in the laboratory determination of relative permeabilities", *Trans. AIME*, Vol. 192, pp. 145-150.
44. Chang, S., (1996), "*Experimental Apparatus For Measurement of Generalized Permeability Coefficients Using Steady State and Unsteady State, Cocurrent and Countercurrent Flow Methods*", M.Sc. Thesis, University of Alberta, Canada.
45. Chatenever, A. and Calhoun, J.C., Jr., (1952), "Visual examinations of fluid behavior in porous media - Part 1", *Trans. AIME*, Vol. 195, pp. 149-156.
46. Chavent, G., (1976), "A new formulation of diphasic incompressible flow in porous media", in *Lecture Notes in Mathematics 503*, Springer, New York.
47. Cheng, P. and Wang, C.Y., (1996), "A multiphase mixture model for multiphase, multicomponent transport in capillary porous media - II. Numerical simulation of the transport of organic compounds in the subsurface", *Int. J. Heat Mass Transfer*, Vol. 39(17), pp. 3619-3632.
48. Childs, E.C., (1945), "The water table, equipotentials, and streamlines in drained land: III", *Soil Sci.*, Vol. 59, pp. 405-415.
49. Chouke, R.L., von Meurs, P. and van der Poel, C., (1959), "The instability of slow, immiscible, viscous liquid-liquid displacements in permeable media", *Trans. AIME*, Vol. 216, pp. 188-194.
50. Cloud, W.F., (1930), "Variation of pressure gradient with distance of rectilinear flow of gas-saturated oil and unsaturated oil through unconsolidated sands", *Trans. AIME*, Vol. 86, pp. 337-350.
51. Collins, R.E., (1961), "*Flow of Fluids Through Porous Materials*", McGraw Hill, New York, N.Y., pp. 161 ff.
52. Corey, A.T. and Rathjens, C.H., (1956), "Effect of stratification on relative permeability", Technical Note, *Trans. AIME*, Vol. 207, pp. 358-360.
53. Craig, F.F., Jr., (1971), "*The Reservoir Engineering Aspects of Waterflooding*", Monograph Vol. 3, SPE of AIME, New York.

54. Craig, F.F., Jr., (1952), "Errors in calculation of gas injection performance from laboratory data", *JPT*, Aug., pp. 23-24(Sec. 1), 6(Sec. 2).
55. Danis, M. and Jacquin, Ch., (1983), "Influence du contraste de viscosités sur les perméabilités relatives lors du drainage: Experimentation et modélisation, *Revue de l'IFP*, Vol. 38(6), pp. 723-733.
56. Darcy, H., (1856), "Les fontaines publiques de la ville de Dyon", *Victor Dalmont*, Paris, France.
57. Davis, L.A., (1980), "VHF electrical measurement of saturation in laboratory floods", SPE Paper No. 8847, presented at the *First Joint SPE/DOE Symposium on Enhanced Oil Recovery*, April 20-23, Tulsa, Oklahoma, USA.
58. De Groot, S.R., (1951), "*Thermodynamics of Irreversible Processes*", North-Holland Publishing Co., Amsterdam.
59. De la Cruz, V. and Spanos, T.J.T., (1983), "Mobilization of oil ganglia", *AIChE J.*, Vol. 29(5), pp. 854-858.
60. Del Riop, J.A. and De Harro, M.L., (1992), "Extended irreversible thermodynamics as a framework for transport phenomena in porous media", *Transport in Porous Media*, Vol. 9, pp. 207-221.
61. Doolen, G.D., Frisch, U., Hasslacher, B., Orszag, S. and Wolfram, S., (1990), *Lattice Gas Methods for Partial Differential Equations*, Addison-Wesley Pub. Co.
62. Drumheller, D.S., (1978), "The theoretical treatment of a porous solid using a mixture theory", *Int. J. Solids Structures*, Vol. 14, pp. 441-456.
63. Dullien, F.A.L. and Dong, M., (1996), "Experimental determination of the flow transport coefficients in the coupled equations of two-phase flow in porous media", *Transport in Porous Media*, Vol. 25, Oct., pp. 97-120.
64. Ehrlich, R., (1993), "Viscous coupling in two-phase flow in porous media and its effect on relative permeabilities", *Transport in Porous Media*, Vol. 11(3), pp. 201-218.

65. Emmett, W.R., Beaver, K.W. and McCaleb, J.A., (1971), "Little Buffalo basin Tensleep heterogeneity and its influence on drilling and secondary recovery", *JPT*, Feb., pp. 161-168.
66. Fatt, I. and Waldemar, A. K., Jr., (1959), "Effect of fractional wettability on multiphase flow through porous media", *Trans. AIME*, Vol. 216, pp. 426-432.
67. Fatt, I., (1953), "The effect of overburden pressure on relative permeability", *JPT.*, October, pp. 15-16.
68. Fatt, I. and Dykstra, H., (1951), "Relative permeability studies", *Trans. AIME*, Vol. 192, pp. 249-256.
69. Ferreol, B. and Rothman, D.H., (1995), "Lattice-Boltzmann simulation of flow through fontainebleau sandstone", *Transport in Porous Media*, Vol. 20, pp. 3-20.
70. Fletcher, J.E., (1949), "Some properties of water solutions that influence infiltration", *Trans. Amer. Geophysical Union*. Vol. 30(4), pp. 548-554.
71. Frisch, U., Hasslacher, B. and Pomeau, Y., (1986), "Lattice-gas automata for the Navier-Stokes equation", *Phys. Rev. Lett.*, Vol. 56(14), pp. 1505-1508.
72. Gao, Y. and Sharma, M.M., (1994a), "A LGA model for dispersion in heterogeneous porous media", *Transport in Porous Media*, Vol. 17, pp. 19-32.
73. Gao, Y. and Sharma, M.M., (1994b), "A LGA model for fluid flow in heterogeneous porous media", *Transport in Porous Media*, Vol. 17, pp. 1-17.
74. Geffen, T.M. and Gladfelter, R.E., (1952), "A note on the X-ray absorption method of determining fluid saturations in cores", *Trans. AIME*, Vol. 195, pp. 322-323.
75. Geffen, T.M., Parrish, D.R., Haynes, G.W. and Morse, R.A., (1952), "Efficiency of gas displacement from porous media by liquid flooding", *Trans. AIME*, Vol. 195, pp. 29-38.

76. Geffen, T.M., Owens, W.W., Parrish, D.R. and Morse, R.A., (1951), "Experimental investigation of factors affecting laboratory relative permeability measurements", *Trans. AIME*, Vol. 192, pp. 99-110.
77. Goode, P.A., (1991), "*Momentum Transfer Across Fluid-Fluid Interfaces in Porous Media*", Ph.D Thesis, Heriot-Watt University, U.K.
78. Goode, P.A. and Ramakrishnan, T.S., (1993), "Momentum transfer across fluid-fluid interfaces in porous media: a network model", *AIChE J.*, Vol. 39(7), pp. 1124-1134.
79. Gray, W.G., (1975), "A derivation of the equations for multi-phase transport", *Chem. Eng. Sci.*, Vol. 30, pp. 229-233.
80. Gray, W.G. and Lee, P.C.Y., (1977), "On the theorems for local volume averaging of multiphase systems", *Int. J. Multiphase Flow*, Vol. 3, pp. 333-340.
81. Greenkorn, R.A., (1983), "*Flow Phenomena in Porous Media*", Marcel Dekker, Inc., New York, USA.
82. Gutman, S., (1990), "Lattice gas methods in porous media computations", *Annual AIChE Meeting (Rock/Fluid Interaction in Petroleum Reservoirs I)*, Nov. 11-16, 1990, Chicago, ILL., USA.
83. Hammervold, W.L., Knutsen, O., Iversen, J.E. and Skjaeveland, S.M., (1998), "Capillary pressure scanning curves by the micropore membrane technique", *Journal of Petroleum Science & Engineering*, Vol. 20, pp. 253-258.
84. Hammervold, W.L. and Skjaeveland, S.M., (1992), "Improvement of diaphragm method for drainage capillary pressure measurement with micro pore membrane", paper presented at the *EUROCAS* meeting, Sept. 8-10, Paris, France.
85. Hassanizadeh, S.M. and Gray, W.G., (1987), "High velocity flow in porous media", *Transport in Porous Media*, Vol. 2, pp. 521-531.
86. Hassanizadeh, M. and Gray, W.G., (1980), "General conservation equations for multi-phase systems: 3. Constitutive theory for porous media flow", *Advances in Water Resources*, Vol. 3, pp. 25-40.

87. Hassanizadeh, M. and Gray, W.G., (1979a), "General conservation equations for multi-phase systems: 2. Mass, momenta, energy, and entropy equations", *Advances in Water Resources*, Vol. 2, pp. 191-203.
88. Hassanizadeh, M. and Gray, W.G., (1979b), "General conservation equations for multi-phase systems: 1. Averaging procedure", *Advances in Water Resources*, Vol. 2, pp. 131-144.
89. Hassler, G.L. and Brunner, E., (1945), "Measurement of capillary pressures in small core samples", *Trans. AIME*, Vol. 160, pp. 114-123.
90. Hassler, G.L., Rice, R.R. and Leeman, E.H., (1936), "Investigations on the recovery of oil from sandstones by gas drive", *Trans. AIME*, Vol. 118, 116-137.
91. Honarpour, M. and Mahmood, S.M., (1988), "Relative-permeability measurements: An overview", *JPT*, Aug., pp. 963-966.
92. Honarpour, M., Koederitz, L. and Harvey, A.H., (1986), "*Relative Permeability of Petroleum Reservoir*", CRC Press. Inc., Boca Raton, FL, USA.
93. Hubbert, M.K., (1950), "Review and Discussion, *Physical Principles of Oil Production* by Morris Muskat", *The J. of Geology*, Vol. 58(6), pp. 655-660.
94. Islam, M.R., (1985), "*An Investigation on the Impact of Flow Regime on Effective Permeabilities*", M.Sc. Thesis, University of Alberta, Canada.
95. Islam, M.R. and Bentsen, R.G., (1987), "Effect of different parameters on two-phase relative permeability", *AOSTRA J. Res.*, Vol. 3, pp. 69-90.
96. Islam, M.R. and Bentsen, R.G., (1986), "A dynamic method for measuring relative permeability", *Journal of Canadian Petroleum Technology*, Jan.-Feb., pp. 39-50.
97. Jennings, H.H., (1957), "Surface properties of natural and synthetic porous media", *Producers Monthly*. Vol. 21(5), pp. 20-24.
98. Johnson, E.F., Bossler, D.P. and Naumann, V.O., (1959), "Calculation of relative permeability from displacement experiments", *Trans. AIME*, Vol. 216, pp. 370-372.

99. Jones, S.C. and Roszelle, W.O., (1978), "Graphical techniques for determining relative permeability from displacement experiments", *JPT*, Vol. 30(5), pp. 807-817.
100. Josendal, V.A., Sandford, B.B. and Wilson, J.W., (1952), "Improved multiphase flow studies employing radioactive tracers", *Trans. AIME*, Vol. 195, pp. 65-76.
101. Kadanoff, L.P., McNamara, G.R. and Zanetti, G., (1989), "From automata to fluid flow: comparisons of simulation and theory", *Physical Review A*, Oct. 15, Vol. 40(8), pp. 4527-4541.
102. Kalaydjian, F., (1990), "Origin and quantification of coupling between relative permeabilities for two-phase flows in porous media", *Transport in Porous Media*, Vol. 5(3), pp. 215-229.
103. Kalaydjian, F., (1987), "A macroscopic description of multiphase flow in porous media involving space-time evolution of fluid/fluid interface", *Transport in Porous Media*, Vol. 2, pp. 537-552.
104. Kalaydjian, F. and Marle, C.M., (1987), "Thermodynamic aspects of multiphase flow in porous media", *2nd Inst. Français Du Pétrole Explor. Res. Conf. (Migration of Hydrocarbons in Sedimentary Basins)*, June 15-19, Carcans, France, pp. 513-531.
105. Kantzas, A., (1990), "Investigation of physical properties of porous rocks and fluid flow phenomena in porous media using computer assisted tomography", *In Situ*, Vol. 14(1), pp. 77-132.
106. Katchalsky, A. and Curran, P.F., (1967), "*Nonequilibrium Thermodynamics in Biophysics*", Harvard University Press, Cambridge, Massachusetts.
107. Kerig, P.D. and Watson, A.T., (1987), "A new algorithm for estimating relative permeabilities from displacement experiments", *SPEE.*, Feb., pp. 103-112.
108. Kerig, P.D. and Watson, A.T., (1986), "Relative permeability estimation from displacement experiments: An error analysis", *SPEJ*, March, pp. 175-182.

109. Killins, C.R., Nielsen, R.F. and Calhoun, J.C., (1953), "Capillary desaturation and imbibition in porous rocks", *Producers Monthly*, Dec., Vol. 18, pp. 30-39.
110. Kimbler, O.K. and Caudle, B.H., (1957), "New technique for study of fluid flow and phase distribution in porous media", *Oil & Gas J.*, Dec. 16, Vol. 55(50), Part-4, pp. 85-88.
111. King, P.R., (1996), "Upscaling permeability: Error analysis for renormalization", *Transport in Porous Media*, Vol. 23, pp. 337-354.
112. Kinny, J.H., Breunig, T.M., Starr, T.L., Haupt, D., Nichols, M.C., Stock, S.R., Butts, M.D. and Saroyan, R.A., (1993), "X-ray tomographic study of chemical vapor infiltration processing of ceramic composite", *Science*, Vol. 26, pp. 789-792.
113. Klute, A., (1967), "Notes on flow water in unsaturated soils", presented at the *M.I.T. Summer Session on Ground Water Hydrology and Flow Through Porous Media*.
114. Kraszewski, A., (1996), "*Microwave Aquametry - Electromagnetic Wave Interaction with Water-Containing Materials*", IEEE Press, New York, USA.
115. Kyte, J.R. and Rapoport, L.A., (1958), "Linear Waterflood behavior and end effects in water-wet porous media", *Trans. AIME*, Vol. 213, pp. 423-426.
116. Laird, A.D.K. and Putman, J.A., (1959), "Three component saturation in porous media by X-ray techniques", *Trans. AIME*, Vol. 216, pp. 216-220.
117. Laird, A.D.K. and Putman, J.A., (1951), "Fluid saturation in porous media by X-ray Technique", *Trans. AIME*, Vol. 192, pp. 275-284.
118. Leas, W.J.; Jenks, L.H. and Russel, C.D., (1950), "Relative permeability to gas", *Trans. AIME.*, Vol. 189, pp. 65-72.
119. Lefebvre du Prey, E.J., (1973), "Factors affecting liquid-liquid relative permeabilities of a consolidated porous medium", *SPEJ*, Vol. 13(1), pp. 39-47.
120. Lelièvre, R.F., (1966), '*Etude d'écoulements disphasiques permanents à contre-courants en milieu poreux – Comparaison avec les*

écoulements de même sens (in French), Ph.D. Thesis, University of Toulouse, France.

121. Leverett, M.C., (1941), "Capillary behavior in porous solids", *Trans. AIME*, Vol. 142, pp. 152-169.
122. Leverett, M.C., (1939), "Flow of oil-water mixtures through unconsolidated sands", *Trans. AIME*, Vol. 132, pp. 149-171.
123. Leverett, M.C. and Lewis, W.B., (1941), "Steady flow of gas-oil-water mixtures through unconsolidated sands", *Trans. AIME*, Vol. 142, pp. 107-116.
124. Levine, J.S., (1954), "Displacement experiments in a consolidated porous system", *Trans. AIME*, Vol. 201, pp. 57-66.
125. Liang, Q., (1993), "*Interaction Between Immiscible Phases Flowing at Different Velocities in Porous Media*", D.E. Thesis, Louisiana Tech University, USA.
126. Liang, Q. and Lohrenz, J., (1994), "Dynamic method of measuring coupling coefficients of transport equations of two-phase flow in porous media", *Transport in Porous Media*, Vol. 15, pp. 71-79.
127. Lin, C.C., (1955), "*The Theory of Hydrodynamic Stability*", Cambridge University Press, UK.
128. Longeron, D., Hammervold, W.L. and Skjaeveland, S.M., (1994), "Water-oil capillary pressure and wettability measurement using micropore technique", paper presented at *The International Symposium of the Society of Core Analysts*, Sept. 12-14, Stavanger, Norway.
129. Longeron, D., (1987), "Study of the influence of thermodynamic parameters on two-phase flow in porous media", *2nd Inst. Francais Du Petrole Explor. Res. Conf. (Migration of Hydrocarbons in Sedimentary Basins)*, June 15-19, Carcans, France, pp. 257-279.
130. Lorenz, P.B., Donaldson, E.C., and Thomas, R.D., (1974), "*Use of Centrifuge Measurements of Wettability to Predict Oil Recovery*", U.S. Bureau of Mines, 7873.

131. Manai, A.A., (1991), *"The measurement of cocurrent and countercurrent relative permeabilities and their use to estimate generalized relative permeabilities"*, M.S. Thesis, University of Alberta, Canada.
132. Mannseth, T., (1991), "Commentary on 'Origin and quantification of coupling between relative permeabilities for two-phase flows in porous media' by F. Kalaydjian". *Transport in Porous Media*, Vol. 6, pp. 469-471.
133. McCaffery, F.G., (1973), *"The effect of wettability on relative permeability and imbibition in porous media"*, Ph.D. Thesis, University of Calgary, Canada.
134. McCaffery, F.G. and Bennion, D.W., (1974), "The effect of wettability on two-phase relative permeabilities", *Journal of Canadian Petroleum Technology*, Oct.-Dec., pp. 42-53.
135. Melrose, J.C. and Brandner, C.F., (1974), "Role of Capillary forces in determining microscopic displacement efficiency for oil recovery by waterflooding", *Journal of Canadian Petroleum Technology*, Oct.-Dec., pp. 54-62.
136. Monaco, R., (1989), *"Discrete Kinetic Theory, Lattice Gas Dynamics and Foundations of Hydrodynamics"*, World Scientific, Singapore.
137. Moore, T.F. and Slobod, R.L., (1956), "The effect of viscosity and capillarity on the displacement of oil by water", *Producers Monthly*, Aug., pp. 20-30.
138. Moore, T.V., (1938), "Behavior of fluids in oil reservoirs", *Bull. Ame. Asso. Pet. Geo.*, Vol. 22(9), pp. 1237-1249.
139. Morse, R.A., Terwilliger, P.K. and Yuster, S.T., (1947), "Relative permeability measurements on small core sample", *Oil & Gas J.*, Aug., pp. 109.
140. Mungan, N., (1971), *"The influence of wettability and laboratory handling on relative permeability measurements using reservoir fluids"*, Research Note, RN-2, February, Petroleum Recovery Institute, Calgary, Canada.
141. Mungan, N., (1964), "Role of wettability and interfacial tension in waterflooding", *SPEJ*, June, Vol. 4, pp. 115-123.

142. Murdoch, A.I. and Kowalski, S.J., (1992), "On fluid-fluid coupling within porous media: A mixture theoretical approach based upon molecular considerations", *Transport in Porous Media*, Vol. 8, pp. 47-70.
143. Muskat, M., (1982), "*The Flow of Homogeneous Fluids through Porous Media*", International Human Resources Development Corporation, Boston, pp. 127 ff.
144. Muskat, M., (1949), "*The Physical Principles of Oil Production*", McGraw Hill, New York.
145. Muskat, M., Wyckoff, R.D., Botset, H.G. and Meres, M.W., (1937), "Flow of gas-liquid mixtures through sands", *Trans. AIME*, Vol. 123, pp. 69-96.
146. Muskat, M. and Meres, M.W., (1936), "The flow of heterogeneous fluids through porous media", *Physics*, Vol. 7, Sept., pp. 346-363.
147. Naar, J., Wygal, R.J. and Henderson, J.H., (1962), "Imbibition relative permeability in unconsolidated porous media", *SPEJ*, March, Vol. 2, pp. 13-17.
148. Narasimhan, T.N., (1980), "A note on volume-averaging", *Advances in Water Resources*, Vol. 3, pp. 135-139.
149. Nind, T.E.W., Ed., (1964), "*Principles of Oil Production*", McGraw Hill, New York, USA.
150. Odeh, A.S., (1959), "Effect of viscosity ratio on relative permeability", *Trans. AIME*, Vol. 216, pp. 346-353.
151. Olson, J.F. and Rothman, D.H., (1997), "Two-fluid flow in sedimentary rock: simulation, transport, and complexity" *J. Fluid Mech.*, Vol. 341, June 25, pp. 343-370.
152. O'Mera, D.J., Jr. and Leas, W.O., (1983), "Multiphase relative permeability measurement using an automated centrifuge", SPE paper No. 12128, presented at the *SPE 58th Ann. Tech. Conf. and Exhib.*, San Francisco, USA.
153. Onsager, L., (1931a), "Reciprocal relations in irreversible processes-I" *Physical Review*, Vol. 37, pp. 405-426.

154. Onsager, L., (1931b), "Reciprocal relations in irreversible processes-II" *Physical Review*, Vol. 38, pp. 2265-2279.
155. Orlov, S.I., (1970), "*Calculation and Designing of Coaxial Resonators*", (in Russian), published by The Soviet Wireless, Moscow, USSR.
156. Osoba, J.S., Richardson, J.G., Kerver, J.K., Hafford, J.A. and Blair, P.M., (1951), "Laboratory measurements of relative permeability", *Trans. AIME*, Vol. 192, pp. 47-56.
157. Outmans, H.D., (1962a), "Transient interfaces during immiscible liquid-liquid displacement in porous media", *SPEJ*, June, pp. 156-164.
158. Outmans, H.D., (1962b), "Nonlinear theory for frontal stability and viscous fingering in porous media", *SPEJ*, June, pp. 165-176.
159. Owens, W.W. and Archer, D.L., (1971), "The effect of rock wettability on oil-water relative permeability relationships", *JPT*, July, pp. 873-878.
160. Parsons, R.W., (1975), "Microwave Attenuation - A new tool for monitoring saturations in laboratory flooding experiments", *SPEJ*, Vol. 15(4), pp. 302-310.
161. Perrine, R.L., (1961), "The development of stability theory for miscible liquid-liquid displacement", *Trans. AIME*, Vol. 222, pp. 17-25.
162. Peters, E.J., (1979), "*Stability Theory and Viscous Fingering in Porous Media*", Ph.D. Thesis, University of Alberta, Canada.
163. Peters, E.J. and Khataniar, S., (1987), "The effect of instability on relative permeability curves obtained by dynamic-displacement method", *SPEFE*, Dec., pp. 469-474.
164. Peters, E.J. and Flock, D.L., (1981), "The onset of instability during two-phase immiscible displacement in porous media", *SPEJ*, Vol. 21(2), pp. 249-258.
165. Philip, J.R., (1972), "Flow in porous media", *Proceedings of the XIII International Congress of Theoretical and Applied Mechanics*, Moscow University, August 21-26, pp. 279-294.

166. Plummer, F.B., Hunter, J.C., Jr. and Timmerman, E.H., (1937), "Flow of mixtures of oil and water through sand", *API Drill. Prod. Pract.*, pp. 417-421.
167. Purcell, W.R., (1950), "Interpretation of capillary pressure data", *Trans. AIME*, Vol. 189, pp. 369-371.
168. Purcell, W.R., (1949), "Capillary pressures - Their measurement using mercury and the calculation of permeability therefrom", *Trans. AIME*, Vol. 186, pp. 39-48.
169. Rachford, H.H., Jr., (1964), "Instability in waterflooding oil from water-wet porous media containing connate water", *SPEJ*, June, pp. 133-148.
170. Rakotomalala, N., Salin, D. and Yortsos, C.Y., (1995), "Viscous coupling in a model porous medium geometry: Effect of fluid contact area", *App. Scientific Res.*, Vol. 55, pp. 155-169.
171. Rapoport, L.A. and Leas, W.J., (1953), "Properties of linear waterfloods", *Trans. AIME*, Vol. 198, pp. 139-148.
172. Rapoport, L.A. and Leas, W.J., (1951), "Relative permeability to a liquid in a liquid-gas system", *Trans. AIME*, Vol. 192, pp. 83-98.
173. Richardson, J.G., (1957), "The calculation of waterflood recovery from steady-state relative permeability data", *Trans. AIME*, Vol. 210, pp. 373-375.
174. Richardson, J.G., Kerver, J.K., Hafford, J.A. and Osoba, J.S., (1952), "Laboratory determination of relative permeability", *Trans. AIME*, Vol. 195, pp. 187-196.
175. Rose, W., (1997), "An upgraded viscous coupling measurement methodology", *Transport in Porous Media*, Vol. 28, pp. 221-231.
176. Rose, W., (1996), "About Transport Processes in porous media", *Handout* distributed in the seminar held by the Alberta Research Council of Canada, July 12, 1996.
177. Rose, W., (1995), "Ideas about viscous coupling in anisotropic media", *Transport in Porous Media*, Vol. 18, pp. 87-93.

178. Rose, W., (1993), "Coupling coefficients for two-phase flow in pore spaces of simple geometry", *Transport in Porous Media*, Vol. 10, pp. 293-296.
179. Rose, W., (1991a), "Richard's assumptions and Hassler's presumptions", *Transport in Porous Media*, Vol. 6(1), pp. 91-99.
180. Rose, W., (1991b), "Critical questions about the coupling hypothesis", *Journal of Petroleum Science & Engineering*, Vol. 5(4), pp. 299-307.
181. Rose, W., (1990a), "Coupling coefficients for two-phase flow in pore spaces of simple geometry", *Transport in Porous Media*, Vol. 5(1), pp. 97-102.
182. Rose, W., (1990b), "Modeling extent of unnoticed coupling effects", *SPE unsolicited paper No. SPE-20379*.
183. Rose, W., (1990c), "Lagrangian simulation of coupled two-phase flows", *Mathematical Geology*, Vol. 22(6), pp. 641-654.
184. Rose, W., (1989), "Data interpretation problems to be expected in the study of coupled two-phase flow of immiscible fluid flows in porous media", *Transport in Porous Media*, Vol. 4, pp. 185-198.
185. Rose, W., (1988a), "Measuring transport coefficients necessary for the description of coupled two-phase flow of immiscible fluids in porous media", *Transport in Porous Media*, Vol. 3(2), pp. 163-171.
186. Rose, W., (1988b), "Attaching new meaning to the equations of Buckley and Leverett", *Journal of Petroleum Science & Engineering*, Vol. 1(3), pp. 223-228.
187. Rose, W., (1969), "Transport through interstitial paths of porous solids", *METU J. of Pure and App. Sci.*, Vol. 2(2), pp. 117-132.
188. Rose, W., (1954), "Problems of relative permeability", *Petroleum Engineer*. Vol. 26(4), pp. B58-B72.
189. Rose, W., (1951), "Some problems of relative permeability measurement", *World Petroleum Cong. Proc., Section-II*, The Hague, pp. 446-459.

190. Rose, W.R. and Bruce, W.A., (1949), "Evaluation of capillary pressure character in petroleum reservoir rocks", *Trans. AIME*, Vol. 186, pp. 127-142.
191. Rothman, D.H., (1990), "Macroscopic laws for immiscible two-phase flow in porous media: Results from numerical experiments", *J. Geophysical Res.*, Vol. 95(B6), pp. 8663-8674.
192. Rothman, D.H., (1988), "Cellular- automation fluids: A model for flow in porous media", *Geophysics*, Vol. 53(4), April, pp. 509-518.
193. Rothman, D.H. and Keller, J.M., (1988), "Immiscible cellular- automation fluids", *J. Stat. Phys.*, Vol. 52(3/4), April, pp. 1119-1127.
194. Saeedi, J., (1979), "*A Comparison of Theoretical and Experimental Saturation profiles in Porous Media*", M.Sc. Thesis, University of Alberta, Canada.
195. Sandberg, C.R., Gournay, L.S. and Sippel, R.F., (1958), "The effect of fluid-flow rate and viscosity on laboratory determinations of oil-water relative permeabilities", *Trans. AIME*, Vol. 213, pp. 36-43.
196. Saraf, D.N. and Fatt, I., (1967), "Three-phase relative permeability measurement using a N.M.R. technique for estimation fluid saturation", *SPEJ*, Sept. pp. 235-242.
197. Sarem, A.M., (1966), "Three-phase relative permeability measurements by unsteady-state methods", *SPEJ*, Sept. pp. 199-205.
198. Sarma, H.K., (1988), "*A study of the impact of instability on the immiscible displacement of one fluid by another*", Ph.D. Thesis, University of Alberta, Canada.
199. Sarma, H.K. and Bentsen, R.G., (1990), "Further experimental validation of the external-drive techniques", *Journal of Canadian Petroleum Technology*, Vol. 29(4), pp. 75-83.
200. Sarma, H.K. and Bentsen, R.G., (1989a), "A new method for estimating relative permeabilities from unstabilized displacement data", *Journal of Canadian Petroleum Technology*, Vol. 28(4), pp. 118-128.

201. Sarma, H.K. and Bentsen, R.G., (1989b), "A study of the impact of instability on relative permeability and capillary pressure", *Journal of Petroleum Science & Engineering*, Vol. 2, pp. 311-330.
202. Sarma, H.K. and Bentsen, R.G., (1989c), "A method for reducing model error when estimating relative permeabilities from displacement data", *Journal of Petroleum Science & Engineering*, Vol. 2, pp. 331-347.
203. Sarma, H.K. and Bentsen, R.G., (1987), "An experimental verification of a modified instability theory for immiscible displacement in porous media", *Journal of Canadian Petroleum Technology*, Vol. 26(4), pp. 88-89.
204. Scheidegger, A.E., (1960), "*The Physics of Flow Through Porous Media*", University of Toronto Press, Toronto, Canada.
205. Schneider, F.N. and Owens, W.W., (1970), "Sandstone and carbonate, two-and three-phase relative permeability characteristics", *SPEJ*, March, pp. 75-84.
206. Scott, P.H. and Rose, W., (1953), "An explanation of the Yuster Effect", *JPT*, Nov. Pp. 19-20.
207. Sigmund, P.M. and McCaffery, F.G., (1979), "An improved unsteady-state procedure for determining the relative permeability characteristics of heterogeneous porous media", *SPEJ*, Vol. 19(1), pp. 15-28.
208. Slattery, J.C., (1970), "Two-phase flow through porous media", *AIChE J.*, Vol. 16(3), pp. 345-352.
209. Slattery, J.C., (1969), "Single-phase flow through porous media", *AIChE J.*, Vol. 15(6), pp. 866-872.
210. Slobod, R.L., Chamber, A. and Prehn, W.L., Jr., (1951), "Use of centrifuge for determining connate water, residual oil, and capillary pressure curves of small core samples", *Trans. AIME*, Vol. 192, pp. 127-134.
211. Snell, R.W., (1959), "Measurement of gas-phase saturation in porous media", *J. Inst. Pet.*, Vol. 45, pp. 259-261.

212. Spanos, T.J.T., de la Cruz, V., Hube, J. and Sharma, R.C., (1986), "An analysis of Buckley-Leverett theory", *Journal of Canadian Petroleum Technology*, Vol. 25(1), pp. 71-75.
213. Spanos, T.J.T. and de la Cruz, V., (1984), "Some stability problems during immiscible displacement in porous media", *AOSTRA J. Res.*, Vol. 1, pp. 63-80.
214. Swanson, B.F., (1979), "Visualizing pores and nonwetting phase in porous rock", *JPT*, Jan., pp. 10-18.
215. Tao, T.M. and Watson, A.T., (1984), "Accuracy of JBN estimates of relative permeability: Part I, Error analysis", *SPEJ*, April, Vol. 24(2), pp. 209-214.
216. Terwilliger, P.L., Wilsey, L.E., Hall, H.N., Bridges, P.M. and Morse, R.A., (1951), "An experimental and theoretical investigation of gravity drainage performance", *Trans. AIME*, Vol. 192, pp. 285-296.
217. Trapp, J.A., (1976), "On the relationship between continuum mixture theory and integral averaged equations for immiscible fluids", *Int. J. Eng. Sci.*, Vol. 14, pp. 991-998.
218. Treiber, L.E., Archer, D.L. and Owens, W.W., (1972), "A laboratory evaluation of the wettability of fifty oil producing reservoirs", *SPEJ*, Vol. 12(6), pp. 531-540.
219. van Genabeek, O. and Rothman, D.H., (1996), "Macroscopic manifestations of microscopic flows through porous media: Phenomenology from simulation", *Annu. Rev. Earth Planet. Sci.*, MIT, Cambridge, Vol. 24, pp. 63-87.
220. Wang, C.Y., (1997), "An alternative description of viscous coupling in two-phase flow through porous media", *Transport in Porous Media*, Vol. 28, pp. 205-219.
221. Wang, C.Y. and Cheng, P., (1996), "A multiphase mixture model for multiphase, multicomponent transport in capillary porous media - I. Model development", *Int. J. Heat Mass Transfer*, Vol. 39(17), pp. 3607-3618.

222. Wang, C.Y. and Beckermann, C., (1993), "A two-phase mixture model of liquid-gas flow and heat transfer in capillary porous media-I, Formulation", *Int. J. Heat Transfer*, Vol. 36(11), pp. 2747-2758.
223. Watson, A.T., Richmond, P.C., Kerig, P.D. and Tao, T.M., (1988), "A regression-based method for estimating relative permeabilities from displacement experiments", *SPEERE*, Aug., pp. 953-958.
224. Welge, H.J., (1952), "A simplified method for computing oil recovery by gas or water drive", *Trans. AIME*, Vol. 195, pp. 91-98.
225. Whitaker, S., (1986), "Flow in porous media II: The governing equations for immiscible, two-phase flow", *Transport in Porous Media*, Vol. 1, pp. 105-125.
226. Whitaker, S., (1973), "The transport equations for multi-phase systems", *Chem. Eng. Sci.*, Vol. 28, pp. 139-147.
227. Whitaker, S., (1967), "Diffusion and dispersion in porous media", *AIChE J.*, May, pp. 420-427.
228. Willhite, G.P., (1986), "*Waterflooding*", Society of Petroleum Engineers, Richardson, TX., USA.
229. Wilson, J.W., (1956), "Determination of relative permeability under simulated reservoir conditions", *AIChE J.*, Vol. 2(1), pp. 94-100.
230. Wolfram, S., (1986a), "Cellular automata fluids 1: Basic theory", *J. Stat. Phys.*, Vol. 45, pp. 471-526.
231. Wolfram, S., (1986b), "Theory and applications of cellular automata", *World Scientific*, Singapore.
232. Wyckoff, R.D. and Botset, H.G., (1936), "The flow of gas-liquid mixtures through unconsolidated sands", *Physics*, Vol. 7, Sept., pp.325-345.
233. Yadav, G.D., Dullien, F.A.L., Chatzis, I. and McDonald, I.F., (1987), "Microscopic distribution of wetting and nonwetting phases in sandstones during immiscible displacement, *SPEERE*, May, Vol. 2, pp. 137-147.
234. Yortsos, Y.C., (1987), "The relationship between immiscible and miscible displacement in porous media", *AIChE J.*, Vol. 33, pp. 1912-1915.

235. Yuster, S.T., (1951), "Theoretical considerations of multiphase flow in idealized capillary systems", *World Petroleum Cong. Proc., Section-II*, The Hague, pp. 437-445.
236. Zanetti, G., (1989), "Hydrodynamics of lattice-gas automata", *Phys. Rev. A.*, Vol. 40(3), August 1, pp.1539-1548.
237. Zarcone, C. and Lenormand, R., (1994), "Détermination expérimentale du couplage visqueux dans les écoulements diphasiques en milieu poreux", *C. R. Acad. Sci., Paris, Series II*, Vol. 318, pp. 1429-1438.

APPENDIX A: PHASE VELOCITY

In this Appendix, phase velocities at various wetting phase saturations, calculated at the breakthrough time for each USCO run, are provided in tabulated form.

Table A1: Calculated phase velocities, USCO (Set 1).

S_l (fraction)	v_l (m/sec)	v_2 (m/sec)
0.8162	3.9243E-05	0
0.8118	3.9203E-05	4.0168E-08
0.8031	3.9118E-05	1.2499E-07
0.7922	3.8996E-05	2.4708E-07
0.7798	3.8837E-05	4.0546E-07
0.7662	3.8636E-05	6.0646E-07
0.7512	3.8378E-05	8.6513E-07
0.7342	3.8036E-05	1.2068E-06
0.7147	3.7574E-05	1.6689E-06
0.6923	3.6941E-05	2.3015E-06
0.6667	3.6075E-05	3.1683E-06
0.6379	3.4899E-05	4.3436E-06
0.6063	3.3290E-05	5.9524E-06
0.5723	3.1335E-05	7.9081E-06
0.5367	2.8909E-05	1.0334E-05
0.5003	2.6032E-05	1.3211E-05
0.4638	2.2733E-05	1.6510E-05
0.4274	1.8995E-05	2.0248E-05
0.3910	1.4633E-05	2.4610E-05
0.3537	9.0004E-06	3.0242E-05
0.3130	0	3.9243E-05

Table A2: Calculated phase velocities, USCO (Set 2).

S_I (fraction)	v_I (m/sec)	v_2 (m/sec)
0.7704	3.7752E-05	0
0.7537	3.7677E-05	7.5050E-08
0.7381	3.7618E-05	1.3388E-07
0.7226	3.7562E-05	1.8969E-07
0.7069	3.7499E-05	2.5327E-07
0.6909	3.7416E-05	3.3586E-07
0.6746	3.7302E-05	4.4967E-07
0.6582	3.7145E-05	6.0684E-07
0.6419	3.6934E-05	8.1767E-07
0.6261	3.6662E-05	1.0894E-06
0.6107	3.6325E-05	1.4270E-06
0.5958	3.5914E-05	1.8374E-06
0.5808	3.5414E-05	2.3381E-06
0.5652	3.4781E-05	2.9711E-06
0.5477	3.3927E-05	3.8248E-06
0.5265	3.2679E-05	5.0730E-06
0.4995	3.0710E-05	7.0415E-06
0.4636	2.7434E-05	1.0317E-05
0.4151	2.1903E-05	1.5849E-05
0.3493	1.2973E-05	2.4779E-05
0.2607	0	3.7752E-05

Table A3: Calculated phase velocities, USCO (Set 3).

S_I (fraction)	v_I (m/sec)	v_2 (m/sec)
0.8413	2.8017E-05	0
0.8341	2.7989E-05	2.8014E-08
0.8263	2.7957E-05	5.9946E-08
0.8179	2.7919E-05	9.8073E-08
0.8086	2.7877E-05	1.4010E-07
0.7982	2.7821E-05	1.9615E-07
0.7866	2.7765E-05	2.5219E-07
0.7735	2.7694E-05	3.2247E-07
0.7588	2.7627E-05	3.9020E-07
0.7422	2.7497E-05	5.2029E-07
0.7236	2.7248E-05	7.6917E-07
0.7028	2.6794E-05	1.2230E-06
0.6796	2.6015E-05	2.0021E-06
0.6538	2.4763E-05	3.2539E-06
0.6253	2.2893E-05	5.1241E-06
0.5937	2.0318E-05	7.6989E-06
0.5591	1.7077E-05	1.0940E-05
0.5210	1.3348E-05	1.4669E-05
0.4795	8.8374E-06	1.9180E-05
0.4342	4.4827E-06	2.3534E-05
0.3850	0	2.8017E-05

APPENDIX B: PHASE PRESSURE (USCO)

In this Appendix, measured, fitted and calculated (Beta = 0.5) phase pressure data along the length of the core, obtained for each USCO run, are provided in tabulated form.

Table B1: Measured phase pressure data, USCO (all Sets).

DD	Set 1		Set 2		Set 3	
	p_1 (Pa)	p_2 (Pa)	p_1 (Pa)	p_2 (Pa)	p_1 (Pa)	p_2 (Pa)
0.00	6480.48	8493.12	19227.06	26697.88	45000.01	50000.21
0.17	6052.51	8136.31	17825.36	26323.49	40751.80	48322.43
0.33	4977.14	8048.96	14642.73	26007.89	38636.75	49748.27
0.50	3856.47	7685.16	16506.74	25596.62	32238.32	48007.35
0.67	2176.27	7545.82	12152.60	25105.28	15268.84	46476.02
0.83	50.01	6978.74	7450.12	24343.85	5000.70	46395.20
1.00	-3850.00	5578.53	1064.56	20523.46	-18242.15	40138.90

* Dimensionless distance

Table B2: Fitted phase pressure data, USC-O (all Sets).

DD	Set 1		Set 2		Set 3	
	p_1 (Pa)	p_2 (Pa)	p_1 (Pa)	p_2 (Pa)	p_1 (Pa)	p_2 (Pa)
0.00	6900.213	8299.429	19000.231	26700.110	46500.012	50400.211
0.05	6669.282	8244.557	18693.021	26655.833	45286.548	50269.048
0.10	6430.316	8205.415	18367.700	26597.363	44030.352	50138.107
0.15	6176.154	8170.517	17997.355	26533.271	42697.942	49989.943
0.20	5904.988	8132.498	17581.804	26464.186	41282.754	49825.422
0.25	5616.563	8087.373	17129.331	26386.549	39785.688	49653.574
0.30	5309.902	8033.799	16646.086	26295.361	38202.601	49483.967
0.35	4982.118	7972.327	16131.398	26185.929	36517.521	49321.201
0.40	4628.064	7904.668	15577.473	26054.720	34700.350	49161.340
0.45	4240.605	7832.948	14971.960	25899.469	32707.876	48990.103
0.50	3811.263	7758.969	14301.848	25718.618	30486.854	48782.625
0.55	3331.017	7683.464	13557.180	25510.245	27977.959	48504.619
0.60	2791.012	7605.363	12733.044	25270.572	25119.389	48114.735
0.65	2182.952	7521.042	11828.337	24992.185	21848.926	47567.955
0.70	1498.942	7423.591	10839.750	24662.083	18103.210	46819.833
0.75	730.543	7302.067	9749.472	24259.662	13813.046	45831.392
0.80	-133.190	7140.757	8505.073	23754.775	8893.515	44574.506
0.85	-1108.920	6918.432	6990.051	23105.963	3227.677	43037.576
0.90	-2223.710	6607.611	4983.503	22258.989	-3357.333	41231.327
0.95	-3521.470	6173.817	2107.412	21145.793	-11123.050	39194.530
1.00	-5071.280	5574.834	-2239.991	19683.974	-20462.470	36999.479

* Dimensionless distance

Table B3: Calculated phase pressure data, Beta = 0.5, USCO (all Sets).

DD	Set 1		Set 2		Set 3	
	p_1 (Pa)	p_2 (Pa)	p_1 (Pa)	p_2 (Pa)	p_1 (Pa)	p_2 (Pa)
0.00	6983.311	8299.401	19300.001	26700.110	46500.201	50400.012
0.05	6753.664	8263.655	18995.729	26661.104	45288.530	50270.747
0.10	6517.074	8226.5637	18671.640	26608.905	44034.337	50141.522
0.15	6266.672	8187.827	18306.464	26550.761	42703.253	49994.495
0.20	6000.697	8146.998	17899.738	26487.122	41288.762	49830.571
0.25	5718.933	8103.466	17457.392	26414.920	39792.072	49659.046
0.30	5420.467	8056.468	16983.366	26329.905	38209.322	49489.728
0.35	5102.502	8005.086	16476.012	26228.061	36524.667	49327.327
0.40	4760.024	7948.247	15928.016	26106.232	34708.012	49167.907
0.45	4386.058	7884.721	15328.585	25962.108	32716.132	48997.179
0.50	3972.319	7813.124	14666.641	25793.705	30495.951	48790.422
0.55	3509.985	7731.914	13933.759	25598.468	27988.715	48513.839
0.60	2990.403	7639.397	13125.601	25372.143	25133.836	48127.118
0.65	2405.464	7533.720	12240.576	25107.555	21871.137	47586.992
0.70	1747.431	7412.876	11274.484	24793.427	18140.274	46851.602
0.75	1007.992	7274.704	10209.860	24413.377	13876.082	45885.423
0.80	176.286	7116.885	8998.798	23945.231	8998.593	44664.573
0.85	-764.294	6936.946	7537.955	23360.794	3396.493	43182.276
0.90	-1840.792	6732.258	5634.512	22626.210	-3097.239	41454.265
0.95	-3097.071	6500.036	2961.815	21703.050	-10738.745	39523.937
1.00	-4602.147	6237.340	-996.562	20550.268	-19917.005	37467.018

* Dimensionless distance

APPENDIX C: CAPILLARY PRESSURE

In this Appendix, fitted capillary pressure data at various wetting phase saturations, obtained for each SSCO run, are provided in tabulated form.

Table C1: Fitted capillary pressure data, SSCO (all Sets).

Set 1		Set 2		Set 3	
S_l (fraction)	P_c (Pa)	S_l (fraction)	P_c (Pa)	S_l (fraction)	P_c (Pa)
0.8162	1199.5242	0.7704	299.8576	0.8413	84.0989
0.8118	1207.5415	0.7537	322.8040	0.8341	91.5353
0.8031	1223.8431	0.7381	345.6092	0.8263	98.1185
0.7922	1245.1955	0.7226	369.6670	0.8179	103.8510
0.7798	1270.1654	0.7069	396.0365	0.8086	108.6335
0.7662	1298.6656	0.6909	425.4926	0.7982	112.3268
0.7512	1331.6106	0.6746	458.5382	0.7866	114.8175
0.7342	1370.5995	0.6582	495.3980	0.7735	116.1270
0.7147	1417.6202	0.6419	536.0353	0.7588	116.5832
0.6923	1474.7712	0.6261	580.2505	0.7422	117.0776
0.6667	1543.9924	0.6107	627.9246	0.7236	119.4335
0.6379	1626.7915	0.5958	679.4603	0.7028	126.9069
0.6063	1723.9800	0.5808	736.4570	0.6796	144.8340
0.5723	1835.4627	0.5652	802.6961	0.6538	181.4137
0.5367	1960.1656	0.5477	885.6519	0.6253	248.5685
0.5003	2096.2092	0.5265	999.1273	0.5937	362.7428
0.4638	2241.4386	0.4995	1168.4592	0.5591	545.3605
0.4274	2394.4021	0.4636	1441.6735	0.5210	822.4423
0.3910	2555.8343	0.4151	1914.4772	0.4795	1222.5430
0.3537	2730.7014	0.3493	2787.8117	0.4342	1771.6680
0.3130	2930.9420	0.2607	4502.9064	0.3850	2482.4830

APPENDIX D: PHASE PRESSURE (SSCO)

In this Appendix, measured phase pressure data along the length of the core, obtained for each SSCO run, are provided in tabulated form.

Table D1: Measured phase pressure data, SSCO (Set 1).

DD	Run 1		Run 2		Run 3		Run 4		Run 5	
	p_1 (Pa)	p_2 (Pa)	p_1 (Pa)	p_2 (Pa)	p_1 (Pa)	p_2 (Pa)	p_1 (Pa)	p_2 (Pa)	p_1 (Pa)	p_2 (Pa)
0.00	--	**	28293.32	30996.31	37153.90	39643.01	33089.01	35227.02	25704.34	27643.15
0.17	--	**	24729.91	28459.81	34161.80	36748.86	30428.98	32687.08	23208.44	25257.56
0.33	--	**	21798.46	25965.49	31269.71	33755.71	27668.96	30247.14	20812.54	22821.98
0.50	--	**	19137.09	22917.40	27977.61	31160.56	25308.93	27407.21	18016.64	20586.39
0.67	--	**	15373.65	19652.57	25285.52	27967.41	22348.90	25167.27	15820.74	18050.81
0.83	--	**	11696.27	16564.57	22193.42	25172.26	19788.88	22527.33	13224.83	15715.22
1.00	--	**	8809.43	12704.64	19201.32	22278.11	17128.85	19987.39	10728.93	13329.63

* Dimensionless distance, ** Not available

Table D1: Continued

DD	Run 6		Run 7		Run 8		Run 9		Run 10	
	p_1 (Pa)	p_2 (Pa)	p_1 (Pa)	p_2 (Pa)	p_1 (Pa)	p_2 (Pa)	p_1 (Pa)	p_2 (Pa)	p_1 (Pa)	p_2 (Pa)
0.00	23136.73	24806.95	20949.03	22664.11	20047.88	21393.74	16803.80	18273.25	10187.03	--
0.17	20784.93	22695.47	18722.02	20518.11	18062.19	19552.84	15238.74	16425.41	9108.66	--
0.33	18413.14	20433.99	16695.02	18422.10	15926.50	17861.94	13473.68	14777.56	8150.29	--
0.50	16179.34	18034.51	14323.01	16126.10	13990.81	15891.04	11508.62	13329.71	7091.92	--
0.67	13669.55	15911.03	12241.00	14230.09	11955.12	14180.14	9943.57	11481.86	6233.55	--
0.83	11297.75	13649.55	9814.00	12134.08	10119.43	12189.24	8178.51	9834.02	5275.18	--
1.00	8905.952	11238.07	7587.00	10088.08	8133.75	10348.34	6213.45	8386.17	4436.81	--

* Dimensionless distance

Table D2: Measured phase pressure data, SSCO (Set 2).

DD	Run 1		Run 2		Run 3		Run 4		Run 5	
	p_1 (Pa)	p_2 (Pa)	p_1 (Pa)	p_2 (Pa)	p_1 (Pa)	p_2 (Pa)	p_1 (Pa)	p_2 (Pa)	p_1 (Pa)	p_2 (Pa)
0.00	--	31489.72	99353.03	103091.5	84805.51	87988.64	79554.29	80600.27	75773.38	77126.69
0.17	--	28504.79	86077.96	91425.61	75953.33	78363.66	69237.15	71788.82	66879.14	68708.19
0.33	--	24713.48	75187.33	79559.68	64969.30	67938.69	59929.23	62777.38	58260.70	60089.69
0.50	--	22283.57	65003.77	68493.76	55826.85	57113.71	51862.36	54165.93	50676.46	52271.20
0.67	--	19693.89	54347.05	56227.83	46585.90	47888.73	43236.47	44754.48	42126.97	43252.70
0.83	--	15010.20	41302.03	44761.90	35170.65	38263.76	33811.89	35743.04	33439.57	35034.20
1.00	--	11206.99	30101.00	33095.97	26228.10	27838.78	25529.18	26531.59	24936.02	26615.70

* Dimensionless distance

Table D2: Continued

DD	Run 6		Run 7		Run 8		Run 9		Run 10	
	p_1 (Pa)	p_2 (Pa)	p_1 (Pa)	p_2 (Pa)	p_1 (Pa)	p_2 (Pa)	p_1 (Pa)	p_2 (Pa)	p_1 (Pa)	p_2 (Pa)
0.00	63293.87	64378.77	52262.26	52744.38	39782.75	40487.68	42540.65	42948.94	10273.19	--
0.17	56674.90	57489.01	46677.50	47370.47	35921.68	36465.72	38265.90	38885.03	9238.97	--
0.33	49849.09	51126.83	40679.07	41234.14	32198.52	32122.03	33991.15	34541.33	8135.81	--
0.50	42954.34	44369.97	35301.16	36752.54	28130.61	29019.39	29854.30	30266.58	7101.60	--
0.67	35990.63	37268.37	30199.04	31788.32	23855.86	25089.38	25303.76	26198.68	5998.44	--
0.83	29164.82	29822.03	25027.97	25789.88	19787.95	20814.63	21029.01	21854.98	4964.23	--
1.00	22674.75	23478.86	20122.69	20343.02	16253.63	16264.09	16773.26	17442.34	3861.06	--

* Dimensionless distance

Table D3: Measured phase pressure data, SSCO (Set 3).

DD	Run 1		Run 2		Run 3		Run 4		Run 5	
	p_1 (Pa)	p_2 (Pa)	p_1 (Pa)	p_2 (Pa)	p_1 (Pa)	p_2 (Pa)	p_1 (Pa)	p_2 (Pa)	p_1 (Pa)	p_2 (Pa)
0.00	--	**	168827.3	171044.0	142445.7	144856.1	123822.9	125409.0	108109.5	109360.0
0.17	--	**	151356.0	158007.5	126794.6	130288.5	109067.9	111210.1	96967.86	97086.90
0.33	--	**	133884.7	144471.0	113143.5	116721.0	97312.86	100511.1	84826.20	83813.80
0.50	--	**	114413.4	132934.5	91492.38	101153.4	82557.82	86812.18	74684.53	74540.71
0.67	--	**	98942.08	118398.2	81841.29	89585.92	69802.78	76113.23	60542.86	59267.61
0.83	--	**	81470.76	105861.5	64190.19	76018.40	54047.74	62414.29	48401.19	47994.51
1.00	--	**	63999.45	92825.23	48539.09	63450.88	41292.70	52215.35	35259.53	35721.41

* Dimensionless distance, ** Not available

Table D3: Continued

DD	Run 6		Run 7		Run 8		Run 9		Run 10	
	p_1 (Pa)	p_2 (Pa)	p_1 (Pa)	p_2 (Pa)	p_1 (Pa)	p_2 (Pa)	p_1 (Pa)	p_2 (Pa)	p_1 (Pa)	p_2 (Pa)
0.00	98726.03	99858.23	105051.8	104672.3	111584.5	111692.2	118072.5	120172.3	61832.34	--
0.17	86915.05	87360.05	94947.96	94503.76	101173.9	100696.0	104744.9	110743.1	54624.40	--
0.33	78104.07	77862.09	81344.08	83335.52	88763.36	88700.04	93417.32	99314.24	48207.30	--
0.50	66293.09	67364.14	71740.21	74167.28	73352.80	78704.07	81089.76	88885.37	41858.23	--
0.67	56482.11	56866.19	58136.33	60999.03	63942.24	64708.09	66762.19	80456.49	32668.52	--
0.83	43671.13	45368.23	48532.45	49830.79	51531.67	52712.11	51434.63	73027.61	25191.63	--
1.00	33860.15	36870.28	35428.58	37662.55	37121.11	39716.13	38107.06	63598.73	17456.20	--

* Dimensionless distance

APPENDIX E: WETTING PHASE SATURATION

In this Appendix, fitted saturation profiles and saturation gradients for the wetting phase at breakthrough times, obtained for each USCO run, are provided in tabulated form.

Table E1: Wetting phase saturation profiles and gradients, USCO (all Sets).

DD	Set 1		Set 2		Set 3	
	S_l (fraction)	(fraction)	S_l (fraction)	(fraction)	S_l (fraction)	(fraction)
0.00	0.8162	-0.0228	0.7704	-0.3168	0.8413	-0.1406
0.05	0.8118	-0.0851	0.7537	-0.3168	0.8341	-0.1488
0.10	0.8031	-0.1450	0.7381	-0.3168	0.8263	-0.1608
0.15	0.7922	-0.2026	0.7226	-0.3168	0.8179	-0.1766
0.20	0.7798	-0.2579	0.7069	-0.3168	0.8086	-0.1962
0.25	0.7662	-0.3109	0.6909	-0.3168	0.7982	-0.2196
0.30	0.7512	-0.3615	0.6746	-0.3168	0.7866	-0.2467
0.35	0.7342	-0.4099	0.6582	-0.3168	0.7735	-0.2777
0.40	0.7147	-0.4559	0.6419	-0.3168	0.7588	-0.3124
0.45	0.6923	-0.4995	0.6261	-0.3168	0.7422	-0.3509
0.50	0.6667	-0.5409	0.6107	-0.3168	0.7236	-0.3932
0.55	0.6379	-0.5799	0.5958	-0.3168	0.7028	-0.4393
0.60	0.6063	-0.6167	0.5808	-0.3168	0.6796	-0.4892
0.65	0.5723	-0.6511	0.5652	-0.3168	0.6538	-0.5428
0.70	0.5367	-0.6831	0.5477	-0.3658	0.6253	-0.6003
0.75	0.5003	-0.7129	0.5265	-0.4692	0.5937	-0.6615
0.80	0.4638	-0.7403	0.4995	-0.6079	0.5591	-0.7265
0.85	0.4274	-0.7654	0.4636	-0.8309	0.5210	-0.7954
0.90	0.3910	-0.7882	0.4151	-1.1380	0.4795	-0.8679
0.95	0.3537	-0.8087	0.3493	-1.5293	0.4342	-0.9443
1.00	0.3130	-0.8268	0.2607	-2.0049	0.3850	-1.0245

* Dimensionless distance

APPENDIX F: ADJUSTED MOBILITY

In this Appendix, adjusted mobilities for the wetting and nonwetting phases at various wetting phase saturations, obtained for each SSCO run are given in tabulated form. Note that, as mentioned in Section 6.2.2, these are not true mobilities; rather, these are mobilities divided by the length (0.60 m) of the core.

Table F1: Wetting phase adjusted mobility data, SSCO (all Sets).

Set 1		Set 2		Set 3	
S_l (fraction)	(m/Pa.s)	S_l (fraction)	(m/Pa.s)	S_l (fraction)	(m/Pa.s)
0.8162	8.5830E-09	0.7704	6.3650E-09	0.8413	1.1693E-09
0.8118	8.4178E-09	0.7537	5.8673E-09	0.8341	1.1228E-09
0.8031	8.0974E-09	0.7381	5.4243E-09	0.8263	1.0747E-09
0.7922	7.7066E-09	0.7226	5.0101E-09	0.8179	1.0243E-09
0.7798	7.2861E-09	0.7069	4.6125E-09	0.8086	9.7078E-10
0.7662	6.8480E-09	0.6909	4.2287E-09	0.7982	9.1377E-10
0.7512	6.3895E-09	0.6746	3.8613E-09	0.7866	8.5305E-10
0.7342	5.9032E-09	0.6582	3.5148E-09	0.7735	7.8865E-10
0.7147	5.3847E-09	0.6419	3.1937E-09	0.7588	7.2087E-10
0.6923	4.8364E-09	0.6261	2.9002E-09	0.7422	6.5024E-10
0.6667	4.2687E-09	0.6107	2.6341E-09	0.7236	5.7756E-10
0.6379	3.6980E-09	0.5958	2.3915E-09	0.7028	5.0385E-10
0.6063	3.1430E-09	0.5808	2.1650E-09	0.6796	4.3030E-10
0.5723	2.6204E-09	0.5652	1.9439E-09	0.6538	3.5822E-10
0.5367	2.1414E-09	0.5477	1.7150E-09	0.6253	2.8895E-10
0.5003	1.7104E-09	0.5265	1.4643E-09	0.5937	2.2380E-10
0.4638	1.3249E-09	0.4995	1.1813E-09	0.5591	1.6399E-10
0.4274	9.7702E-10	0.4636	8.6460E-10	0.5210	1.1058E-10
0.3910	6.5399E-10	0.4151	5.3053E-10	0.4795	6.4604E-11
0.3537	3.3762E-10	0.3493	2.1671E-10	0.4342	2.7184E-11
0.3130	0	0.2607	0	0.3850	0

Table F2: Nonwetting phase adjusted mobility data, SSCO (all Sets).

Set 1		Set 2		Set 3	
S_I (fraction)	(m/Pa.s)	S_I (fraction)	(m/Pa.s)	S_I (fraction)	(m/Pa.s)
0.8162	0	0.7704	0	0.8413	0
0.8118	5.2017E-11	0.7537	3.9263E-11	0.8341	1.0004E-11
0.8031	1.5509E-10	0.7381	7.6182E-11	0.8263	2.0668E-11
0.7922	2.8570E-10	0.7226	1.1264E-10	0.8179	3.2293E-11
0.7798	4.3276E-10	0.7069	1.4963E-10	0.8086	4.5139E-11
0.7662	5.9395E-10	0.6909	1.8748E-10	0.7982	5.9468E-11
0.7512	7.7247E-10	0.6746	2.2599E-10	0.7866	7.5541E-11
0.7342	9.7427E-10	0.6582	2.6470E-10	0.7735	9.3620E-11
0.7147	1.2058E-09	0.6419	3.0300E-10	0.7588	1.1397E-10
0.6923	1.4724E-09	0.6261	3.4038E-10	0.7422	1.3684E-10
0.6667	1.7768E-09	0.6107	3.7660E-10	0.7236	1.6250E-10
0.6379	2.1188E-09	0.5958	4.1188E-10	0.7028	1.9122E-10
0.6063	2.4948E-09	0.5808	4.4710E-10	0.6796	2.2325E-10
0.5723	2.8984E-09	0.5652	4.8400E-10	0.6538	2.5885E-10
0.5367	3.3211E-09	0.5477	5.2535E-10	0.6253	2.9829E-10
0.5003	3.7537E-09	0.5265	5.7517E-10	0.5937	3.4182E-10
0.4638	4.1883E-09	0.4995	6.3888E-10	0.5591	3.8971E-10
0.4274	4.6204E-09	0.4636	7.2355E-10	0.5210	4.4222E-10
0.3910	5.0525E-09	0.4151	8.3804E-10	0.4795	4.9962E-10
0.3537	5.4968E-09	0.3493	9.9322E-10	0.4342	5.6215E-10
0.3130	5.9797E-09	0.2607	1.2022E-09	0.3850	6.3004E-10

CURRICULUM VITAE

OF

MUHAMMAD AYUB

HOME ADDRESS (PREFERRED)	OFFICE ADDRESS
312 RH, Michener Park Edmonton, Alberta Canada, T6H 4M5 Phone. (780) 433-3170 E-Mail: mayub@ualberta.ca	220-CEB Building University of Alberta Edmonton, AB., Canada, T6G 2G7 Phone. (780) 492-2875 FAX: (780) 492-0249

Qualifications

- **Ph.D. in Petroleum Engineering**, University of Alberta, Edmonton, Alberta, Canada, Spring 2000.
- **M.Sc. in Petroleum Engineering**, King Fahd University of Petroleum and Minerals (KFUPM), Dhahran, Saudi Arabia, June 1989.
- **B.Sc. in Petroleum Engineering**, University of Engineering and Technology, Lahore, Pakistan, with HONORS (Distinction), 1985.

Experience

- 1995 - 2000
- **Research Assistant**, University of Alberta, Edmonton, Alberta, Canada. Responsibilities included: To develop a comprehensive computer-based experimental set-up to conduct steady state and unsteady state displacement experiments whereby dynamic saturation and dynamic capillary pressure profiles can be measured with an excellent precision. All instrumentation, survey, designing, purchasing, fabrication, testing, data acquisition, data analysis and interpretation, etc. Supervised and graded undergraduate laboratories, assignments and reports, etc.

- May 1995-
Sep. 1995.
- **Research Associate** (Summer Assistance), Alberta Research Council, Edmonton, Canada. Extensively involved in a project entitled "Technology Scanning". Responsibilities included: To collect the latest information (using the data bases of various world renowned organizations through INTERNET, libraries, CD-ROM, and Personnel Communications etc.) about technologies related to the oil and gas industry of Western Canada, Comprehensive review of state-of-the-art technologies and their applications; Recommendations for further development and possible methods for problem solving; Writing comprehensive reports from marketing and selling point of view; and making presentations before management, etc.
- 1989 to 1994
- **Research Scientist**, King Fahd University of Petroleum and Minerals, Dhahran, Saudi Arabia. Handling research projects funded by the Saudi Arabian Government related to Petroleum Engineering. Performed all tune-up operations and worked as technical expert of waterflooding, core analysis, reservoir rocks fluids properties, computer aided interpretation of data, prepare regular technical reports and conducted special studies on subjects such as hot and cold waterflooding for reservoirs with a Tarmat problem.
 - Complete handling (experimentation, result interpretations and report writing) of research related to In-Situ Combustion of the Tarmat of the Saudi Arabian Oil Reservoirs; one of the major problems faced by the Saudi's and many other Middle Eastern's Oil Industries. Played an active role in finalizing the progress report of the research projects. Contributions in design and fabrications of new physical reservoir models for various problems. Attended many seminars, symposiums organized by the University and ARAMCO.
- 1986 to 1989
- **Research Assistant**, King Fahd University of Petroleum and Minerals. Responsibilities included, research experimentation to investigate the Tarmat reservoirs. Extensively involved in waterflooding experiments, techniques, strategies, and interpretation of data collected. Expert in handling almost all types of equipment used in petroleum engineering laboratories.

- 1985 to 1986 • **Assistant Production Engineer**, Oil and Gas Development Corporation (OGDC) of Pakistan, the largest petroleum-company in the country. Involved in Well Testing, Reserve Estimation, Reservoir Monitoring and Characterization, Production activities like PLT, RFT, DST and different Production Logging output evaluations and interpretations. Consulting with Service Companies on various aspects of the performance and progress of various jobs assigned by the OGDC. Also got three-month training about Well Testing and Well Logging from Schlumberger.
- 1985 • **Lecturer**, University of Engineering and Technology, Lahore, Pakistan. Taught undergraduate courses like Production Engineering and Well Testing. Supervised and demonstrated laboratory experiments to the students.

Honors and Awards

- Awarded First Prize for the best presentation at the Annual SPE Student Paper Contest (Canadian Section) held in Calgary, January 23, 1999.
- Awarded Third Prize for the best presentation at the Annual CIM Student Paper Contest held in Calgary, June 14, 1999.
- Tuition Scholarships awarded by the Faculty of Graduate Studies and Research, University of Alberta, 1997 and 1998.
- Travel grant awarded by the Faculty of Graduate Studies and Research, University of Alberta, June 1999.
- Awarded financial support from the Imperial Oil of Canada to complete Ph.D. related research, 1998-2000.
- Awarded financial support from the Natural Science and Engineering Research Council (NSERC) of Canada to complete Ph.D. related research, 1997-2000.
- Awarded Scholarships by the Norcen Energy Resources Ltd., Calgary, Canada, September 1995, and September 1996, for the best academic performance.

- Awarded financial support from the Alberta Research Council of Canada to complete Ph.D. related research, 1997.
- Awarded Canadian SPE Scholarship, 1996-97 and 1998-99.
- Awarded Research Assistantship to complete M.Sc., by the University of Petroleum and Minerals, Dhahran, Saudi Arabia, 1986 - 1989.
- B.Sc. Engineering Degree with Honors and Distinction. First position in the Department of Petroleum Engineering throughout 1980 to 1984.
- University Merit Scholarships, Merit Certificates, and Gold Medals for best academic performance in 1981, 82, 83, and 84.
- Fellowship and Gold Medal from Oil and Gas Development Corporation, Pakistan, for best academic performance, 1984.
- Gold Medal from Qamar Traders, Lahore, Pakistan, for best academic performance, 1984.

Professional Skills

- Excellent analytical, experimental and data handling skills; excellent oral and written communication skills.
- Worked extensively with PC, MAC, (WINDOWS, DOS, MS-WORD, POWER-POINT, EXCEL, INTERNET etc.) and IBM mainframe, working knowledge of FORTRAN, BASIC, LabVIEW, GRAPHICS, WSCRIPT, SPSS, Maple, and SAS, etc.

Short Courses

- Completed an extensive short course in “Basic Corrosion Engineering” offered by the College of Applied Engineering at the King Fahd University of Petroleum and Minerals, Dhahran, Saudi Arabia. (Dec. 19 - 23, 1992).
- Completed an extensive short course in “Introduction to Statistical Analysis System” (SAS BASE / STAT / GRAPH), offered by the DPC at the King Fahd University of Petroleum and Minerals, Dhahran, Saudi Arabia. (Jan. 09 - 20, 1993).

- Attended several seminars, workshops on LabVIEW; an excellent software for data acquisition and instrument control, 1996-2000.

Professional Affiliation

- Member, Society of Petroleum Engineers (SPE), USA.
- Member, Petroleum Society of CIM, Canada.
- Life Member, Pakistan Engineering Council, Pakistan.

Publications

- **Ayub, M.**, "The Experimental Testing of the Impact of Interfacial Coupling on Two-Phase Flow in Porous Media," Ph.D. Thesis in Petroleum Engineering, Department of Civil and Environmental Engineering, University of Alberta, Edmonton, Alberta, Canada, Spring 2000.
- **Ayub, M.**, "A Method for Measurement of Dynamic Saturation Profiles," Paper presented and won the FIRST AWARD at the annual SPE Student Paper Contest (Canadian Section), Calgary, January 23, 1999.
- **Ayub, M.**, Bentsen, R. G., "Measurement of Dynamic Saturation Profiles", accepted for publication, Journal of Canadian Petroleum Technology, 2000. Also awarded THIRD PRIZE for the best presentation at the Annual CIM Student Paper Contest held in Calgary, June 14, 1999
- **Ayub, M.**, Bentsen, R. G., "Interfacial viscous coupling: a myth or reality?" Journal of Petroleum Science and Engineering, Vol. 23, pp. 13-26, 1999.
- Abu-Khamsin, S. A., **Ayub, M.**, Menouar, H., Al-Marhoun, M. A., "Waterflooding in a Tarmat Reservoir Laboratory Model," Journal of Petroleum Science and Engineering," Vol. 9, pp. 251-261, 1993.
- **Ayub, M.**, "The Effects of Tar Viscosity and Thickness on Oil Recovery in a Tarmat Reservoir Model," M.Sc. Thesis, Petroleum Engineering Department, King Fahd University of Petroleum and Minerals, Dhahran, Saudi Arabia, June 1989.

Technical Reports: Three comprehensive technical reports were written and presented during my stay at Alberta Research Council, Edmonton, Alberta, Canada. May 1995 to Sep. 1995.

1. **Ayub, M.**, "Horizontal Well Drilling Opportunities in Western Canada," Internal Report #1, Technology Scanning, Energy Technologies Department, Alberta Research Council, Edmonton, Canada, June 1995.
2. **Ayub, M.**, "Opportunities for Natural Gas Utilization in Refrigeration Technologies," Internal Report #2, Technology Scanning, Energy Technologies Department, Alberta Research Council, Edmonton, Canada, Aug. 1995.
3. **Ayub, M.**, "Opportunities for Handling Waxy Crude Oils," Internal Report #3, Technology Scanning, Energy Technologies Department, Alberta Research Council, Edmonton, Canada, Sept. 1995.

Graduate Level Courses Taken

University of Alberta

- Modeling in Petroleum Engineering
- Reservoir Simulator Development
- Secondary Recovery
- Fluid Mechanics of Natural Gas Production
- Heavy Oil Recovery
- Numerical and Analytical Solution of Porous Media Flow Problems
- Advanced Well Test Analysis
- Environmental Geotechnics
- Engineering Geology and Terrain Analysis
- Colloids and Interfaces
- Graduate Seminar

King Fahd University of Petroleum and Minerals

- Advanced Well Testing
- Advanced Production Engineering
- Advanced Reservoir Engineering
- Intermediate Well Logging
- Special Topics in Petroleum Engineering
- Enhanced Oil Recovery
- Petroleum Economics
- Reservoir Simulation
- Applied Regression
- Computer Programming
- Graduate Seminar